Discrete Dynamical Systems and Applications

Tutorial Workshop

Urbino (Italy)

June 30 - July 3, 2010

Contents

1 ACKNOWLEDGEMENTS

Discrete Dynamical Systems and Applications
Tutorial Workshop
Urbino (Italy) June 30 - July 3, 2010

The organization of this Tutorial Workshop has been possible due to the support of the following institutions, which we warmly thanks:

- The GNFM, Gruppo Nazionale di Fisica Matematica
- The Atheneum of Urbino
- The Department of Economics and Quantitative Methods

2 PROGRAM

June 30, Wednesday

9:00 -10:45 Gian Italo Bischi

Introduction to one-dimensional smooth discrete dynamical systems: fixed points, cycles, stability, local bifurcations, basins and their bifurcations.

Break

11:00 -12:45.Laura Gardini.

Global properties of one-dimensional smooth discrete dynamical systems. Noninvertible maps, homoclinic bifurcations and chaotic sets, trapping intervals and critical points.

13: Lunch

15:00 -16:45. Iryna Sushko.

One-dimensional continuous piecewise-smooth dynamical systems. Border-collision bifurcations.

Break

17:00 -18:00. Fabio Lamantia.

Examples and applications of one-dimensional discrete dynamical systems in economic, social and ecological systems.

18:00 -19:00. Discussion with the Participants.

———————————————————————————

July 1, Thursday

9:00-10:45. Gian Italo Bischi.

Two-dimensional discrete dynamical systems, local bifurcations, critical curves, absorbing areas, chaotic areas, basins of attraction and related bifurcations due to contacts with critical curves.

Break

11:00-12:45. Laura Gardini.

Homoclinic bifurcations and global bifurcations of attractors and basins in two-dimensional noninvertible maps.

13: Lunch

15:00-16:45. Anna Agliari.

Closed invariant curves and their bifurcations in two-dimensional maps.

Break

17:00-18:00. Iryna Sushko.

Two-dimensional piecewise-smooth maps.

18:00-19:00. Discussion with the Participants.

July 2, Friday

9:00-10:45. Laura Gardini and Fabio Tramontana.

One-dimensional discontinuous dynamical systems.

Break

11-12:45 Roberto Dieci.

Applications to Economics: modeling interacting markets with higher-dimensional discrete dynamical systems.

13: Lunch

15:00-16:00. Gian Italo Bischi and Anna Agliari.

Global bifurcations in applied models.

16-16.45 Roberto Dieci.

Applications to financial markets: higher-dimensional dynamical systems in heterogeneous-agent asset pricing models.

Break

17:00-18:00. Fabio Tramontana.

Examples and applications of discrete dynamical systems in economic, social and ecological systems.

18:00-19:00. Discussion with the Participants.

July 3, Saturday

9:00-10:30. Numerical tools

Fabio Lamantia: Mathematica

Davide Radi: Matlab

Fabio Tramontana: Visual Basic and numerical problems.

10:30-12:45. Participants' space: discussion, open problems, examples.

Remark

besides the present one, other material for the participants can be downloaded from the web site:

http://www.econ.uniurb.it/bischi/urbino2010.html

2.1 List of participants

Alessio Emanuele Biondo, Università di Catania, Italy (ae.biondo@unict.it)
Emiliano Biosa, Università di Sassari, Italy (ebiosa@uniss.it)
Marcello Budroni, Università di Siena e di Sassari, Italy (mabudroni@uniss.it)
Alessandro Calamai, Università Politecnica delle Marche, Ancona, Italy (calamai@dipmat.univpm.it)
Giovanni Cignali, Università di Bologna, Italy (giovanni.cignali@unibo.it)
Fatima Correia, University of Evora, Portugal (mfac@uevora.pt)
Carla Dias, Istituto Politécnico de Portalegre, Portugal.(carlald.dias@gmail.com)
Linda Dimare, Università di Pisa, Italy (dimarelinda@alice.it)
Particia Dominguez, Universidad Autónoma de Puebla, México (pdsoto@fcfm.buap.mx)
Davide Farnocchia, Università di Pisa, Italy (farnocchia@mail.dm.unipi.it)
Matteo Franca, Università Politecnica delle Marche, Ancona, Italy (franca@dipmat.univpm.it)
Luca Gori, Università di Pisa, Italy (dr.luca.gori@gmail.com)
Anna Jonssons, University of Umea, Sweden (anna.jonsson@cerum.umu.se)
Daniele Linaro, Università di Genova (daniele.linaro@unige.it)
Rafik Mouzaia, Università di Annaba, Algeria (mouzaia_rafik@yahoo.fr)
Giorgia Oggioni, Università di Brescia, Italy (oggioni@eco.unibs.it)
Delio Panaro, Università di Pisa, Italy (skiuski@gmail.com)
Anastasia Panchuk, Institute of Mathematicis, Kiev, Ukraine (nasyap@imath.kiev.ua)
Carmen Pellicer-Lostao, Universidad de Zaragoza, Spain (carmen.pellicer@unizar.es)
Barbara Przebieracz, University of Silesia, Katowice, Poland (przebieraczb@gmail.com)
Rossana Riccardi, Università di Pisa, Italy (riccardi@ec.unipi.it)
Marco Rocco, Università di Bergamo, Italy (marco.rocco@unibg.it)
Julia Slipantschuk, University of Aberdeen, Switzerland (juliasl@student.ethz.ch)
Michalis Smyrnakis, University of Bristol, GB (M.Smyrnakis@bristol.ac.uk)
Mauro Sodini, Università di Pisa, Italy (m.sodini@ec.unipi.it)
Lisa Svendsberget, University of Umea, Sweden (lisv0037@ad.umu.se)
Shu Zhang, Cyna (zhsh886@yahoo.com.cn)
Ruifeng Zhang, University of Trieste (rzhang@ictp.it)

Tutors

Anna Agliari, Catholic University, Piacenza, Italy (anna.agliari@unicatt.it)
Gian-Italo Bischi, University of Urbino, DEMQ, Italy (bischi@uniurb.it)
Roberto Dieci, University of Bologna, Italy (roberto.dieci@unibo.it)
Laura Gardini, University of Urbino, DEMQ, Italy (laura.gardini@uniurb.it)
Fabio Lamantia, University of Calabria, Cosenza, Italy (lamantia@unical.it)

Tönu Puu, CERUM Centre for Regional Science, Umea, Sweden (tonu.puu@cerum.umu.se)

Davide Radi, University of Urbino, DEMQ, Italy (radidavide85@gmail.com)

Iryna Sushko, National Academy of Sciences of Ukraine, Kiev, Ukraine (sushko@imath.kiev.ua)

Fabio Tramontana, Università Politecnica delle Marche, Ancona, Italy (f.tramontana@univpm.it)

3 Definitions and preliminary notions.

The object of the present work is to describe some properties on the complex world of the nonlinear dynamics in discrete systems. Let us consider a dynamic model which is described by iterating some process:

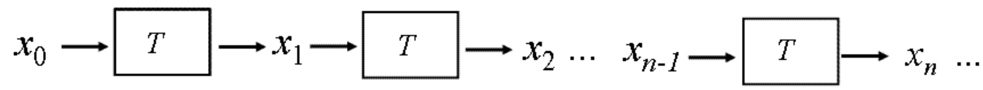

Fig.1 Iterative process

The state of the system changes under the action of some function, here represented (Fig.1) by T. The state x may be a scalar or a vector of state variables. The state (or phase) space is a set $X \subseteq R^m$ where m is an integer denoting the dimension of the vector state variable x, $m \in \{1, 2, 3...\}$, and $T : X \to X$. A discrete dynamical system (DDS for short) is represented by the standard notation

$$x_{n+1} = T(x_n) \quad or \quad x' = T(x) \tag{1}$$

The object of the theory of DDS is that to understand which kind of values will be obtained asymptotically, and this depending on the initial value (or initial condition, i.c. henceforth) x_0 in the phase space. Also important will be the *bifurcations*, which are responsible of the changes in the qualitative behaviors of the trajectories of the iterative process. To this scope we recall that the bifurcations are studied in the parameter space, which includes all the parameters which are considered in the model under study. Whenever the parameters have a fixed value we have a dynamic system whose invariant sets in the phase space of interest are our object of investigation, as well as the description of the dynamic behavior associated with the points in the phase space (are the trajectories converging to the same set ? are some of them uninteresting for us because associated to divergent dynamics ? and so on). Then, as the parameters are varied, things may change smoothly (as under a deformation, we shall say "via an homeomorphism", which is a continuous invertible function) or some drastic change may occur, in which case we say that a bifurcation takes place. Roughly speaking, we say that a bifurcation takes place at some specific parameters setting when the dynamics occurring "before" and "after" (when the condition is not fulfilled) cannot be obtained one from the other by a smooth change (via an homeomorphism).

To study DDS it is important to introduce first a few definitions and terms. Let us consider a map $x' = T(x)$, T is defined from X into itself. The point x' is called the *rank-1 image* of x. A point x such that $T(x) = x'$ is called a *rank-1 preimage* of x'. The point $x(n) = T^n(x)$,

$n \in \mathbb{N}$, is called image of rank-n of the point x, where T^0 is identified with the identity map and $T^n(\cdot) = T \circ T^{n-1}(\cdot) = T(T^{n-1}(\cdot))$. A point x such that $T^n(x) = y$ is called rank-n preimage of y.

Let $A \subset X$ be a such that $T(A) \subseteq A$, then A is called *trapping set.* We have two kinds of trapping set: either (a) $T(A) = A$, then A is called *invariant set,* or (b) $T(A) \subset A$ than A is strictly mapped into itself, and in this case $T^{n+1}(A) \subseteq T^n(A)$ for any $n > 0$. When A is a compact set then the intersection of the nested sequence of sets is a closed nonempty invariant set, say $B = \cap_{n>0} T^n(A)$, then $T(B) = B$ (note that the number of iterations necessary to get the invariant set B may be finite or infinite). For our purposes it is important to stress the properties of an invariant set $A \subseteq X$. As by definition any point of $T(A)$ is the image of at least one point of A, we have that for an invariant set $A \subseteq X$, for which $T(A) = A$, this propery holds for any point in A, that is:

Property 1. If T is invariant on A then any point of A has at least one rank-1 preimage in A, and iteratively: any point of A has an infinite sequence of preimages in A.

The behaviour of points in a neighburhood of an invariant set A depends on the local dynamics (A may be attracting, repelling, or neither of the two).

An *attracting set* is a closed invariant set A which possess a *trapping neighborhood,* that is, a neighborhood U, with $A \subset Int(U)$, such that $A = \cap_{n \geq 0} T^n(U)$ (as in the case of the set B constructed above). In other words, if A is an attracting set for T, then a neighborhood U of A exists such that the iterates $T^n(x)$ tend to A for any $x \in U$ (and not necessarily enter A). An *attractor* is an attracting set with a dense orbit.

The *basin of attraction* of an attracting set A, $\mathcal{B}(A)$, it the set of all the points whose trajectory has the limit set in A (roughly speaking, whose trajectory tends to A).

$$\mathcal{B}(A) = \{x | T^n(x) \to A \quad \text{as } n \to +\infty\}.$$

As the attracting set possesses a neighborhood U of points having this property, then the basin is made up of all the possible preimages of U: $\mathcal{B}(A) = \cup_{n \geq 0} T^{-n}(U)$. Sometimes it is useful to consider as neighborhood U the *immediate basin*, which is the largest connected component of the basin which contains the attracting set A.

A *repelling set* is a compact invariant set K which possesses a neighborhood U such that for any point $x_0 \in U \backslash K$, the trajectory $x_0 \to x_1 \to \ldots$ must satisfy $x_n \notin U$ for at least one value of $n \geq 0$ (but such a trajectory may also come back again in U, as it occurrs when homoclinic trajectories exist). A *repellor* is a repelling set with a dense orbit.

It is worth noticing that this definition is a very strict one (as we shall see below, by using this definition a saddle cycle cannot be called repelling, but only unstable). Some authors use "expanding" in its place, keeping a more soft definition for a repelling set saying that a closed invariant set K which is not attracting is called *repelling if however close to K there are points whose trajectories goes away from K*. And as usual a *repellor* is defined as a repelling set containing a dense orbit. This less restrictive definition allows, when applied to a cycle, to say that *attractor* (*repellor*) is synonymous of asymptotically stable (unstable), however it is worth noticing that in this case we have further to distinguish when a repelling cycle is expanding or not.

Regarding the *invariant sets*, the simplest case is that of "*fixed point*". We say that x^* is a fixed point (or equilibrium point) of the DDS if it satisfies

$$x^* = f(x^*)$$

That is: starting in that point the system never changes. Then, given that it is very difficult to be exactly in a fixed point, it is important to understand when (i.e. under which conditions) starting from a different state and iterating the process we are approaching the equilibrium, and when this occurs for all the points in a suitable neighborhood, we call it *attracting:* The definition given above is fulfilled. When for some points, also very close to an equilibrium, the process will lead the state far away from it, then it is unstable.

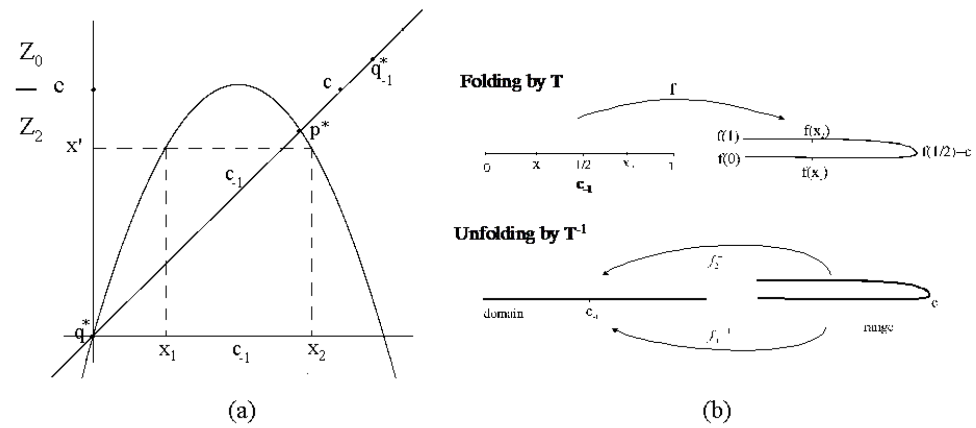

Fig.2

A map T is said to be noninvertible (or "many-to-one", see Fig.2), if distinct points $x \neq y$ exist which have the same image, $T(x) = T(y) = x'$. This can be equivalently stated by saying that points exist which have several rank-1 preimages, i.e. the inverse relation $x = T^{-1}(x')$ may be multi-valued. Geometrically, the action of a noninvertible map T can be described by saying that it "folds and pleats" the plane, so that two distinct points are mapped into the same point. Equivalently, we could also say that several inverses are defined, and these inverses "unfold" the plane. For a noninvertible map T, the space $\mathbb{R}^m$ can be subdivided into regions Z_k, $k \geq 0$, whose points have k distinct rank-1 preimages (Fig.3). Generally, as the point x' varies in $\mathbb{R}^m$, pairs of preimages appear or disappear as this point crosses the boundaries which separate different regions. Hence, such boundaries are characterized by the presence of at least two coincident (or merging) preimages. This leads to the definition of the critical sets, one of the distinguishing features of noninvertible maps (Mira et al., [89]): The *critical set* CS of a continuous map T is defined as the locus of points having at least two coincident $rank-1$ preimages, located on a set CS_{-1} called *set of merging preimages*. The critical set CS is the n-dimensional generalization of the notion of critical value (when it is a local minimum or maximum value) of a one-dimensional map[1], and of the notion of *critical curve* LC of a noninvertible two-dimensional map (from the French "Ligne Critique"). The set CS_{-1} is the generalization of the notion of critical point (when it is a local extremum point) of a one-dimensional map, and of the fold curve LC_{-1} of a two-dimensional noninvertible map. The critical set CS is generally formed by $(n-1)$-dimensional hypersurfaces of $\mathbb{R}^m$, and portions of CS separate regions Z_k of the phase space characterized by a different number of $rank-1$ preimages, for example Z_k and Z_{k+2} (this is the standard occurrence).

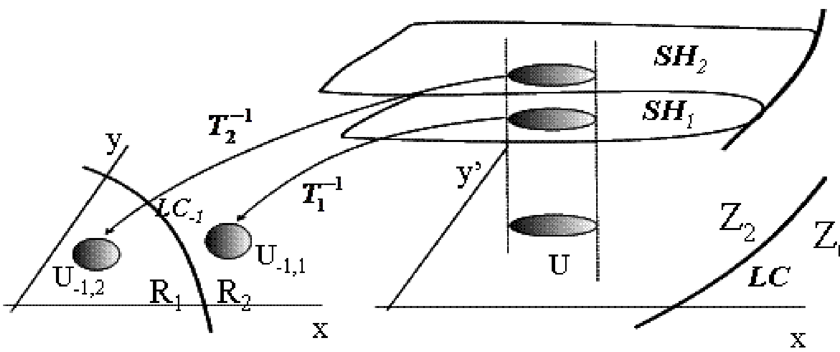

Fig.3

[1] This terminology, and notation, originates from the notion of critical points as it is used in the classical works of Julia and Fatou.

4 One-dimensional phase-space.

Let us consider first the case of a 1D phase space, as all the main properties of dynamical systems and chaotic behaviors can be well introduced in this space. As a very simple example consider the function $f(x) = \sqrt{x}$:

$$x' = \sqrt{x}$$

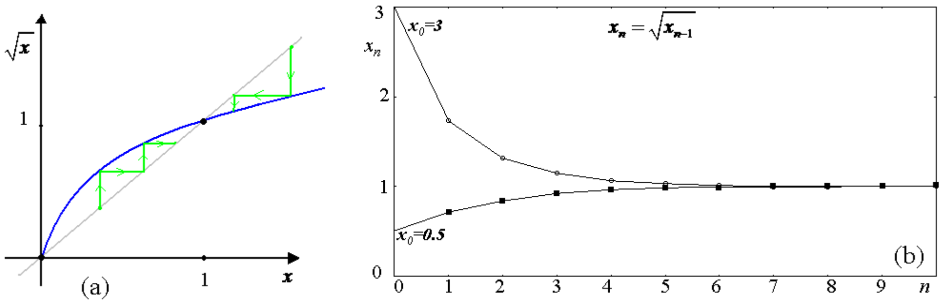

Fig.4 Convergence to the stable fixed point.

Then it is easy to see that $x^* = 1$ is a stable fixed point of this model (Fig.4). Starting from any point as i.c. and iterating, the process shall converge to the stable fixed point. From the graph of the function it is easy to see this result also graphically, by using the "stair-process". The stability can be obtained analytically from the slope of the tangent to the function in the fixed point. This follows from the linearization theorem. It is very easy to prove the property in the linear case: a straight line with slope in modulus (or absolute value) lower (higher) than 1 has a stable (unstable) fixed point.

For a nonlinear function the stability/instability is a local property, which may be investigated by the first order approximation of the function in the fixed point. We can summarize as follows:

$$\begin{aligned} &-1 < S = f'(x^*) < 1 \ : \ locally \ stable \ fixed \ point \\ &S = +1 \ bifurcation \ (fold, \ transcritical \ or \ pitchfork) \\ &S = -1 \ flip \ bifurcation \end{aligned}$$

In the case of monotone increasing one-dimensional functions (Fig.5) the only possible invariant sets are fixed points which are alternating: one stable, one unstable. The basins of attractions of the stable fixed points are bounded by the unstable fixed points or by infinity.

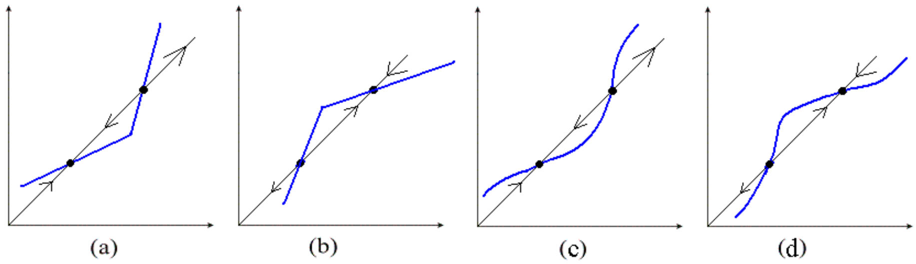

Fig.5 Increasing functions, piecewise linear and nonlinear smmoth.

In the linear case we can see that at the bifurcation occurring when the slope is equal to -1, a new kind of dynamics occurs: all the points belong to a 2-cycle (Fig.6).

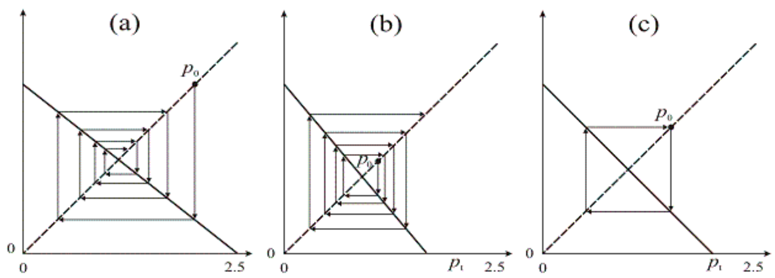

Fig. 2

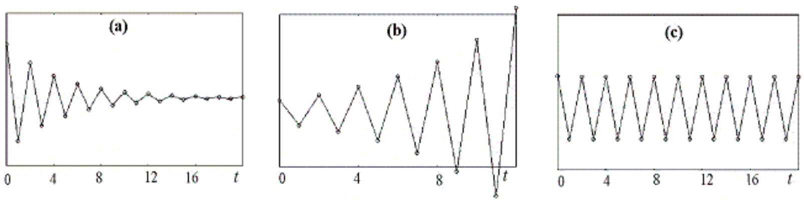

Fig. 3

Fig.6 Decreasing linear functions

In the generic case of a decreasing one-dimensional function the only possible invariant sets are *one fixed point, and 2-cycles*, which are alternating: one stable, one unstable.

We can already see a generic feature: if the slope in the fixed point is positive (resp. negative) then locally we have monotonic dynamics (resp. alternating dynamics), as qualitatively shown in Fig.7a and Fig.7b, respectively.

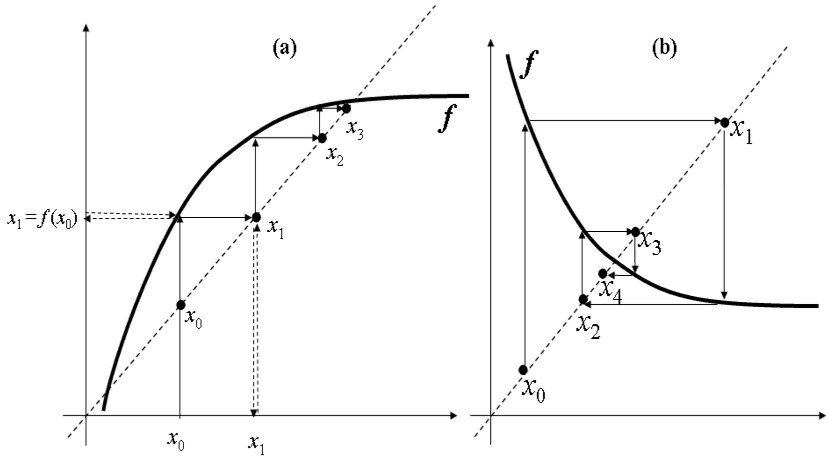

Fig.7 Monotone dynamics or alternating dynamics.

Moreover we have seen that cycles may occur. A $k-$cycle is a sequence of k distinc points x_i, $i = 1, 2, ..., k$ visited iteratively by the map, and such that $f^k(x_i) = x_i$ for any point x_i. That is, stated in other words, each of the periodic points is a fixed point of the map $f^k = f \circ f \circ ... \circ f$. The stability/instability of a cycle is determined by the stability/instability condition of a fixed point of the map f^k and from the chain rule we have, for each point x_i of the cycle,

$$S = \frac{d}{dx}(f^k(x))|_{x_i} = \prod_{j=1}^{k} f'(x_j) \tag{2}$$

Summarizing, if we consider a one–dimensional map $x_{n+1} = f(x_n)$ and a $k-$cycle of points $\{x_1, ..., x_k\}$, $k \geq 1$ (for $k = 1$ we have a fixed point), the condition $|S| < 1$ (resp. > 1) is a sufficient condition to conclude that the $k-$cycle is an attractor (resp. repellor), as S is the slope, or eigenvalue, in any point x_i of the map f^k.

We have not considered the bifurcation cases in which $|S| = 1$, because the behavior depends on the kind of bifurcation. This can be found in several textbooks ([104], [49], [50], [30], [70]), and we simply recall that the bifurcations associated with $S = -1$ are related to a period-doubling of the cycle, and it is frequently called *flip bifurcation*. That is, crossing this bifurcation value, when suitable transversality conditions are satisfied, then a stable $k-$cycle becomes unstable and a stable $2k-$cycle (of double period) appears around it. While the bifurcations associated with $S = +1$ may be of three different kinds: (i) either related to a *fold bifurcation*, giving rise to a pair of $k-$cycles, one attracting and one repelling, (ii) or to a *change of stability* (also called *transcritical*), a pair of stable/unstable cycles merge after which they exchange their stability, i.e. become unstable/stable respectively, (iii) or a *pitchfork* *bifurcation* occurs at which a stable $k-$cycle becomes unstable and two new $k-$cycles appear around it, both stable.

As observed several years ago by the pioneers of such studies ([92], [103], [85], [86], [82], [87]) still in the one-dimensional case we can see that once that the monotonicity (i.e. the invertibility property) is lost, then very complicated paths may occur, which may be predictable or not (although the model is completely deterministic). As a standard example let us consider the simple logistic map (whose graph is a parabola):

$$x' = f(x) \quad , \quad f(x) = \mu x(1-x) \quad , \quad \mu \in [3,4] \tag{3}$$

which for $\mu > 3$ has the origin as unstable fixed point and the positive fixed point which may be stable or unstable, depending on the slope (or eigenvalue) in that point. This map has a unique critical point $c = \mu/4$, which separates the real line into the two subsets (see Fig.8): $Z_0 = (c, +\infty)$, where no inverses are defined, and $Z_2 = (-\infty, c)$, whose points have two rank-1 preimages. These preimages can be computed by the two inverses

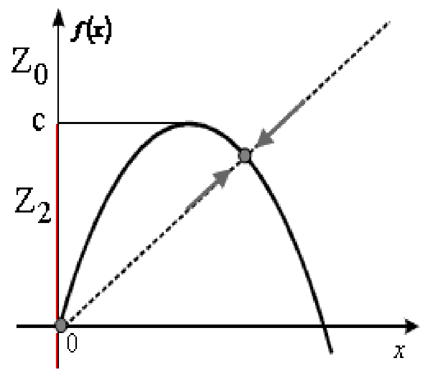

Fig.8 Logistic map

$$x_1 = f_1^{-1}(x') = \frac{1}{2} - \frac{\sqrt{\mu(\mu - 4x')}}{2\mu}; \quad x_2 = f_2^{-1}(x') = \frac{1}{2} + \frac{\sqrt{\mu(\mu - 4x')}}{2\mu}. \tag{4}$$

If $x' \in Z_2$, its two rank-1 preimages, computed according to (4), are located symmetrically with respect to the point $c_{-1} = 1/2 = f_1^{-1}(\mu/4) = f_2^{-1}(\mu/4)$. Hence, c_{-1} is the point where the two merging preimages of c are located. The map f folds the real line, the two inverses unfold it (Fig. 1b). As the map (3) is differentiable, at c_{-1} the first derivative vanishes. However, note that in general a critical point may even be a point where the map is not differentiable. This happens for continuous piecewise differentiable maps such as the well known tent map or other piecewise linear maps. In these maps critical points are located at the kinks where two branches with slopes of opposite sign join and local maxima and minima are located.

As an *equivalent model*, we may consider any function which is obtained by using a change of variable with an homeomorphism h (a continuous and invertible function). We are so introducing the concept of "*topological conjugacy*": let

$$F = h \circ f \circ h^{-1} \tag{5}$$

then the maps F and f are called topologically conjugated, and it can be proved that *topologically conjugated maps have the same dynamics*: all the trajectories can be put in one-to-one correspondence by using the homeomorphism h.

It is easy to see that via a linear homeomorphism we can transform the logistic map into the Myrber's map (Myrber was the first author who studied in details the bifurcations of such non-invertible one-dimensional maps, still in 1963):

$$x' = F(x) \quad : \quad F(x) = x^2 - b \tag{6}$$

For $b \in [0, 2]$ we have $F : I \to I,\ I = [q^*_{-1}, q^*]$ where q^* is the repelling positive fixed point. At $b = 0$ the slope at the stable fixed point p^* is zero (also called superstable), and then, increasing b, the slope from positive becomes negative, reaching the value -1 and a flip bifurcation takes place, leading to the appearance of a stable cycle of period 2 (Fig.9).

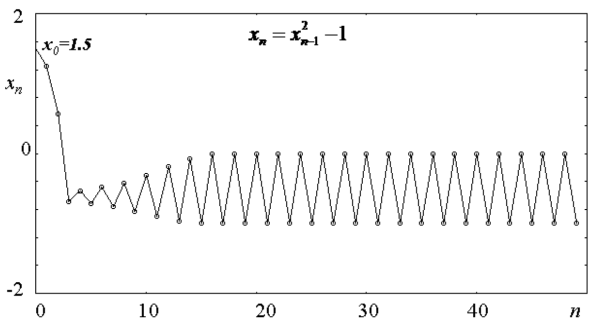

Fig.9 Attracting 2-cycle

From the shape of the second iterate of the function (Fig.10) we can see that locally the fixed point of the map F^2 ($2-$cycle of F) behaves as previously for the fixed point of the function F: the stable $2-$cycle becomes superstable. After that, the slope becomes negative, reaching the value -1, and so on. By self-similarity all the cycles of period 2^n will be generated and become unstable leading, as n tends to infinity, to a critical bifurcation value $b = b_2^{\infty}$ after which the map has a so-called chaotic behavior, because a set Λ invariant for the map, i.e. $F(\Lambda) = \Lambda$, on which the restriction is chaotic always exists.

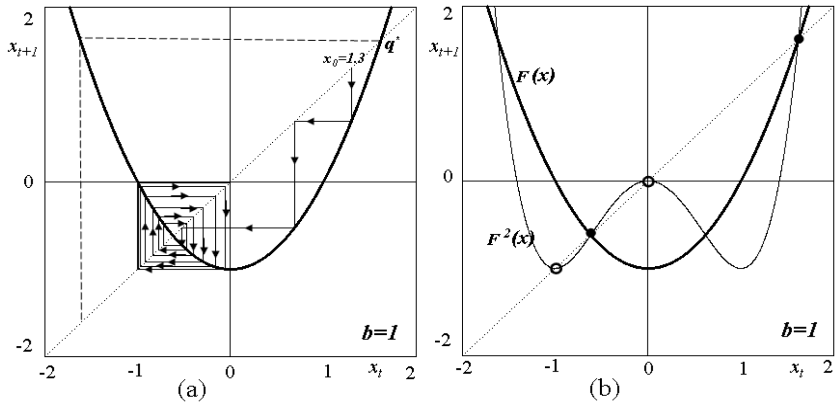

Fig.10 Superstable 2-cycle

This is often represented in a bifurcation diagram (Fig.11) which shows the asymptotic behavior of a generic point of the interval $I = [q_{-1}^*, q^*]$ as a function of the parameter b.

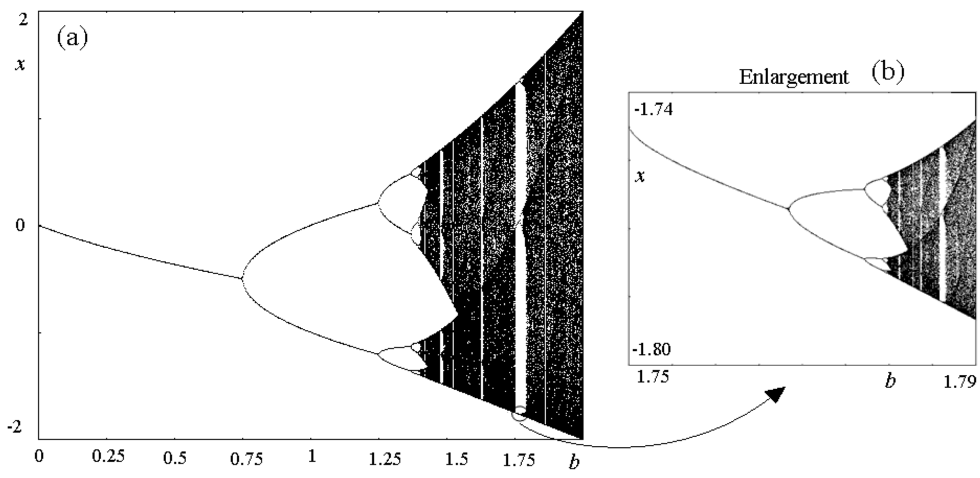

Fig.11 Bifurcation diagram

The bifurcation diagram is "self-similar" as for any period (and several boxes exist having the same period) we can repeat the period-doubling route to chaos described above. As an example the enlargement shows the "box" associated with the period-3 cycle: a pair of these cycles appear by saddle node-bifurcation (see Fig.12a), and the stable one, for the map F^3, will have the same bifurcation structure.

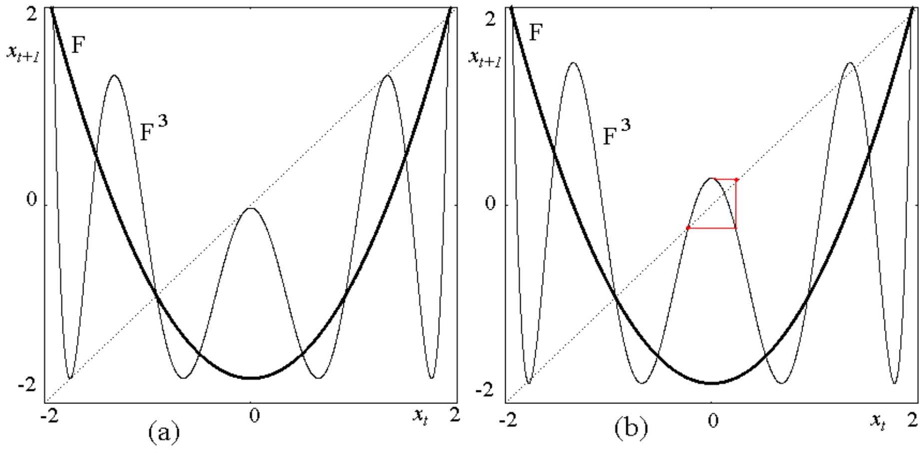

Fig.12 Box of the 3-cycle

We also note that although in a chaotic regime the dynamic behavior is unpredictable, some global properties can still be very useful. For example the iterates of the critical point determine cyclical intervals or one single interval inside which the trajectories are confined, and such intervals are trapping: starting in a different point of the interval $I = [q^*_{-1}, q^*]$ a trajectory enters such absorbing interval from which it will never escape (Fig.13).

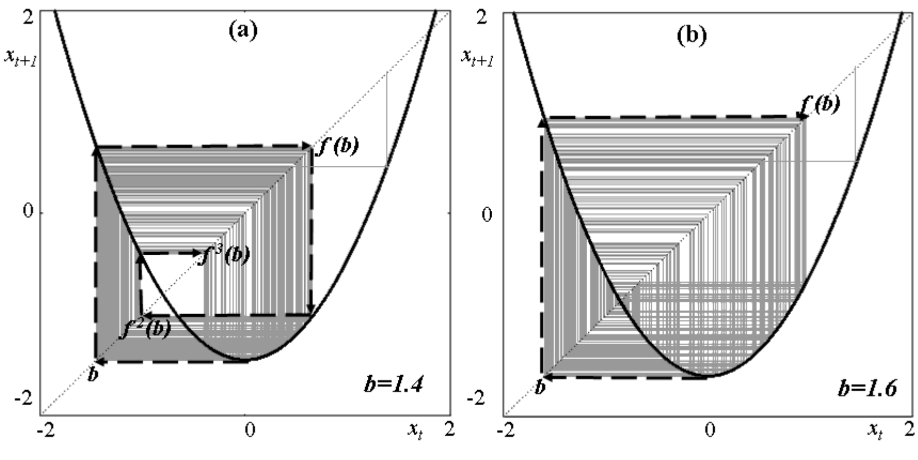

Fig.13 Absorbing intervals

A "final bifurcation" is known to occur at the bifurcation value $b = 2$, when the preimage of the unstable fixed point becomes equal to the critical value, that is: the invariant interval $I = [q^*_{-1}, q^*]$ becomes an invariant chaotic interval (Fig.14a), and after, for $b > 2$, the generic trajectory will be divergent. However a set which is invariant inside I exists also for $b > 2$. As we shall see, it is a Cantor set on which the restriction of the map F is chaotic. Notice that in two iterations all the points of the segment in the middle in Fig.14b are mapped above the unstable fixed point q^*, and then will diverge to $+\infty$. The two distinct preimages of this middle part will give two more intervals, one inside I_0 and one inside I_1, whose points are mapped, let us say "outside" q^*, in three iterations, and we continue this proces. Leaving from the old interval all the points whose trajectory will be divergent we are left with an invariant set Λ which is a Cantor set.

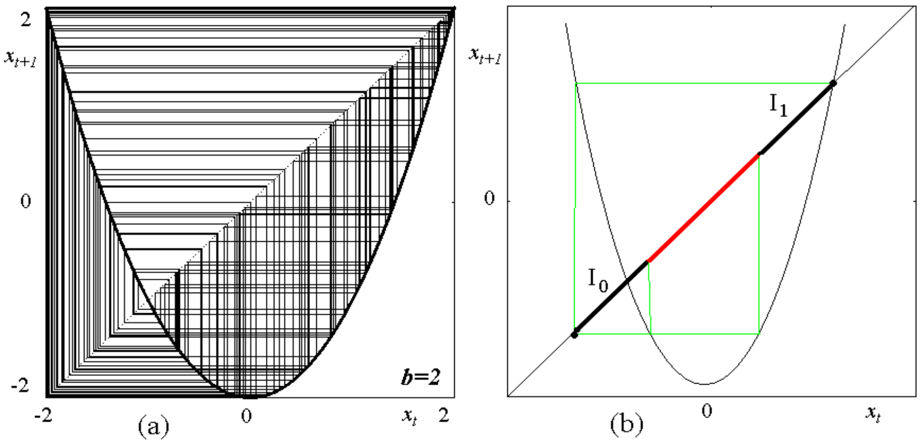

Fig.14 Full chaos in (a) and chaos in a Cantor set in (b).

A set Λ is a *Cantor set* if it is *closed, totally disconnected and perfect*[2]. The simplest example is the "Middle-third Cantor set": start with a closed interval I and remove the open "middle third" of the interval (see Fig.15). Next, from each of the two remaining closed intervals, say I_0 and I_1, remove again the open "middle thirds", and so on. After n iterations, we have 2^n closed intervals inside the two intervals I_0 and I_1.

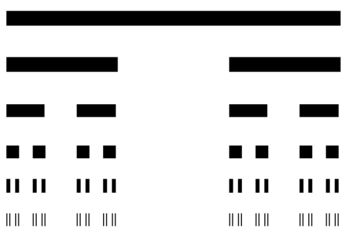

Fig.15 Middle-third Cantor set

It is quite clear the similarity of this construction with that of the invariant set for the Myrberg's map for any $b > 2$. Considering our unimodal

[2]Totally disconnected means that it contains no intervals (i.e. no subset $[a, b]$ with $a \neq b$) and perfect means that every point is a limit point of other points of the set.

map, for any point ξ belonging to the interval $I = [q^*_{-1}, q^*]$ there are two distinct inverse functions, say $F^{-1}(\xi) = F_0^{-1}(\xi) \cup F_1^{-1}(\xi)$, where

$$F_0^{-1}(\xi) = -\sqrt{b+\xi} \quad , \quad F_1^{-1}(\xi) = +\sqrt{b+\xi} \tag{7}$$

The set of points whose dynamics is bounded forever in the interval I can be obtained removing from the interval all the points which exit the interval after n iterations, for $n = 1, 2, ...$ Thus let us start with the two closed disjoint intervals

$$F^{-1}(I) = F_0^{-1}(I) \cup F_1^{-1}(I) = I_0 \cup I_1, \tag{8}$$

(see (Fig.14ab), i.e. we have removed the points leaving I after one iteration. Next we remove the points exiting after two iterations obtaining four closed disjoint intervals

$$F^{-2}(I) = I_{00} \cup I_{01} \cup I_{10} \cup I_{11},$$

defining in a natural way $F^{-1}(I_0) = F_0^{-1}(I_0) \cup F_1^{-1}(I_0) = I_{00} \cup I_{10}$ and $F^{-1}(I_1) = F_0^{-1}(I_1) \cup F_1^{-1}(I_1) = I_{01} \cup I_{11}$. Note that if a point x belongs to I_{01} (or to I_{11}) then $F(x)$ belongs to I_1 (i.e. one iteration means dropping the first symbol of the index). Continuing the elimination process we have that $F^{-n}(I)$ consists of 2^n disjoint closed intervals (satisfying $F^{\ -(n+1)}(I) \subset F^{-n}(I)$), and in the limit we get

$$\Lambda = \cap_{n=0}^{\infty} F^{-n}(I) = \lim_{n\to\infty} F^{-n}(I). \tag{9}$$

The set Λ is closed (as intersection of closed intervals), invariant by construction (as $F^{-1}(\Lambda) = F^{-1}(\cap_{n=0}^{\infty} F^{-n}(I)) = \cap_{n=0}^{\infty} F^{-n}(I) = \Lambda$). Let us consider $b > 2$ and such that $|F'(x)| > 1$ for any $x \in I_0 \cup I_1$ (the property holds for any $b > 2$, but the proof is more complicated, it can be found in [30]), then Λ cannot include any interval (because otherwise, since F is expanding, after finitely many application of F to an interval, we ought to cover the whole set $I_0 \cup I_1$). Thus Λ is totally disconnected, and perfect by construction, so that it is a Cantor set.

Moreover, by construction, to any element $x \in \Lambda$ we can associate a symbolic sequence, called Itinerary, or address, of x in the backward dynamics, $S_x = (s_0 s_1 s_2 s_3 ...)$ with $s_i \in \{0, 1\}$, i.e. S_x belongs to the set of all one-sided infinite sequences of two symbols Σ_2. S_x comes from the symbols we put as indices to the intervals in the construction process, and there exists a one-to-one correspondence between the points $x \in \Lambda$ and the elements $S_x \in \Sigma_2$. Also, from the construction process we have that if x belongs to the interval $I_{s_0 s_1 ... s_n}$ then $F(x)$ belongs to $I_{s_1 ... s_n}$. Thus the action of the function F on the points of Λ corresponds to the application of the "shift map σ" to the itinerary S_x in the code space Σ_2:

$$\begin{aligned} &if \quad x \in \Lambda \ has \ S_x = (s_0 s_1 s_2 s_3 ...) \\ &\qquad then \\ &F(x) \in \Lambda \ has \ S_{F(x)} = (s_1 s_2 s_3 ...) = \sigma(s_0 s_1 s_2 s_3 ...) = \sigma(S_x) \end{aligned} \tag{10}$$

Given a point $x \in \Lambda$ how do we construct its itinerary S_x? In the obvious way: we put $s_0 = 0$ if $x \in I_0$ or $s_0 = 1$ if $x \in I_1$, then we consider $F(x)$ and we put $s_1 = 0$ if $F(x) \in I_0$ or $s_1 = 1$ if $F(x) \in I_1$, and so on. It follows that F is chaotic in Λ, because it is topologically conjugated with the shift map, which is the prototype of the chaotic map. We recall that, following the definition of chaos given by Devaney [30], *an invariant set is chaotic under the action of a map F if*

1) there exist infinitely many periodic orbits, dense in the invariant set
2) there exist an aperiodic trajectory dense in the set

As a consequence of the above two conditions we have that the sensitivity with respect to the initial conditions also exists (which often is added as a third condition).

Indeed, it is easy to see that the two properties hold. If fact from the correspondence given above we have that each periodic sequence of symbols of period k represents a periodic orbit with k distinct points, and thus a so-called $k-$cycle. Since the elements of Σ_2 can be put in one-to-one correspondence with the real numbers[3], we have that the periodic sequences are dense in the space, thus (1): the periodic orbits are dense in Λ. Also there are infinitely many aperiodic sequences (i.e. trajectories) which are dense in Λ thus (2) also is satisfied, and we also have sensitivity with respect to the initial conditions.

4.1 Iterated Function System (IFS)

The construction process previously used, with the two contraction functions in (7) leading to the Cantor set in (9), can be repeated with any number of contraction functions defined in a complete metric space D of any dimension[4], as it is well known since the pioneering work by Barnsley (see [17], [18]). Let us recall the definition of an IFS:

Definition. *An Iterated Function System (IFS) $\{D; H_1, ...H_m\}$ is a collection of m mappings H_i of a compact metric space D into itself.*

[3]We can think for example of the representation of the numbers in binary form.

[4]or better (D, d) where d denotes the function distance

We can so define $W = H_1 \cup ... \cup H_m$. Denoting by s_i the contractivity factor of H_i then the contractivity factor of W is $s = max\{s_1, ...s_m\}$, and for any point or set $X \subseteq D$ we define

$$W(X) = H_1(X) \cup ... \cup H_m(X).$$

The main property of this definition is given in the following theorem:

Theorem (Barnsley 1988 [18] p. 82). Let $\{D; H_1, ...H_m\}$ *be an IFS. If the* H_i *are contraction functions then there exists a "unique attractor"* Λ *such that* $\Lambda = W(\Lambda)$ *and* $\Lambda = \lim_{n\to\infty} W^n(X)$ *for any non-empty set* $X \subseteq D$.

The existence and uniqueness of the set Λ is guaranteed by the theorem and it is also true that given any point or set $X \subseteq D$ by applying each time one of the m functions H_i the sequence tends to the same set Λ.

In the case previously described with the Myrberg's map we have $D = I$, $H_1 = F_0^{-1}$, $H_2 = F_1^{-1}$.

In general, if the sets $D_i = H_i(D)$ $i \in \{1, ..., m\}$ are disjoint, we can put the elements of Λ in one-to-one correspondence with the elements of the code space on m symbols Σ_m. The construction is the generalization of the process described above for the two inverses of the Myrberg's function. Let $U_0 = D$ and define

$$\begin{aligned}
U_1 &= W(U_0) = H_1(D) \cup ... \cup H_m(D) = D_1 \cup ... \cup D_m \subset U_0 \\
U_2 &= W(U_1) = W^2(U_0) = H_1(U_1) \cup ... \cup H_m(U_1) = D_{11} \cup ... \cup D_{mm} \subset U_1 \\
&\quad ... \\
U_n &= W(U_{n-1}) = W^n(U_0) \subset U_{n-1}
\end{aligned}$$

i.e. all the disjoint sets of U_1 are identified with one symbol belonging to $\{1, ..., m\}$, all the disjoint sets of U_2 are identified with two symbols belonging to $\{1, ..., m\}$ (m^2 in number) and so on, all the disjoint sets of U_n are identified with n symbols belonging to $\{1, ..., m\}$ (m^n in number). And in the limit, as $\Lambda = \lim_{n\to\infty} U_n = \lim_{n\to\infty} W^n(U_0) = \cap_{n=0}^{\infty} W^n(U_0)$, each element $x \in \Lambda$ is in one-to-one correspondence with the elements $S_x \in \Sigma_m$, where $S_x = (s_0 s_1 s_2 s_3 ...)$, $s_i \in \{1, ..., m\}$.

Moreover, for any element $x \in \Lambda$ we can define a transformation (or map) F on the elements of Λ by using the inverses of the functions H_i (the so called *shift transformation* or *shift dynamical system* in Barsnley 1988, p. 144):

$$if \quad x \in H_i(D) \quad then \quad F(x) = H_i^{-1}(D)$$

so that we can also associate an induced dynamic to the points belonging to Λ, and the rule described above holds for F, i.e. if $x \in$

Λ has itinerary $S_x = (s_0 s_1 s_2 s_3 ...)$ then $F(x) \in \Lambda$ has itinerary $S_{F(x)} = (s_1 s_2 s_3 ...) = \sigma(s_0 s_1 s_2 s_3 ...) = \sigma(S_x)$. *Clearly, when the functions H_i are distinct inverses of a unique function f then the induced dynamic system is the same, as $F = f$.*

4.2 The chaos game and Random IFS

As a second relevant example (besides the logistic map) let us consider another well known IFS with three functions, the so-called *chaos game*. Choose three different points A_i, $i = 1, 2, 3$, in the plane, not lying on a straight line. Let D be the closed set bounded by the triangle with vertices given by the three points A_i, and consider the system $\{D; H_1, H_2, H_3\}$ where the H_i are linear contractions in D with center A_i and contractivity factor 0.5. Then choose an arbitrary initial state x_0 in D. An orbit of the system is obtained by applying one of the three maps H_i, after throwing a dice. More precisely, $x_{n+1} = H_i(x_n)$ with $i = 1$ after throwing 1 or 2, $i = 2$ after throwing 3 or 4, $i = 3$ after throwing 5 or 6. For any initial state $x_0 \in D$, plotting the points of this orbit after a short transient gives Fig.16a. This fractal shape is called the Sierpinski triangle and it is the unique attractor of the chaos game. Almost all the orbits generated in the chaos game are dense in the Sierpinski triangle

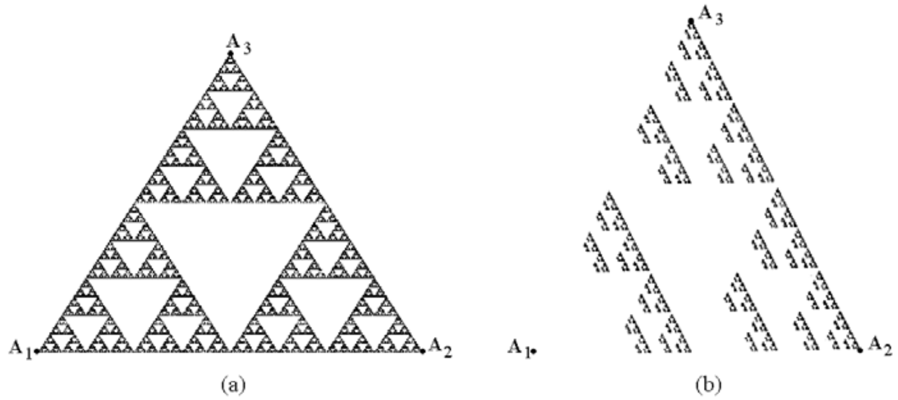

Fig.16 (a) Sierpinski triangle, unique attractor Λ of the ITF $\{D; H_1, H_2, H_3\}$. (b) A subset Λ^* of the Sierpinski triangle is the unique attractor of the RIFS $\{D; H_1, H_2, H_3\}$ with the restriction that H_1 is never applied twice consecutively.

Moreover, in Barnsley (1988, p. 335) it is also shown how, besides the standard IFS, we can consider a Random IFS (RIFS for short, or IFS with probabilities) by associating a probability $p_i > 0$ to each function H_i, such that $\Sigma_{i=1}^{m} p_i = 1$. Considering a point $x_0 \in D$ then we choose recursively

$$x_{n+1} \in \{H_1(x_n), ..., H_m(x_n)\}$$

and the probability of the event $x_{n+1} = H_i(x_n)$ is p_i. The iterated points always converge to the unique attractor Λ of the standard IFS, but the density of the points over the set Λ reflects in some way the chosen probabilities p_i. However, we note that if the probabilities in the RIFS are strictly positive, $p_i > 0$, then the unique attractor does not change, and the iterated points are dense in Λ.

This may be very useful and convenient when using IFS theory applied to backward dynamic models. Using an approach similar to the Random IFS, we can define a Restricted IFS (or IFS with restrictions) imposing that, depending on the position of a point $x \in D$ not all the maps H_i can be applied but only some of them. Stated differently, we can impose some restrictions on the order in which the functions can be applied. As an example let us consider the chaos game described above, but now with some restrictions, that is: The order in which the three different maps H_i are applied is not completely random, but subject to certain restrictions. Suppose for example that the map H_1 is never applied twice consecutively, i.e. whenever H_1 is applied then the next map to be applied is either H_2 or H_3. Let Σ_3 be the code space on three symbols, and let $\Sigma^* \subset \Sigma_3$ be the subset of all sequences which do not have two consecutive 1's. The chaos game $\{D; H_1, H_2, H_3\}$ with the restriction so described has a unique attractor Λ^* whose points are in one-to-one correspondence with the restricted space Σ^*. A typical orbit of this chaos game with restrictions, after a short transient, is shown in Fig.16b. The unique attractor of the chaos game with restrictions is a subset of the Sierpinski triangle, the attractor of the chaos game. In fact, the attractor contains precisely those points of the Sierpinski triangle whose itinerary, or addresses, do not have two consecutive 1's.

This example shows that when some restrictions upon the order in which the maps are applied is imposed, then a unique fractal attractor can arise, which is some subset of the unique attractor of the IFS.

In the following sections we shall see how IFS are related in a natural way to non-uniquely defined forward sequences within a backward model. We will also see that the forward states can be described by IFS, whenever the uniquely defined dynamics has homoclinic trajectories due to the existence of a snap-back repellor.

In the next section we shall show applications of the above theorem associated with the existence of homoclinic orbits.

5 Homoclinic theorem in 1D.

Note that the main property in the previous construction is the existence of two disjoint intervals, I_0 and I_1, such that

$$F^k(I_0) \supset I_0 \cup I_1 \quad \text{and} \quad F^k(I_1) \supset I_0 \cup I_1$$

for a suitable k, and indeed this propery is the key feature in any dimension, i.e. to prove the existence of chaos for maps in R^n whith $n \geq 1$. We shall recall this in general in Section 5, but let us here briefly recall its application to the one-dimensional case, where a similar property (leading to the construction of an invariant set on which the restriction of the map is chaotic) can be repeated whenever we have a homoclinic trajectory to some fixed point or cycle. A homoclinic trajectory to a cycle is one which tends to the cycle in the forward process, and in some backward one. For example, in a unimodal map it is easy to see when the unstable fixed point p^* becomes homoclinic (also called snap back repeller, after Marotto [79]). See also Fig.17 where in a neighborhood U of p^* we can find two intervals I_0 and I_1 such that $f^k(I_0) \supset I_0 \cup I_1$ and $f^k(I_1) \supset I_0 \cup I_1$ for a suitable k.

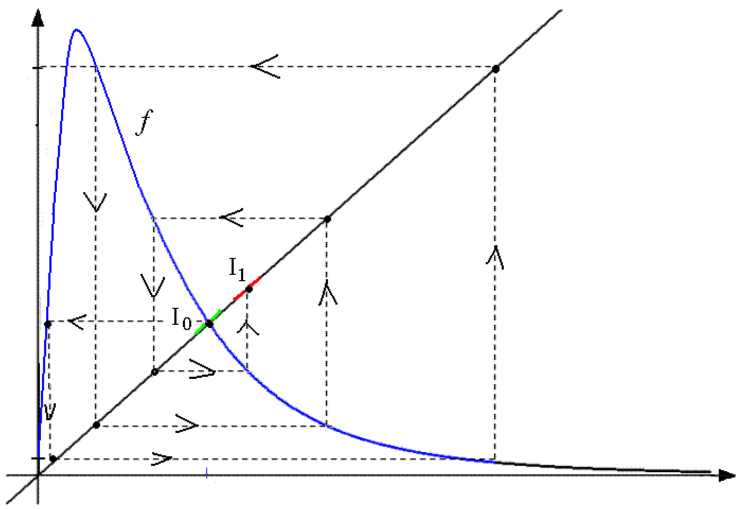

Fig.17 Homoclinic trajectory

In general we can state the following property for a unimodal map with a local maximum (and a similar property with obvious changes holds for a unimodal map with a local minimum):

Let x_m be the maximum point of a unimodal continuous map of an interval into itself, say $f : I \to I$, smooth in $I \backslash \{x_m\}$, with a unique unstable fixed point x^*, and a sequence of preimages of x_m tends to x^*. Then the first homoclinic orbits (all critical) of the fixed point x^* occur when the critical point satisfies $f^3(x_m) = x^*$. For $f^3(x_m) < x^*$ the *fixed point is a snap-back repellor. There exists a closed invariant set $\Lambda \subseteq [f^2(x_m), f(x_m)] \subseteq I$ on which the map is topologically conjugate to the shift automorphism, and thus f is chaotic, in the sense of Devaney (i.e. topological chaos, with positive topological entropy).*

The proof of the bifurcation condition is immediate, as for $f^3(x_m) > x^*$ the fixed point x^* has no rank-1 preimages in I, while at $f^3(x_m) = x^*$ the critical point is homoclinic and infinitely many homoclinic trajectories exist, all critical. When $f^3(x_m) < x^*$ then infinitely many noncritical homoclinic orbits exist (close to those critical at the bifurcation value, that is, the homoclinic points are obtained by the same sequences of preimages of the function). So that the fixed point x^* becomes a snap-back repellor.

Then the existence of chaotic dymanics associated with noncritical homoclinic orbits, let us call it "homoclinc theorem", is well known in a one-dimensional space (see for example [79], [30], [40]). In Section 5 we shall give a different proof of this "homoclinc theorem" for expanding cycles in any dimension $n \geq 1$, by using the ITS.

It is plain that the same result (that is, the existence of a closed invariant set Λ on which the map is chaotic) holds for any cycle (periodic point of any period), when it is a snap-back repellor (i.e. when homoclinic orbits exist), because the proposition above can be applied to fixed points of the map f^k, for any $k > 1$ (in suitable intervals for f^k, corresponding to cyclical intervals for f).

In Fig.11, showing the bifurcation diagram of the Myrberg's map, such invariant sets with chaotic dynamics occur for any $b > b_2^{\infty}$ (which represents the limit of the first period doubling sequence, after which the cycles of period 2^n become homoclinic in decreasing order of period).

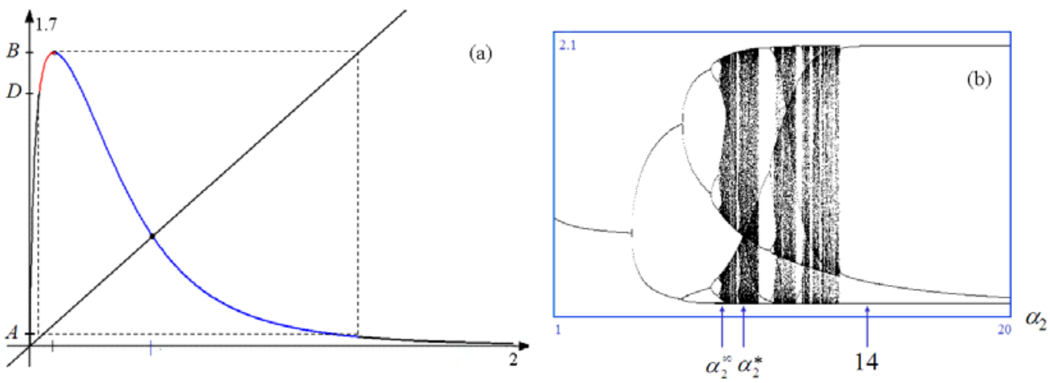

Fig.18

A remarkable application of this theorem in the economic context occurs in the study of models formulated in the so called "backward dynamics". That is, as discrete models in the form $x_t = F(x_{t+1})$, and the interest is in the behavior of the *forward values* of the state variable $(x_t, x_{t+1}, x_{t+2}...)$. Two well known examples are the overlapping generations (OLG)-model (e.g. Grandmont, 1985 [45], [46], [101], [47]) and the cash-in-advance model (e.g. Woodford, 1994 [117], Michener and Ravikumar, 1998 [84]). There are no problems when the function $F(.)$ is invertible (as $x_{t+1} = F^{-1}(x_t)$ is a standard dynamical system), while difficulties arise in the cases in which the function $F(.)$ has not a unique inverse, and difficulties may also arise in the interpretation of the models. Mathematically, this kind of models have been investigated considering the space of all possible sequences, which is a space of infinite dimension (the so-called Hilbert Cube), and is known as Inverse Limit Theory (for the interested reader we refer to [60], [61] and the references therein). As applications to economic models see [83], [65], [66]. However, the inverse limit approach is rather abstract (as it always considers infinitely many states all together at once, without a real selection of the states step by step), so we prefer to follow a different approach, which is based on the theory of Iterated Function Systems. As stated above, we show a kind of "bridge" between the theory of Dynamical Systems and the theory of IFS, which is useful to describe *fractal "attractors" in the forward states of backward models*. In [43] it is proposed this technique applied to a one-dimensional model due to Grandmond, where the shape of the one-dimensional unimodal map $f_\mu(.)$ is reported in Fig.18a (whose bifurcation diagram is shown in Fig.18b). Another example is in [83], where it is proposed an overlapping generation model represented by the backward model with the one-dimensional logistic map $x_t = f_\mu(x_{t+1}) = \mu x_{t+1}(1 - x_{t+1})$ already seen in Section 2, and topologically conjugated with the Myrberg's map.

Let us consider the one-dimentional unimodal map $f_\alpha(.)$ shown in Fig.18a and let α^* the bifurcation value at which the unstable fixed point becomes a snap-back repellor. Then for any $\alpha > \alpha^*$ there are noncritical homoclinic orbits of x^*. Let us consider an example, and let $O(x^*) = \{x^*, x_1, x_2, ...x_p, ...\}$ be the homoclinic orbit (an example is given in Fig.17) such that $x_1 = f_1^{-1}(x^*)$ (while $x^* = f_0^{-1}(x^*)$), and $x_i = f_0^{-1}(x_{i-1})$ for any $i > 1$.

Let U be a neighborhood of x^* in which $f_\mu(.)$ is expanding and such that $U_1 = f_0^{-4} \circ f_1^{-1}(U) \subset U$, $U_0 = f_0^{-5}(U)$ (clearly $U_0 \cap U_1 = \varnothing$). Then we have that $G = f_0^{-5}(.)$ and $F = f_0^{-4} \circ f_1^{-1}(.)$ are contractions in $S = U_0 \cup U_1$. Thus $\{S; F, G\}$ is *an Iterated Function System (*IFS*)* which has a unique attractor $\Lambda \subset S$: an invariant Cantor set on which f_α is chaotic.

To find some particular sequences in the forward process, for any initial condition $x_0 \in S$ let us consider the following rule: whenever we apply the left inverse f_1^{-1} then we apply the right inverse f_0^{-1} for at least 4 times consecutively, i.e. any number q of times with the only restriction $q \geq 4$. It is clear that the sequence of forward states of the backward model always belongs to the set $A = \bigcup_{i=0}^{4} S_i$ where $S_0 = S$, $S_1 = f_1^{-1}(S)$, $S_i = f_0^{-1}(S_{i-1})$ for $i = 2, 3, 4$, and the points have a kind of chaotic behavior in this set.

The "rules" which we may construct leading to bounded forward sequences (which seem chaotic) are infinitely many. Thus it depends on the applied meaning of the model to have meaningful rules or not. In the economic context such rules may be associated to "sunspot" dynamics ([25], [117], [13]).

6 Dynamics in higher dimensional spaces.

After the one-dimensional case let us consider $m-$dimensional dynamical systems $T : X \to X$, $X \subset R^m$, $m > 1$. The definition of the local stability of a fixed point x^* can be easily extended by using the linearization of the map, that is, the Jacobian matrix evaluated at the fixed point $J_T(x^*)$. When all the eigenvalues are less than 1 in absolute values then the fixed point is locally attracting, when one eigenvalue is higher than 1 in absolute values then the fixed point is unstable.

For real eigenvalues we have properties similar to those already described in the one-dimensional case. That is, when one eigenvalue λ crosses through $\lambda = -1$ then a flip bifurcation may occur, while when one eigenvalue λ crosses through $\lambda = +1$ then we may have a saddle-node or a transcritical or a pitchfork bifurcation. However now we have one more kind of bifurcation, related with a pair of complex conjugated eigenvalues which cross the modulus 1. This new kind of bifurcation is the discrete analogue of the Hopf bifurcation for flows (dynamical systems in continuous time), and it is called Neimark-Sacker (NS for short) bifurcation in the discrete case (associated with the names of the researchers who first and independently studied this kind of bifurcation). The existence of complex eigenvalues is also reflected in the dynamic behaviors of the trajectories, which are oscillating around the equilibrium, spiraling toward it when attracting or spiraling far from it when unstable. The NS bifurcation is associated with the existence of closed invariant curves around the fixed point or cycle (which, as usual, can be studied as a fixed point for the iterated map). Let us recall here the *Neimark-Sacker bifurcation theorem* for a two-dimensional map ([50], [70]):

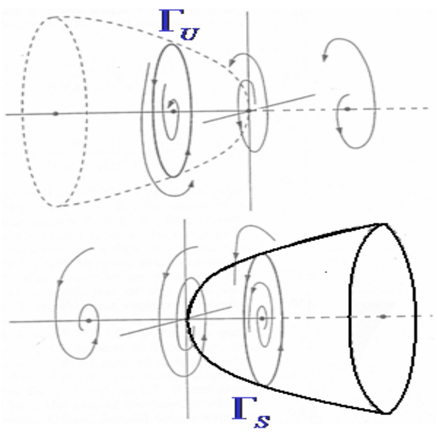

Fig.19

Let $F_\mu : \mathbb{R}^2 \to \mathbb{R}^2$ *be a one-parameter family of 2D maps which has a smooth family of fixed points* $x^*(\mu)$ *at which the eigenvalues are complex conjugates* $\lambda(\mu)$, $\overline{\lambda}(\mu)$. *Assume*

(1) $|\lambda(\mu_0)| = 1$, *but* $\lambda^j(\mu_0) \neq 1$ *for* $j = \overline{1,4}$;

(2) $\frac{d}{d\mu}(|\lambda(\mu_0)|) = d \neq 0$. *(transversality condition)*

Then there is a smooth change of coordinates h *so that the expression* $hF_\mu h^{-1}$ *in polar coordinates has the form* $hF_\mu h^{-1}(r, \theta) = (r(1 + d(\mu - \mu_0) + ar^2), \theta + c + br^2)+$ *higher-order terms. If, in addition,*

(3) $a \neq 0$,

then there is a 2D surface Σ *(not necessarily infinitely differentiable) in* $\mathbb{R}^2 \times \mathbb{R}$ *having quadratic tangency with the plane* $\mathbb{R}^2 \times \{\mu_0\}$ *which is invariant for* F_μ. *If* $\Sigma \cap (\mathbb{R}^2 \times \{\mu_0\})$ *is larger than a point, then it is a simple closed curve.*

The sign of the coefficients d and a determine the direction and stability of the bifurcating orbits, while c and b give information on the rotation numbers. The NS bifurcation is called supercritical (when $a < 0$) or subcritical (when $a > 0$) (Fig.19). We remark that numerically one can deduce the type of the bifurcation just from the stability of the fixed point at the bifurcation value: If the fixed point is locally attracting (resp., repelling), then the NS bifurcation is supercritical (resp., subcritical).

A qualitative example is shown in Fig.20, where we can see that after its appearance, via supercritical NS bifurcation, a closed invariant curve Γ may undergo several local and global bifurcations, leading to chaotic dynamics which often are related with an annular shape.

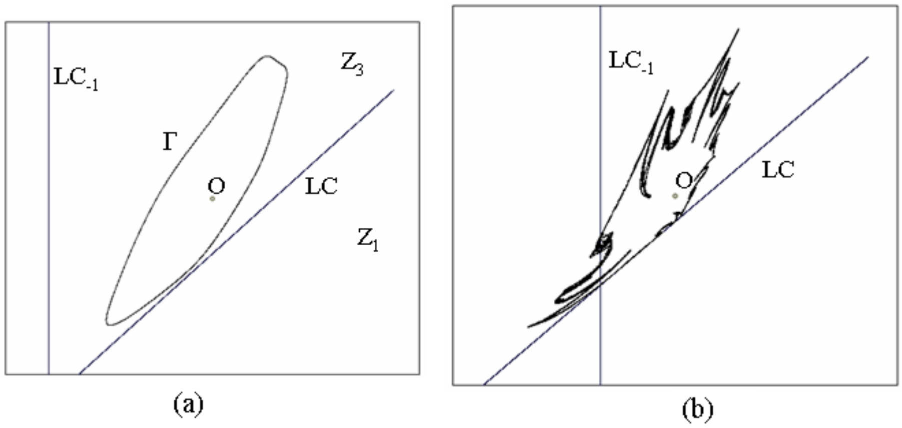

Fig.20

Let us notice that for 2D *linear maps* the condition $a \neq 0$ is obviously not satisfied, and not only at the fixed point, but in the whole region of definition of the map. And, indeed, considering a linear map, say, F_μ, with complex-conjugate eigenvalues $\lambda(\mu)$, $\overline{\lambda}(\mu)$, if $|\lambda(\mu_0)| = 1$ then the fixed point $x = x^*(\mu_0)$ of F_μ is a center, so that the trajectory of any point $x \neq x^*(\mu_0)$ belongs to a related invariant ellipse and is either periodic, or quasiperiodic, depending on the parameters. For $\mu \neq \mu_0$ the fixed point is either a globally attracting focus or a repelling focus (in which case the trajectory of any point $x \neq x^*(\mu)$ goes to infinity). Thus the bifurcation which occurs in a 2D linear map when its complex-conjugate eigenvalues cross the unit circle is called *center bifurcation.*

In the particular case of a 2D map

$$T \ : \begin{cases} x' = F_1(x,y) \\ y' = F_2(x,y) \end{cases}$$

then the stability analysis at a fixed point $X^* = (x^*, y^*)$ is quite simple. Let $J_T(X^*)$ be the jacobian matrix evaluated at the fixed point, of elements J_{ij}, then we have to consider the eigenvalues, roots of the characteristic polynomial

$$P(\lambda) = \det(J_T(X^*) - \lambda I) = \lambda^2 - Tr\lambda + Det = 0$$

where

$$Tr = J_{11} + J_{22} \quad , \quad Det = J_{11}J_{22} - J_{12}J_{21}$$

then the following conditions are necessary and sufficient to have all the eigenvalues less than 1 in modulus:

$$\begin{array}{ll} i) & P(1) = 1 - Tr + Det > 0 \\ ii) & P(-1) = 1 + Tr + Det > 0 \\ iii) & Det < 1 \end{array}$$

In the parameter plane (Tr, Det) the three conditions i), ii), iii) are three straight lines which bound a triangle (known as *stability triangle,* see Fig.21), and when the parameters are such that the representative point (Tr, Det) is inside the triangle then the fixed point is locally attracting. The bifurcation occurring when $P(1) = 0$ is associated with one eigenvalues equal to $+1$, the one occurring when $P(-1) = 0$ is associated with one eigenvalues equal to -1, while the NS bifurcation is associated with the condition $Det = 1$ (the curve inside the triangle separates real from complex eigenvalues).

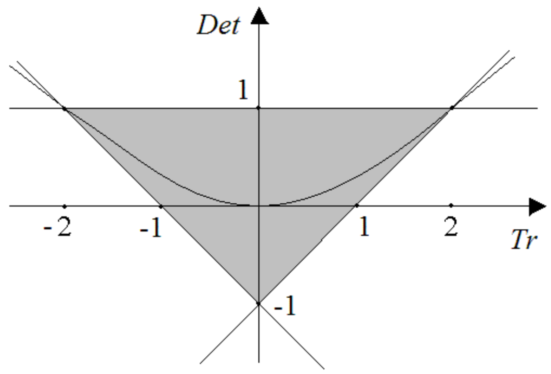

Fig.21 Stability triangle

6.1 Quadratic map.

In the case of maps in R^m, $m > 1$, chaotic dynamics may occur (associated with homoclinic orbits) also in invertible maps (as a standard example we may refer to the Henon map). While the true extension of the properties of the Myrberg map can be analyzed in a two-dimensional non-invertible map. As a prototype let us consider the map T defined by

$$T \; : \begin{cases} x' = ax + y \\ y' = b + x^2 \end{cases}$$

which was considered in [89] and [1]. The points which are the analogue of the critical points of a one-dimensional map are now associated with the vanishing of the Jacobian determinant. Here we have

$$J_T(x,y) = \begin{bmatrix} a & 1 \\ 2x & 0 \end{bmatrix} \quad , \quad \det J_T(x,y) = -2x$$

then the set defined by $\det J_T(x,y) = 0$, here $x = 0$, represents the so called critical line LC_{-1} (from the french *Ligne Critique*, see in [51],

[52]), and its image, $LC = T(LC_{-1})$ here the line of equation $y = b$, is a set which separates the phase plane into two regions: Z_0 and Z_2. Each point belonging to Z_0 has no rank-1 preimage, while each point belonging to Z_2 has two distinct rank-1 preimages, located one on the right and one on the left of LC_{-1}.

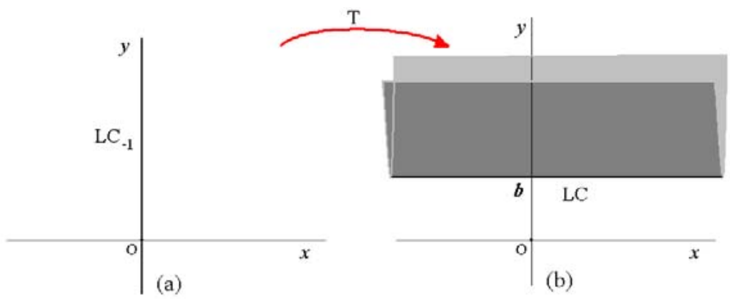

Fog.22 Foliation of the plane

In a generic two-dimensional map, and in analogy of the one-dimensional case, the set LC_{-1} is included in the set where $\det J_T(x, y)$ changes sign, since T is locally an orientation preserving map near points (x, y) such that $\det J_T(x, y) > 0$ and orientation reversing if $\det J_T(x, y) < 0$. Also in this case, when the map is continuously differentiable the points of LC_{-1} necessarily belong to the set where the Jacobian determinant vanishes, and $LC = T(LC_{-1})$ belongs to boundaries which separate regions Z_k characterized by a different number of preimages. In order to give a geometrical interpretation of the action of a multi-valued inverse relation T^{-1}, it is useful to consider a region Z_k as the superposition of k sheets, each associated with a different inverse. Such a representation is known as *Riemann foliation* of the plane (see e.g. Mira et al., [89]). Different sheets are connected by folds joining two sheets, and the projections of such folds on the phase plane are arcs of LC. This is shown in the qualitative sketch of Fig.22, where the case of a $Z_0 - Z_2$ noninvertible map is considered. This graphical representation of the unfolding action of the inverses gives an intuitive idea of the mechanism which causes the creation of non-connected basins for noninvertible maps of the plane.

We can easily extend the definition given above to the m-dimensional case. It is clear that the relation $CS = T(CS_{-1})$ holds, and the points of CS_{-1}, in which the map is continuously differentiable, are necessarily points where the Jacobian determinant vanishes. In fact, in any neighborhood of a point of CS_{-1} there are at least two distinct points which are mapped by T in the same point. Accordingly, the map is not locally invertible in points of CS_{-1}.

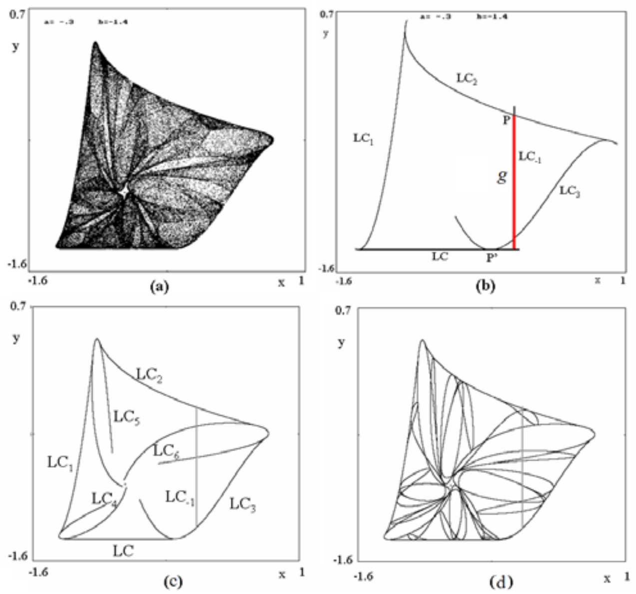

Fig.23

As it occurs in one-dimensional maps, where absorbing intervals are bounded by the images of the critical point, also now the images of the critical curve (also called critical curves of higher rank) are used to bound absorbing areas as well as chaotic areas. An example of chaotic area is shown in Fig.23, and in [89] it is proved that the boundary of the chaotic area is given by portions of critical curves belonging to the images of the segment (called generating arc g) of LC_{-1} belonging to the area itself.

The white area in Fig.24 shows the basin of attraction of the chaotic attractor, while gray points denote points having divergent trajectories. The basins also may have a fractal (or chaotic) structure, and a basin may be simply connected, or connected but not simply or disconnected (which cannot occur in invertible maps), as we shall see in Section 7.

The bifurcations leading to changes in the structure of the basins (connected, multiply connected or disconnected) are called *contact bifurcations* (see in [89]) because they are due to the contact of the frontier of the basin with the critical set LC. While bifurcations leading to changes in the structure of the chaotic areas (reunion of chaotic pieces, explosion to a wide area, final bifurcation, etc.) are also called *contact bifurcations* but due to the contact of two (at least) *different invariant sets*.

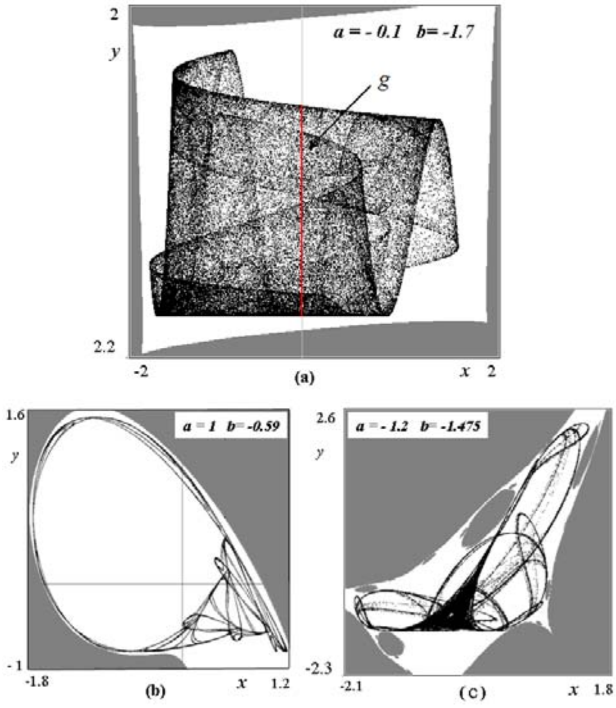

Fig.24

It is clear now that things may be extended also to dynamics of a map T in higher dimensions ($m \geq 3$), although the related properties are more complicated for the analysis.

As already recalled, the simplest analysis is that of the local stability of equilibria. In particular we mention that when all the eigenvalues are in modulus higher than 1 then the fixed point (clearly unstable) is called expanding. Among the relevant notions associated with fixed points and $k-$cycles (fixed points of the map T^k) we always have the notion of homoclinic trajectories, as these are the basic tools to rigorously show the existence of chaotic dynamics. For expanding fixed points the extension of the properties of the one-dimensional case is very simple, and related with the properties of $T^k(I_0) \supset I_0 \cup I_1$ and $T^k(I_1) \supset I_0 \cup I_1$ for a suitable k, as we shall see in the next Section.

However, homoclinic orbits may now also be related with saddle cycles. For example, in a two-dimensional case, a saddle fixed point S or cycle $\mathcal{C}$ is characterized by a stable manifold, or more generally by a stable set, denoted as $W^s(\mathcal{C})$ which is defined as the set of points whose forward trajectory tends to $\mathcal{C}$ (and in 2D it is made up of two branches $\{\omega_1 \cup \omega_2\}$), and by an unstable set, denoted as $W^u(\mathcal{C})$ which is defined as the set of points for which at least a sequense of preimages exist leading to $\mathcal{C}$ (and in 2D it is made up of two branches $\{\alpha_1 \cup \alpha_2\}$) Then whenever we have $W^s(\mathcal{C}) \cap W^u(\mathcal{C}) \neq \varnothing$ we have homoclinic points and chaotic sets exist associated with a homoclinic orbit. A point $q \in W^s(\mathcal{C}) \cap W^u(\mathcal{C})$ is called homoclinic to $\mathcal{C}$ as the sequence of its forward images tends to $\mathcal{C}$ and a suitable sequence of preimages also tends to $\mathcal{C}$. The chaotic dynamics associated to such a homoclinic orbit is well known since the works of Smale (Smale horseshoe) and the homoclinc tangle associated to it, shown in Fig.25, will be described in Section 6.

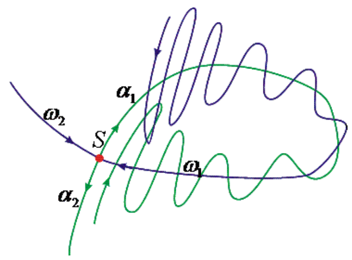

Fig.25 Homoclinic tangle in a saddle fixed point S.

Before closing this section we recall that in higher dimensions the existence of a closed invariant curve may occur not only via a NS bifurcation, as stated in Section 3, but also via global bifurcations connected with the homoclinic tangles of saddle cycles, as we shall see in Section 6.

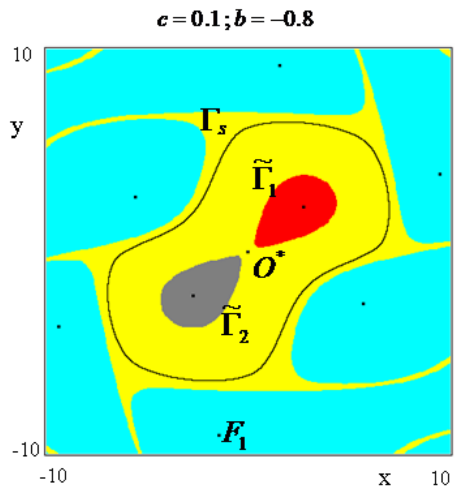

Fig.26

As an example, in Fig.26 we show several closed invariant curves, whose existence is not related with a NS bifurcation. In that example we have an attracting curve Γ_S and two repelling curves $\widetilde{\Gamma}_1$ and $\widetilde{\Gamma}_2$.This case, occurring in a simple invertible map, may be found in [6].

7 Homoclinic theorem for expanding periodic points.

Here we recall how chaotic behaviors exist in a dynamical system whenever we have transverse (which means non critical) homoclinic orbits of expanding cycles, also called *snap-back repellors* by Marotto. Without loss of generality we can deal with an *expanding fixed point* x^* of a $\mathcal{C}^{(1)}$ map T from a space X into itself, $X \subset R^m$ with $m \geqq 1$, as for a cycle of period k we can consider the map T^k ($k-th$ iterate of T).

We recall that a fixed point x^* is hyperbolic if all the eigenvalues of $J_T(x^*)$ are different from 1 in modulus, when all are higher then 1 in modulus, then x^* is expanding. Also, a homoclinic trajectory of a fixed point x^* is called non degenerate (or non critical, or transverse) if $\det J_T(.) \neq 0$ in all the points of the homoclinic trajectory.

Definition. *A fixed point x^* of a smooth dynamical system is called a snap-back repellor if it possesses a neighborhood U such that the Jacobian matrix has all the eigenvalues higher than* 1 *in modulus in all the points of U, and in U there exist a homoclinic point of x^*.*

It is well known (as recalled before) that in any neighborhood of a nondegenerate homoclinic trajectory we can find an invariant set Λ in which a suitable iterate of T, and thus T, is chaotic in the sense of Li and Yorke [71]. For the proof we refer to [30], [79], [80]. Here we give a different proof, showing its connection with the IFS ([40], [43], [115]).

The proof consists in showing that in any neighborhood U of x^* we can find two disjoint compact sets, U_0 and U_1, $U_0 \cap U_1 = \varnothing$, such that for a suitable k we have

$$T^k(U_0) \supset U_0 \cup U_1 \text{ and } T^k(U_1) \supset U_0 \cup U_1 \tag{11}$$

thus for the map T^k there exists an invariant chaotic set $\Lambda \subset U_0 \cup U_1$. In the following we illustrate:

(I) how the set property in (11) is used to construct an invariant Cantor set $\Lambda \subset U_0 \cup U_1$, on which T^k, and thus T, is chaotic;

(II) how the set property in (11) can be found associated with a given homoclinic trajectory;

(**III**) an economic application.

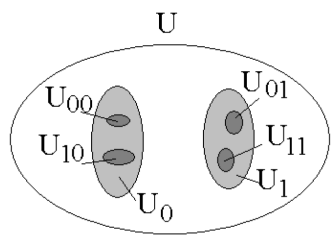

Fig.27 Qualitative picture showing the application of F and G on the sets U_0 and U_1.

(I) We repeat here the process already used in Section 2 in the 1D space. Let us consider $\widetilde{T} = T^k$. As, from (11), $\widetilde{T}(U_0) \supset U_0$ then a suitable inverse, say $F = \widetilde{T}_0^{-1}$, exists such that $F(\widetilde{T}(U_0)) = U_0$, and as $\widetilde{T}(U_1) \supset U_1$ (from (11) as well) then a suitable inverse, say $G = \widetilde{T}_1^{-1}$, exists such that $G(\widetilde{T}(U_1)) = U_1$.

Let $S = U_0 \cup U_1$ then $F(S)$ is made up of two disjoint pieces $U_{00} \subset U_0$ and $U_{10} \subset U_0$, and the action of the map $\widetilde{T}$ on such sets may be read on the symbols which label the set, dropping the first symbol: $\widetilde{T}(U_{00}) = U_0$ and $\widetilde{T}(U_{10}) = U_0$ (see the qualitative picture in Fig.27). Similarly $G(S)$ is made up of two disjoint pieces $U_{01} \subset U_1$ and $U_{11} \subset U_1$, and the action of the map $\widetilde{T}$ on such sets may be read on the symbols which label the set, dropping the first symbol: $\widetilde{T}(U_{01}) = U_1$ and $\widetilde{T}(U_{11}) = U_1$. And so on, by repeating this mechanism we construct, in the limit process, a set $\Lambda \subset S = U_0 \cup U_1$, $\Lambda = \cap_{n=0}^{\infty}(F \cup G)^n(S)$. The elements (or sets) V_s of Λ are in $1-1$ correspondence with the elements $s = (s_0 s_1 s_2 s_3 ...)$ ($s_i \in \{0, 1\}$) of the space $\sum_2$ of (one sided) infinite sequences on two symbols. Moreover the action of the map $\widetilde{T}$ in Λ corresponds to the action of the shift map σ to elements of Σ_2, that is: if x is a point of Λ and $x \in V_s$ then $\widetilde{T}(x) \in V_{\sigma(s)}$ (when $s = (s_0 s_1 s_2 s_3 ...)$ the shift map drops the first symbol $\sigma(s) = (s_1 s_2 s_3 ...)$).

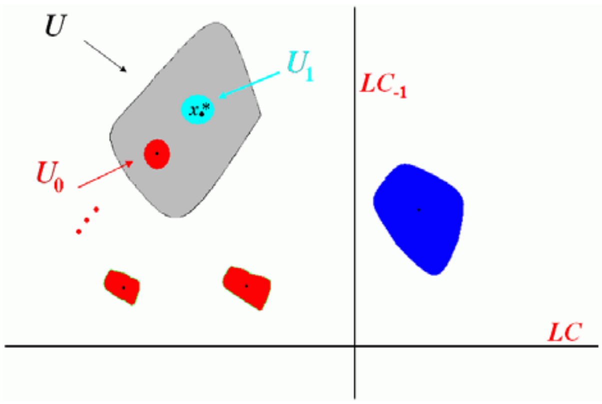

Fig.28 Homoclinic trajectory in the phase plane, and neighborhoods I_0 and I_1.

This set Λ constructed up to now, without any other information on the map $\widetilde{T}$, is *invariant* ($\widetilde{T}(\Lambda) = \Lambda$), and its elements satisfy $V_s \neq \varnothing$ for any s, and $V_s \cap V_{s'} = \varnothing$ for $s \neq s'$: It is what we call *a set with Cantor like structure*, and its elements V_s are closed and compact (and thus Λ is closed and compact) and simply connected if so are the starting sets U_0 and U_1.

When F and G are "contraction mappings" then Λ is a classical

Cantor set of points. In fact, if the inverses F and G of $\widetilde{T}$ are contractions in U (or in $S = U_0 \cup U_1$), the we can apply the IFS theory which states that $\{U; F, G\}$ is *an Iterated Function System (*IFS*)* (or $\{S; F, G\}$ is a IFS) which has a unique attractor $\Lambda \subset U$ (or S): an invariant Cantor set on which the map $\widetilde{T}$ is chaotic.

(II) Now we show that the conditions in (11) are satisfied, and the functions constructed in **(II)** are contractions, when we have a repelling fixed point (or cycle), unstable node or unstable focus, and a non degenerate homoclinic trajectory, which means that the preimages of the fixed point belonging to the considered homoclinic orbit are not on the critical curves (while degenerate homoclinic trajectories denote homoclinic explosions). So that we prove the following:

Theorem. If a fixed point x^* is expanding for a $\mathcal{C}^{(1)}$ map T in $X \subseteq R^m$ with a non degenerate homoclinic orbit, then in any neighborhood of the homoclinic orbit there exist an invariant set Λ on which T is chaotic.

Proof. Consider a compact neighborhood U of x^* in which T is expanding (i.e. all the eigenvalues of $J_T(x)$ are higher then 1 in modulus for all the points x in U). Let us first show that under the assumptions of the theorem we can always find two disjoint compact sets in U, U_0 and U_1, $U_0 \cap U_1 = \varnothing$, such that for a suitable k we have $T^k(U_0) \supset U_0 \cup U_1$ and $T^k(U_1) \supset U_0 \cup U_1$. Then we show that two suitable inverses are contractions, so that the result comes from the properties descibed in (I).

Let $O(x^*) = \{x^*, x_1, x_2, ...x_p, ...\}$ be the homoclinic orbit, and let T_1^{-1} be the local inverse, satisfying $T_1^{-1}(x^*) = x^*$ and T_0^{-1} the inverse such that $T_0^{-1}(x^*) = x_1$, while the point x_p is such that the repeated applications of T_1^{-1} to x_p converge to x^*. Notice that $T_0^{-1}(U) \cap U = \varnothing$. The nondegeneracy implies that $DetJ_T(x_i) \neq 0$ in all the points of the homoclinic orbit. The expansivity in a neighborhood implies that T_1^{-1} is a contraction in U or locally homeomorphic to a contraction, but we can choose a suitable integer p such that T_1^{-p} is a contraction in U. Define $G = T_1^{-p}$, and $U_1 = G(U)$. Then we apply to U the sequence of inverses which follow the homoclinic orbit until we have again points located inside U (see the qualitative picture in Fig.28). Define $F = T_1^{-s} \circ ...T_1^{-1} \circ T_0^{-1}$ where the integer s is such that $F(U) \subset U$ and F is a contraction in U. Define $U_0 = F(U)$. Obviously $x^* \in U_1$, U_1 and U_0 are disjoint (because $T_1^{-1}(U)$ and $T_0^{-1}(U)$ are disjoint by construction), and thus all the applications of the inverses by T_1^{-1} give disjoint sets, and by properly choosing the integers p and s (number of local inverses with T_1^{-1}) in the construction of G and F we can assume $k = p$ and such that $T^k(U_0) = U \supset U_0 \cup U_1$ and $T^k(U_1) = U \supset U_0 \cup U_1$, so that $\{U; F, G\}$ is *an Iterated Function System (IFS)* which has a unique attractor $\Lambda \subset U$:

an invariant cantor set on which T^k, and thus T, is chaotic, which ends the proof.

(**III**) An application of this theorem to a two dimensional model in backword dynamics is described in [43] from an overlapping generation model due to Grandmond [45], to which we refer for its deduction. Here let us briefly say that it refers to a map T of the plane into itself of so-called $Z_0 - Z_2$ type: there exists a critical line LC_{-1} in which $DetJ_T(X) = 0$ for any $X \in LC_{-1}$, mapped into a line $LC = T(LC_{-1})$ which separates the plane in to regions: Z_0 whose points have no rank-1 preimages and Z_2 whose points have two distinct rank-1 preimages, $T_R^{-1}(.)$ and $T_L^{-1}(.)$ giving one point on the right and one point on the left of LC_{-1}, respectively. Explicitely, we have that the backward dynamics is described by the two-dimensional backward map

$$(x_t, y_t) = T(x_{t+1}, y_{t+1}) = (f[a(1 - \delta + \frac{1}{a})x_{t+1} - ay_{t+1}], y_{t+1}).$$

where the function f is unimodal, and its shape is reported in Fig.17 and Fig.18. Thus we have the two inverses of T, associated with the two distinct inverses of f, given by

$$T_i^{-1} : \begin{cases} x_{t+1} = y_t \\ \quad y_{t+1} = (1 - \delta + \frac{1}{a})y_t - \frac{1}{a}f_i^{-1}(x_t) \end{cases}$$

where $i = L, R$. At suitable values we have the fixed point X^* of the function T, at the L side with respect to LC_{-1}, which is an unstable focus, with homoclinic points, i.e. it becomes a snap-back repellor. Then we may consider backword dynamics as follows. For a suitable neighbourhhood U we have that $U_0 = F(U) = T_L^{-7} \circ T_R^{-1}(U) \subset U$ is disjoint from $U_1 = G(U) = T_L^{-8}(U)$, and F and G are contractions in U (see Fig.28). Then $\{U; F, G\}$ constitutes an IFS.

Moreover, as discussed in Section 2, we can also consider the IFS with probabilities, or Random Iteration Function System (RIFS) $\{U; F, G; p_1, p_2\}$, $p_i > 0$, $p_1 + p_2 = 1$, which means that given a point $x \in U$ we consider the trajectory obtained by applying the function F with probability p_1 or the function G with probability p_2, that is, one of the functions is selected at random, with the given probabilities. The sequence of points is trapped in U, i.e. the forward trajectory cannot escape, and the qualitative shape of the asymptotic orbit has the set Λ as a “ghost” underlying it. Some points in Λ are visited more often than others, that is, typical forward trajectories may be described by an invariant measure with support on the fractal set Λ.

Thus "the generic forward trajectory" obtained in this way is a random sequence of points in the bounded region obtained by the starting interval U and its images with the functions which are involved in the definition of the contractions of the IFS. In our example, the set including all the forward states includes U, $T_R^{-1}(U)$, $T_{RL}^{-2}(U)$, ..., $T_{RL...L}^{-(8)}$, that is, the trajectory always belongs to the set

$$A = U \cup T_L^{-1}(U) \cup T_{RL}^{-2}(U) \cup ... \cup T_{RL...L}^{-(8)}.$$

Moreover, it is not always necessary to apply the function T_L^{-1} only once in a row. In fact IFS may be constructed in which two consecutive applications of T_L^{-1} can occur. Thus we can conclude that "the generic forward trajectory" (with the only constraint that we cannot apply the function T_R^{-1} when it leads outside of the curve LC) is a random sequence of points in the bounded regions.

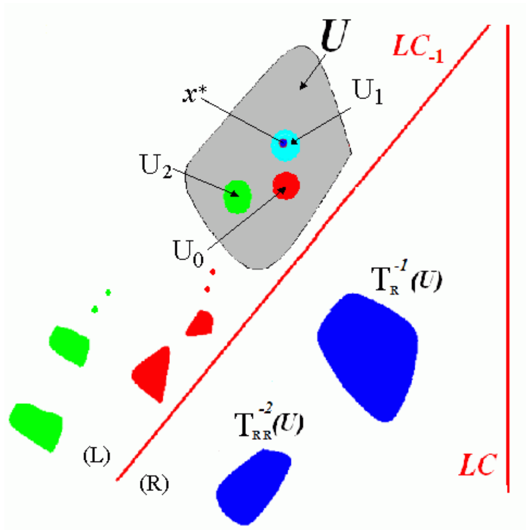

Fig.29 Qualitative description of the construction of the different sets belonging to U, involved in the IFS similar to the "chaos game" associated with the two-dimensional model.

As for the 1D case, we have infinitely many choices to construct such functions and related invariant chaotic sets Λ. Let us construct an example of IFS, using two (instead of one) iterations of the right inverse map to the set U. That is we consider the neighborhood U of X^* given above (i.e. such that the two eigenvalues of J_T are in modulus larger than 1 in all points of U). Then apply to U the right inverse map $T_R^{-1}(U)$ twice, after which the left inverse map T_L^{-1} is applied n times, where n is such that the final set is again located inside U. Such an integer exists because we are following a homoclinic trajectory (whose existence has been previously verified), thus applying the left inverse map repeatedly the sequence of sets will converge to the fixed point X^*. In our example we need $k = 11$ consecutive applications of T_L^{-1} to obtain a set U_2

such that $U_2 \subset U$. In this way we have built a suitable inverse function $\widetilde{F} = T_{RRL...L}^{-(2+k)}$, with $k = 11$ and we can assume that it is a contraction in the euclidean norm in U (if not, we adapt $\widetilde{F}$ by appling the left inverse map T_L^{-1} as many times as necessary). Then we have $U_1 = \widetilde{G}(U) = T_L^{-(13)}(U)$, $U_2 = F(U) = T_{RL...L}^{-(13)}(U)$ and $U_3 = \widetilde{F}(U) = T_{RRL...L}^{-(13)}(U)$., Define $H_1 = \widetilde{G} = T_L^{-(13)}$, $H_2 = F = T_{RL...L}^{-(13)}$ and $H_3 = \widetilde{F} = T_{RRL...L}^{-(13)}$, which are all contractions so that $\{U; H_1, H_2, H_3\}$ is an IFS (Fig.29).

As a third example, we will obtain an IFS similar to the chaos game describing forward trajectories. As shown for the 1-D case, we may consider the Random Iteration Function Systems, say RIFS $\{U; H_1, H_2, H_3; p_1, p_2, p_3\}$, $p_i > 0$, $p_1+p_2+p_3 = 1$, which means that given a point $x \in U$ we consider the trajectory obtained by applying the function H_i with probability p_i, that is, at each date one of the functions is selected at random, with the given probabilities. Then the random sequence of points is trapped in U, i.e. the forward trajectory cannot escape, and the asymptotic orbit is always dense in the chaotic set, although the distribution of points on the fractal set may be uneven, as some regions may be visited more often than others depending on the magnitude of the probabilities. An example of trajectory is shown in Fig.30.

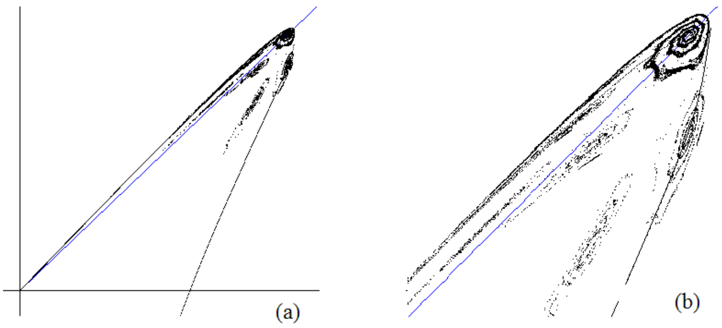

Fig.30 A trajectory of the RIFS in (a). An enlarged part in (b).

8 Global Bifurcations of Invariant Sets and Homoclinic Tangles

The aim of this Section is to illustrate some global bifurcations related to the appearance/disappearance of closed invariant curves, and to the interaction between coexisting cycles and other invariant curves. We shall see that such bifurcations are related to saddle connections, which may be associated with homoclinic tangles. These global bifurcations may arise both in invertible and non invertible maps. To achieve our goal, we shall start considering an introductory example and then we shall turn on some economic models, where the above cited bifurcations take place.

8.1 Stable and unstable sets. Homoclinic tangle.

Let us consider a generic smooth map $T : \mathbb{R}^2 \to \mathbb{R}^2$. As already defined in Section 1, we recall that a set $E \subset \mathbb{R}^n$ is *invariant* for the map T if it is mapped onto itself, $T(E) = E$. This means that if $x \in E$ then $T(x) \in E$, which also means that each point of E is the forward image of at least one point of E. As we have seen, the simplest examples of invariant sets are the fixed points and the cycles of the map. More generally, the attracting (repelling) sets and the attractors (repellors) of a map are invariant sets. An *attracting set* A is a closed invariant set for which a neighborhood U of A exists such that the trajectories starting in U converge to A. Here, a closed invariant set A which is not attracting is called *repelling* if however close to A there are points whose trajectories goes away from A. This definition is more suitable in this section due to the fact that we are explicitly interested in trajectories which are convergent to some invariant set which is not attracting (for example when we have a saddle cycle, then it is not an attractor, but neither an expanding repellor). Thus let us call as repelling any invariant set which is not attracting.

Given a point x, denote by $\tau(x)$ its trajectory (i.e. the sequence of states $T^n(x)$ for $n \geq 0$), then we are interested in the asymptotic behavior of the trajectory (i.e. what is the behavior of $T^n(x)$ for $n \to \infty$?) so we also introduce the $\omega-$*limit set* of a point x, $\omega(x)$, which is the limit set of the trajectory $\tau(x)$ (so a point $q \in \omega(x)$ if it is a limit point of $\tau(x)$ which means that there exists an increasing sequence of integers $n_1 < n_2 < ... < n_k ...$ such that the points $T^{n_k}(x)$ tend to q as $k \to \infty$). The set $\omega(x)$ is invariant and gives an idea of the long run behavior of the trajectory from x.

The same definition can be associated with the backward iterations of T, so obtaining the $\alpha-$*limit set* of x: A point $q \in \alpha(x)$ if there exists an increasing sequence $n_1 < n_2 < ... < n_k...$ such that the points $T_{j_k}^{-n_k}(x)$, for a suitable sequences of inverses j_k in case of a noninvertible map, tend to q as $k \to \infty$ (clearly such a point q belongs to the limit set of $\cup_{n\geq 0} T^{-n}(x)$).

In the particular case of a fixed point p^* of T we define the *stable and unstable sets of* p^* as

$$W^{st}(p^*) = \left\{ x : \lim_{n\to+\infty} T^n(x) = p^* \right\}$$

$$W^{un}(p^*) = \left\{ x : \lim_{n\to+\infty} T_{j_n}^{-n}(x) = p^* \right\}$$

respectively, where $T_{j_n}^{-n}$ means for a suitable sequence of inverses. This means that the stable set of p^* is the set of points x having p^* as ω-limit set and the unstable set of p^* is given by the points having p^* in their α-limit set.

If p^* is an asymptotically stable fixed point, then its stable set coincides with its basin of attraction, $B(p^*)$, and its unstable set is not empty if the map is noninvertible in p^*. If p^* is an expanding fixed point, then its unstable set is a whole area and its stable set is not empty if the map is noninvertible in p^*.

Other important sets in the study of the global properties of a map T are the stable and unstable sets of an hyperbolic[5] saddle fixed point p^*. Indeed, if the map T admits several disjoint attracting sets, the stable sets of some saddles (fixed points or cycles) often play the role of separatrices between basins of attraction.

If p^* is a hyperbolic saddle and T is smooth in a neighborhood U of p^* in which T has a local inverse denoted by T_1^{-1}, the *Stable Manifold Theorem* states the existence of the local stable and unstable sets (defined in such a neighborhood U of p^*) as

$$W_{loc}^{S}(p^*) = \{x \in U : x_n = T^n(x) \to p^* \text{ and } x_n \in U\}$$
$$W_{loc}^{U}(p^*) = \left\{x \in U : x_{-n} = T_1^{-n}(x) \to p^* \text{ and } x_{-n} \in U\right\}.$$

The set $W_{loc}^{S}(p^*)$ (resp. $W_{loc}^{U}(p^*)$) is a one-dimensional curve as smooth as T, passing through p^* and tangent at p^* to the eigenvectors associated with the stable (resp. unstable) eigenvalue. Then the *global stable set* is made up of all the preimages of any rank of the points of the local stable set:

$$W^S(p^*) = \bigcup_{n\geq 0} T^{-n}\left(W_{loc}^{S}(p^*)\right) \tag{12}$$

[5] A fixed point p^* is said hyperbolic if the jacobian matrix evaluated at p^* has no eigenvalues of unit modulus.

where T^{-n} denotes all the existing preimages of rank$-n$, and the global unstable set is made up of all the forward images of the points of the local unstable set:

$$W^U(p^*) = \underset{n\geq 0}{\cup} T\left(W^U_{loc}(p^*)\right). \tag{13}$$

If the map T is invertible, the stable and unstable sets of a saddle p^* are invariant manifolds of T. If the map is noninvertible, the stable set of p^* is backward invariant, but it may be strictly mapped into itself (since some of its points may have no preimages), and it may be not connected. The unstable set of p^* is an invariant set, but it may be not backward invariant and (contrarily to what occurs in invertible maps) self intersections are allowed.

It is worth to observe that analogous concepts are also given for continuous flows, but the main difference here is that the stable and unstable sets are not trajectories, but union of different trajectories (indeed infinitely many distinct trajectories).

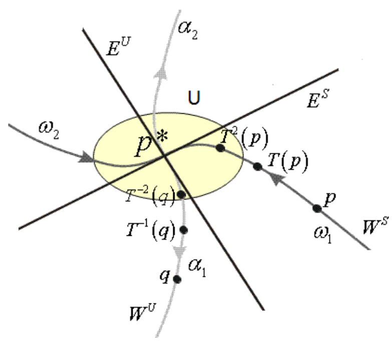

Fig.31 Stable set and unstable set of a saddle.

A qualitative representation of the local stable and unstable sets, W^S_{loc} and W^U_{loc}, of a saddle fixed point p^* is given in Fig.31, where E^S and E^U are the eigenvectors. In the following, we shall consider the stable (resp. unstable) set of a saddle as given by the union of two branches merging in p^* denoted by ω_1 and ω_2 (resp α_1 and α_2) because all the points in these branches have p^* as $\omega-$*limit set* (resp. in their $\alpha-$*limit set).*

$$W^S(p^*) = \omega_1 \cup \omega_2 \quad , \quad W^U(p^*) = \alpha_1 \cup \alpha_2$$

The concepts of stable and unstable sets can be easily extended to a cycle of period k, say $\mathcal{C} = \{p_1^*, p_2^*, ..., p_k^*\}$, simply considering the union of the stable (unstable) sets of the points of the cycle considered as k fixed points of the map T^k. For example

$$W^{st}(\mathcal{C}) = \bigcup_{i=1}^{k} W^{st}(p_i^*) \quad , \quad W^{st}(p_i^*) = \left\{x : \lim_{n\to+\infty} T^{kn}(x) = p_i^*\right\}$$

and analogously for the unstable set. In particular, for a $k-$cycle saddle we obtain the stable and unstable sets from (12) and (13) with the map T^k instead of T, that is

$$W^S(\mathcal{C}) = \bigcup_{i=1}^{k} W^S(p_i^*) = \bigcup_{i=1}^{k} (\omega_{1,i} \cup \omega_{2,i})$$
$$W^U(\mathcal{C}) = \bigcup_{i=1}^{k} W^U(p_i^*) = \bigcup_{i=1}^{k} (\alpha_{1,i} \cup \alpha_{2,i})$$

The importance of the stable and unstable sets is related to the fact that they are global concepts, that is, they are not defined only in a neighborhood of the fixed point (or cycle). Thus, being interested in the global properties of the map G, we may study its invariant sets, through a continuous dialogue between analytic, geometric and numerical methods, and focus our attention on the basins of attraction of its attractors and on the stable and unstable sets of some of its saddle points or cycles.

If the map is nonlinear, the stable and unstable sets may intersect, i.e. it may exist a point q such that

$$q \in W^S(p^*) \cap W^U(p^*).$$

Such a point q is a *homoclinic point* and it is easy to see that if a homoclinic point exists then infinitely many homoclinic points must also exist, accumulating in a neighborhood of p^*. Intuitively, this can be understood observing that the forward orbit of q and a suitable backward sequence is also made up of homoclinic points, and converge to p^*. The union of the forward orbit and a suitable backward orbit of a homoclinic point q is called a *homoclinic orbit of* p^*, or *orbit homoclinic to* p^*:

$$o(q) = \{..., q_{-n}, ..., q_{-2}, q_{-1}, q, q_1, q_2, ..., q_n, ...\}$$

where $q_n = T^n(q)$ and $T^n(q) \to p^*$ while $q_{-n} = T_{j_n}^{-n}(q)$ and $T_{j_n}^{-n}(q) \to p^*$ is a suitable backward orbit. More generally, an *orbit homoclinic to a cycle* approaches the cycle asymptotically both through forward and backward iterations, so that it always belong to the intersection of the stable and unstable sets of the cycle.

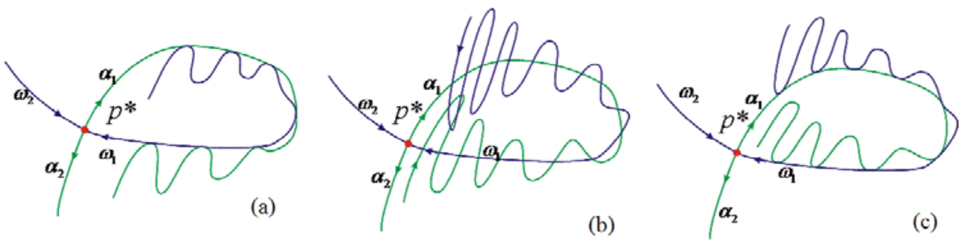

Fig.32 Homoclinic tangle

The appearance of homoclinic orbits of a saddle point p^* corresponds to a *homoclinic bifurcation* and implies a very complex configuration of W^S and W^U, called *homoclinic tangle*, due to their winding in the proximity of p^*. The existence of an homoclinic tangle is often related to a sequence of bifurcations occurring in a suitable parameter range, and qualitatively shown in Fig.32. First, a homoclinic tangency (Fig.32a) between one branch, say ω_1, of the stable set of the saddle p^* and one branch of the unstable one, say α_1, followed (Fig.32b) by a transversal crossing between ω_1 and α_1, that gives rise to a homoclinic tangle, and by a second homoclinic tangency (Fig.32c) of the same stable and unstable branches, occurring at opposite side with respect to the previous one, which closes the sequence. It is worth to recall that in the parameter range in which the manifolds intersect transversely, an invariant set exists such that the restriction of the map to this invariant set is *chaotic,* that is, the restriction is topologically conjugated with the shift map, as stated in the Smale-Birkhoff Theorem (see for example in [50], [87], [116], [54], [70]). Thus we say that the map possesses a *chaotic repellor* Λ, made up of infinitely many (countable) repelling cycles and uncountable aperiodic trajectories. In the case shown in Fig.32 such a chaotic repellor certainly exists after the first homoclinic tangency and disappears after the second one. Before and after the homoclinic tangle (i.e. before the first and after the last homoclinic tangencies), the dynamic behavior of the two branches involved in the bifurcation must differ: The invariant set towards which α_1 tends to (or equivalently the ω-limit set of the points of α_1) and the invariant set from which ω_1 comes from (or equivalently the α-limit set of the points of ω_1) before and after the two tangencies are different. Also at the bifurcation value, as in Fig.32a, are different from those of Fig.32c. Thus we can detect the occurrence of such a sequence of bifurcations looking at the asymptotic behavior of the sets W^S and W^U.

We observe that if the saddle is a cycle $\mathcal{C} = \{p_1^*, p_2^*, ..., p_k^*\}$, we may have homoclinic orbits of p_i^*, $i = 1, ..., k$, belonging to the stable and unstable sets of the periodic point p_i^* (considered as fixed points of the map T^k): In such a case we say that there exists points homoclinic to $\mathcal{C}$. But it may also occur that the unstable set $W^U(p_i^*)$ transversely intersects $W^S(p_{i+1}^*)$, $i = 1, ..., k$ and $p_{k+1}^* = p_1^*$: In such a case we have *heteroclinic points* and *heteroclinic tangle* denotes the corresponding configuration of W^S and W^U sets.

In the following, we shall see that, apart from the connection to chaotic dynamics, the homoclinic (heteroclinic) tangles play a fundamental role in the bifurcations involving invariant closed curves.

8.2 Invariant closed curves

Beside fixed points and cycles, invariant closed curves are possible attracting or repelling sets for a map of the plane. Such curves correspond to quasi-periodic or periodic (eventually, of very large period) trajectories and may emerge from a Neimark-Sacker (NS for short) bifurcation. Let us briefly recall the properties of such particular sets.

Assume that $E^* = (x^*, y^*)$ is a fixed point of a smooth map G, for which the Jacobian matrix DG in E^* has complex-conjugate eigenvalues (i.e., E^* is a focus). As long as the eigenvalues are in modulus less than one, the focus is stable and locally (in a small neighborhood of E^*) the trajectories belong to spirals and tend to the fixed point. When the eigenvalues exit the unit circle (belonging in modulus greater than one), the focus becomes unstable (repelling) and locally the trajectories still belong to spirals, however they have a different asymptotic behavior. The crossing of the complex eigenvalue trough the unitary circle corresponds to a *NS bifurcation*. The analytical conditions at which it occurs, and the so called "resonant cases", recalled in Section 4 now belong to standard dynamical results which can be found in many textbooks, see for example [62], [63], [50], [70], [116]. A NS bifurcation is related with closed invariant curves, existing in a neighborhood of the fixed point, and develops in two different ways, said subcritical and supercritical types (see Fig.19 in Section 4). If the NS bifurcation is of subcritical type, then the fixed point E^* becomes unstable, merging with a repelling closed curve Γ_U (existing when E^* is attracting). It is worth noting that in such a case the closed repelling curve is generally the boundary of the basin of attraction of the stable fixed point. After the bifurcation the asymptotic behaviour of a point close to the fixed point depends on the nonlinearity of the map (it may converge to another attracting set or diverge). Otherwise, if the NS is of supercritical type, then the fixed point E^* becomes unstable and an attracting closed curve Γ_S appears, surrounding it. Thus, after the bifurcation, the points close to E^* converge to such closed invariant curve.

In a neighborhood of the bifurcation value, the closed invariant curve Γ (stable or unstable) is homeomorphic to a circle, and the restriction of the map to Γ is conjugated with a rotation on the circle. Thus the dynamics on Γ are either periodic or quasiperiodic, depending on the rotation number. Roughly speaking, the rotation number represents the average number of turns of a trajectory around the fixed point. When the rotation number is rational, say q/p, it means that a pair of periodic orbits of period p exists on Γ, and to get the whole periodic orbit a trajectory makes q turns around the fixed point. The dynamics occurring in such a case on Γ are qualitatively shown in Fig.33a in case of a supercritical bifurcation (Γ_S is attracting): The closed curve is made up by the unstable set of the saddle cycle, and Γ_S is also called a saddle-(stable) node connection. Instead, Fig.33b shows the subcritical case (Γ_U is repelling): The closed curve is made up by the stable set of the saddle cycle, and Γ_U is also called a saddle-(unstable) node connection.

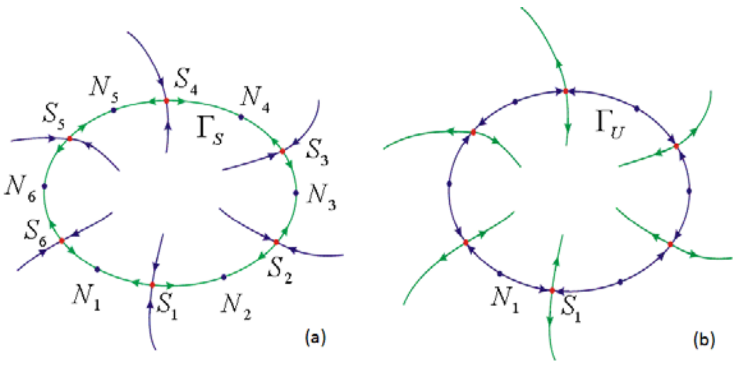

Fig.33 Saddle-node connections

When the rotation number is irrational, the trajectories of G on the closed curve Γ are all quasiperiodic. That is, each point on Γ gives rise to a trajectory on the invariant curve which never comes on the same point, and the closure of the trajectory is exactly Γ.

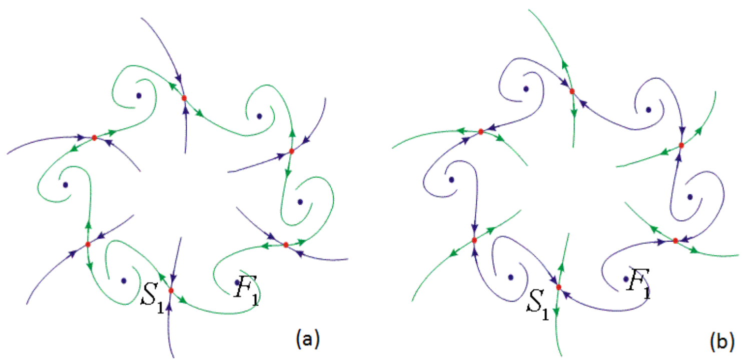

Fig.34 Saddle-focus connections

It is worth to observe here that the destruction of the invariant closed curve may occur in two different ways: Either because the invariant closed curve Γ becomes no longer homeomorphic to a circle, or because the restriction of the map on Γ becomes no longer conjugate with a rigid rotation or an invertible map of the circle. The first case naturally occurs when the cycle node (stable or unstable) on Γ becomes a focus: Fig.34 qualitatively represents this case, together with a saddle-focus connection, which may be stable (Fig.34a) or unstable (Fig.34b).

Investigating the bifurcation of a fixed point of G as a function of two parameters, we have described in Section 4 how to derive the so called *stability triangle* (see Fig.21) whose boundaries represent the stability loss due to different properties of the eigenvalues. That is, one side represents a flip-bifurcation (one eigenvalue equal to -1), another side a fold or pitchfork-bifurcation (one eigenvalue equal to $+1$), and a third side the NS bifurcation (complex eigenvalues in modulus equal to $+1$). In the supercritical case, such a portion of bifurcation curves is the starting point of so called "periodicity tongues", or *Arnol'd tongues,* associated with different rational rotation numbers q/p. A peculiar property of such tongues is associated with the summation rule ([87], [54], [57]): Between any two tongues with rotation numbers q_1/p_1 and q_2/p_2 there is also a tongue associated with the rotation number $q'/p' = (q_1 + q_2)/(p_1 + p_2)$.

Crossing transversely an Arnold tongue we observe the *frequency locking* phenomenon. At the crossing of one boundary of the tongue, two cycles (an attracting node and a saddle) appear via saddle-node bifurcation and the invariant closed curve is given by the saddle-node connection. As the opposite boundary is approached, the periodic points of the two cycles move on the curve, until a second saddle-node bifurcation takes place and cause the disappearance of the cycle.

It is clear that properties and bifurcations similar to those described above for a fixed point can occur also for a $k-$cycle of any period $k > 1$, simply considering the k periodic points as fixed points of the map G^k. In such a case the closed invariant curves Γ_k of the map G^k belong to a $k-$cyclical set for the map G.

Several examples of bifurcation diagrams and invariant closed curves Γ with periodic or with quasiperiodic trajectories, will be shown in the following examples, associated with different economic models. In particular we shall give a survey of possible mechanisms leading to the appearance/disappearance of a closed curve, when this phenomenon is not related to a NS bifurcation. This is the case, for example, associated with the appearance of the repelling closed curve involved in the subcritical NS bifurcation. And even when a pair of parameters are let to vary in a parameter plane outside the stability triangle, from the region close to a supercritical pitchfork (or flip) bifurcation curve towards the region where a supercritical NS bifurcation occurs, then global bifurcations associated with (attracting and repelling) closed invariant curves must necessarily occur. In continuous dynamical systems one of the mechanism associated with the appearance and disappearance of closed invariant curves involves a *saddle connection*: A branch of the stable set of a saddle point (or cycle) merges with a branch of the unstable one (of the same saddle or a different one), giving rise to an invariant closed curve.

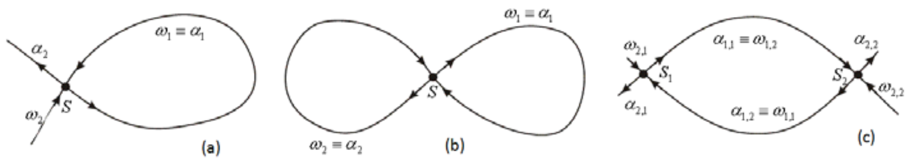

Fig.35 Saddle connections: (a) homoclinic loop (b) double homoclinic loop (c) heteroclinic loop

When the involved saddle is a fixed point, the saddle connection can be due to the merging of one branch of the stable set and one of the unstable set, as in Fig.35a: We shall call such a situation *homoclinic loop*. Otherwise, if both the branches of the stable and unstable sets are involved in the saddle connection we obtain an eight-shaped structure that we shall call *double homoclinic loop* (see Fig.35b).

Homoclinic loops and double homoclinic loops can also involve a saddle cycle of period k, being related to the map G^k, but in this case we can also obtain a *heteroclinic loop*: Indeed, the map G^k exhibits k saddles points and a branch of the stable set of a saddle may merge with a branch of another periodic point of the saddle cycle.

Stated in other words, if S_i, $i = 1, ..., k$, are the periodic points of the saddle cycle and $\alpha_{1,i} \cup \alpha_{2,i}$ ($\omega_{1,i} \cup \omega_{2,i}$) are the unstable (stable) sets of S_i, then a heteroclinic loop is given by the merging, for example, of the unstable branch $\alpha_{1,i}$ of S_i with the stable branch $\omega_{1,j}$ of a different periodic point S_j. Then each periodic point of the saddle cycle is connected with another one, and an invariant closed curve is so created that connects the periodic points of the saddle cycle. In Fig.35c an heteroclinic loop is shown, related to a pair of saddles (or a saddle cycle of period 2).

All these loops correspond to structurally unstable situations and cause a qualitative change in the dynamic behavior of the dynamical system. Since they cannot be predicted by a local investigation, i.e., a study of the linear approximation of the map, we classify them as global bifurcations. Indeed, we study this kind of bifurcation looking at the asymptotic behavior of the stable and unstable sets of the saddle: If a bifurcation associated with a loop has occurred, before and after the bifurcation the involved branch of the unstable set converges to different attracting sets, and the points of the involved stable branch have a different α-limit set, as well.

Although homoclinic and heteroclinic loops may also occur in discrete dynamical systems, in this case they are frequently replaced by homoclinic tangles, as described in Section 8.1. That is, a tangency between the unstable branch $W_1^U(S) = \cup\alpha_{1,i}$ with the stable one $W_1^S(S) = \cup\omega_{1,i}$ occurs, followed by transverse crossings of the two manifolds, followed by another tangency of the same manifolds, but on opposite sides.

8.3 Appearance of an invariant closed curve. A simple example

Let us start to investigate the mechanisms leading to the appearance of closed invariant curves. As a first step we analyze the global bifurcation associated with the appearance of the repelling closed curve involved in a subcritical NS bifurcation. To do that we consider the simple example studied in [9], where interested readers may found major details. This map allows us to investigate interesting situations that may be found also in many economic applications related to business cycle models (e.g. [67],[72],[8],[73],[10]), duopoly models (e.g. [93], [3],[4],[5]) and models describing financial market wit heterogeneous agents (e.g. [44],[36]).

Let us consider the family of two-dimensional maps depending on 5 real parameters: a, b, c, d and k given by:

$$T:\begin{cases} x' = ax + bky + cky^2 + dky^3 \\ y' = -bx + ay + cx^2 + dx^3 \end{cases} \tag{14}$$

The map in (14) has the origin $E^* = (0,0)$ as a fixed point. Analyzing the local stability of the fixed point E^*, through the triangle of stability, we obtain that it is locally stable if

$$\begin{cases} -1 < a < 1 \\ b = 0 \end{cases} \cup \begin{cases} -1 < a \le 0 \\ -\frac{(a+1)^2}{b^2} < k < \frac{1-a^2}{b^2} \end{cases} \cup \begin{cases} 0 < a < 1 \\ -\frac{(a-1)^2}{b^2} < k < \frac{1-a^2}{b^2} \end{cases}$$

Furthermore, if $k = -(a-1)^2/b^2$ (and $0 < a < 1$) one of the eigenvalues is -1 and a flip bifurcation occurs, whereas if $k = -(a+1)^2/b^2$ (and $-1 < a < 0$) a fold bifurcation occurs, being one eigenvalue equal to 1. The particular case $a = 0$ and $k = -1/b^2$ corresponds to a bifurcation of codimension 2, being the eigenvalues equal to 1 and -1. The study of the occurrence of these bifurcations is beyond the aim of this section.

In order to study the bifurcation occurring when $0 < k = (1-a^2)/b^2$ we follow [50], Theorem 3.5.2 (or [70], Theorem 4.6). At this purpose, let us set $\Omega = \{(a,k) : -1 < a < 1 \wedge k > 0\}$.

Proposition 1 *If $b \neq 0$, $(a,k) \in \Omega$ with $a \notin \{0, -0.5\}$ and*

$$3db\left(a^2+b^2-1\right) - c^2\left(a^2-b^2-1\right)(a+1)(2a-3) \neq 0 \tag{15}$$

then at

$$k = k_N = \frac{1-a^2}{b^2}$$

the fixed point E^* undergoes a Neimark-Sacker bifurcation.

Proof. See [9] ∎

The NS bifurcation is of *supercritical* type if $A = 3db\left(a^2 + b^2 - 1\right) - c^2\left(a^2 - b^2 - 1\right)(a+1)(2a-3) < 0$ and subcritical in the opposite case $A > 0$. Here we consider this latter case.

From Proposition 1, we also deduce that the parameter value $(-0.5, 3/4b^2) \in \Omega$ corresponds to a 1 : 3 resonant case and $(0, 1/b^2) \in \Omega$ to a 1 : 4 resonant case. This means that at these parameter values the closed invariant curve might appear in a very peculiar way, or there might be several invariant curves bifurcating from the fixed point.

In the following, we shall fix the values of b, c, d and consider the maps in (1) as depending only on the parameters a and k belonging to the parameter space $\Omega = \{(a,k) : -1 < a < 1 \wedge k > 0\}$. This restriction of the map family allows us to focus on the scenarios associated with the occurrence of the subcritical Neimark-Sacker bifurcation. As an example, in our simulations, we set $b = -0.4$, $c = -6$ and $d = 150$ and, from Proposition 1, we obtain that the Neimark-Sacker bifurcation is of subcritical type if a ranges in the interval $[-0.897\,23, 0.661\,03]$.

If we look at the phase-space just after the occurrence of the subcritical NS bifurcation, we observe that the bounded trajectories converge to an invariant closed curve Γ_S, surrounding the repelling focus E^* (see Fig.36a), as it occurs when the NS is of supercritical type. But a more accurate inspection permits to note that the attracting closed curve Γ_S is quite far from the fixed point. This observation exclude the occurrence of a NS bifurcation of supercritical type and suggests that two invariant closed curves, one attracting and one repelling have to appear when E^* is stable. The repelling one decreases in size, merging with E^* at the bifurcation value, leaving Γ_S as the unique attractor. The two invariant closed curves are represented in Fig.36b.

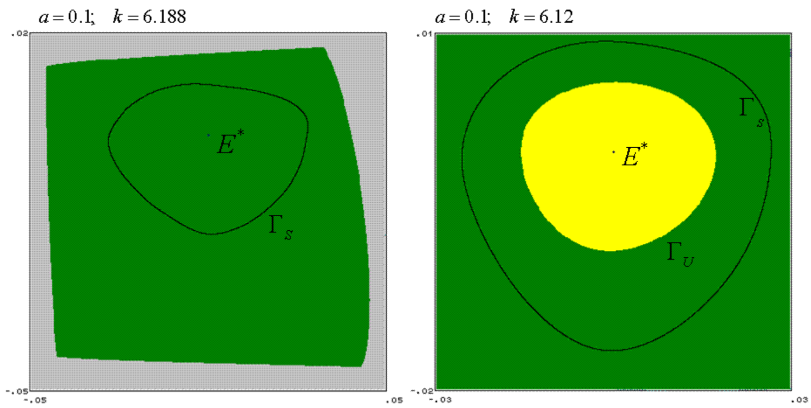

Fig.36

The scenario represented in Fig.36b may have some important implications when occurring in some economic model. Indeed we have that the system converges to its dynamic equilibrium for small perturbations, but shows no such tendency for larger shocks. Indeed, due to the existence of a repelling curve which bounds the basin of attraction of the stable fixed point, small shocks of the system have no effects on its dynamical behaviour, but large enough shocks may lead to an aperiodic (or periodic with large period) fluctuations or to an unfeasible trajectory (*corridor stability*). We can also describe a *hysteresis effect* related to such a scenario. Consider the system close to its equilibrium, before the NS bifurcation occurring at the value k_N. As k crosses the critical value k_N, the trajectories of the system converge to a large closed invariant curve. The loss of stability in such a bifurcation thus recall a *catastrophe*. Moreover, if the parameter k is decreased again, the system does not return to its previous equilibrium but rests in steady oscillation. This effect is illustrated in Fig.37a, where a bifurcation diagram is obtained with increasing and decreasing values of the parameter k and considering at each step as initial condition the state reached at the previous iteration, and in Fig.37b, where a trajectory of the system is represented versus and obtained assuming that a exogenous shock on the k parameter occurs when the fixed point is still stable, causing the destabilization of E^*. A restoration of the original value of k does not imply the trajectory again convergent to the fixed point, since the state of the system now belong to the basin of attraction of the attracting closed curve coexisting with the stable focus E^*. A qualitative sketch of the this hysteresis effect is ginven in Fig.37c

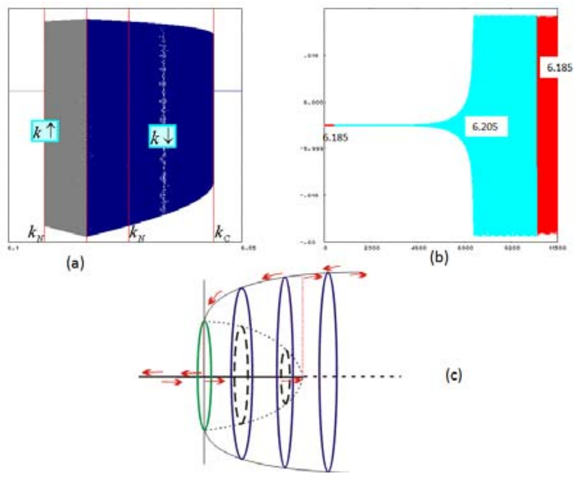

Fig.37 (a) Bifurcation diagramm. (b) Trajectory. (c) Qualitative picture

Our aim here is to study the bifurcation leading to the appearance of the two invariant curve, and by numerical investigation, we can observe that when they appear they are very close to each other, as in Fig.38 obtained just after the bifurcation.

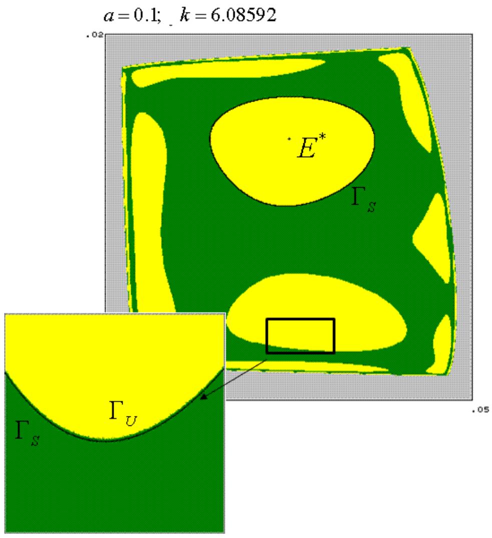

Fig.38

The particular configuration of Fig.38 recalls the bifurcation scenario of a saddle-node bifurcation, where at the bifurcation value a half-stable invariant set appear, attracting points located on one side and repelling those located on the other side. After the bifurcation, we observe the splitting of such a set into a saddle and a node. And indeed, in many books such a bifurcation is called saddle-node bifurcation of closed invariant curves, in analogy to what occurs in flows.

In order to understand the mechanism that leads to such a configuration of the state-phase we look at the case of periodic orbits, whose existence is suggested by the bifurcation diagram of Fig.37a, since in such cases, as we known, the existence of an invariant closed curve is due to a heteroclinic connection (either a saddle-node connection or a saddle-focus connection) and the bifurcation mechanisms associated with the appearance of heteroclinic connections are simpler to investigate, since they can be detected following the asymptotic behaviour of the stable and unstable sets of the saddle cycle. The periodicity regions related to the maps in (1) are shown in Fig.39, where a two parameters bifurcation diagram is represented in the parameter plane (a, k). In such a figure we observe two quite large regions: the stability region of E^* (the yellow points) and the divergence region (the gray points). Only a small portion of the bifurcation curve (pointed out by an arrow in Fig.39) plays the role of boundary separating these two regions: this means that at the corresponding parameter constellations after the occurrence of the subcritical NS bifurcation the generic trajectory is divergent. But in the other portion of the bifurcation curve we see periodicy regions issuing from the NS curve, before reaching the divergence region, denoting that at least an attractor at finite distance exists after the NS bifurcation. In particular, the small regions in different colors correspond to the periodicity regions, each one related to an attracting cycle. The enlargement of two of them (corresponding to attracting cycles of period 4 and 5) is proposed in order to appreciate the fact that they originate below the NS bifurcation curve.

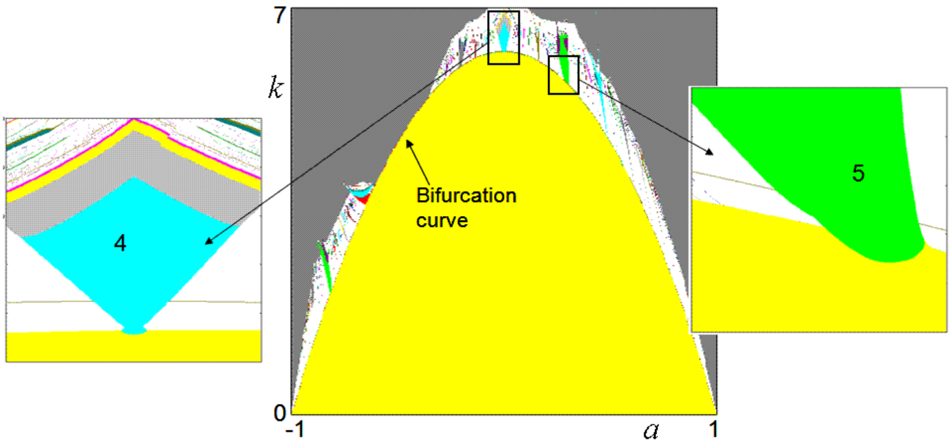

Fig.39 Two parameters bifurcation diagram.

This means that in such a case immediately before the destabilization of the fixed point two or more attractors coexist. In the generic case, the attracting cycle appears through a saddle-node bifurcation, which gives also rise to a saddle cycle of the same period, and coexists with the stable fixed point E^*. The stable set of the saddle cycle separates the basins of attraction of the two attractors and the two branches of the unstable set reach the fixed point and the attracting node cycle, respectively. Then, at the appearance of the cycles no closed invariant curves exist, while we know that a repelling closed curve must emerge before the Neimark-Sacker bifurcation and must shrink, coalescing with the fixed point at the bifurcation value. How such a curve appears is the question we aim to deal.

8.3.1 Saddle-node bifurcation for closed curves

We start our analysis considering the periodicity region in which a cycle of period 4 exists and the particural case of the subfamily of T obtained by setting $a = 0$ in (14), that is, the family

$$T_0 = \begin{cases} x' = bky + cky^2 + dky^3 = f(y) \\ y' = -bx + cx^2 + dx^3 = g(x) \end{cases} \tag{16}$$

As we have seen in Proposition 1, this is a very particular case since the fixed point E^* undergoes a local bifurcation corresponding to a $1:4$ resonant case, being E^* a node which bifurcates with pure immaginary eigenvalues (equal to $\pm i$).

The study of the asymptotic behaviour of the maps in (16) can be developed in a simple way once we observe that the maps belonging to the family T_0 are such that T_0^2 (the second iterate of T_0) results in a de-coupled map:

$$T_0^2\left(x,y\right) = T_0\left(f\left(y\right),g\left(x\right)\right) = \left(f\left(g\left(x\right)\right),g\left(f\left(y\right)\right)\right) = \left(F\left(x\right),G\left(y\right)\right) \tag{17}$$

Maps having this property, that we shall call "*square separate*", have been studied in-depth in [20].

The main feature is that the dynamic behaviour of the map T_0 can be deduced from the one-dimensional map $F\left(x\right)$ (or $G\left(y\right)$) in (17), obtained by the composition of the two components of T_0. Indeed there exists a correspondence between the cycles of map $F\left(x\right)$ and those of T_0. In particular, if x^* is a fixed point of F, then $\left(x^*,g\left(x^*\right)\right)$ is a fixed point of T_0 with eigenvalues[6] $\lambda_1 = \sqrt{F'\left(x^*\right)}$ and $\lambda_2 = -\sqrt{F'\left(x^*\right)}$. If x_1^* and x_2^* are fixed points of $F\left(x\right)$ then $\left\{\left(x_1^*,g\left(x_2^*\right)\right),\left(x_2^*,g\left(x_1^*\right)\right)\right\}$ is a cycle of period 2 of T_0, with eigenvalue $\lambda_1 = F'\left(x_1^*\right)$ and $\lambda_2 = F'\left(x_2^*\right)$. We deduce that the map T_0 has no saddle fixed points, but saddle cycles may emerge, for instance when F has two fixed points, one attracting and one repelling.

The local bifurcations of the one-dimensional map F correspond to local bifurcations of T_0; indeed, whenever a bifurcation occurs causing the appearance (disappearance) of cycles of the map F, many cycles of the map T_0 simultaneously appear (disappear) at the same parameter values. Such bifurcations of the two-dimensional map are often of particular type, due to the presence of two eigenvalues that simultaneously cross the unit circle. In particular, a fold bifurcation of a fixed point of F causes the appearance of two fixed points of T_0, one stable and one unstable, as well as a saddle cycle of period 2.

Moreover, we have that a vertical (horizontal) segment is mapped into a horizontal (vertical) segment by a square separate map and the same holds for the preimages. Consequently, as the saddle cycles always have eigenvectors parallel to the coordinate axes (see [20]), their unstable and stable sets consist of the union of vertical and horizontal segments and the basins of attraction of the different attracting sets are rectangles, if connected, or have many components with rectangular shape.

Let us return to the maps we are interested in and consider the one-dimensional map

$$F\left(x\right) = bk\left(-bx+cx^2+dx^3\right)+ck\left(-bx+cx^2+dx^3\right)^2+dk\left(-bx+cx^2+dx^3\right)^3 \tag{18}$$

[6] In the following, the symbol $F'\left(x\right)$ denotes the first derivative of $F\left(x\right)$.

obtained by the composition of the two components of the map T_0 in (16). The map F in (18) admits $\mathbf{e}^* = 0$ as a fixed point and, being $F'(0) = -b^2k < 0$, we obtain that if $k < 1/b^2$ the fixed point is stable. Furthermore, by using a center manifold reduction we obtain that if $db + c^2 + b^2c^2 - b^3d < 0$ (and in particular this holds in relation to the parameters we are considering) the bifurcation occurring at $k = 1/b^2$ is a flip of subcritical type[7]. This means that an unstable cycle $\mathbf{r}^*$ of period 2 exists when the fixed point is still stable and, at the bifurcation, it merges with $\mathbf{e}^*$, leaving an unstable fixed point. Then, we have that when $k < 1/b^2$, the cycle $\mathbf{r}^*$ appears through a fold bifurcation together with a stable one, $\mathbf{n}^*$, of the same period. Then, if the parameter k ranges in $[k_{sn}, 1/b^2]$, where k_{sn} is the saddle-node bifurcation value, the one-dimensional map F exhibits the coexistence of two attractors, $\mathbf{e}^*$ and the 2-cycle $\mathbf{n}^*$, whose immediate basins are separated by the periodic points of $\mathbf{r}^*$.

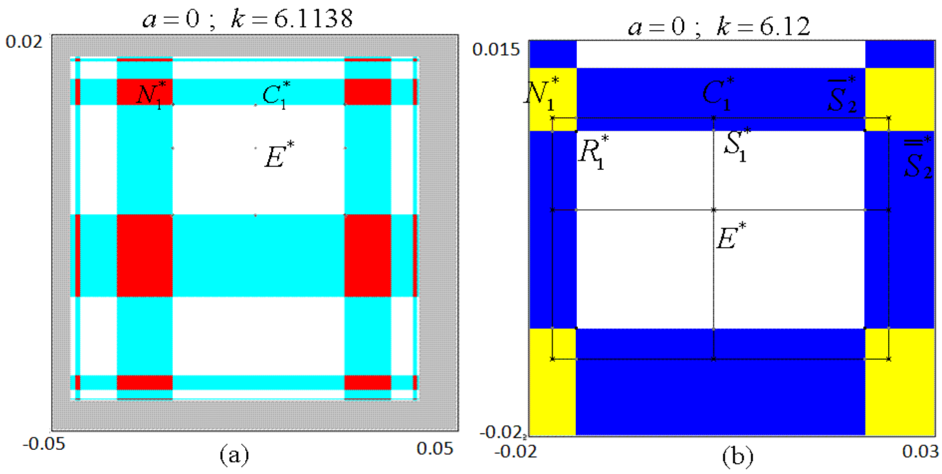

Fig.40

Coming back to the two-dimensional map in (16), the above detected saddle-node bifurcation of F^2 (the second iterate of F) causes the sudden appearance of six cycles of period 4 of the map T_0, shown in Fig.40b, as described in [20]. Two of these cycles, the attracting node N^* and the repelling one R^*, correspond to the cycles $\mathbf{n}^*$ and $\mathbf{r}^*$ respectively. Moreover 4 further cycles of period 4 exist: two of them, the saddles $\overline{S}^*$ and $\widehat{S}^*$, due to the coexistence of N^* and R^*, and two, a stable node C^* and a saddle S^*, due to the coexistence of the cycles N^* and R^* with the stable fixed point E^*. Summarizing, as a result of the saddle-node bifurcation of T_0 occurring at $k = k_{sn}$ we obtain three coexisting attractors, the fixed point and the period 4 cycles C^* and N^*, a repelling

[7]See, for example, Th. 3.5.1 in [50].

cycle R^*, and three saddle cycles, S^*, $\overline{S}^*$ and $\widetilde{S}^*$. The basins of attraction of E^* and C^* are made up by rectangular components separated by the stable set of the saddle S^* which gives rise to a heteroclinic connection with the periodic points of the repelling cycle R^*. Such a repelling closed curve bounds the immediate basin of attraction of E^*. The stable sets of the two saddle cycles $\overline{S}^*$ and $\widetilde{S}^*$ separate the basins of attractions of the two cycles C^* and N^* while the unstable ones connect the periodic points of the two stable cycles, giving rise to a second invariant closed curve (see Fig.40b). The two unstable cycles R^* and S^* are those also involved in the flip bifurcation of the fixed point E^*, indeed as the value $k = 1/b^2$ is approached, the heteroclinic connection between the two cycles shrinks, merging with E^* at the subcritical bifurcation.

Then, starting from the one-dimensional map in (18) we have seen that two local bifurcations occur for the map T_0, a “saddle-node” bifurcation, giving rise to six cycles of period 4 and a “subcritical flip” bifurcation, at which two of the cycles of period 4, a saddle and a repelling node, merge with E^* leaving an unstable node. The noticeable point here is that immediately after the occurrence of the first bifurcation two closed curves appear in the phase-space, one attracting, made up by the unstable sets of the two saddle cycles $\overline{S}^*$ and $\widetilde{S}^*$, and one repelling, made up by the stable set of the saddle cycle S^*, as qualitatively represented in Fig.41b.

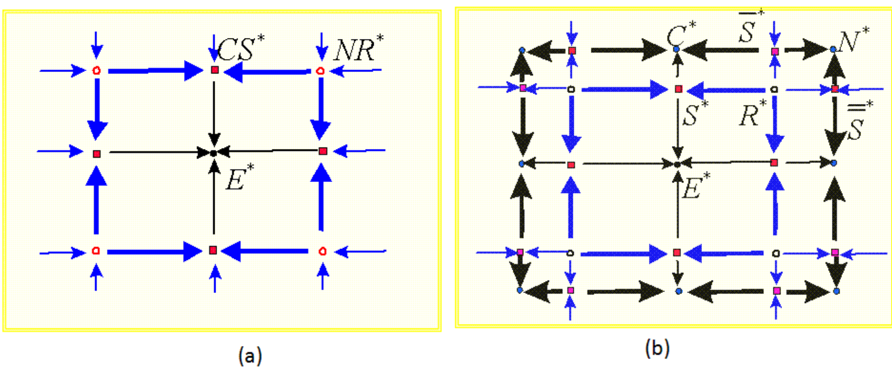

Fig.41 Qualitative representation of the "saddle-node" bifurcation for closed curves

In order to explain such an appearance, we analyze the map at the bifurcation value $k = k_{sn}$. At such a value the two cycles N^* and R^* coalesce in a unique cycle (that we shall call NR^*) as well as the cycles C^* and N^* in the cycle CS^*. The Jacobian matrix of T_0 evaluated at NR^* has the eigenvalues equal to ± 1 then NR^* is bifurcating along both the directions of the eigenvectors (eigen-directions for short). Furthermore, due to the square separate property of T_0, the eigen-directions are vertical or horizontal and, consequently, their portions running away from NR^* must reach the cycle CS^* (see Fig.41a and Fig.40a). On the other hand, the cycle CS^* bifurcates with a unique eigenvalue equal to 1, the second one being smaller than 1 in modulus, and along the eigenvector associated with the eigenvalue 1 the two cycles C^* and S^* will appear. We conclude that at the bifurcation a heteroclinic connection exists between the two cycles CS^* and NR^* which surrounds the attracting fixed point E^*. It attracts the trajectories starting from the external (with respect to the closed curve) portion of the phase-plane and repels those having initial condition belonging to the internal one. This is a structurally unstable situation, which evolves in the appearance of the two invariant closed curves of Fig.41b.

Summarizing, in this first scenario we have seen that the periodic orbits appear through a saddle-node of codimension 2, that is, to a bifurcation occurring with two eigenvalues which cross the unit circle at the same time. This particular situation allows us to obtain, at the bifurcation, a *half-stable* invariant closed curve which is attracting from outside and repelling from inside. Such a curve can be seen as the merging of the two invariant closed curves, one repelling and one attracting, that appear immediately after the bifurcation. Thus, we observe a *saddle-node bifurcation of invariant closed curves*, given by the coalescence of two closed invariant curves, one attracting and one repelling, followed by their splitting (or their annihilation if the movement of the parameters is reversed). Such a bifurcation, quite common in continuous flows, is instead not generic when we deal with two-dimensional maps and its occurrence in the map we are considering seems strongly related to one of the properties of the map itself. We refer, in particular, to the "*square separate*" property, that is, to the fact that the second iterate of the map results in a de-coupled map.

8.3.2 Saddle connections

In order to consider a more generic situation we set $a = 0.3$ and let k range in $[5.5713, 5.635]$, so that the parameters belong to the periodicity region in which an attracting cycle of period 5 exists. Indeed, at $k < 5.5713$ a saddle-node bifurcation causes the appearance of a stable cycle of period 5 as well as a saddle-cycle of the same period. Immediately after such a local bifurcation no invariant closed curves exist, as shown in Fig.42a where the attracting cycle is turned in a focus C^*, while at $k = 5.635$ two invariant closed curves exist (see Fig.42b), a repelling one and a stable heteroclinic connection between the periodic points of the saddle with those of the attracting cycle, turned into a focus (i.e., the attracting curve is a saddle-focus connection). Looking at the stable and unstable sets of the saddle cycle, we can observe that

- i) the branch of the unstable set converging to the fixed point E^* in Fig.42a, after the appearance of the repelling closed curve converges to the cycle C^*;

ii) both the branches of the stable set of the saddle come from the frontier of the bounded trajectories in Fig.42a, while in Fig.42b one of them exits from the repelling closed curve.

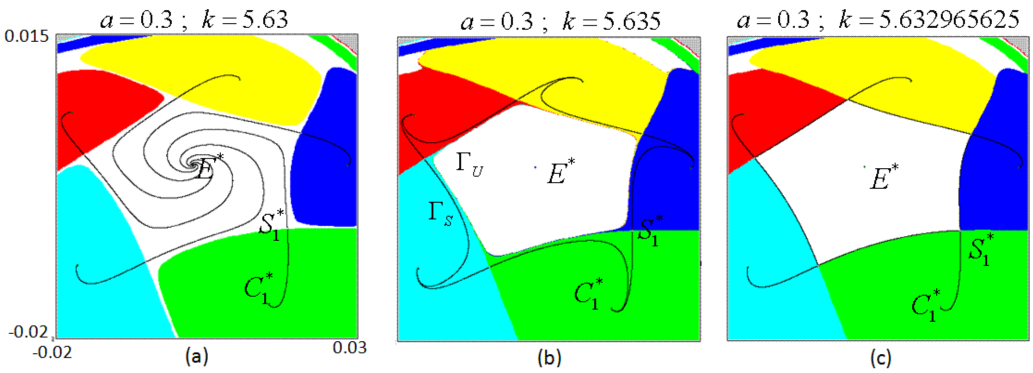

Fig.42

The enlargements in Fig.43 illustrate the different behaviour of the stable and unstable sets of the saddle cycle S^*.

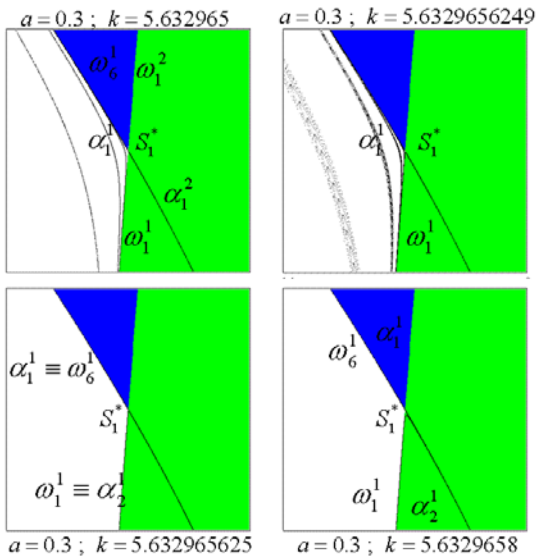

Fig.43

This suggest that the appearance of the repelling closed curve can be explained by the merging of a branch of the stable set of a saddle cycle S with a branch of the unstable set of the same cycle. Such a merging gives rise to a structurally unstable closed connection (*saddle connection*) between the periodic points of S, which develops causing the appearance of two invariant closed curves, one attracting and one repelling. The merging of the branches belonging to the stable and unstable sets of the saddle cycle can be observed around at $k = 5.632965625$ (see Fig.42c).

We summarize in Fig.44a qualitative sketch of this bifurcation. Before the bifurcation, Fig.44a, an attracting focus cycle coexists with the stable fixed point; the basins of attraction of the two attractors are separated by the stable manifold of the saddle cycle. The unstable branch $W_1^U = \cup\alpha_{1,i}$ tends to the fixed point and $W_2^U = \cup\alpha_{2,i}$ to the focus cycle. As the bifurcation value is approached, the stable branch $\omega_{1,i}$ of the saddle periodic point S_i approaches the unstable branch $\alpha_{1,j}$ of S_j, so preparing the homoclinic connection. At the bifurcation (Fig.44b) we have that the two branches $\omega_{1,i}$ and $\alpha_{1,j}$ merge giving rise to a connection between the periodic points of the saddle cycle: the attracting cycle is external to such a connection and the branch W_2^U still converges to it. The stable fixed point is internal to the saddle connection which bounds its basin of attraction. Immediately after the bifurcation, an invariant repelling close curve is created (from which the branch W_1^S comes out, rolling up). The unstable branch W_1^U converges to the focus cycle, creating with W_2^U another closed invariant curve, attracting, given by the saddle-focus connection (see Fig.44c).

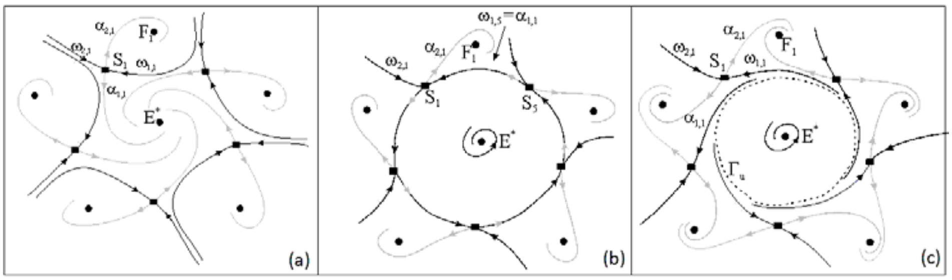

Fig.44

This global mechanism, that does not involve saddle-node bifurcation for closed curves, neither bifurcations of codimension 2, seems more generic and it has been observed in different models ([6], [3], [5], [7]) and, as we shall see in the next section, it works also when we study the interactions between periodic and quasi periodic trajectories.

Moreover a saddle connection may also lead to the appearance of an attracting closed curve, as shown in ([5]). We illustrate such a mechanism making use of the qualitative picture in Fig.45 where a pair of cycles of period 5, a saddle and a repelling focus, is considered.

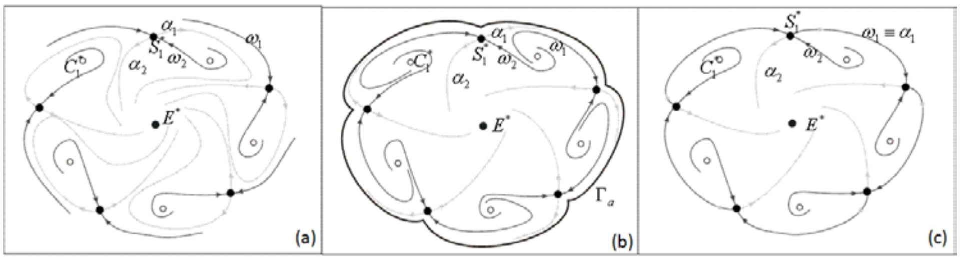

Fig.45

Before the bifurcation, in Fig.45a, a repelling focus cycle and a saddle cycle coexist with the attracting fixed point. The unstable set of the saddle cycle converges to E^* and the two branches of the stable one come from different repelling sets: in particular, ω_2 issues from the repelling focus. Approaching the bifurcation, the unstable branch α_1, turning around the periodic points of the repelling focus is closer and closer to the stable branch ω_1. At the bifurcation, these two branches merge, creating a structurally unstable situation given by the saddle connection of the periodic points of the saddle cycle (Fig.45b). Immediately after the bifurcation, in Fig.45 c an attracting closed curve Γ_a appears, surrounding the periodic points of the cycles, at which converges the unstable branch α_1. At the same time, the stable branch ω_1 gives rise with ω_2 to a repelling heteroclinic connection with the periodic points of the focus cycle and separates the basins of attraction of E^* and Γ_a.

Then, we can conclude that if the cycle C, involved in the global bifurcation with the saddle S, is attracting then the closed curve appearing after the saddle connection is repelling, together with an attracting saddle-connection. If the cycle C, involved in the global bifurcation with the saddle S, is repelling then the closed curve appearing after the first step is attracting, together with a repelling saddle-connection. In particular, in this latter case when the repelling cycle involved in it is a node instead of a focus the two invariant closed curves may appear very close to each other, and this is really what is numerically observed when performing the study of the dynamical behaviours of the model, as in Fig.38.

It is worth to observe here that the bifurcations represented in Fig.45c and Fig.45c are simply a schematic representation. Indeed we are dealing with a discrete model and thus it is possible that they occur with an *homoclinic tangle*, that is in a certain parameter range the contact between the stable and unstable set is opened by their quadratic tangencies, at which homoclinic orbits appear (and related complex dynamics), followed by transversal intersection and closed by a second quadratic tangencies at the opposite side which destroy all the homoclinic orbits. Some examples will be shown in the next section.

8.3.3 Saddle-node bifurcation of a cycle

Finally, we show a further example, to illustrate a different mechanism leading to two closed invariant curves and involving two pair of cycles, appearing via two different saddle-node bifucations. We fix $a = 0.001$, so that we slightly pertub the square separated map and we are inside to the period 4 periodicity region. We follow a bifurcation path increasing k from $\overline{k}_{sn}$, value at which a saddle-node bifurcation causes the appearance of an attracting cycle C^* of period 4 as well as a saddle cycle S^* of the same period. Immediately after such a bifurcation we obtain the situation represented in Fig.46a, where the stable fixed point E^* coexist with the two cycles and the basins of attraction of E^* and C^* are separated by the stable set of the saddle cycle S^*. The two branches of the unstable set of S^*, α_1 and α_2, converge to E^* and to C^*, respectively.

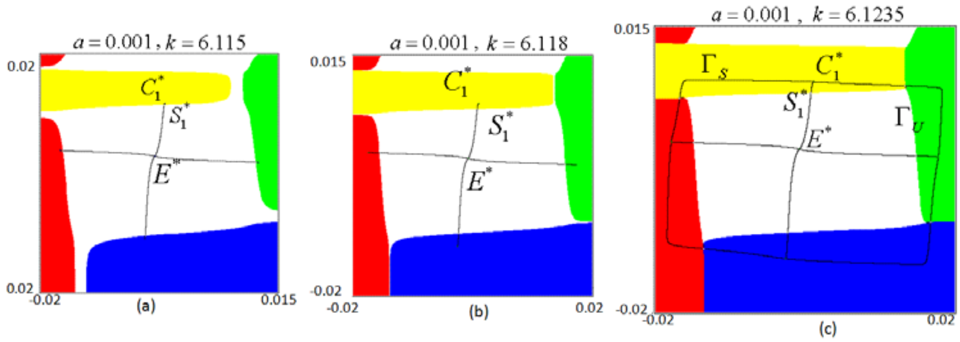

Fig.46

As the parameter k increases, each branch ω_1^i of the periodic point S_i^* of the saddle cycle approach the branch ω_2^{i+1} of the subsequent periodic point S_{i+1}^*, as in Fig.46b where the two branches are very close, suggesting that a bifurcation is going to occur. Notice that at this parameter constellation no invariant closed curve exists, since the stable set of the saddle cycle exits from the frontier of the set of bounded trajectories and the unstable one connects the saddle with the two different attractors.

The situation now detected is quite different from that previously described, where the appearance of the repelling curve was associated with an homoclinic connection of a saddle cycle, caused by the merging of a branch of its *stable* set with a branch of the *unstable* one. Now, we are faced with a new mechanism since only the *stable* set of the saddle cycle is involved in the bifurcation. Since the two branches of the stable set cannot merge, the situation of Fig.46b suggests that some invariant set is appearing. And this is just what we observe increasing the parameter k, as shown in Fig.46c. The attractors are still given by the fixed point E^* and the attracting cycle C^* of period 4; the unstable set of the saddle cycle S^* exhibits the same behaviour as in Fig.46b, reaching both the attractors, but now the basins of attraction of E^* is bounded by a repelling closed curve Γ_U. This closed curve is made up by the stable set of the saddle cycle S^*, now coming from the periodic points of a repelling node cycle, R^*, of period 4. The appearance of the cycle R^* is due to a standard saddle-node bifurcation which gives also rise to a saddle cycle $\overline{S}$ of period 4. The stable set of this latter saddle cycle separates the basins of attraction of the four fixed points C_i^*, $i = 1, 2, 3, 4$, of the map T^4, fourth iterate of the map T. The unstable set of the saddle $\overline{S}$ connects the periodic points of the attracting cycle C^*, so giving rise to an attracting closed curve Γ_S. Then, due to the occurrence of the saddle-node bifurcation, we obtain the appearance of two invariant closed curves, one attracting and one repelling, and Fig.47 gives a qualitative representation of the mechanism associated with such an appearance.

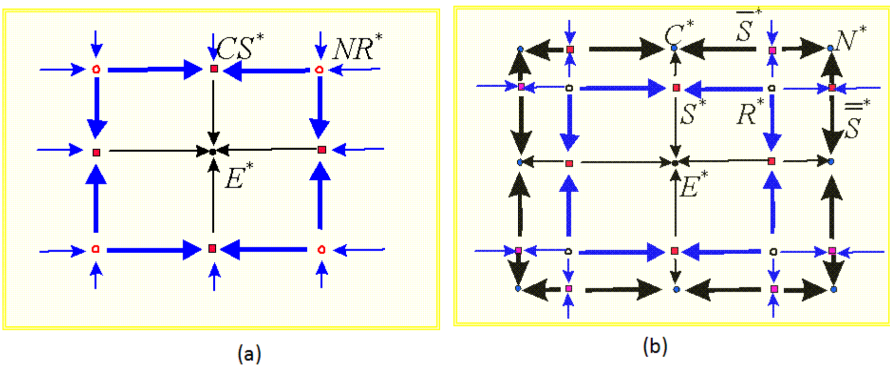

Fig.47

We start from a phase space in which an attracting cycle C^* coexists with a stable fixed point E^*, the basins of attraction being separated by the stable set of a saddle cycle S^*, as in Fig.47a. In this framework a saddle-node bifurcation of the map T^4 occurs and causes the appearance of a repelling cycle R^* of period 4 of the map T together with a saddle cycle $\overline{S}$ of the same period. It is worth to observe that the occurring bifurcation is associated with the eigenvalue $\lambda_1 = 1$ while $|\lambda_2| > 1$. Then, at the saddle-node bifurcation value, we observe the appearance of a cycle of period 4 ($R\overline{S}$ in Fig.47b) which is half-stable along the eigenvector associated with λ_1. Along this direction we have a structurally unstable situation, characterized by a branch (the external one, with respect to a fictitious line joining the periodic points of the cycles) whose points converge to $R\overline{S}$ while the internal one reaches the saddle cycle S^*. Furthermore, the eigenvector associated with λ_2 has a branch (the external one) converging to the attracting cycle C^*, while the internal one belongs to the stable set of the saddle cycle S^*. As a result, we obtain an invariant closed curve, made up by the stable set of the saddle S^* which connects the periodic points of the cycle $R\overline{S}$. Immediately after the bifurcation (Fig.47b) the cycle $R\overline{S}$ splits up into a repelling node cycle R^* and a saddle cycle $\overline{S}$; the stable set of the saddle S^* persists to give rise to a repelling closed curve, connecting the periodic points of R^*, and an attracting closed curve appears, made up by the unstable set of the saddle $\overline{S}$ which connects the periodic points of the cycle C^*. Comparing Fig.47b and Fig.41b we remark that the two bifurcation mechanisms are quite different, even if both are due to a saddle-node bifurcation of the map T and T_0, respectively. Indeed, while in this latter case at the bifurcation value the two invariant curves coalesce and are half-stable, the sequence commented above gives not the merging of the two curves, since at the bifurcation a unique heteroclinic connection exists and is attracting only along a branch of the eigenvector associated with the eigenvalue 1.

8.4 Interaction between invariant closed curves and cycles. A business cycle model

In this section we consider a map T that exhibits some multistability phenomena, at least one of the attractor being a closed curve. In such situations, the invariant closed curve may interact with the other attractors and interesting dynamic phenomena may occur, often associated with homoclinic or heteroclinic tangles. In particular, we shall show two different global bifurcations. The first one causes the transition from one repelling closed curve to two disjoint repelling closed curves; the second one causes the transition from an attracting closed invariant curve, say Γ_a, with a pair of cycles of period k outside it, a saddle S and an attracting one, C, to a wider attracting closed invariant curve, say Γ_b, with the two cycles inside it.

In order to illustrate the mechanisms associated with these phenomena, we consider the following discrete-time version of the Kaldor nonlinear model of the business cycle

$$\begin{cases} Y_{t+1} = Y_t + \alpha \left(I_t - (Y_t - C_t) \right) \\ K_{t+1} = I_t + (1 - \delta) K_t \end{cases} \tag{19}$$

where the dynamic variables Y_t and K_t represent the income (or output) level and the capital stock in period t, respectively, and both the investment I_t and the consumption C_t (or equivalently the savings $S_t = Y_t - C_t$) are assumed to depend in general on Y_t and K_t.

The first equation in (19) views the output level as reacting over time to the excess demand or, put differently, to the difference between ex-ante investment (I_t) and saving ($S_t = Y_t - C_t$). The *speed of adjustment* is measured by the parameter α ($\alpha > 0$), where a value of α smaller than 1 means a prudent reaction by firms, while a value of α greater than 1 denotes rash reactions and coordination failure.

The second equation in (19) models the capital stock as being increased by realized investment (here assumed to coincide with ex-ante investment) $I_t = I_t(K_t, Y_t)$, and decreased by depreciation δK_t, where δ ($0 < \delta < 1$) represents the *capital stock depreciation rate.*

The discrete dynamical equations (19) (or, alternatively, their continuous-time counterparts) provide the common structure of several versions of the Kaldor model, which have been proposed in the literature up to now (see [33], [57], [48], [23], [8], [10] among others), and a different example will be also shown below. Such models are able to produce both periodic or quasi-periodic trajectories and further dynamic scenarios, ranging from chaotic fluctuations to coexistence of different attractors, once the investment and the savings function I_t and S_t are specified in a way consistent with Kaldor's original qualitative assumptions.

The assumptions about consumption (C_t) and investment (I_t), which are the same as in [57], [74] and [8], are

- **Consumption**

  At each time t, the consumption is a nonlinear sigmoid shaped function of income:

$$C_t = c_0 + \frac{2}{\pi} c_1 \arctan\left(\frac{\pi c_2}{2c_1}(Y_t - Y^*)\right) \tag{20}$$

  where Y^* denotes the exogenously assumed equilibrium (or normal) level of income and c_0, c_1, c_2 are positive parameters. The consumption is therefore an increasing function of income (ranging between $c_0 - c_1$ and $c_0 + c_1$): however, while for extreme values of income consumption remains nearly constant, i.e. the fraction of income spent for consumption decreases as income increases, there exists a region around the normal level Y^* where consumption increases rapidly at a rate close to c_2, which represents the consumption propensity at Y^* (we assume $0 < c_2 < 1$). The consumption function (20), or equivalently the inverted S-shaped savings function $S_t = Y_t - C_t$, reflects the view that the proportion of income which is saved is higher in non-ordinary periods, when Y_t is far from Y^*, because in such periods people perceive a larger portion of their income as being transitory.

- **Investment**

At each time t, the investment is a linear function of income and capital stock. Precisely it is assumed that (gross) investment responds to a gradual adjustment of the actual capital stock to the desired capital stock

$$I_t = b\left(K_t^d - K_t\right) + \delta K_t$$

where K_t^d is the desired stock of capital at time t, which is assumed linear in current output, $K_t^d = kY_t$, k represents the desired *capital-output ratio* (which will be considered as an exogenous parameter here) and b, $0 < b < 1$, is the capital stock adjustment parameter. Therefore the investment function can be rewritten as a linear function of income and capital, as follows

$$I_t = bkY_t - (b - \delta)K_t \tag{21}$$

where the Kaldorian negative relation between investment and capital stock is fulfilled provided that $b > \delta$.

Substituting the consumption and investment functions (20)-(21) in model (19) we get

$$\begin{cases} Y_{t+1} = (1 - \alpha + \alpha bk)\, Y_t + \alpha\left(c_0 + \frac{2}{\pi} c_1 \arctan\left(\frac{\pi c_2}{2c_1}\left(Y_t - Y^*\right)\right) - (b - \delta)\, K_t\right) \\ K_{t+1} = b\left(kY_t - K_t\right) + K_t \end{cases} \tag{22}$$

from which the coordinates of the exogenous fixed point can be easily obtained

$$\begin{cases} Y^* = \frac{c_0}{1-k\delta} \\ K^* = kY^* = \frac{kc_0}{1-k\delta} \end{cases}$$

In order to simplify the analysis of the model (22), we normalize the fixed point to $(0, 0)$, by reformulating the model in terms of deviations

$$\begin{cases} x_t = K_t - kY^* \\ y_t = Y_t - Y^* \end{cases} \tag{23}$$

With the new coordinates (23), the dynamical system (22) is represented by the following map

$$T : \begin{cases} x' = (1 - b)\, x + bky \\ y' = \alpha\,(\delta - b)\, x + (1 - \alpha + \alpha bk)\, y + \frac{2}{\pi}\alpha c_1 \arctan\left(\frac{\pi c_2}{2c_1} y\right) \end{cases} \tag{24}$$

Note first that the map T is independent on c_0, which means that c_0 is only a "location" parameter and does not affect the asymptotic behaviour of the system. Second, though the map T depends on 6 parameters, in our analysis we will assume b, k, δ, c_1 as fixed parameters, and we will perform stability and bifurcation analysis in the parameter space

$$\Omega = \{(\alpha, c_2) : \alpha > 0 \text{ and } 0 < c_2 < 1\}$$

The properties of the map T in (24) are studied in [8], at which the interested reader is addressed for major details. We only recall here the symmetric property of T, whose implications is that any invariant set of T either is symmetric with respect to the origin, or it admits a symmetric invariant set, and the existence of a region in the parameter space where the map is not invertible (being a $Z_1 - Z_3 - Z_1$ map). In our analysis we shall consider a parameter range in which T is invertible. Even the existence of the fixed points and the local stability of the exogenous fixed point (obtained as usual by the localization of the eigenvalues of the Jacobian matrix) is performed in [8] and we only recall the main results:

Proposition 2 *The map T in (24) has*

- *the unique fixed point $E^* = (0,0)$, if $c_2 \leq 1 - k\delta$ or $1 - \delta k \leq 0$*
- *three fixed points, $E^* = (0,0)$ and two further points, P^* and Q^*, symmetric with respect to E^*, if $c_2 > 1 - k\delta > 0$.*

Proposition 3 *Assume $\delta k < 1$, $b < 1$.*

- *If $b > \delta$ and $(2-b)^2 > bk(4 - 4\delta + \delta b)$ the fixed point $E^* = (0,0)$ is locally asymptotically stable if the parameters α and c_2 belong to the region $OABCD$ of the plane (α, c_2), with vertices $O = (0,0)$, $A = \left(\frac{2(2-b)}{2-b-bk(2-\delta)}, 0\right)$, $B = \left(\frac{(b-2)^2}{bk(b-\delta)}, \frac{(2-b)^2 - bk(\delta b - 4\delta + 4)}{(-2+b)^2}\right)$, $C = \left(\frac{b}{k(b-\delta)}, 1 - \delta k\right)$, $D = (0, 1 - \delta k)$, where the sides AB, BC and CD belong to the hyperbola of equation*

$$c_2 = c_{2f}(\alpha) = \frac{\alpha - 2}{\alpha} - \frac{bk(2-\delta)}{2-b} \tag{25}$$

to the hyperbola of equation

$$c_2 = c_{2N}(\alpha) = 1 + \frac{b - \alpha bk(1-\delta)}{\alpha(1-b)} \tag{26}$$

an to the line $c_2 = 1 - \delta k$, respectively;

- *if* $b > \delta$ *and* $(2-b)^2 < bk(4-4\delta+\delta b)$ *the fixed point* $E^* = (0,0)$ *is locally asymptotically stable if the parameters* α *and* c_2 *belong to the region OBCD of the plane* (α, c_2)*, with vertices* $O = (0,0)$*,* $B = \left(\frac{b}{bk(1-\delta)-(1-b)}, 0\right)$*,* $C = \left(\frac{b}{k(b-\delta)}, 1-\delta k\right)$*,* $D = (0, 1-\delta k)$*, where the sides BC and CD belong to the hyperbola of equation*

$$c_2 = c_{2N}(\alpha) = 1 + \frac{b - \alpha bk(1-\delta)}{\alpha(1-b)}$$

an to the line $c_2 = 1 - \delta k$*, respectively;*

- *if* $b < \delta$ *the fixed point* $E^* = (0,0)$ *is locally asymptotically stable if the parameters* α *and* c_2 *belong to the region OABD of the plane* (α, c_2)*, with vertices* $O = (0,0)$*,* $A = \left(\frac{2(2-b)}{2-b-bk(2-\delta)}, 0\right)$*,* $B = \left(\frac{2-b}{k(\delta-b)}, 1-\delta k\right)$*,* $D = (0, 1-\delta k)$*, where the sides AB and BD belong to the hyperbola of equation*

$$c_2 = c_{2f}(\alpha) = \frac{\alpha-2}{\alpha} - \frac{bk(2-\delta)}{2-b}$$

an to the line $c_2 = 1 - \delta k$*, respectively.*

Moreover if the point (α, c_2) *exits the stability region by crossing the side AB, then a supercritical flip bifurcation occurs at which* E^* *becomes a saddle point and a period 2 attracting cycle appears; if the point* (α, c_2) *exits the stability region by crossing the side BC, then a Neimark bifurcation occurs at which* E^* *is transformed from a stable focus to an unstable focus and an attracting closed invariant curve appears around it; if the point* (α, c_2) *exits the stability region by crossing the side CD, then a supercritical pitchfork bifurcation at which two stable fixed points are created close to* E^**, which becomes a saddle.*

In the following we shall consider $\delta \leq b$, so that self-sustained oscillatory behavior around the unstable fixed point E^* occur, and $(2-b)^2 < bk(4-4\delta+\delta b)$. In this parameter region the exogeneous fixed point can be destabilized only via pitchfork bifurcation or via a NS bifurcation and we shall follow a bifurcation path starting from a point corresponding to two stable fixed points P^* and Q^* and an unstable fixed point E^*, located in the middle, i.e. a situation of *bi-stability* (without oscillations), and moving towards a region where self-sustained oscillations exist (see Fig.48).

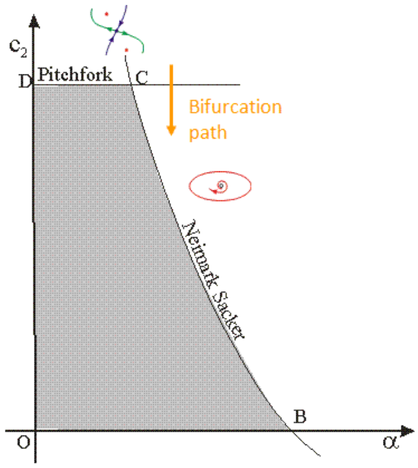

Fig.48

However, our global analysis will point out that long-run oscillatory behavior is possible even for high values of c_2 (beyond the pitchfork boundary), in parameter ranges where two further equilibria P^* and Q^* exist and are stable, or where they exist unstable but further stable periodic orbits exist. This will reveal phenomena of coexistence of the Kaldorian business cycle with other possible long-run dynamic outcomes, where the role played by the initial condition will be crucial.

8.4.1 From one repelling closed curve to two repelling ones

Immediately after the pitchfork bifurcation of the exogenous fixed point E^*, two attracting fixed points, the nodes P^* and Q^*, appear, located at symmetric positions with respect to the saddle E^*. Their basins of attraction are separated by the stable manifold $W^S(E^*)$. The unstable set $W^U(E^*)$ reaches the two fixed points: more precisely, a branch, say α_1, tends to P^* whereas the other one, say α_2, goes to Q^*.

The phase portrait of Fig.49a shows an example of this situation: it has been obtained at $\alpha = 1.5$ and $c_2 = 0.98$, then quite far from the bifurcation. Indeed at this parameter values the two nodes have turned into stable foci and the stable set of the saddle exhibits some convolutions separating the basins of attraction of P^* and Q^*, $\boldsymbol{B}(P^*)$ and $\boldsymbol{B}(Q^*)$ respectively, represented in red and gray respectively.

As the speed of adjustment α increases, the set $W^S(E^*)$ involves more and more, winging around the fixed points P^* and Q^*, as shown in Fig.49b. Consequently, the basin boundary appear to be more complicated and a trajectory starting from the region where the convolutions get thicker is subject to greater uncertainty about its long run behaviour. In fact, a slight perturbation of an initial condition taken in such a region may cause a crossing of the basin boundary and consequently the convergence to a different equilibrium.

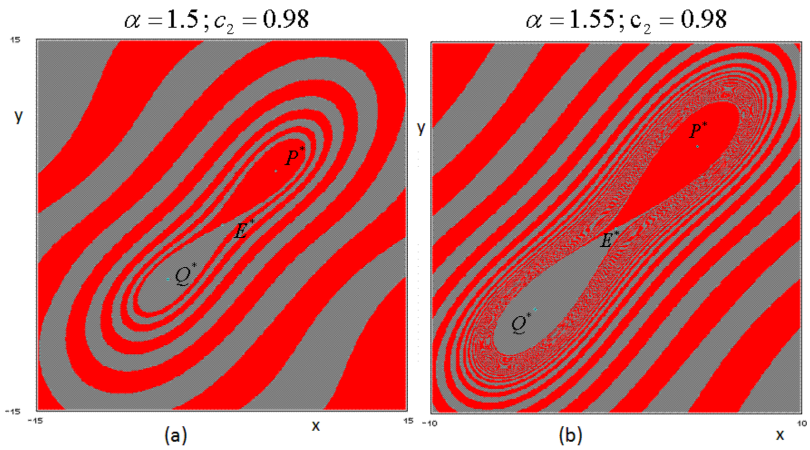

Fig.49

Moreover this basin structure suggests that some global bifurcation is about to occur. Indeed, when α is slightly increased, as in Fig.50a, an attracting closed curve Γ appears in the area where there was many convolutions of $W^S(E^*)$. This means that long-run quasi-periodic self-sustaining fluctuations are now a possible outcome, as well as dampened oscillations converging to the fixed points: three typical trajectories, starting from initial condition taken in the three different basins, are represented versus time in Fig.50b.

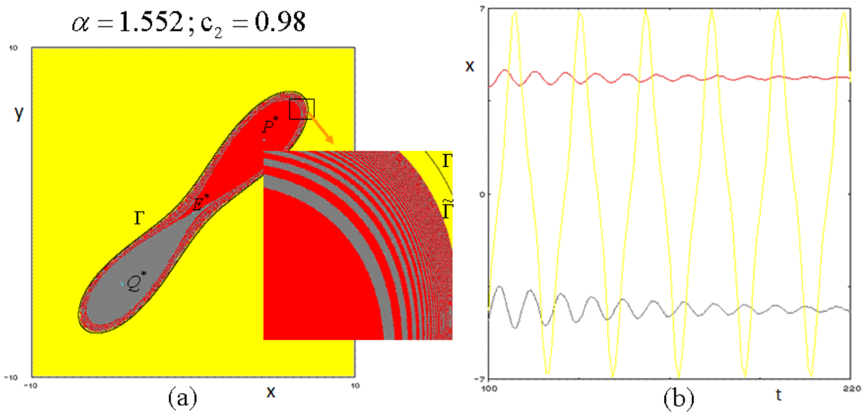

Fig.50

The basins of attraction of P^* and Q^* are still separated by the stable manifold of the saddle E^*, but, differently from the case illustrated in Fig.49, now the preimages of the points of $W^S(E^*)$ accumulate on a repelling closed curve $\widetilde{\Gamma}$, appeared with Γ and very close to it (see Fig.50). The appearance of Γ and $\widetilde{\Gamma}$ could be due in principle to a "saddle-node" bifurcation for closed curves, given that the two curves are very close each other, but we know that such a bifurcation is very infrequent in discrete maps. Then a mechanism similar to that described in the previous section may be conjectured in this case: a saddle cycle appears via saddle-node together with a repelling (attracting) node cycle of the same period, then a saddle connection made up by the merging of two branches of the stable and unstable manifolds of the saddle gives rise to an attracting (repelling) closed invariant curve and to a heteroclinic connection between the periodic points of the two cycles made up by the stable (unstable) set. These two invariant closed curves appear very close to each other and if the period of the cycle is very high they look like those of Fig.50a.

Whatever be the underlying mechanism, the appearance of the two invariant closed curves, one attracting and one repelling, has a noticeable effect on the asymptotic behaviour of the model, since three attractors now coexist (the two equilibria, $P^*$and Q^*, and the closed curve Γ), the basins $\mathcal{B}(P^*)$ and $\mathcal{B}(Q^*)$ are strongly reduced and the majority of the trajectories are quasi-periodic (or periodic of very high period), since the curve $\widetilde{\Gamma}$ is now the basin boundary of Γ.

Moreover the repelling closed curve $\widetilde{\Gamma}$ is involved in other important qualitative change in the structure of the basins of attraction as the adjustment speed is increased further. Indeed, as we can see in Fig.51a, it progressively reduces in size and shrinks in proximity of the saddle E^*. Up to now, initial conditions taken close to the exogenous equilibrium give rise to trajectories converging to P^* or Q^*, but this is not true in the parameter constellation of Fig.51c, where trajectories starting close to E^* exhibit self-sustaining oscillations.

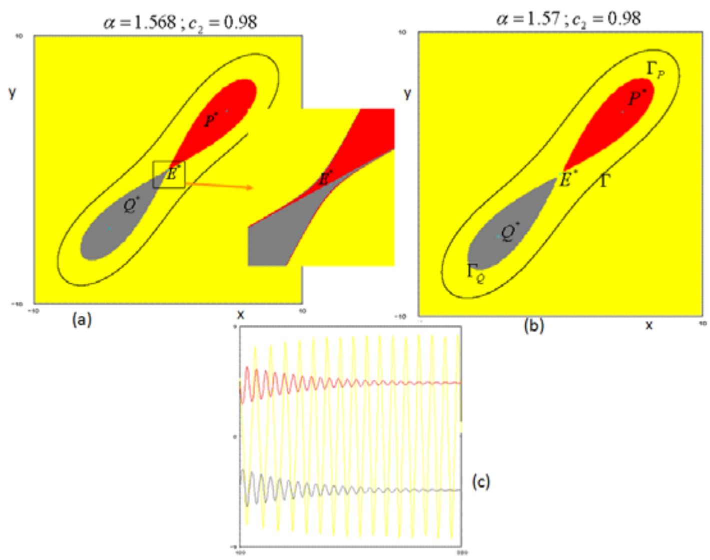

Fig.51

This means that the points of the unstable manifold of E^* no longer reach the two equilibria but converge to Γ. This change in the asymptotic behaviour of $W^U(E^*)$ proves that a global bifurcation has occurred, involving both the unstable branches of the saddle E^*. Indeed in the phase portrait of Fig.51b we can observe the splitting of $\widetilde{\Gamma}$ into two repelling closed curves, Γ_P and Γ_Q, each one bounding the basin of the corresponding fixed point. These two repelling closed curves are the α-limit sets of the points of the two branches ω_1 and ω_2 of the stable set $W^S(E^*)$, which have modified their behaviour as well. Then we deduce that when the parameter α ranges from 1.568 to 1.57, a homoclinic bifurcation of E^* occurs, whose effect is the transition from one "big" repelling closed curve, basin boundary of the attracting set $\{P^*, Q^*\}$, to two "small" repelling closed curves, basin boundaries of $\mathcal{B}(P^*)$ and $\mathcal{B}(P^*)$ respectively. This situation can be classified as a *double homoclinic loop*, since it involves both the branches of the stable and unstable sets of the saddle E^*: its evolution is represented in Fig.52, where some enlargements of the phase space as well as of the stable and unstable sets of E^* are shown.

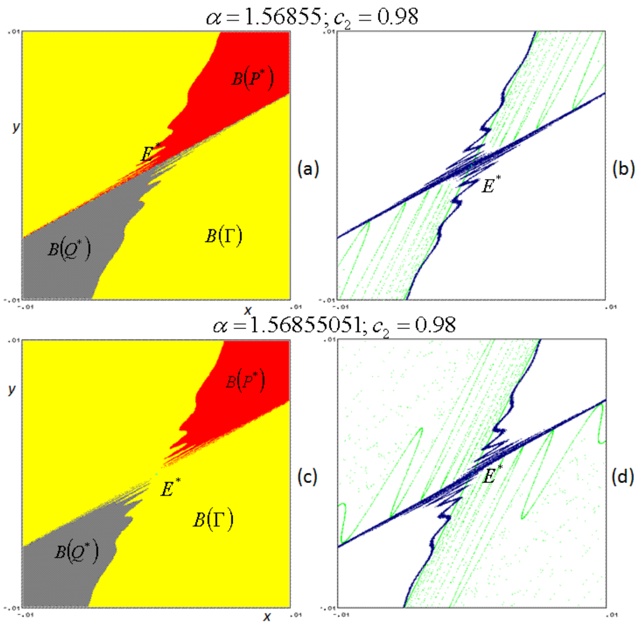

Fig.52

The first homoclinic tangency is shown in Fig.52a,b, obtained at $\alpha = 1.56855$: the branch α_1 of $W^U(E^*)$ converges to P^* and it is completely contained in its basin of attraction; the same is true for α_2 with respect to the fixed point Q^*. The stable branches have a complex structure: the repelling closed curve Γ is replaced by a strange repellor, generated by the tangency and separating the basins of $\{P^*, Q^*\}$ and Γ. After the transversal crossing of $W^S(E^*)$ and $W^U(E^*)$, at which more and more homoclinic points of E^* are created, the second homoclinic tangency occurs at $\alpha = 1.5685501$, as shown in Fig.52c,d, and closes the tangle. The homoclinic points of E^* disappear as well as the chaotic repellor, leaving the two disjoint curves Γ_P and Γ_Q as boundaries of the basins of attraction of P^* and Q^*, respectively. After the homoclinic tangle both the branches of $W^U(E^*)$ converge to the attracting closed curve Γ and those of the stable set $W^S(E^*)$ come from the repelling closed curve Γ_P and Γ_Q.

A different illustration of this homoclinic tangle, occurring in a very narrow parameter α range, is proposed in Fig.53, where we show the asymptotic behaviour of the whole unstable set of the saddle E^*. In Fig.53a, obtained at the same parameter value as Fig.53a corresponding to the first homoclinic tangency, the points of $W^U(E^*)$ converge to the two equilibria, forming an eight-shaped structure; then, in Fig.53b the unstable set $W^U(E^*)$ enters the basin of attraction of the attracting closed curve Γ as well as that of the attracting set $\{P^*, Q^*\}$: the separator of the three basins of attraction is a chaotic repellor, associated with the infinitely many periodic points existing close to the homoclinic trajectories. As α is further increased, more and more points of $W^U(E^*)$ converge to Γ until at the second homoclinic tangency, shown in Fig.53c, no points of the unstable set converge to the two stable foci.

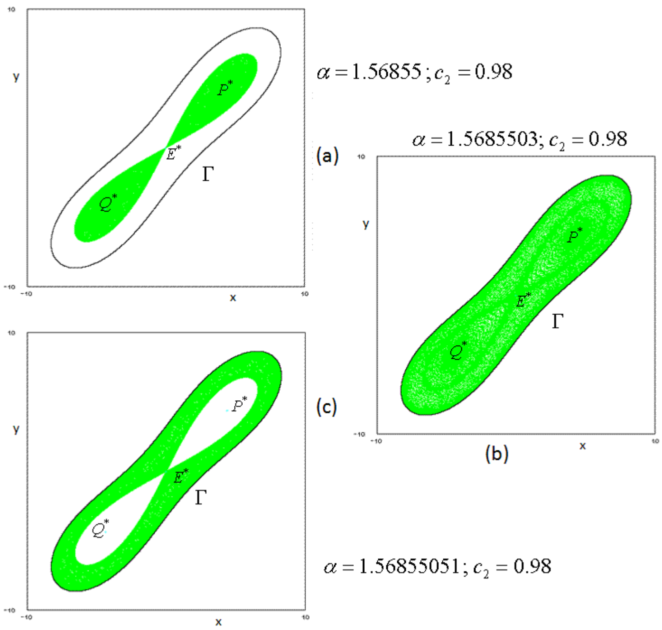

Fig.53

As the parameter α further increases, the two repelling closed curves Γ_P and Γ_Q become smaller and smaller, until a new bifurcation value $\alpha = \widetilde{\alpha}_N$ is reached at which a Neimark subcritical bifurcation occurs:

the two repelling closed curves collapse in P^* and Q^* respectively and at $\alpha > \widetilde{\alpha}_N$ the attracting closed curve Γ is the unique surviving attractor, since the two fixed points become unstable foci.

8.4.2 Interaction between coexisting invariant curve and cycles.

After the subcritical Neimark bifurcation of P^* and Q^*, the saddle E^* coexists with two repelling foci, from which the stable set $W^S(E^*)$ comes. The points of the unstable manifold $W^U(E^*)$ converges to the attracting closed curve Γ surrounding the three unstable fixed points.

This situation persists until at a certain value of α, say α_{sn}, a saddle-node bifurcation occurs, causing the appearance of two cycles of period 8, a saddle, S, and a stable node, C , which turns into a stable focus cycle immediately after. The two cycles are located outside the attracting closed curve and, as α increases from α_{sn}, a larger and larger portion of trajectories exhibits period-8 oscillations, as shown in Fig.54a, where the basins of attraction of the two attractors are represented in yellow and light blue. The points close to the endogenous equilibrium E^* still give rise to quasi-periodic fluctuations.

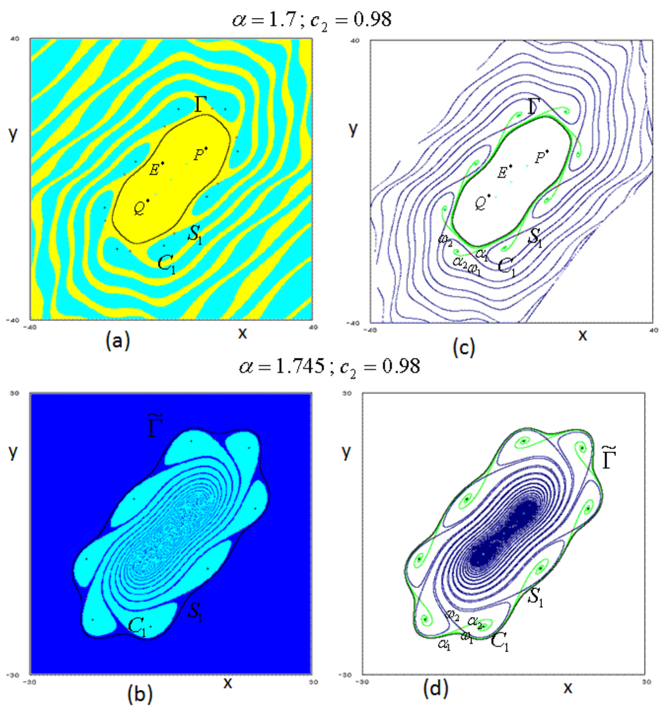

Fig.54

The phase portrait shown in Fig.54b is completely different: quasi-periodic and period-8 trajectories still coexist, but now the attracting closed curve $\widetilde{\Gamma}$ surrounds the stable focus cycle C and the majority of the trajectories exhibit quasi-periodic motion. Moreover the long run behaviour of trajectories starting in the area close to E^* is no longer predictable, since a small shock on them may have strong consequences given the many and many convolution of the separatrix of the two basins in this area.

The global mechanisms which cause this important modification in the basin structures, transforming an attracting closed curve, coexisting with a stable cycle external to it, in a larger one, surrounding it, has to involves the stable and unstable sets of the saddle, since they change behaviour. Indeed, in Fig.54a, obtained at $\alpha = 1.7 > \alpha_{sn}$, two attractors exist, the closed curve Γ and a focus cycle C, surrounding the curve, while the two basins, $\mathcal{B}(C)$ and $\mathcal{B}(\Gamma)$, are separated by the stable manifold $W^S(S) = \omega_1 \cup \omega_2$ of the saddle S. Both the branches of the stable manifold have as α-limit set the frontier of the set of bounded trajectories. The branches of the unstable one $W^S(S)$ reach the attracting closed curve (α_1) and the stable focus cycle (α_2). While, in Fig.54b, two attractors still exist, the closed curve Γ and the focus cycle C, surrounded by the curve; the stable manifold of the saddle cycle still separate the basins of attraction of the two attractors, but its α-limit set now belongs to the attracting set given by the three fixed points. Moreover, the branches of the unstable one play the opposite role, α_1 reaching the stable focus and α_2 the attracting closed curve. Then, to understand the bifurcation, we follow these invariant sets, increasing slowly the parameter α.

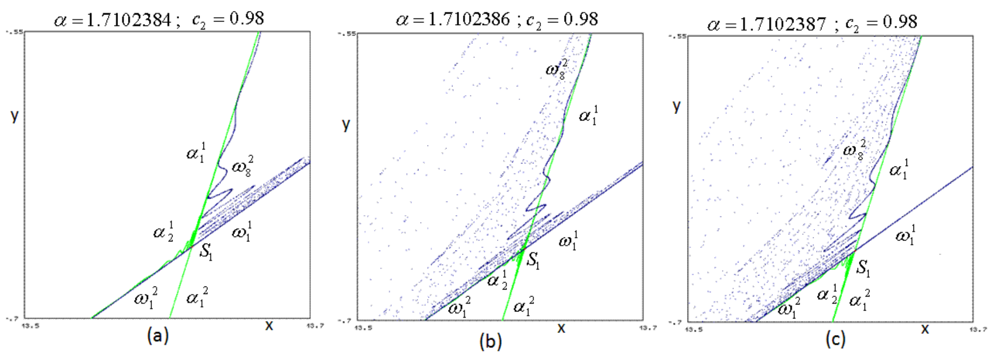

Fig.55

As the parameter α is increased, the two branches ω_1 and α_1 start to oscillate until a homoclinic tangency occurs. More precisely, at $\alpha = 1.7102384$ the stable branch $\alpha_{1,i}$ of the periodic point S_i has a tangential contact with the unstable branch $\omega_{1,j}$ of a different periodic point S_j (see Fig.55a) and this occurs cyclically for all the periodic points of the saddle S. This contact is the starting point of a heteroclinic tangle, which develops in a transversal crossing of the involved inner branches

(Fig.55b) and closes at $\alpha = 1.7102387$, at which value a second cyclical homoclinic tangency occurs (Fig.55c). Observe that at the end of the heteroclinic tangle, the two branches α_1 and ω_1 (but not α_2 and ω_2) have exchanged they reciprocal position with respect to Fig.55a. Approaching the heteroclinic tangle, the curve Γ exhibits more and more oscillations, as in Fig.56a obtained at the same parameter values of Fig.55a, before its disappearance. Moreover during the tangle a chaotic repellor $\mathcal{R}$ is created in the area occupied by the transversal crossing of the two manifolds. The presence of the chaotic repellor can be detected by looking the map T^8 and, in particular, to the basins of attraction of its 8 stable fixed points given by the periodic points of the attracting cycle C. As we show in Fig.56b, such basins, well separated in a portion of the phase-space, are instead strongly intermingled in the area occupied by the transversal crossing of the two manifolds, denoting the existence of infinitely many repelling cycles which cause an erratic behaviour of the trajectories converging to the different fixed points.

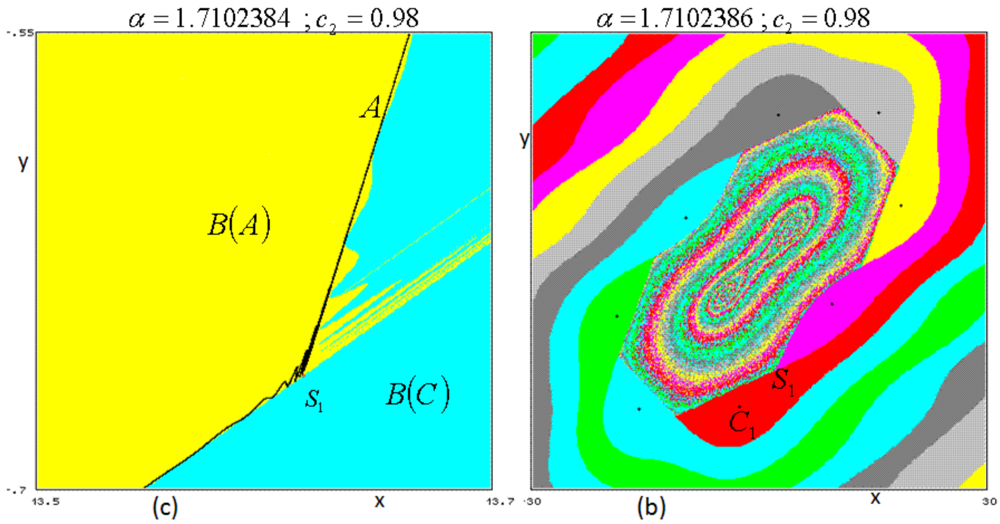

Fig.56

The existence of the $\mathcal{R}$ has important effects on the long run behaviour of the trajectories starting from the area occupied by the chaotic repellor, since they have a very long transient part before to reach the period 8 oscillations.

The effects of the observed heteroclinic tangle are illustrated in Fig.57: the attracting closed curve Γ disappears, or better, it comes into resonance with the cycle, forming an attracting set with the saddle S and the focus cycle C, with C the attractor within it. leaving the focus cycle C as unique attractor (Fig.57a). More precisely, Γ has been replaced by the heteroclinic connection of the periodic points of the cycles, made up by the unstable manifold of the saddle S which reach the periodic points of the focus cycle (Fig.57b).

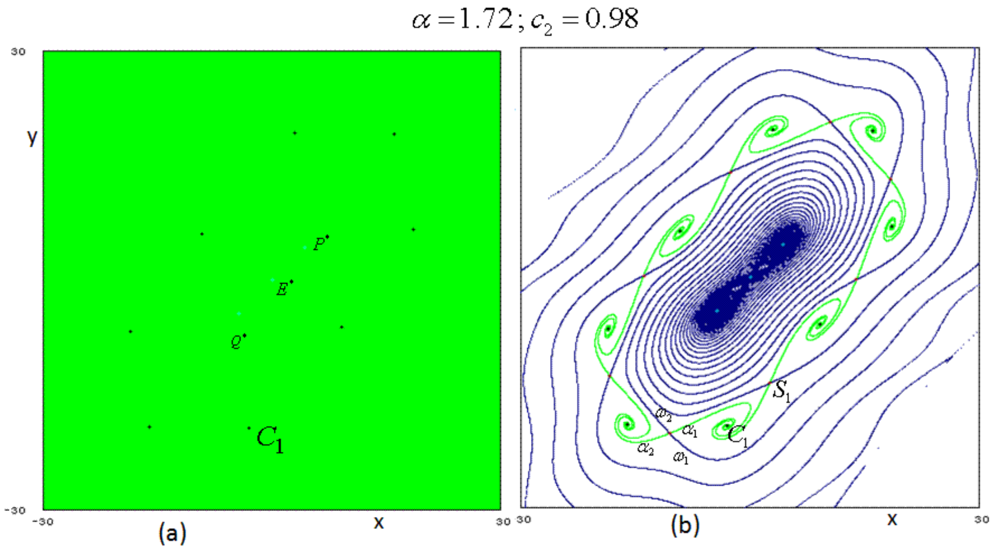

Fig.57

With a similar mechanism the final situation of Fig.54b is obtained. Indeed, increasing α the two outer branches α_2 and ω_2 approach each other, oscillating. This is the prelude to a new heteroclinic tangle, still occurring in a very small range of the parameter α: the first tangential contact between the unstable branch $\alpha_{2,i}$ of the periodic point S_i and the stable branch $\omega_{2,j}$ of a different periodic point S_j is followed by their transversal crossing and then by the homoclinic tangency occurring at the opposite side with respect to the previous one (as illustrated in Fig.58).

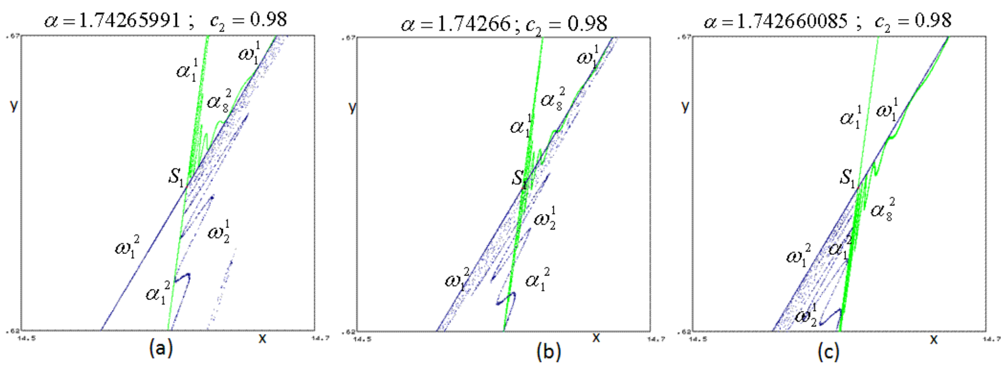

Fig.58

In the area occupied by the transversal crossing of the invariant sets, a chaotic repellor appears at the first homoclinic tangency (see Fig.59a), persists during the transversal crossing phase and disappears at the closing of the tangle: consequently, the trajectories starting close to it have a longer transient part before converging to the period 8 cycle. But the main effect of this global bifurcation is the appearance of an attracting closed curve $\widetilde{\Gamma}$, which replaces the heteroclinic connection between the periodic points of the cycles S and C. As soon as it has appeared, it exhibits many oscillations, as shown in Fig.59b obtained at the same parameter value as Fig.58c, and surrounds the periodic points of the attracting cycle. As α increases, $\widetilde{\Gamma}$ becomes smoother and smoother reaching the shape of Fig.54b.

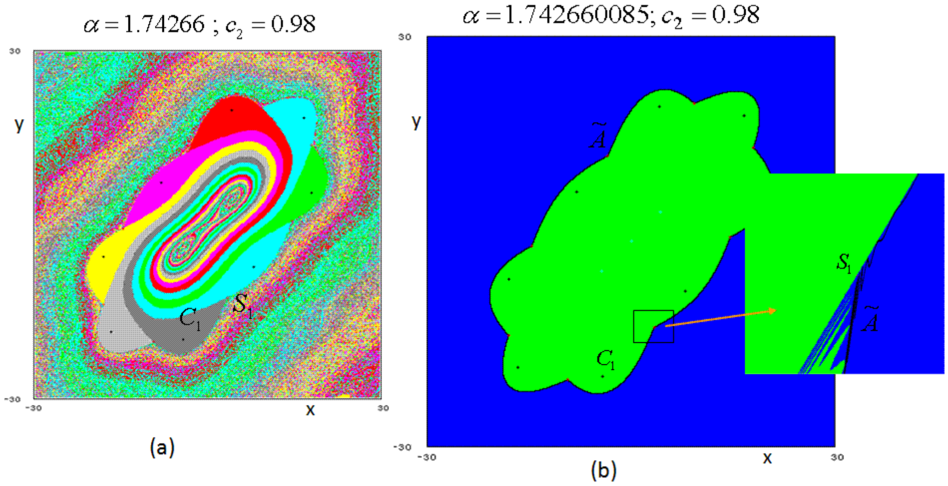

Fig.59

To sum up, we qualitatively describe the sequence of bifurcations causing the transition from an attracting closed invariant curve with a pair of cycles outside it, a saddle and an attracting one, into another wider attracting closed invariant curve, occurring via heteroclinic loops of the saddle. Let us consider the situation described in Fig.60. In Fig.60a we have an attracting closed invariant curve Γ_a, and a pair of cycles that have been created via a saddle-node bifurcation outside Γ_a. Such external cycles do not form an heteroclinic connection, whereas the stable set of the saddle S bounds the basin of attraction of the related attracting fixed points C_i of the map T^k. The unstable branches $\alpha_{1,i}$ of S_i tend to the attracting curve Γ_a, while the unstable branches $\alpha_{2,i}$ of S_i tend to the attracting cycle. At the bifurcation (Fig.60b) we may have that the closed invariant curve Γ_a merges with the unstable branches $W_1^U(S) = \cup\alpha_{1,i}$ and with the stable ones $W_1^S(S) = \cup\omega_{1,i}$ as well, in a *heteroclinic loop*, or tangle, of the saddle S, causing the disappearance of the attracting closed invariant curve Γ_a, and leaving another closed invariant curve, see Fig.60c, which is now the heteroclinic connection

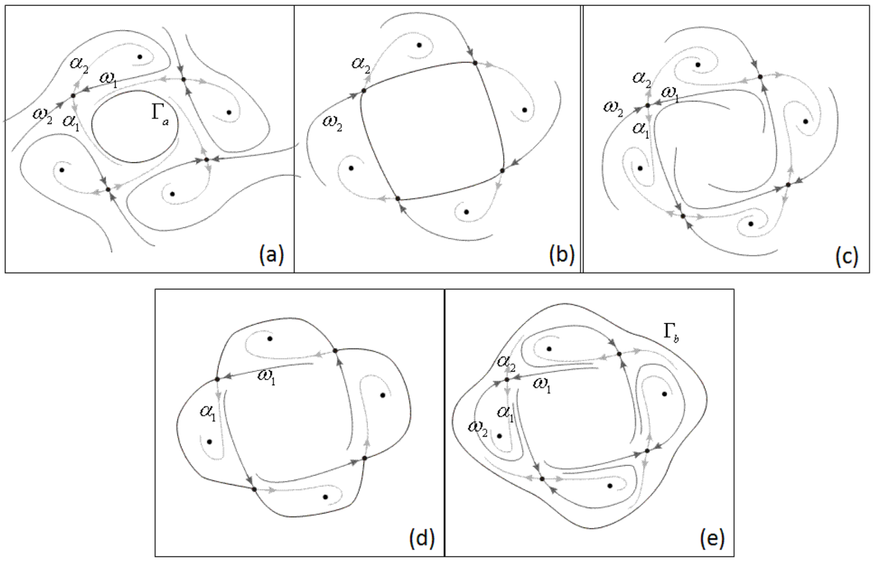

Figure 1: Fig.60

involving the saddle S and the related attracting cycle C. After the bifurcation of the heteroclinic loop a closed curve still exists, but differently from Γ_a it includes the two cycles on it (Fig.60c).

Starting from this situation, a second heteroclinic loop (or tangle) may be formed. The heteroclinic connection turns into a heteroclinic loop in which the unstable branches $W_2^U(S) = \cup\alpha_{2,i}$ merge with the stable ones $W_2^S(S) = \cup\omega_{2,i}$ (see Fig.60d). After the bifurcation a new closed attracting curve exists, say Γ_b, and the two cycles are both inside Γ_b (Fig.60e). The stable set of the saddle S separates the basins of attraction of the k attracting fixed points C_i of the map T^k. The unstable branches $\cup\alpha_{1,i}$ tend to the attracting cycle while the unstable branches $\cup\alpha_{2,i}$ tend to Γ_b.

As we have seen, in the case of discrete dynamical systems, the dynamic behaviors more frequently observed is such that the heteroclinic loop of Figs.60b,d are replaced by homoclinic tangles. That is, a tangency occurs between the two manifolds involved in the bifurcation, followed by transverse intersections and a tangency again on the opposite side, after which all the homoclinic points of the saddle S, existing during the tangle, are destroyed.

It is worth noticing that all the unstable periodic points associated with the first homoclinic tangle, due to $W_1^U(S) \cap W_1^S(S) \neq \emptyset$, are in the region interior to the set of periodic points of the saddle S, whereas in the strange repellor associated with the second homoclinic tangle, in which $W_2^U(S) \cap W_2^S(S) \neq \emptyset$, all the unstable cycles are "outside" the saddle cycle S. Notice also that before the first heteroclinic loop (tangle) of Fig.60 we have two distinct attracting sets: Γ_a and the stable $k-$cycle outside it; after the second one of Fig.60, we have again two distinct attractors: Γ_b, which is wider than Γ_a, and the $k-$cycle inside it, while between the two heteroclinic loops only one attractor may survive, that is the k-cycle.

9 Basin of attraction and related contact bifurcations.

In this section we recall some definitions and properties associated with the basins of attractiong sets. Let us consider an $m-$dimensional map $x' = T(x)$ and an invariant attracting set $A \subset \mathbb{R}^m$ (thus it is mapped into itself, $T(A) = A$, i.e. if $x \in A$ then $T^n(x) \in A$ for any $n > 0$). As already defined, the *Basin of attraction of* A is the set of all the points that generate trajectories converging to A

$$\mathcal{B}(A) = \{x | T^n(x) \rightarrow A \quad \text{as } n \rightarrow +\infty\}. \tag{27}$$

Starting from the definition of attracting set, let $U(A)$ be a neighborhood of a A whose points converge to A. Of course $U(A) \subseteq \mathcal{B}(A)$, but note that also the points of the phase space which are mapped inside U after a finite number of iterations belong to $\mathcal{B}(A)$. Hence, the *total basin of* A (or briefly the basin of A) is given by

$$\mathcal{B}(A) = \bigcup_{n=0}^{\infty} T^{-n}(U(A)), \tag{28}$$

9.1 One-dimensional maps

Let us start with one-dimensional, continuous and noninvertible maps, to we illustrate how non-connected basins of attraction arise. Furthermore, we show how the global bifurcations that cause their qualitative changes can be described in terms of contacts between critical points and the basins' boundaries.

Let us first take a look at iterated invertible maps though. If $f : I \rightarrow I$ is a continuous and increasing function, then the only invariant sets are the fixed points (as already remarked in Section 1). When many fixed points exist, say $x_1^* < x_2^* < ... < x_k^*$, they are alternatingly stable and unstable: the unstable fixed points are the boundaries that separate the basins of the stable ones. Starting from an initial condition where the graph of f is above the diagonal, i.e. $f(x_0) > x_0$, the generated trajectory is an increasing sequence converging to the stable fixed point on the right, or it is diverging to $+\infty$. On the other hand, starting from an initial condition such that $f(x_0) < x_0$, the trajectory is a decreasing sequence converging to the fixed point on the left, or it is diverging to $-\infty$ (see Fig.61a, where p^* is a stable fixed point, and its basin is bounded by two unstable fixed points q^* and r^*, where $q^* < p^*$ and $r^* > p^*$). If $f : I \rightarrow I$ is a continuous and decreasing map, the only possible invariant sets are one fixed point and cycles of period 2. Periodic points of the cycles of period 2 are located around the fixed point, the unstable ones being boundaries of the basins of the stable ones (see Fig.61b, where a stable fixed point x^* exists, and its basin is bounded by the periodic points α_1, α_2 of an unstable cycle of period 2).

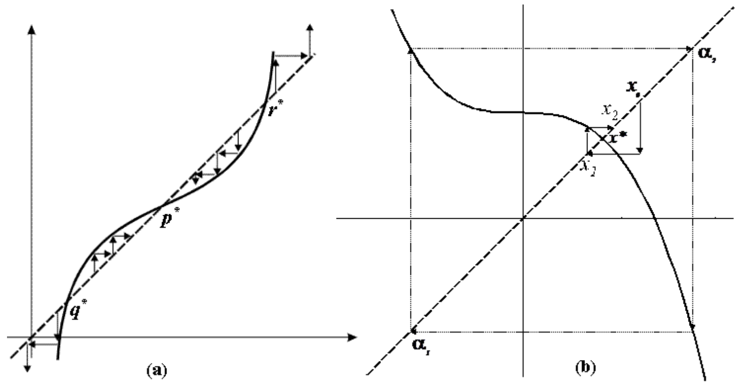

Fig.61

In general, in the case of one-dimensional invertible maps the only kinds of attractors are fixed points and cycles of period two. In the first case, the basin is an open interval which includes the fixed point, and in the second case, the basin is the union of two open intervals, each one including an attracting periodic point.

Obviously, if the map is invertible, the basins of the attracting sets are simple. This may be no longer true if the map is noninvertible. In this case the structure of a basin may be very complicated. Non-connected portions of the basins may be created, given by open intervals that do not include any point of the related attractor. As a first example, let us consider the logistic map (3) (Fig.8 of Section2), a noninvertible $Z_0 - Z_2$ map whose graph is represented again in Fig.62.

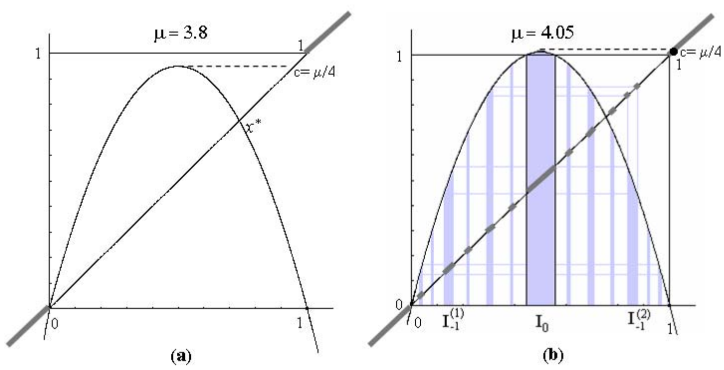

Fig.62

For $\mu < 4$ every initial condition $x_0 \in (0, 1)$ generates bounded sequences, converging to a unique attractor A (which may be the fixed point $x^* = (\mu - 1)/\mu$ or a more complex attractor, periodic or chaotic). Initial conditions out of the interval $[0,1]$ generate sequences diverging to $-\infty$. The boundary that separates the basin of attraction $\mathcal{B}(A)$ of the attractor A, from the basin $\mathcal{B}(\infty)$ is formed by the unstable fixed point $q^* = 0$ and its rank-1 preimage (different from itself), $q^*_{-1} = 1$. Observe that, of course, a fixed point is always preimage of itself, but in this case also another preimage exists because $q^* \in Z_2$. If $\mu < 4$, as in Fig.62a, then $q^*_{-1} > c = \mu/4$, where c is the critical point (maximum) that separates Z_0 and Z_2. Hence, $q^*_{-1} \in Z_0$. When we increase μ, at $\mu = 4$ we have $q^*_{-1} = c = 1$, and a contact between the critical point and the basin boundary occurs. This is a global bifurcation, which changes the structure of the basin (really it destroys the basin). For $\mu > 4$ (Fig.62b) we have $q^*_{-1} < c$, and the portion $\left(q^*_{-1}, c\right)$ of $\mathcal{B}(\infty)$ enters Z_2. This implies that new preimages of that portion are created, which belong to $\mathcal{B}(\infty)$ according to (28). As we know, almost everything will then belong to the basin of divergent trajectories, the only points which are left on the interval I are the points belonging to the chaotic invariant set Λ, as described in Section 2 (on which the restriction of the map is still chaotic).

A similar situation occurs for a unimodal $Z_0 - Z_2$ map where the attractor at infinity is replaced by an attracting fixed point, as the one shown in Fig.63a. As in the previous example, we have an attractor A, which may be the fixed point x^* (or some other invariant set around it), with a simply connected basin bounded by the unstable fixed point q^* and its rank-1 preimage q^*_{-1}. This example differs with respect to the previous one in so far as in this case initial conditions taken in the complementary set generate trajectories converging to the stable fixed point z^*. This means that the basin $\mathcal{B}(z^*)$ is formed by the union of two non-connected portions: $B_0 = (-\infty, q^*) \subset Z_2$, which contains z^* (it is usually called *immediate basin*, the largest connected component of the basin which contains the attractor) and $B_1 = \left(q^*_{-1}, +\infty\right) = f^{-1}(B_0) \subset Z_0$. In Fig.63a the two non-connected portions of the basin $\mathcal{B}(z^*)$ are marked by bold lines. Interesting effects occur, if some parameter variation causes an increase of the critical point c (maximum value) until it crosses the basin boundary q^*_{-1}. If this happens, the interval (q^*_{-1}, c), which is part of B_1, enters Z_2, and infinitely many non-connected portions of $\mathcal{B}(z^*)$ emerge in the interval (q^*, q^*_{-1}). Note that the total basin can still be expressed as the union of all the preimages of any rank of the immediate basin B_0.

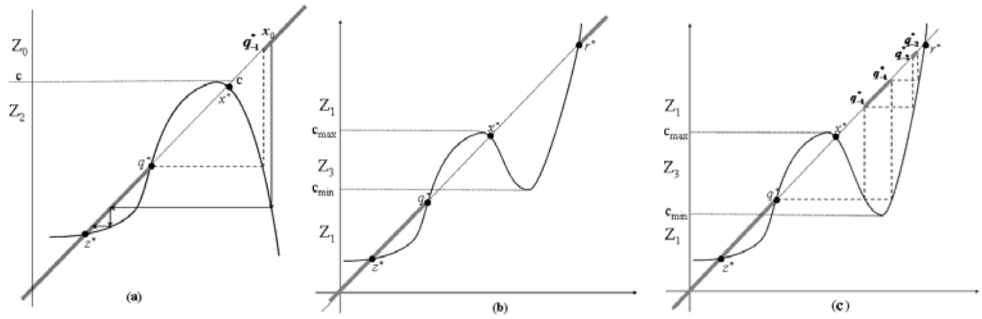

Fig.63

Another interesting situation is obtained if we change the right branch of the map of Fig.63a by folding it upwards such that another critical point, a minimum, is created. Such a situation is shown in Fig.63b. This is a noninvertible $Z_1 - Z_3 - Z_1$ map, where Z_3 is the portion of the codomain bounded by the relative minimum value $c_{\min}$ and relative maximum value $c_{\max}$. In the situation shown in Fig.63b we have three attractors: the fixed point z^*, with $\mathcal{B}(z^*) = (-\infty, q^*)$, the attractor A around x^*, with basin $\mathcal{B}(A) = (q^*, r^*)$ bounded by two unstable fixed points, and $+\infty$ (i.e. positively diverging trajectories) with basin $\mathcal{B}(+\infty) = (r^*, +\infty)$. In this case all the basins are immediate basins, each being given by an open interval. In the situation shown in Fig.63b, both basin boundaries q^* and r^* are in Z_1, so they have only themselves as unique preimages (like for an invertible map). However, the situation drastically changes if, for example, some parameter changes causes the minimum value $c_{\min}$ to move downwards, until it goes below q^* (as in Fig.63c). After the global bifurcation, when $c_{\min} = q^*$, the portion $(c_{\min}, q^*)$ enters Z_3, so new preimages $f^{-k}(c_{\min}, q^*)$ appear with $k \geq 1$. These preimages constitute non-connected portions of $\mathcal{B}(z^*)$ nested inside $\mathcal{B}(A)$, and are represented by the thick portions of the diagonal in Fig.63c.

9.2 Two-dimensional maps.

To better understand the subject, we consider a first example taken from Bischi and Kopel [22]: a dynamic duopoly game in the tradition of Cournot. In contrast to the early models on oligopoly dynamics, in their model players form adaptive expectations and players' reaction functions are unimodal. This framework gives rise to a situation of multistability, where the basins of each stable Nash equilibrium is a rather complicated set. The second example presents a dynamic brand competition model proposed by Bischi, Gardini and Kopel [21]. In this game a unique and stable fixed point exists, but the basin of the fixed point can have a very complicated structure. Several other examples may be fowd in [89], [2], [96], [97].

9.2.1 Example 1: Quantity-setting duopoly games with adaptive expectations

The first example we present is a dynamic Cournot duopoly game with unimodal reaction functions. The two quantity-setting firms produce homogeneous goods and, since they do not know the competitor's output, they try to predict this quantity using an adaptive scheme. Let $x_1(t)$ and $x_2(t)$ be the outputs at time period t. The two players determine their production quantities of the next period, $x_1(t+1)$ and $x_2(t+1)$, by solving the optimization problems

$$\underset{x_1}{Max}\, \Pi_1\left(x_1, x_2^e(t+1)\right); \ \underset{x_2}{Max}\, \Pi_2\left(x_1^e(t+1), x_2\right) \tag{29}$$

where Π_i is the profit of player i, and $x_i^e(t+1), i=1,2$ represent the predictions for the output of the competitor. The solutions of the optimization problems (assumed to be unique) are denoted by

$$\begin{array}{l} x_1(t+1) = r_1\left(x_2^e(t+1)\right) \\ x_2(t+1) = r_2\left(x_1^e(t+1)\right) \end{array} \tag{30}$$

where r_1 and r_2 are called the *Best Replies* (or reaction functions). In the original work of Cournot [26], as well as in much of the literature which followed, *naive expectations* $x_i^e(t+1) = x_i(t)$ have been considered. Under the assumption of naive expectations each firm expects or predicts that the quantity offered by the competitor in the next period will be the same as in the current period. The time evolution of the duopoly system is then represented by the two-dimensional discrete dynamical system

$$\left(x_1(t+1), x_2(t+1)\right) = \left(r_1\left(x_2(t)\right), r_2\left(x_1(t)\right)\right) \tag{31}$$

which is also referred to as the *Cournot tâtonnement process*. In contrast to this, in Bischi and Kopel [22] firms are assumed to revise their beliefs according to the adaptive expectations scheme

$$\begin{array}{l} x_1^e(t+1) = x_1^e(t) + \alpha_1\left(x_1(t) - x_1^e(t)\right) \\ x_2^e(t+1) = x_2^e(t) + \alpha_2\left(x_2(t) - x_2^e(t)\right) \end{array} \tag{32}$$

If the relations (30) are inserted into (32), one gets the following two-dimensional dynamical system in the belief space

$$\begin{array}{l} x_1^e(t+1) = (1-\alpha_1)\, x_1^e(t) + \alpha_1 r_1\left(x_2^e(t)\right) \\ x_2^e(t+1) = (1-\alpha_2)\, x_2^e(t) + \alpha_2 r_2\left(x_1^e(t)\right) \end{array}. \tag{33}$$

Of course, the quantities chosen by the competitors can be obtained by the transformations $x_1(t) = r_1\left(x_2^e(t)\right)$, $x_2(t) = r_2\left(x_1^e(t)\right)$, i.e. by a mapping from the belief space into the action space. The fixed points of the dynamical system (33), defined by $x_i^e(t+1) = x_i^e(t)$, $i = 1, 2$, i.e.

$$\begin{aligned} x_1^e(t) &= r_1\left(x_2^e(t)\right) \\ x_2^e(t) &= r_2\left(x_1^e(t)\right) \end{aligned} \tag{34}$$

are located at the intersections of the two reaction curves and are independent of the adjustment coefficients α_1 and α_2. In other words, a fixed point is a situation where beliefs are not further revised and quantities do not change, and at the fixed points the expected outputs coincide with the realized ones. Hence, in belief space we are considering a situation where beliefs are consistent and this corresponds to a Nash equilibrium in the quantity space. In Bischi and Kopel [22] the following reaction functions have been considered

$$\begin{aligned} r_1(x_2) &= \mu_1 x_2\left(1 - x_2\right) \\ r_2(x_1) &= \mu_2 x_1\left(1 - x_1\right) \end{aligned} \tag{35}$$

It has been shown elsewhere (see Kopel, [69]) that if the competitors regard their products as strategic complements over a certain range of the set of admissible actions, the functions given in (35) can be derived as Best Responses, and the parameters μ_i, $i = 1, 2$ measure the intensity of the positive externality the actions of one player exert on the payoff of the other player.

To simplify the notation, we rename the expected outputs by setting $x(t) = x_1^e(t)$ and $y(t) = x_2^e(t)$. Inserting the reaction functions specified in (35) into (33), the time evolution of the competitors' beliefs is obtained by the iteration of the two-dimensional map $T : (x, y) \to (x', y')$ defined by

$$\begin{aligned} x' &= (1 - \alpha_1)\, x + \alpha_1 \mu_1 y\,(1 - y) \\ y' &= (1 - \alpha_2)\, y + \alpha_2 \mu_2 x\,(1 - x) \end{aligned} \tag{36}$$

Under the assumption $\mu_1 = \mu_2 = \mu$, the fixed points can be expressed by simple analytical expressions: besides the trivial solution $O = (0, 0)$, a positive symmetric equilibrium exists for $\mu > 1$, given by $S = ((\mu - 1)/\mu, (\mu - 1)/\mu)$. Two further equilibria $E_1 = (\bar{x}, \bar{y})$ and $E_2 = (\bar{y}, \bar{x})$ exist for $\mu > 3$, where $\bar{x} = \left(\mu + 1 + \sqrt{\psi}\right)/2\mu$, $\bar{y} = \left(\mu + 1 - \sqrt{\psi}\right)/2\mu$ with $\psi = (\mu + 1)(\mu - 3)$. These equilibria are located in symmetric positions with respect to the diagonal Δ. The corresponding Nash equilibria have the same entries. As shown in Bischi and Kopel [22], a wide range of parameters μ, α_1, α_2 exists such that E_1 and E_2 are both stable. Accordingly, a problem of equilibrium selection arises, which leads to the question of the delimitation of the two basins of attraction $\mathcal{B}(E_1)$ and $\mathcal{B}(E_2)$.

As already remarked, the properties of the inverses of the map become important in order to understand the structure of the basins and their qualitative changes. The map (36) is a noninvertible map. This can be deduced from the fact that given a point $(x', y') \in \mathbb{R}^2$, its rank-1 preimages may be up to four; they can be computed by solving the fourth degree algebraic system (36) with respect to x and y. The critical curves are computed as follows: LC_{-1} coincides with the set of points in which the Jacobian determinant vanishes, i.e. $\det J_T = 0$, where

$$J_T(x,y) = \begin{bmatrix} 1-\alpha_1 & \alpha_1\mu_1(1-2y) \\ \alpha_2\mu_2(1-2x) & 1-\alpha_2 \end{bmatrix} \tag{37}$$

and $LC = T(LC_{-1})$. So, LC_{-1} is an equilateral hyperbola, of equation

$$\left(x-\frac{1}{2}\right)\left(y-\frac{1}{2}\right) = \frac{(1-\alpha_1)(1-\alpha_2)}{4\alpha_1\alpha_2\mu_1\mu_2}. \tag{38}$$

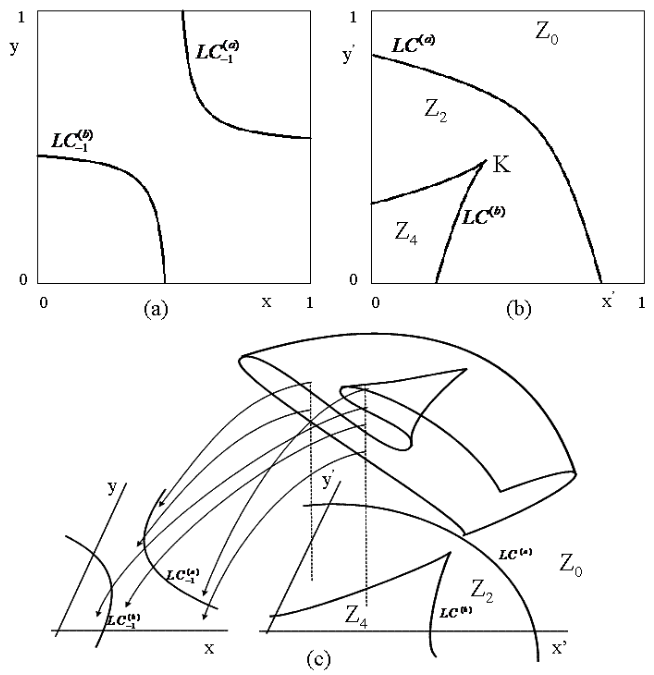

Fig.64

Since LC_{-1} is formed by the union of two disjoint branches, say $LC_{-1} = LC^{(a)}_{-1} \cup LC^{(b)}_{-1}$, it follows that also $LC = T(LC_{-1})$ is the union of two branches, say $LC^{(a)} = T(LC^{(a)}_{-1})$ and $LC^{(b)} = T(LC^{(b)}_{-1})$, see Figs.64a,b. The branch $LC^{(a)}$ separates the region Z_0, whose points have no preimages, from the region Z_2, whose points have two distinct rank-1 preimages. The other branch $LC^{(b)}$ separates the region Z_2 from Z_4, whose points have four distinct preimages. Any point of $LC^{(a)}$ has two coincident rank-1 preimages, located at a point of $LC^{(a)}_{-1}$, and any point of

$LC^{(b)}$ has two coincident rank-1 preimages, located at a point of $LC_{-1}^{(b)}$, plus two further distinct rank-1 preimages, called *extra preimages*. Following the terminology of Mira et al. [89], we say that the map (36) is a noninvertible map of $Z_4 > Z_2 - Z_0$ type, where the symbol ">" denotes the presence of a cusp point in the branch $LC^{(b)}$ (see Fig.64b). The corresponding *Riemann foliation* is shown in Fig.64c. Different sheets are connected by folds joining two sheets, and the projections of such folds on the phase plane are arcs of LC. The cusp point of LC is characterized by three merging preimages at the junction of two folds.

In order to study the structure of the basins and explain the global bifurcations that change their qualitative properties, we first consider the symmetric case of players with homogeneous expectations, i.e. $\alpha_1 = \alpha_2 = \alpha$. In this case, the map (36) has a symmetry property, as it remains the same if the variables x and y are swapped. Formally, we have $T(P(x,y)) = P(T(x,y))$, where $P : (x,y) \to (y,x)$ is the reflection through the diagonal $\Delta = \{(x,x), x \in \mathbb{R}\}$. This symmetry property implies that the diagonal Δ is a trapping subspace for the map T, i.e. $T(\Delta) \subseteq \Delta$. The trajectories embedded in Δ are governed by the restriction of the two-dimensional map T to Δ, i.e. $f = T|_\Delta : \Delta \to \Delta$. The map f, obtained by setting $x = y$ and $x' = y'$ in (36), is given by $x' = f(x) = (1 + \alpha(\mu - 1))x - \alpha\mu x^2$. In the symmetric case of homogeneous players we can give a complete analytical characterization of the global bifurcation that transforms the basins from simply connected sets to multiply connected. In fact, the following result is given in Bischi and Kopel [22]:

If $\mu_1 = \mu_2 = \mu$ and $\alpha_1 = \alpha_2 = \alpha$ and the equilibria E_1 and E_2 are both stable, then the common boundary $\partial\mathcal{B}(E_1) \cap \partial\mathcal{B}(E_2)$ which separates the basin $\mathcal{B}(E_1)$ from the basin $\mathcal{B}(E_2)$ is given by the stable set $W^s(S)$ of the saddle point S. If $\alpha(\mu+1) < 1$ then $W^s(S) = OO_{-1}^{(1)}$, where $O = (0,0)$ and $O_{-1}^{(1)} = \left(\frac{1+\alpha(\mu-1)}{\alpha\mu}, \frac{1+\alpha(\mu-1)}{\alpha\mu}\right)$, and the two basins are simply connected sets. If $\alpha(\mu+1) > 1$ then the two basins are non-connected sets, formed by infinitely many simply connected components.

The bifurcation occurring at $\alpha(\mu+1) = 1$ is a *global bifurcation*. It cannot be revealed by a study of the linear approximation of the dynamical system and the occurrence of such a bifurcation can be characterized by a contact between the stable set of the symmetric fixed point S and a critical curve. In order to explain this, we start from a set of parameters such that both of the basins are simply connected, like in Fig.65a, where $\mu_1 = \mu_2 = \mu = 3.4$ and $\alpha_1 = \alpha_2 = \alpha = 0.2 < 1/(\mu+1)$. For this set of parameters, four fixed points exist, indicated by O, S, E_1 and E_2. The fixed points O and S are saddle points, whereas the Nash equilibria E_1

and E_2 are both stable, each with its own basin of attraction. These basins, $\mathcal{B}(E_1)$ and $\mathcal{B}(E_2)$, are represented by white and light grey respectively (the dark grey region represents the set of initial conditions which generate unbounded trajectories; we could refer to this set as the basin of infinity). In this situation, any bounded trajectory starting with $x_1^e(0) > x_2^e(0)$ ($x_1^e(0) < x_2^e(0)$) converges to E_1 (E_2). In economic terms this means that an initial difference in the expectations of the competitors uniquely determines which of the equilibria is selected in the long run. Expectations of the players become self-fulfilling: if $x_1^e(0) > x_2^e(0)$ ($x_1^e(0) < x_2^e(0)$) then $x_1^e(t) > x_2^e(t)$ ($x_1^e(t) < x_2^e(t)$) for any t and equilibrium E_1, where firm 1 dominates the market (equilibrium E_2 at which firm 2 dominates the market) is selected in the long run. In contrast to this, the situation shown in Fig.65b, where the value of the parameter μ is the same, but $\alpha_1 = \alpha_2 = 0.5 > 1/(\mu+1)$, is quite different. In fact, in this case the basins are no longer simply connected sets. Many portions of each basin are present, both in the region above and below the diagonal, and the adjustment process of our dynamic game starting with initial beliefs $x_1^e(0) > x_2^e(0)$ (or $x_1^e(0) < x_2^e(0)$) may lead to convergence to either of the equilibria.

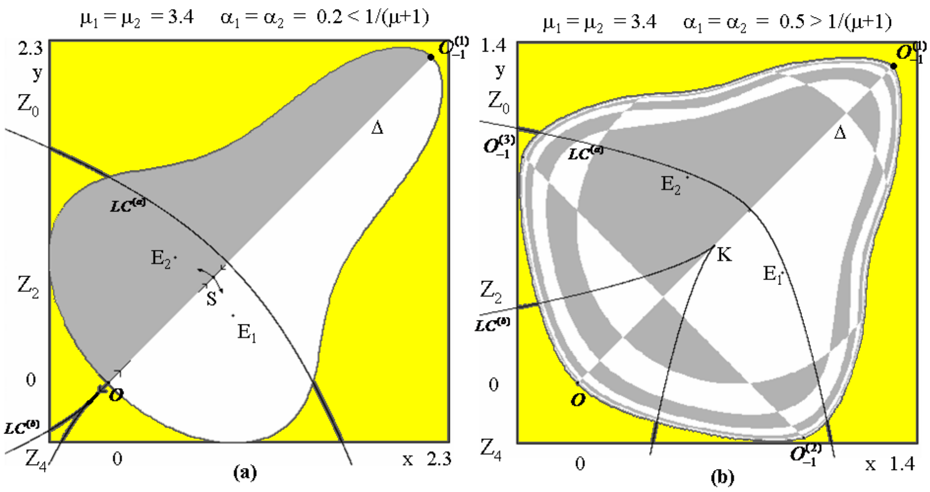

Fig.65

Now let us turn to an explanation of the global bifurcation which causes the transition between these rather different structures of the basins. First notice that the boundary separating $\mathcal{B}(E_1)$ and $\mathcal{B}(E_2)$ contains the symmetric equilibrium S as well as its whole stable set $W^s(S)$. In fact, just after the creation of the two stable fixed points E_1 and E_2 for $\mu = 3$, the symmetric equilibrium $S \in \Delta$ is a saddle point. The two branches of the unstable set $W^u(S)$ departing from it reach E_1 and E_2 respectively. Hence, since a basin boundary is backward invariant (see

Mira et al., [89], [88]), not only the local stable set $W^s_{loc}(S)$ belongs to the boundary that separates the two basins, but also its preimages of any rank: $W^s(S) = \bigcup_{k\geq 0} T^{-k}\left(W^s_{loc}(S)\right)$. Because of the symmetry property of the system (36) with homogeneous players, the local stable set of S belongs to the invariant diagonal Δ. As long as $\alpha\,(\mu+1) < 1$, the whole stable set $W^s(S)$ belongs to Δ and is given by $W^s(S) = OO^{(1)}_{-1}$, where $O^{(1)}_{-1}$ is the preimage of O located along Δ. Observe that if $\alpha\,(\mu+1) < 1$ holds, the cusp point K of the critical curve $LC^{(b)}$ has negative coordinates and, consequently, the whole segment $OO^{(1)}_{-1}$ belongs to the regions Z_0 and Z_2, see Fig.65a. This implies that the two preimages of any point of $OO^{(1)}_{-1}$ belong to Δ (they can be computed by the restriction f of T to the invariant diagonal Δ). This proves that the segment $OO^{(1)}_{-1}$ is backward invariant, i.e. it includes all its preimages. The structure of the basins $\mathcal{B}\,(E_i)$, $i = 1, 2$, is very simple: $\mathcal{B}\,(E_1)$ is entirely located below the diagonal Δ and $\mathcal{B}\,(E_2)$ is entirely located above it. Both of the basins $\mathcal{B}\,(E_1)$ and $\mathcal{B}\,(E_2)$ are simply connected sets.

Their structure becomes a lot more complex for $\alpha\,(\mu+1) > 1$. In order to understand the bifurcation occurring at $\alpha\,(\mu+1) = 1$, we consider the critical curves of the map (36). At $\alpha\,(\mu+1) = 1$ a contact between $LC^{(b)}$ and the fixed point O occurs, due to the merging between O and the cusp point K.[8] For $\alpha\,(\mu+1) > 1$, the portion KO of $W^S_{loc}\,(S)$ belongs to the region Z_4, where four inverses of T exist. This implies that besides the two rank-1 preimages on Δ, the points of KO have two further preimages, which are located on the segment $O^{(2)}_{-1}O^{(3)}_{-1}$ of the line Δ_{-1}. Since $OO^{(1)}_{-1} = W^s_{loc}(S) \subset \partial\mathcal{B}\,(E_1) \cap \partial\mathcal{B}\,(E_2)$, also its preimages of any rank belong to the boundary which separates $\mathcal{B}\,(E_1)$ from $\mathcal{B}\,(E_2)$. So the rank-1 preimages of the segment $O^{(2)}_{-1}O^{(3)}_{-1}$, which exist because portions of it are included in the regions Z_2 and Z_4, belong to $W^s\,(S)$ as well, being preimages of rank-2 of $OO^{(1)}_{-1}$. This repeated procedure, based on the iteration of the multi-valued inverse of T, leads to the construction of the whole stable set $W^s(S)$.

Similar results can be obtained in the case of heterogeneous players,

[8] To compute the coordinates of the cusp point of $LC^{(b)}$ notice that in any point of LC_{-1} at least one eigenvalue of DT vanishes. In the point $C_{-1} = LC^{(a)}_{-1} \cap \Delta = (c_{-1}, c_{-1})$, with $c_{-1} = (\alpha\,(\mu-1)+1)\,/2\alpha\mu$, the eigenvalue $z_{\parallel}$ with eigendirection along Δ vanishes, and its image $C = LC^{(a)} \cap \Delta = (c, c)$ with $c = f(c_{-1}) = (\alpha\,(\mu-1)+1)^2\,/4\alpha\mu$ is the point at which $LC^{(a)}$ intersects Δ. This corresponds to the unique critical point of the restriction of T to Δ. At the other intersection of LC_{-1} with Δ, given by $K_{-1} = LC^{(b)}_{-1} \cap \Delta = (k_{-1}, k_{-1})$ with $k_{-1} = (\alpha\,(\mu-1)-1)\,/2\alpha\mu$ the eigenvalue $z_{\perp}$ vanishes, and the curve $LC^{(b)} = T(LC^{(b)}_{-1})$ has a *cusp point* (see e.g. Arnold et al., 1986) $K = LC^{(b)} \cap \Delta = (k, k)$ with $k = f(k_{-1}) = (\alpha\,(\mu+1)-1)\,(\alpha\mu+3(1-\alpha))\,/4\alpha\mu$

where the heterogeneity arises e.g. due to different speeds of adjustment $\alpha_1 \neq \alpha_2$. The main difference with respect to the homogeneous case lies in the fact that the diagonal Δ is no longer invariant. Even if the fixed points remain the same, the basins are no longer symmetric with respect to Δ. Nevertheless, many of the arguments given above continue to hold in the case of heterogeneous beliefs. In particular, the boundary which separates the basin of equilibrium E_1 from that of E_2 is still formed by the whole stable set $W^s(S)$, but in the case $\alpha_1 \neq \alpha_2$ the local stable set $W^s_{loc}(S)$ is not along the diagonal Δ. The contact between $W^s(S)$ and $LC^{(b)}$, which causes the transition from simple to complex basins, does not occur at O (since now $O \notin W^s(S)$) and no longer involves the cusp point of $LC^{(b)}$. So, the parameter values at which such contact bifurcations occur cannot be computed analytically.

In Fig.66a, obtained with $\mu = 3.6$, $\alpha_1 = 0.55$ and $\alpha_2 = 0.7$, the two equilibria E_1 and E_2 are stable, and their basins are connected sets. An asymmetry in the expectation formation process has a negligible effect on the local stability properties of the equilibria, but it results in an evident asymmetry in the basins of attraction. As shown in Fg.66a, when $\alpha_2 > \alpha_1$ the extension of $\mathcal{B}(E_2)$ is, in general, greater than the extension of $\mathcal{B}(E_1)$.

Moreover, the situation is not always as simple as in Fig.66a. The symmetric equilibrium S is a saddle fixed point and is included in the boundary – the whole stable set $W^s(S)$ – which separates the two basins. It can be noticed that in the simple situation shown in Fig.66a, the whole stable set $W^s(S)$ is entirely included inside the regions Z_2 and Z_0. However, the fact that a portion of $W^s(S)$ is close to LC suggests that a contact bifurcation may occur if, e.g., the adjustment coefficients are slightly changed. In fact, if a portion of $\mathcal{B}(E_1)$ enters Z_4 after a contact with $LC^{(b)}$, new rank-1 preimages of that portion will appear near $LC^{(b)}_{-1}$. This is the situation illustrated in Fig.66b, obtained after a small change of α_1. The portion of $\mathcal{B}(E_1)$ inside Z_4 is denoted by H_0. It has two rank-1 preimages, denoted by $H^{(1)}_{-1}$ and $H^{(2)}_{-1}$, which are located at opposite sides with respect to $LC^{(b)}_{-1}$ and merge on it (by definition the rank-1 preimages of the arc of $LC^{(b)}$ which bound H_0 must merge along $LC^{(b)}_{-1}$). The set $H_{-1} = H^{(1)}_{-1} \cup H^{(2)}_{-1}$ constitute a non-connected portion of $\mathcal{B}(E_1)$. Moreover, since H_{-1} belongs to the region Z_4, it has four rank-1 preimages, denoted by $H^{(j)}_{-2}$, $j = 1, ..., 4$ in Fig.66b, which constitute other four "islands"[9] of $\mathcal{B}(E_1)$. Points of these "islands" are mapped into H_0 after two iterations of the map T. Indeed, infinitely many higher rank preimages of H_0 exist, thus giving infinitely many smaller and smaller

[9] We follow the terminology introduced in Mira et al. 1994 [88].

disjoint "islands" of $\mathcal{B}(E_1)$. Hence, at the contact between $W^s(S)$ and LC, the basin $\mathcal{B}(E_1)$ is transformed from a simply connected into a non-connected set, constituted by infinitely many disjoint components. The larger connected component of $\mathcal{B}(E_1)$ which contains E_1 is the *immediate basin* $\mathcal{B}_0(E_1)$, and the whole basin is given by the union of the infinitely many preimages of $\mathcal{B}_0(E_1)$: $\mathcal{B}(E_1) = \bigcup_{k\geq 0} T^{-k}(\mathcal{B}_0(E_1))$. Observe that even if small differences between the adjustment speeds have negligible effects on the properties of the attractors, they may cause remarkable asymmetries in the structure of the basins, which can only be detected when the global properties of the economic model are studied.

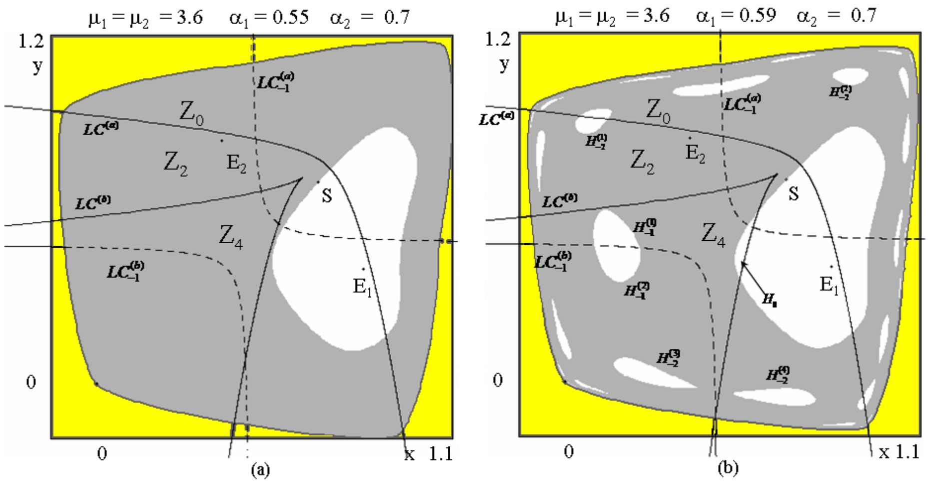

Fig.66

So, as in the one-dimensional case, the global bifurcation which causes a transformation of a basin from connected set into the union of infinitely many non-connected portions, is caused by a contact between a critical set and a basin boundary. However, since the equations of the curves involved in the contact often cannot be analytically expressed in terms of elementary functions, the occurrence of contact bifurcations can only be revealed numerically. This happens frequently in the study of nonlinear dynamical systems of dimension greater than one: results on global bifurcations are generally obtained through an interplay between theoretical and numerical methods, and the occurrence of these bifurcations is shown by computer-assisted proofs, based on the knowledge of the properties of the critical curves and their graphical representation. This "modus operandi" is typical in the study of global bifurcations of nonlinear two-dimensional maps.

9.2.2 Example 2: A rent-seeking/competition game

The second dynamic model we present is used to describe a market game where a population of consumers can choose between two brands of homogeneous goods which are produced by two competing firms. Let x_1 and x_2 represent the marketing efforts of two firms (e.g. advertising effort) and B the total sales potential of the market (in terms of customer market expenditures). If firm 1's effort is x_1 and firm 2's effort is x_2, then the shares of the market (in terms of sales) accruing to firm 1 and to firm 2 are Bs_1 and $Bs_2 = B - Bs_1$, where

$$s_1 = \frac{ax_1^{\beta_1}}{ax_1^{\beta_1} + bx_2^{\beta_2}}\ ,\ s_2 = \frac{bx_2^{\beta_2}}{ax_1^{\beta_1} + bx_2^{\beta_2}}\ . \tag{39}$$

The terms $A_1 = ax_1^{\beta_1}$ and $A_2 = bx_2^{\beta_2}$ represent the recruitment of customers by firm 1 and 2, given the firms' efforts x_1 and x_2. The parameters a and b denote the relative effectiveness of the effort made by the firms. Since $\frac{dA_1}{dx_1}\frac{x_1}{A_1} = \beta_1$ and $\frac{dA_2}{dx_2}\frac{x_2}{A_2} = \beta_2$, the parameters β_1 and β_2 denote the elasticities of the attraction of firm (or brand) i with regard to the effort of firm i. A dynamic model is obtained by assuming that the two competitors adjust their marketing efforts in response to the profits achieved in the previous period:

$$T : \begin{cases} x_1\left(t+1\right) = x_1(t) + \lambda_1 x_1(t)\left(B\frac{[x_1(t)]^{\beta_1}}{[x_1(t)]^{\beta_1}+k[x_2(t)]^{\beta_2}} - x_1(t)\right) \\ \\ x_2\left(t+1\right) = x_2(t) + \lambda_2 x_2(t)\left(B\frac{[x_2(t)]^{\beta_2}}{[x_1(t)]^{\beta_1}+k[x_2(t)]^{\beta_2}} - x_2(t)\right) \end{cases} \tag{40}$$

The parameters $\lambda_i > 0, i = 1, 2$, measure the rate of this adjustment and $k := b/a$.

An important feature of the map (40) is that the two coordinate axes are invariant lines, since $T(x_1, 0) = (x_1', 0)$ and $T(0, x_2) = (0, x_2')$. The dynamics of (40) along the axis $x_i = 0$ are governed by one-dimensional maps $x_j' = f_j(x_j)$, where f_j is the restriction of T to the corresponding axis. The map f_j is given by $f_j(x_j) = (1 + \lambda_j B)\, x_j - \lambda_j x_j^2$. It is conjugate to the standard logistic map (**??**) by the homeomorphisms $x_j = x\left(1 + \lambda_j B\right)/\lambda_j$, where the parameters μ is given by $\mu = 1 + \lambda_j B$. Thus, the properties of the trajectories embedded in the invariant axes can be easily deduced from the well-known properties of the standard logistic map (3).

The fixed points of the map (40) are the solutions of the system

$$\begin{cases} x_1\left(B\frac{x_1^{\beta_1}}{x_1^{\beta_1}+kx_2^{\beta_2}} - x_1\right) = 0 \\ x_2\left(B\frac{kx_2^{\beta_2}}{x_1^{\beta_1}+kx_2^{\beta_2}} - x_2\right) = 0 \end{cases} \tag{41}$$

There are three evident “boundary solutions”,

$$O = (0,0)\,;\;\; E_1 = (B,0)\,;\;\; E_2 = (0,B)\,, \tag{42}$$

but O is not a fixed point because the map is not defined in it. The fixed points E_1 and E_2 are related to the positive fixed points of the one-dimensional quadratic maps f_1 and f_2 governing the dynamics along the invariant axes. There is also another fixed point, interior to the positive quadrant $\mathbb{R}^2_+$, given by

$$E_* = (x_1^*, B - x_1^*)\,. \tag{43}$$

The coordinate $x_1^* \in (0,B)$ is the unique solution of the equation $F(x) = k^{\frac{1}{1-\beta_2}} x^{\frac{1-\beta_1}{1-\beta_2}} + x - B = 0$, since F a continuous function with $F(0) < 0$, $F(B) > 0$ and $F'(x) > 0$ for each $x > 0$. With a given set of parameters B, β_1 and β_2, the positive fixed point E_* is locally asymptotically stable for sufficiently small values of the adjustment speeds λ_1 and λ_2. It loses stability as one or both of the adjustment speeds are increased and more complex attractors are created around it.

In the following we focus our attention on the global properties of the map (40), in particular on the boundaries of the *feasible set* $\mathcal{B}$. This feasible set is defined as the set of points which generate trajectories which are entirely in the positive orthant (feasible trajectories). A feasible trajectory may converge to the positive fixed point E_*, to other more complex attractors inside $\mathcal{B}$ or to a one-dimensional invariant set embedded inside a coordinate axis (the last occurrence means that one of the two brands disappears). Trajectories starting outside of the set $\mathcal{B}$ represent infeasible evolutions of the economic system. As proved in Bischi, Gardini and Kopel [21], (40) is a noninvertible map of $Z_4 > Z_2 - Z_0$ type, and the qualitative shape of the critical curves, as well as the Riemann foliation, are similar to the ones of the previous example, see Fig.64c. As before, starting from the knowledge of the global properties of the map (40), we illustrate how the boundaries of the feasible set changes when a structural parameter of the game is changed. By using the method of critical curves, we try to reveal the mechanism which is responsible for these changes.

With values of the parameters β_i in the range $(0.2, 0.3)$, our numerical investigation has shown that the invariant coordinate axes are transversely repelling, i.e. they act as repelling sets with respect to trajectories approaching them from the interior of the nonnegative orthant. Moreover, for the parameters used in our simulations, we have observed only one attractor inside $\mathcal{B}$, although more than one coexisting attractors may exist, each with its own basin of attraction. On the basis of this numerical evidence, in what follows we will often speak of a unique bounded and positive attracting set $\mathcal{A}$, which attracts the generic feasible trajectory, even if its existence and uniqueness are not rigorously proved. Let $\partial\mathcal{B}$ be the boundary of $\mathcal{B}$. Such a boundary can have a simple shape, as in the situation shown in Fig.67a, where the attractor $\mathcal{A}$ is the fixed point E_* and $\mathcal{B}$ is represented by the white region. However, the basin can also have a very complex structure, as in Fig.67b, where, again, $\mathcal{B}$ is given by the white points and $\mathcal{A}$ is a chaotic attractor represented by the black points inside $\mathcal{B}$.

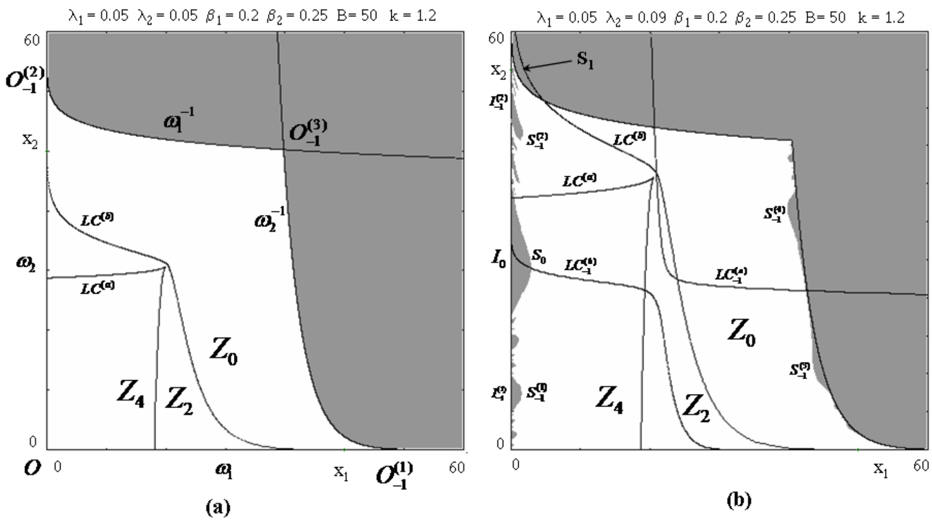

Fig.67

An exact determination of $\partial\mathcal{B}$ is the main goal of the remainder of this analysis. Let us first consider the dynamics of T restricted to the invariant axes. We know that the maps f_j that govern the dynamics along the invariant axes are topologically conjugated to the logistic map (3). This insight is important, and the reader is urged to recall the properties of this one-dimensional map (see Section 2). For $\lambda_1 B \leq 3$ (corresponding to $\mu \leq 4$), we can deduce that bounded trajectories along the x_1 axis are obtained, as long as the initial conditions are taken inside the segment $\omega_1 = OO_{-1}^{(1)}$. The point $O_{-1}^{(1)}$ is the rank-1 preimage of the origin O computed for the one-dimensional restriction f_1, i.e.

$$O_{-1}^{(1)} = \left(\frac{1+\lambda_1 B}{\lambda_1}, 0\right). \tag{44}$$

Divergent trajectories along the x_1 axis are obtained starting from an initial condition out of the segment ω_1. Analogously, when $\lambda_2 B \leq 3$, bounded trajectories along the invariant x_2 axis are obtained provided that the initial conditions are taken inside the segment $\omega_2 = OO_{-1}^{(2)}$. In this case the point $O_{-1}^{(2)}$ is the rank-1 preimage of the origin computed for the restriction f_2, i.e.

$$O_{-1}^{(2)} = \left(0, \frac{1+\lambda_2 B}{\lambda_2}\right). \tag{45}$$

Divergent trajectories along the x_2 axis are obtained starting from an initial condition out of the segment ω_2. Consider now the region bounded by the segments ω_1 and ω_2 and their rank-1 preimages $\omega_1^{-1} = T^{-1}(\omega_1)$ and $\omega_2^{-1} = T^{-1}(\omega_2)$. Such preimages can be analytically computed as follows. Let $X = (p, 0)$ be a point of ω_1, i.e. $0 < p < \frac{1+\lambda_1 B}{\lambda_1}$. Its preimages are the real solutions of the algebraic system obtained from (40) with $(x_1', x_2') = (p, 0)$:

$$\begin{cases} x_1\left(1+\lambda_1 B \frac{x_1^{\beta_1}}{x_1^{\beta_1}+kx_2^{\beta_2}} - \lambda_1 x_1\right) = p \\ \\ x_2\left(1+\lambda_2 B \frac{kx_2^{\beta_2}}{x_1^{\beta_1}+kx_2^{\beta_2}} - \lambda_2 x_2\right) = 0 \end{cases} \tag{46}$$

It is easy to see that the preimages of the point X are either located on the same invariant axis $x_2 = 0$ (in the points whose coordinates are the solutions of the equation $f_1(x_1) = p$) or on the curve of equation

$$x_1 = \left[kx_2^{\beta_2}\left(\frac{\lambda_2 B - \lambda_2 x_2 + 1}{\lambda_2 x_2 - 1}\right)\right]^{\frac{1}{\beta_1}}. \tag{47}$$

Analogously, the preimages of a point $Y = (0, q)$ of ω_2, i.e. $0 < q < \frac{1+\lambda_2 B}{\lambda_2}$, belong to the same invariant axis $x_1 = 0$ (in the points whose coordinates are the solutions of the equation $f_2(x_2) = q$), or lie on the curve of equation

$$x_2 = \left[\frac{x_1^{\beta_1}}{k}\left(\frac{\lambda_1 B - \lambda_1 x_1 + 1}{\lambda_1 x_1 - 1}\right)\right]^{\frac{1}{\beta_2}}. \tag{48}$$

It is straightforward to see that the curve (47) intersects the x_2 axis in the point $O_{-1}^{(2)}$ given in (45), the curve (48) intersects the x_1 axis in the point $O_{-1}^{(1)}$ given in (44), and the two curves (47) and (48) intersect at a point $O_{-1}^{(3)}$ interior to the positive orthant (see Fig.67a). The point $O_{-1}^{(3)}$ is another rank-1 preimage of the origin. The four preimages of the origin are the vertexes of a "quadrilateral" $OO_{-1}^{(1)}O_{-1}^{(3)}O_{-1}^{(2)}$, whose sides are ω_1, ω_2 and their rank-1 preimages ω_1^{-1} and ω_2^{-1}, which are located on the curves of equation (47) and (48). All the points outside this quadrilateral cannot generate feasible trajectories. In fact, points located on the right of ω_2^{-1} are mapped into points with negative x_1 coordinate after one iteration, as can be easily deduced from the first line of (40). Points located above ω_1^{-1} are mapped into points with negative x_2 coordinate after one iteration, as can be deduced from the second line of (40).

The boundary of $\mathcal{B}$ is given, in general, by the union of all preimages (of any rank) of the segments ω_1 and ω_2:

$$\partial\mathcal{B}(\infty) = \left(\bigcup_{n=0}^{\infty} T^{-n}(\omega_1)\right) \cup \left(\bigcup_{n=0}^{\infty} T^{-n}(\omega_2)\right). \tag{49}$$

As long as $\lambda_1 B \leq 3$ and $\lambda_2 B \leq 3$ the boundary of $\mathcal{B}$ has the simple shape shown in Fig.67a, because no preimages of higher rank of ω_1 and ω_2 exist. This is due to the fact that ω_1^{-1} and ω_2^{-1} are entirely included inside the region Z_0 of the plane whose points have no preimages. The situation is different when the values of the parameters are such that some portions of these curves belong to the regions Z_2 or Z_4 whose points have two and four preimages respectively. In this case preimages of higher order of ω_1 and ω_2 exist, say ω_1^{-k} and ω_2^{-k}, which form new portions of $\partial\mathcal{B}$. Such preimages of ω_1 and ω_2 of rank $k > 1$ bound regions whose points are mapped out of the feasible set $\mathcal{B}$ after k iterations. In such a case the shape of the boundary of $\mathcal{B}$ becomes far more complex. This change is due to a global bifurcation that can be explained by using the critical curves.

If λ_1 or λ_2 are increased so that the bifurcation value $\lambda_b = 3/B$ is crossed by at least one of them, then $\partial\mathcal{B}$ changes from smooth to fractal. To see this, we fix the parameters B, k, β_1, β_2 and λ_1 and vary the speed of adjustment λ_2. As λ_2 is increased, the branch $LC^{(b)}$ of the critical curve that separates Z_0 from Z_2 moves upwards, and at $\lambda_2 = 3/B$ it has a contact with ω_1^{-1} at the point $O_{-1}^{(2)}$. After this contact, a segment of ω_1^{-1} enters the region Z_2, so that a portion S_1 of the infeasible set, bounded by $LC^{(b)}$ and ω_1^{-1}, now has two preimages (see Fig.67b). These two preimages, say $S_0^{(1)}$ and $S_0^{(2)}$, merge in points of $LC_{-1}^{(b)}$ (as the points of $LC^{(b)}$ have two merging preimages belonging to $LC_{-1}^{(b)}$) and form a "grey tongue" issuing from the x_2 axis (denoted by S_0 in Fig.67b, with $S_0 = S_0^{(1)} \cup S_0^{(2)}$). S_0 belongs to the "grey set" of points that generate infeasible trajectories because the points of S_0 are mapped into S_1, so that negative values are obtained after two iterations. Again, it is important to recall the fact that along the axes the dynamical behavior is governed by one-dimensional maps which are conjugate to the logistic map. We already know that the logistic map undergoes a global bifurcation at $\mu = 4$, where a contact between the critical point and the basin boundary occurs. This global bifurcation changes the structure of the basin for the one-dimensional map. A similar mechanism is at work here. To see this, look at the intersection of the "main tongue" S_0 with the x_2 axis. This gives a set I_0 around the critical point c_2 of the restriction f_2. Of course, I_0 corresponds to the "main hole in the middle part" of the logistic map with $\mu > 4$ (Fig.62b, or in the Myrberg's map for $b > 2$, see Fig.14b). However, we already know that I_0 has an infinite sequence of further preimages, $I_{-1}^{(1)}$ and $I_{-1}^{(2)}$, and so on. Accordingly, the set S_0 is only the first of infinitely many preimages of S_1. Preimages of S_1 of higher rank form a sequence of smaller and smaller grey tongues issuing from the x_2 axis, whose intersection with the x_2 axis correspond to the infinitely many preimages I_{-k} of the main hole I_0. Only some of them are visible in Fig.67b, but smaller tongues become numerically visible by enlargements, as it usually happens with fractal curves. The fractal structure of the boundary of $\mathcal{B}$ is a consequence of the fact that the tongues are distributed along the segment ω_2 of the x_2 axis according to the structure of the intervals I_{-k} described in Section 2, whose complementary set is a Cantor set. In the situation shown in Fig.67b the main tongue S_0 has a wide portion in the region Z_4. Hence, besides the two preimages along the x_2 axis (denoted by $S_{-1}^{(1)}$ and $S_{-1}^{(2)}$ in Fig.67b) issuing from the intervals $I_{-1}^{(1)}$ and $I_{-1}^{(2)}$, two more preimages exist. Hence, in the two-dimensional case the structure of the basin is even more complex. The additional preimages are denoted by $S_{-1}^{(3)}$ and $S_{-1}^{(4)}$ in Fig.67b, and are located at opposite sides with respect to $LC_{-1}^{(a)}$. The tongues $S_{-1}^{(3)}$ and $S_{-1}^{(4)}$ belong to Z_0, hence they do not give rise to new sequences of tongues. On the other hand, $S_{-1}^{(1)}$ and $S_{-1}^{(2)}$ have further preimages, since they are located inside Z_4 and Z_2 respectively. If the preimages are two, as in the case of $S_{-1}^{(2)}$, they form two tongues issuing from the x_2 axis. In the case of four preimages, as in the case of $S_{-1}^{(1)}$, two of them are tongues issuing from the x_2 axis and two are tongues issuing from the opposite side, i.e. ω_2^{-1}.

As λ_2 is further increased, $LC^{(b)}$ moves upwards, the portion S_1 enlarges and, consequently, all its preimages (i.e. the infinitely many tongues) enlarge and become more pronounced. This causes the occurrence of another global bifurcation, that changes the set $\mathcal{B}$ from simply connected to multiply connected (or connected with holes). The mechanism is similar to the one described in Mira et al. [89], [88] and Abraham et al. [1]. This second global bifurcation occurs when a tongue, belonging to Z_2, has a contact with $LC^{(a)}$ and subsequently enters the region Z_4. If such a contact occurs out of the x_2 axis, it causes the creation of a pair of new preimages. These preimages merge along $LC_{-1}^{(a)}$ and their union is a *hole* (or *lake*, following the terminology introduced in Mira et al. [88]) inside the feasible set $\mathcal{B}$. Accordingly, a set of points that generate infeasible trajectories has been created, and this set is surrounded by points of the feasible set $\mathcal{B}$. Such a situation is shown in Fig.68a, where a tongue has crossed $LC^{(a)}$ and the set H_1 is now in Z_4. The hole H_0 of infeasible points is the preimage of the set H_1, and is completely included in the feasible set. As λ_2 is further increased, other tongues cross $LC^{(a)}$ and, hence, new holes are created, giving a complicated structure of $\mathcal{B}$ like the one shown in Fig.68b, where many holes inside $\mathcal{B}$ are clearly visible.

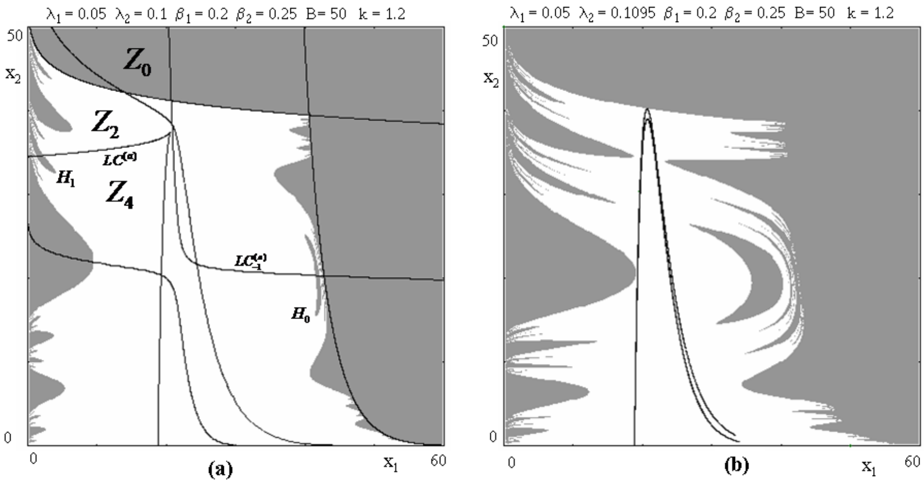

Fig.68

To sum up, the transformation of the set $\mathcal{B}$ from a simply connected region with smooth boundaries into a multiply connected set with fractal boundaries occurs through two types of global bifurcations, both due to contacts between $\partial\mathcal{B}$ and branches of the critical set LC. In Fig.68b it can be noticed that also the attractor inside $\mathcal{B}$ changed its structure. For low values of λ_2, as in Fig.68a, the attractor is the fixed point E_*, to which all the trajectories starting inside the set $\mathcal{B}$ converge. As λ_2 increases, E_* loses stability through a flip (or period doubling) bifurcation, at which E_* becomes a saddle point, and an attracting cycle of period 2 is created near it. As λ_2 is further increased, a sequence of period doublings occurs, similar to the well-known Myrberg (or Feigenbaum) cascade for one-dimensional maps, which creates a sequence of attracting cycles of period 2^n followed by the creation of chaotic attractors, which may be cyclic chaotic sets or a connected chaotic set. So, both kinds of complexities can be observed in this model, even if there are no relations between them (for more details see Bischi, Gardini and Kopel, [21]).

10 Piecewise smooth systems.

In this section we shall consider maps which are not continuously differentiable or not continuous. These maps may undergo bifurcations which are not described by those already seen in the previous Sections. In fact, in such cases a new kind of bifurcation may occur, which involves the disconitinuity point or set, which is the locus in which the discontinuity occurs (either in the first derivative or in the function definition). These new kind of bifurcations are nowadays known as "Border Collision Bifurcations" (BCB henceforth). This kind of bifurcation is a quite recent topic of research. We shall consider here only piecewise smooth continuous systems, giving some results for maps in 1D and 2D phase spaces.

10.1 1D map.

A recent application in the conomic context (see Gardini, Sushko and Naimzada, 2008 [39]) may be useful to introduce the subject associated with a one-dimensional piecewise smooth map. Besids this work we refer to [53], [59], [75], [77], [94], [95], [31], [15], [106], [107], for some works related to one-dimensional piecewise smooth maps.

Let us consider the model first proposed by Matsuyama in [81], which describes the interaction of two sources of economic growth: The mechanism of capital accumulation and the process of technical change and innovation. Matsuyama constructed a one-dimensional dynamic model described by two different functions, each of which characterizes a different regime: The Solow regime, with high rates of growth, no innovations and a competitive market structure, as in the neoclassical model, and the Romer regime, with low rates of growth, innovations and a monopolistic market structure, as in the neo-shumpeterian model. In this model the dynamics often alternates between the two different regimes: There is a trade off between growth and innovation. Analytically the model is represented by a piecewise smooth unimodal map, $x_{t+1} = \phi(x_t)$, where the function $\phi(x)$ is given by

$$\phi(x) = \begin{cases} f(x) = Gx^{1-\frac{1}{\sigma}} & if \quad 0 < x < 1 \;\; (\textit{Solow regime}) \\ g(x) = \frac{Gx}{1+\theta(x-1)} & if \qquad\quad x > 1 \;\; (\textit{Romer regime}) \end{cases} \tag{50}$$

with $\theta = (1-\frac{1}{\sigma})^{1-\sigma}$, and $\sigma > 1$. The independent variable x_t corresponds to the independent variable k_t in the original paper [81], that is, $x_t = \frac{K_t}{N_t \sigma F \theta}$ where K_t stands for capital, N_t the number of types of intermediate goods introduced up to time t, and F is some constant. The output Y_t is related to the amount of capital K_t, and the available types of intermediates, N_s, $0 < s < t$, through a production function. The model is closed assuming that a constant proportion of the output, Y_t, is left to be used as capital in the next period. When the state is $x_t < 1$ then no innovation occurs and no new intermediates are introduced, the *viceversa* takes place in the case $x_t > 1$. The two parameters of the model are G and σ. Increasing G the gross rate of growth changes, the fixed point from the Solow region ($0 < x < 1$) enters the Romer region ($x > 1$) and for $\sigma > 2$ is destabilized. The parameter σ denotes the demand elasticity of the intermediate good (and the monopoly margin), and also has a meaning in determining the share of labor ($\frac{1}{\sigma}$).

Besides Matsuyama, the same model was also considered by Mitra in [90], Mukherjy in [91], and the complete analysis is reported in Gardini et al. 2008, to which we refer for further details. Here we shall here recall haw the use of the BCB is fundamental for the undestanding of the bifurcations occurring in the dynamics of the model.

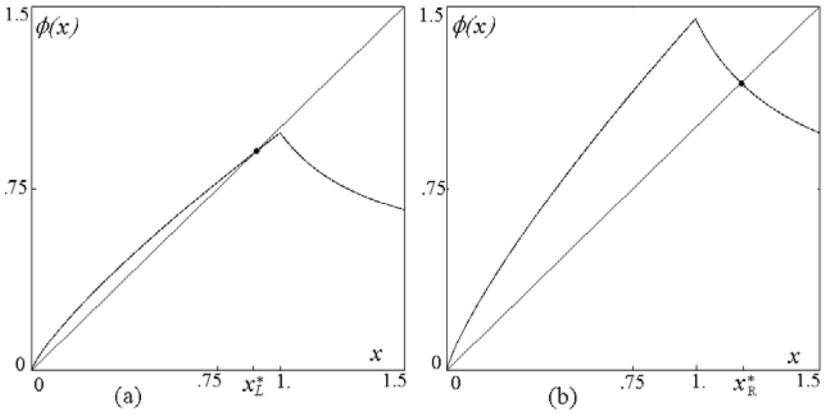

Fig.69 The function $\phi(x)$ with the globally attracting fixed point x_L^* in the Solow regime at $G = 0.98$, $\sigma = 5$ (a), and x_R^* in the Romer regime at $G = 1.45$, $\sigma = 5$ (b).

It is easy to see that for $1 < \sigma < \infty$ we have $1 < \theta < e$, and this is the range of interest: $\sigma > 1$. The function $f(x)$ on the left side (Solow regime) is monotonic increasing, because $f'(x) = G(1 - \frac{1}{\sigma})x^{-\frac{1}{\sigma}} > 0$. It has a unique fixed point $x_L^* = G^\sigma$ which exists (in its region of definition: $x < 1$) as long as $G < 1$, and when it exists, it is always stable, as $0 < f'(x_L^*) = (1 - \frac{1}{\sigma}) < 1$. Furthermore, it is globally attracting except for the origin. As the origin is always a repelling fixed point, we have restricted our interval of interest to $x > 0$. As mentioned in the Introduction, at $G = 1$ a bifurcation occurs, and for $G > (\theta - 1)$ the fixed point in the Romer regime ($x > 1$) is globally asymptotically stable. In fact, the function $g(x)$ defining the regime for $x > 1$ is monotonic decreasing and convex (as $g'(x) = -\frac{G(\theta-1)}{(1+\theta(x-1))^2} < 0$, and $g''(x) > 0$) and it has a unique fixed point $x_R^* = 1 + \frac{G-1}{\theta}$ which exists (in its region: $x > 1$) for any

$G > 1$, but it may be stable or unstable. From $g'(x_R^*) = -(\frac{\theta-1}{G})$ we have that it is locally stable for $G > (\theta - 1)$, and it is easy to see that it is also globally attracting.

In .Fig.69a, we show the shape of the function $\phi(x)$ when the fixed point x_L^* is globally attracting ($G < 1$), while in Fig.69b, x_R^* is globally attracting ($G > (\theta-1)$). We also see immediately that at the bifurcation value $G = 1$, when the fixed point is $x^* = 1$, we have the left side derivative of the function $\phi_L'(1) = (1 - \frac{1}{\sigma}) < 1$ and independently on the value of the derivative of the function on the right, this is enough to prove that the fixed point $x^* = 1$ is globally attracting. In fact, any point with $x > 1$ is mapped in one iteration on the left side with $x < 1$ from which the iterations converge (increasing monotonically) to the fixed point $x^* = 1$. Similarly, due to the monotonicity of the functions on the right side for $G > (\theta - 1)$, with $g(1) = G$ and $g(G) = \frac{G^2}{1+\theta(G-1)} > 1$, we have that any point $x \in (0, 1)$ will reach the region $x > 1$ in a finite number of iterations, and the region $x > 1$ is mapped into itself, with the fixed point globally attracting.

From the previous observations it follows that the interesting region is the interval $1 < G < (\theta - 1)$, and the dynamics of the model as G varies in this interval depend on the value of the other parameter σ. At the bifurcation value $G = (\theta - 1)$ all the points in the interval $[1, G]$ belong to 2-cycles (stable but not asymptotically stable). In fact, the bifurcation value $G = (\theta - 1)$ is a degenerate flip bifurcation: all the points of the segments $[1, x_R^*)$ and $(x_R^*, 1]$ are 2-cycles. We can show this by using the change of variable which puts x_R^* in the origin. That is, let $y = x - x_R^*$ then

$$H_R(y) = g(y + x_R^*) - x_R^* = \frac{(1-\theta)y}{\theta y + G} \tag{51}$$

and

$$H_R^2(y) = H_R{}^\circ H_R(y) = \frac{(1-\theta)^2 y}{y(\theta(1-\theta) + G\theta) + G^2} \tag{52}$$

so that at the bifurcation value $G = (\theta - 1)$ we have $H_R^2(y) = y$. Any i.c. with $x > 0$ will be mapped into the interval $[1, G]$ in a finite number of iterations, thus ending in a 2-cycle with both states in the Romer regime. It was also shown in [81] that for $G < (\theta - 1)$ there exists a 2-cycle, the dynamics "oscillate" between the Solow regime and the Romer regime, and the dynamics of the map in (50) always belong to the *absorbing interval* $[g(G), G]$. Any point with i.c. $x > 0$ will enter this interval in a finite number of iterations, from which it will never escape since $\phi([g(G), G]) \subseteq [g(G), G]$.

The rigorous proof of the bifurcations occurring in the map in (50) are not easy, because of the complex analytical expressions. However, a numerical proof can first be given. In Fig.70 we present a two-dimensional bifurcation diagram in the (G, σ)-parameter plane in which different gray tonalities correspond to different dynamic regimes of the map (50).

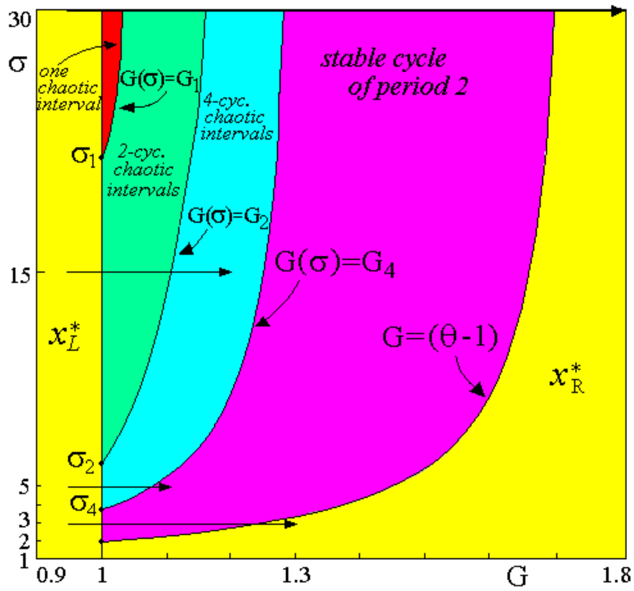

Fig.70 Bifurcation diagram in the (G,σ)-parameter plane. The lightest gray color corresponds to the parameter values at which the map ϕ has a stable fixed point (which is x_L^* for $G < 1$, or x_R^* for $G > 1$, $G > (\theta - 1)$), followed by a strip related to the parameter values at which the map ϕ has an attracting cycle of period 2, and in sequence gray tonalities correspond to 4-, 2- and 1-piece chaotic intervals, respectively.

Let us here consider the parameter values corresponding to the existence of a two-cycle. Since in the Romer regime the function $g(x)$ is decreasing and convex, we have that the first derivative $g'(x)$ is negative and it increases as x increases from 1 (but remaining $g'(x) < 0$). It follows that if the derivative in the critical point satisfies $-1 < g'(1)$ we must have $-1 < g'(x) < 0$ for any $x > 1$. From the expression $g'(1) = -G(\theta - 1)$ we have that $|g'(1)| < 1$ whenever both the conditions hold, $G < 1$ and $\theta \leq 2$, which corresponds to $\sigma \leq 2$. Moreover, in the (G, σ)-parameter plane the bifurcation curve of equation $G = (\theta - 1)$ issues from the point $(G, \sigma) = (1, 2)$ and is increasing and convex - as can be seen in Fig.2 (this fact was also proven in [91]). Thus, the line $\sigma = 2$ never intersects the bifurcation curve $G = (\theta - 1)$ (apart from the issuing point). So, all the interesting dynamics occur at fixed values of σ with $\sigma > 2$, otherwise we must have a stable fixed point (either on the left, if $G < 1$, or on the right, if $G > 1$). It follows that in order to detect a stable 2-cycle we must have $\sigma > 2$, which corresponds to $(\theta - 1) > 1$. Now let us assume that $\sigma > 2$ is fixed and G decreases, starting from some value $G > (\theta - 1)$ for which x_R^* is stable (see Fig.70). Then, as we have seen above, the loss of stability of x_R^* occurs via a degenerate bifurcation: At the bifurcation value $G = (\theta - 1)$ all the points of a segment are 2-cycles. In particular $\{1, G\}$ forms a 2-cycle. After the bifurcation, for $G < (\theta - 1)$, the fixed point x_R^* is unstable. Furthermore no stable 2-cycle can exist with both the points on the right, in the Romer regime. This is proved by the fact that we have $g'(x) < -1$ for all the points x in the interval $[1, G]$, because in the iterated map $H_R \circ H_R(y)$ we have the slope equal to 1 in all the points of a segment (see Fig.71a where $\phi(x)$ and $\phi^2(x)$ are shown at the bifurcation value $G = (\theta - 1)$), while after the bifurcation (see Fig.71b, where $G < (\theta - 1)$) we have the slope greater than 1 in the segment $x \in [1, G]$.

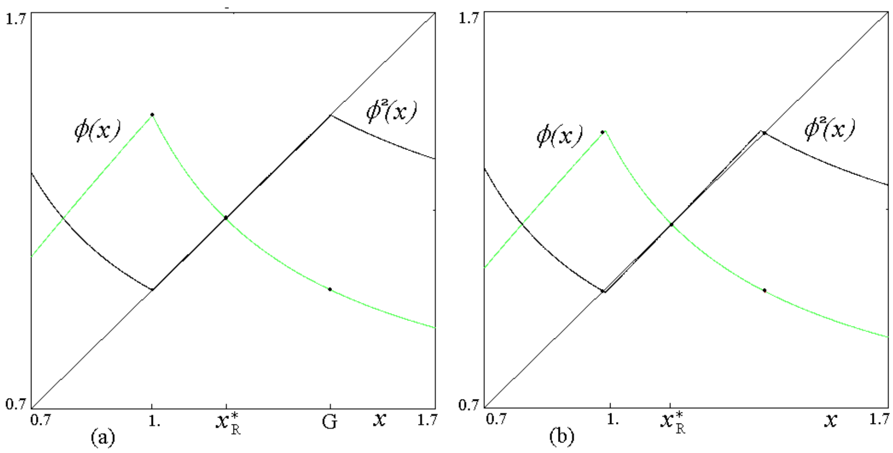

Fig.71 The functions $\phi(x)$ and $\phi^2(x)$ at the critical flip bifurcation value $G = (\theta - 1) = 1.441408$, $\sigma = 5$ (a) and after, at $G = 1.4 < (\theta - 1)$ (b).

This is rigorously proved by using

$$\frac{d}{dy} H_R^2(y) = \frac{(1-\theta)^2 G^2}{[y(\theta(1-\theta) + G\theta) + G^2]^2} = \frac{(\frac{1-\theta}{G})^2}{[\frac{y(\theta(1-\theta)+G\theta)}{G^2} + 1]^2}$$

from which we have $\frac{d}{dy} H_R^2(0) > 1$. Moreover, from $(\theta - 1) > G$, we have $\theta(\theta - 1) > G\theta$ so that $G\theta + \theta(1 - \theta) < 0$, and for y in a right neighborhood of 0 the denominator of $\frac{d}{dy} H_R^2(y)$ is less than 1, and thus $\frac{d}{dy} H_R^2(y) > (\frac{1-\theta}{G})^2 > 1$. From the considerations given above, it follows that a unique 2-cycle exists after the bifurcation, for $G < (\theta - 1)$, with one point of the cycle in the Solow regime and one point in the Romer regime, $\{x_L, x_R\}$. From stable (inside the wide region) it becomes unstable as

G decreases reaching the value $G = G_4$ in Fig.70. The local stability of this unique 2-cycle was already studied in [91], and a sufficient condition for its stability is given, depending on the points of the 2-cycle:

$$|\phi'(x_L)\phi'(x_R)| = \frac{x_L^{\frac{1}{\sigma}}(1-\frac{1}{\sigma})(\theta-1)}{G^2} < 1. \tag{53}$$

The bifurcation occurs when $|\phi'(x_L)\phi'(x_R)| = 1$ in (53), once that the explicit expression of x_L is there inserted, but this is not known, thus it is difficult to obtain an explicit form. However, a different way to get the bifurcation condition comes from considering the images of the critical point $x = 1$ (or equivalently of its first iterate $x = G$). It can be noticed that the bifurcation occurring at $G = (\theta - 1)$ increasing G, for the existing stable 2-cycle (with points $x_L < 1 < x_R$) corresponds to a border-collision bifurcation: The periodic point x_L merges with the critical point $x = 1$, which is a 2-cycle at this parameter value. The condition $G = (\theta - 1)$ may thus be written also as $\phi(G) = 1$ or $\phi^2(1) = 1$, which reads explicitly also as $g^2(1) = 1$. Similarly, at the bifurcation in which the stable 2-cycle becomes unstable as G decreases, one might think that a stable $4-$cycle would appear. Let us first describe what occurs via an example.

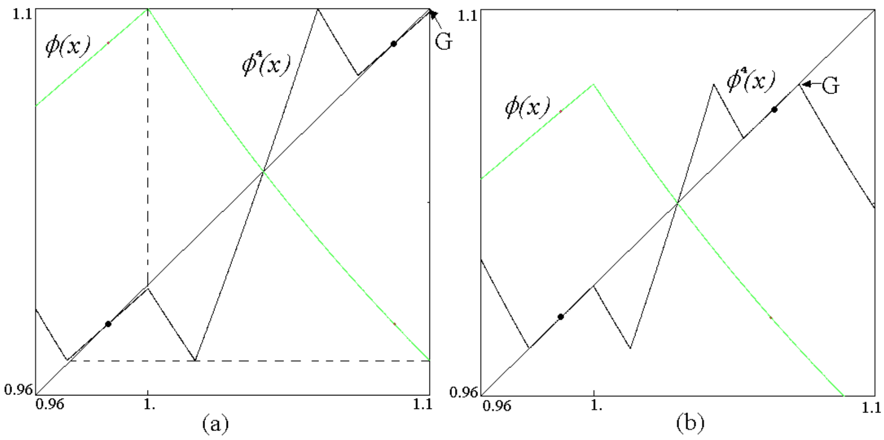

Fig.72 The functions $\phi(x)$ and $\phi^4(x)$ at the parameter values $G = 1.1$, $\sigma = 5$ in (a) and $G = 1.073$, $\sigma = 5$ in (b), for which the map ϕ has the attracting 2-cycle.

In Fig.72a ($G = 1.1$), we show the same example considered by Mukherji ($\sigma = 5$) at a value of G in which the 2-cycle is stable. We can see that this corresponds to two stable fixed points for the iterated map $\phi^2(x)$. It can be also seen that the bifurcation structure is quite similar to the critical situation occurring at the bifurcation of the fixed point. That is, as G decreases approaching the bifurcation value, in the graph of $\phi^4(x)$

two segments tend to collide with the diagonal. In fact this can clearly be seen in Fig.72b ($G = 1.073$), although the parameters are only close to the bifurcation value and the iterations of the critical point still tend to the stable 2-cycle. The bifurcation occurs at approximately $G = 1.0725$, as shown in Fig.73a, where we have indeed that the points 1, G, $g(G)$, and $f \circ g(G)$ form a 4-cycle, and the points of the segments $[g(G), 1]$, $[f^{\circ} g(G), G]$ are all fixed points for the map $\phi^4(x)$ (corresponding to all 4-cycles for ϕ and only one 2-cycle with periodic points approximately in the center of the two intervals). It can be noticed that at the bifurcation value, $|\frac{d}{dx}\phi^4(x)| \geq 1$ for all the points of the absorbing segment of the map, thus it is impossible to get a stable 4-cycle after the bifurcation. In fact, after the bifurcation (see Fig.73b), also the segments previously on the diagonal now have slopes higher than 1, thus we have $|\frac{d}{dx}\phi^4(x)| > 1$ in all the points of the absorbing interval.

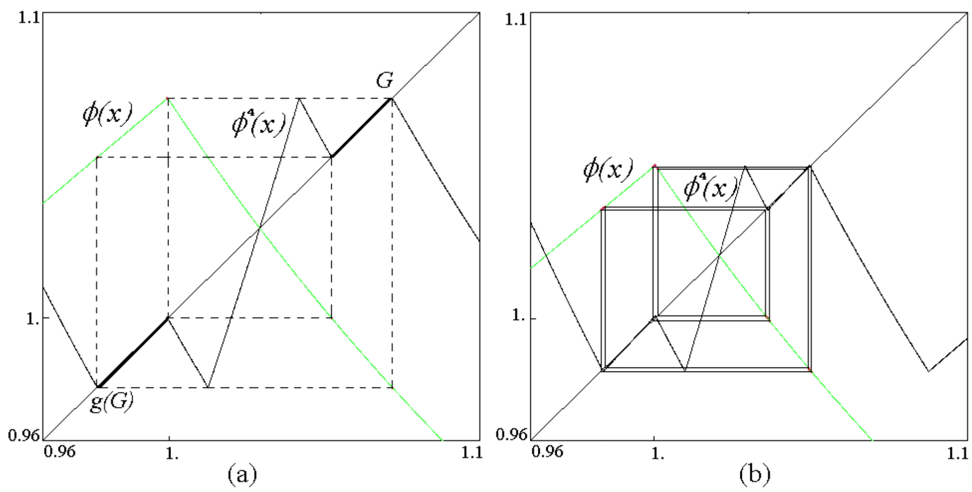

Fig.73 The functions $\phi(x)$ and $\phi^4(x)$ at the parameter values $G = 1.0725$, $\sigma = 5$, are related approximately to the critical flip bifurcation of the 2-cycle in (a) and after the bifurcation, at $G = 1.05$, $\sigma = 5$, when the map ϕ has 4-cyclical chaotic intervals in (b).

It turns out that a stable 4-cycle is impossible. Moreover, any cycle of any period cannot be stable, because ϕ^4 is expanding in the absorbing interval $[g(G), G]$. Instead, all the asymptotic trajectory inside this interval tend to the unique attractor, which is chaotic and made up of 4 cyclical chaotic intervals for the map ϕ (corresponding to four invariant chaotic intervals for ϕ^4), which are bounded by the images of the critical point, that is: $\phi^i(1)$ for $i = 1, 2, ..., 8$ (i.e., $G, g(G), ...$). The considerations given above also show that the bifurcation condition in (53) is equivalent to the condition $\phi^4(1) = 1$ (the critical point must be periodic of period four), which is given by

$$g \circ f \circ g^2(1) = 1. \tag{54}$$

We can so state the following:

Proposition. *The stability region of the 2-cycle of the map in (50), shown in Fig.70, for any fixed value* $\sigma > 2$, *is bounded by the curves of implicit equations* $g^2(1) = 1$ *(which corresponds explicitly to* $G = (\theta - 1)$*) and* $g \circ f \circ g^2(1) = 1$ *(implicit equation for* $G(\sigma) = G_4$*).*

The critical bifurcation of the 2-cycle (related with its stability/ instability) also corresponds to the bifurcation curve at which the 4 pieces chaotic intervals undergo a border collision bifurcation, and thus the condition is obtained either from $\phi^4(1) = 1$ which corresponds to the condition given in (54), or from the equality in (53) (but there, the coordinate of the point x_L of the 2-cycle is not analytically known). We have seen numerically that for any fixed value of $\sigma > \sigma_4$ ($\simeq 3.825$) the equation given in (54) has a single solution, which we have called G_4 in the Proposition.

10.1.1 Chaotic intervals

Really the proof given in the previous subsection of the dynamics of the map is numerical, but the slopes of the function ϕ^4 in the absorbing interval are easy to see (as the pieces of the function look almost piecewise linear, and it is enough to compare the slopes with the two diagonals). So we state that also the bifurcation occurring for the attracting 2-cycle is critical (as it is proved for the fixed point), and no stable cycle can exist. Moreover, as it is easy to see numerically that , the slopes become steepest as G further decreases towards 1, so the condition $|\frac{d}{dx}\phi^4(x)| > 1$ persists at any lower value of G up to 1. Thus no period-doubling bifurcation occurs at the 2-cycle as G decreases, crossing through the value $G = G_4$, at which the equation $g \circ f \circ g^2(1) = 1$, or equivalently $g \circ f \circ g(G) = 1$, holds, while chaotic regimes exist. Indeed, as we see in Fig.70, it is also correct to say that cycles of period three cannot exist, but the chaotic regimes exist anyhow. As we have already seen in Sections 2 and 3 it is enough to have homoclinic trajectories for a fixed point or cycle to have also chaotic dynamics. And in this specific case the chaotic set is also of full measure. In fact, considering the fixed point, when the condition $\phi^3(1) = x_R^*$ is satisfied we have that the map is chaotic in the whole interval $[g(G), G]$. It is worth noticing that the condition given in Sections 2 and 3 says nothing about the density of the chaotic set Λ. Indeed, Λ may also be a set of points of zero measure in I, and in such a case the chaotic dynamics, although existing, is not detectable by numeric simulations of a generic trajectory. The situation is different when the chaotic set is an interval or cyclical chaotic intervals (as it occurs, for example, exactly at the homoclinic bifurcation value of a cycle). The appearance of such *full measure chaotic intervals* is indeed what occurs in our model (50) whenever the fixed point and the 2-cycle are not stable, as stated in the following

Proposition. *For any fixed value* $\sigma > 2$ *when the fixed point and the 2-cycle of the map in (50) are unstable, the attractors are full measure chaotic intervals.*

In fact, the dynamics which may occur as G is further decreased below the value $G = G_4$ are always chaotic: After the 2-cycle, 4-cyclical chaotic intervals appear, which may merge (say at $G = G_2$) into 2-cyclical chaotic intervals, which in turn may merge (say at $G = G_1$) into one chaotic interval (see Fig.70).

The bifurcation curve at which 4-cyclical chaotic intervals merge in pairs into 2-pieces chaotic intervals (and vice-versa) is *the first homoclinic bifurcation of the repelling* 2*-cycle* (which was external to the four chaotic intervals). Thus this bifurcation occurs when $\phi^6(1) = (\phi^2)^3(1) = x_L$ in the Solow regime or, equivalently, when the fifth iterate of the point of maximum ($x = 1$) merges into the periodic point x_R in the Romer regime, $\phi^5(1) = x_R$, which corresponds to

$$g^2 \circ f \circ g^2(1) = x_R. \tag{55}$$

Although it is quite complicated to find it in explicit form analytically, we have numerically seen that for any fixed value of $\sigma > \sigma_2$ ($\simeq 6.123$) the equation given in (55) has a single solution, which we call G_2.

The 2-cyclical chaotic intervals are always bounded by the images of the critical point (now $\phi^i(1)$ for $i = 1, 2, 3, 4$ i.e., $G, g(G), ...$, that is $[g(G), g \circ f \circ g(G)]$, $[f \circ g(G), G]$). However this does not occur at the low value of σ (as $\sigma = 5$ in the above example). Indeed the chaotic regime may not be reached either, as can be seen also from Fig.70. The dynamic behaviors of the map as G decreases or increases depend on the value of σ, for $2 < \sigma < \sigma_4$ we can only have a stable 2-cycle and chaotic intervals never occur at any value of G, while chaotic intervals occur for any $\sigma > \sigma_4$.

To illustrate the dynamic behavior let us show a few figures of one-dimensional bifurcation diagrams (or orbit diagrams) at fixed values of σ. Fig.s 74-75 show the asymptotic behavior of the state variable x (in the vertical axis) as a function of G (in the horizontal axis). As already remarked, it is worth noticing that whichever is the value of σ, as it is easy to see from the analytical expression of $g(G)$, as G tends to 1 $g(G)$ also tends to 1, so that the whole absorbing interval $[g(G), G]$ shrinks to one point, the point of maximum $x = 1$ and also maximum value $G = 1$ (and attracting fixed point). Each figure represents the dynamics occurring at a crossection of the bifurcation diagram in Fig.70, at fixed values of σ (the crossections are indicated in Fig.70 by the straight lines with arrows).

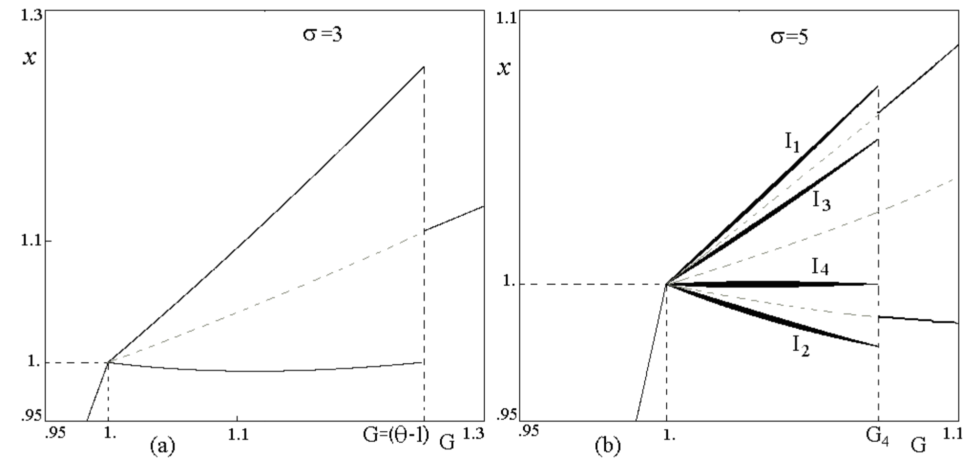

Fig.74 One-dimensional bifurcation diagrams of the map ϕ. $\sigma = 3$, $g \in [0.95, 1.3]$, in (a); $\sigma = 5$, $g \in [0.95, 1.1]$, in (b).

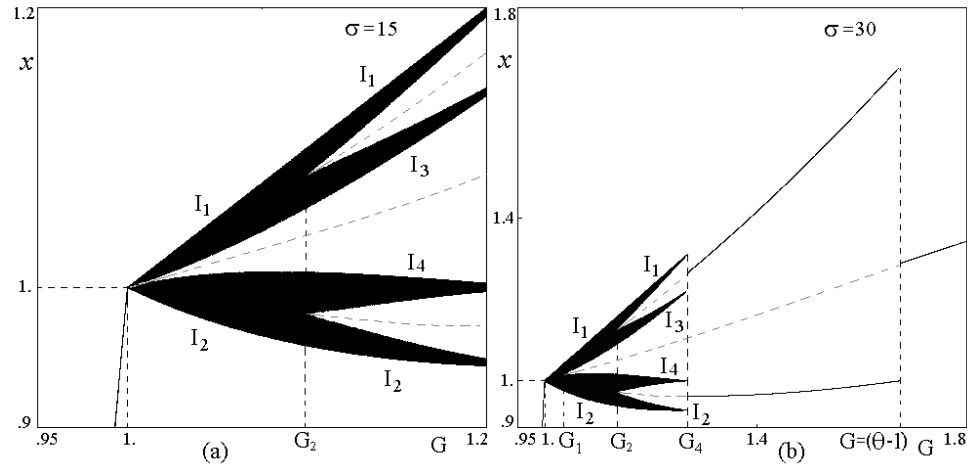

Fig.75 One-dimensional bifurcation diagrams of the map ϕ. $\sigma = 15$, $g \in [0.95, 1.2]$, in (a); $\sigma = 30$, $g \in [0.95, 1.8]$, in (b).

The bifurcation curves represented there, separating the different kinds of chaotic intervals, have been done numerically, by using the analytical conditions related with the homoclinic bifurcations of the relevant cycles. One is the equation given in (55), while the bifurcation curve at which 2 pieces chaotic intervals merge into a single one (or vice-versa a chaotic interval splits into two cyclical chaotic intervals) occurs *when the fixed point in the Romer regime becomes homoclinic.* So the condition is obtained when the third iterate of the point of maximum ($x = 1$) merges into the fixed point, $\phi^3(1) = x_R^*$, which in our case corresponds to

$$f \circ g^2(1) = x_R^* \tag{56}$$

i.e. $f \circ g(G) = x_R^*$, and more explicitly reads as follows:

$$G\left(\frac{G^2}{1+\theta(G-1)}\right)^{\left(1-\frac{1}{\sigma}\right)} = 1 + \frac{G-1}{\theta}. \tag{57}$$

We have seen numerically that for any fixed value of $\sigma > \sigma_1$ ($\simeq 21.231$) the equation given in (57) has a single solution, which we call G_1 (for example, at $\sigma = 50$, value used by Mitra, we have $G_1 = 1.024254692$, at $\sigma = 22$, value used by Mukherji, we have $G_1 = 1.001468146$, at $\sigma = 30$, value used in the bifurcation diagram in Fig.75b we have $G_1 = 1.0123131$).

10.1.2 Border-collision bifurcation at $G = 1$

We have seen before that the bifurcations occurring at the fixed point and the 2-cycle, which are critical bifurcations, may also be considered as border-collision bifurcations. In fact, the bifurcation of the fixed point occurring for any value of $\sigma > 2$ at $G = (\theta - 1)$, may be characterized as $\phi^2(1) = 1$, and the critical bifurcation of the 2-cycle (related with its stability/instability) also corresponds to the bifurcation curve at which 4 pieces chaotic intervals undergo a border collision bifurcation, and thus the condition is $\phi^4(1) = 1$. However, the main role of the border-collision bifurcation is clearly the one observed in the model when, at a fixed values of σ, the parameter G is increased and the stable fixed point in the Solow regime merges the point $x = 1$. The kinds of dynamics that will be observed after the border-collision bifurcation occurring at $G = 1$ comes from the following

Theorem. *The border-collision bifurcation of the fixed point $x^* = 1$ of the map ϕ given in (50), occurring at $G = 1$ for any $\sigma > 1$, gives rise (as G increaeses) to*

- *an attracting fixed point x_R^* if $1 < \sigma < 2$;*
- *an attracting cycle of period 2 if $2 < \sigma < \sigma_4 \simeq 3.825$;*
- *attracting 4-cyclical chaotic intervals if $\sigma_4 < \sigma < \sigma_2 \simeq 6.123$;*
- *attracting 2-cyclical chaotic intervals if $\sigma_2 < \sigma < \sigma_1 \simeq 21.231$;*
- *an attracting chaotic interval if $\sigma > \sigma_1$.*

Proof. The theorem can be proved by using the normal form of the border-collision bifurcation occurring in one-dimensional piecewise smooth maps first proposed in [95]. According to Theorem 3 stated in [95] applied to the map ϕ given in (50), the result of the border-collision bifurcation of the fixed point depends on the left and right side derivatives of $\phi(x)$ evaluated at $x = 1$ for $G = 1$, here denoted α and β, respectively:

$$\alpha = \lim_{x\to 1_-} \frac{d}{dx}\phi(x), \qquad \beta = \lim_{x\to 1_+} \frac{d}{dx}\phi(x). \tag{58}$$

The related normal form is given by the skew-tent map $\psi : y \mapsto \psi(y)$ defined by the function

$$\psi(y) = \begin{cases} \alpha y + \varepsilon, & y \leq 0, \\ \beta y + \varepsilon, & y \geq 0. \end{cases} \tag{59}$$

Here ε is a bifurcation parameter such that as ε varies through 0, the local bifurcations of the piecewise linear map ψ and the piecewise smooth map ϕ are of the same kind. That is, the border-collision bifurcation occurring for the fixed point $x^* = 1$ of the map ϕ at $G = 1$ is of the same kind as the border-collision bifurcation of the fixed point $y^* = 0$ of the map ψ occurring at $\varepsilon = 0$.

The dynamics of the piecewise linear map ψ have already been studied (see [75], [95], [15] and references therein), and depend on the slopes α and β of the linear functions. All the possible kinds of border-collision bifurcation of the fixed point x^* are classified according to the partition of the (α, β)-parameter plane into subregions in which the same qualitative dynamics take place.

We summarize these results in Fig.76, which schematically shows the related one-dimensional bifurcation diagrams for the border-collision of the fixed point of the map ψ. The cases $0 < \alpha < 1$, $\beta < -1$, and $\alpha < -1$, $0 < \beta < 1$ (see the dashed regions in Fig.76), have been studied by many authors. They are qualitatively the same case due to the symmetry of the (α, β)-parameter plane with respect to the line $\alpha = \beta$. It has been shown that for $\varepsilon > 0$ ($\varepsilon < 0$, respectively), all trajectories are bounded and the map ψ can have an attracting cycle of any period $k \geq 2$, denoted q_k, as well as a cyclic chaotic interval of any period $m \geq 1$, denoted Q_m. This means that varying ε through 0 from $\varepsilon < 0$ to $\varepsilon > 0$ (from $\varepsilon > 0$ to $\varepsilon < 0$, respectively) we can have the border-collision bifurcation from the attracting fixed point x^* to any one of such attractors. The region $\alpha > 1$, $\alpha/(1-\alpha) < \beta < -1$ (and $\alpha < -1$, $1 < \beta < \alpha/(\alpha + 1)$) includes subregions corresponding to the transition from no attractor to cyclic chaotic intervals Q_m of period $m = 2^k$, $k = 0, ..., l$, where $l \to \infty$ as $(\alpha, \beta) \to (1, -1)$ ($(\alpha, \beta) \to (-1, 1)$, respectively).

Now we write the coefficients of the normal form (59) in terms of the parameter σ. From (58) we get

$$\alpha = \left(1 - \frac{1}{\sigma}\right), \qquad \beta = (1 - \theta) \tag{60}$$

so that we have $0 < \alpha < 1$ and $\beta < 0$. Moreover, from $1 < \theta < e$ we have that $1 - e < \beta < 0$. Thus, the region of our interest in the (α, β)-parameter plane is $0 < \alpha < 1$, $1 - e < \beta < 0$ (see the thick rectangle in Fig.76).

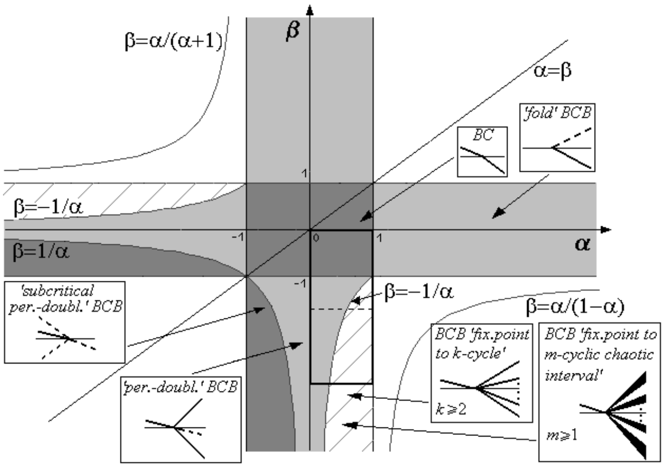

Fig.76

The partition of the (α, β)-parameter plane into the regions with qualitatively similar dynamics of the map ψ at $\varepsilon < 0$ (for $\beta > \alpha$) and at $\varepsilon > 0$ (for $\beta < a$). Corresponding BCB of the fixed point of ψ, occuring at $\varepsilon = 0$ as ε varies from $\varepsilon < 0$ to $\varepsilon > 0$, are shown schematically by means of one-dimensional bifurcation diagrams (the same kinds of BCB occur for $\alpha < \beta$ as ε varies from $\varepsilon > 0$ to $\varepsilon < 0$): The thick and dashed lines indicate attracting and repelling cycles, respectively. The thin lines correspond to the border point.

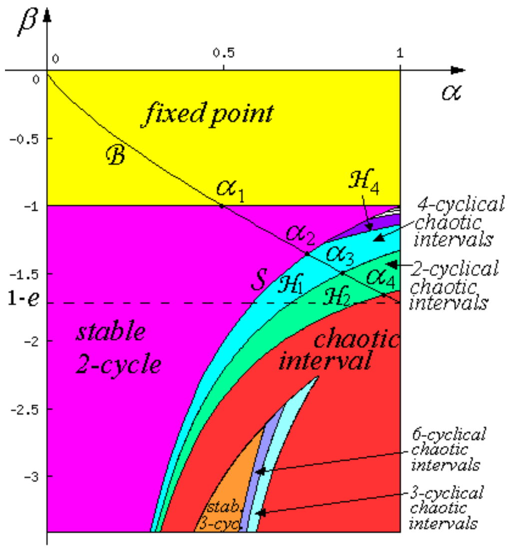

Fig.77

The enlarged window of Fig.76 where the BCB curve B of the fixed point $x^* = 1$ of the map ϕ is shown, as well as the critical flip bifurcation curve S of the 2-cycle of the map ψ, the homoclinic bifurcation curves H_i, $i = 1, 2, 4$ of the corresponding cycles of ψ and the bifurcation curves related to the 3-cycle of ψ.

Substituting first $\theta = (1 - \frac{1}{\sigma})^{1-\sigma}$ and then $\sigma = 1/(1-\alpha)$ into (60) we get the expression of the border-collision curve of the fixed point $x^* = 1$ in terms of the parameters α and β, which is denoted as $\mathcal{B}$,

$$\mathcal{B}: \qquad \beta = 1 - \alpha^{\alpha/(\alpha-1)}. \tag{61}$$

Fig.77 presents an enlargment of the rectangle of interest in Fig.76, and in it the curve $\mathcal{B}$ is shown. By using the analytic expressions of the bifurcation curves as given in [75], we can describe the regions of the (α, β)-parameter plane which are crossed by the curve $\mathcal{B}$. We can see that $\mathcal{B}$ intersects:

1) the straight line $\beta = -1$ at a point P which is $(\alpha, \beta) = (0.5, -1)$, related to the (critical) flip bifurcation of the fixed point y^*;

2) the curve, denoted as $\mathcal{S}$, given by

$$\mathcal{S}: \qquad \beta = -\frac{1}{\alpha},$$

related to the (critical) flip bifurcation of the 2-cycle (after which the curve $\mathcal{B}$ enter a region of 4-cyclical chaotic intervals). The intersection point is denoted by α_4, i.e., $\mathcal{B} \cap \mathcal{S} = \alpha_4$;

3) the curve, denoted as $\mathcal{H}_2$, given by

$$\mathcal{H}_2: \qquad \alpha = \frac{-1 - \sqrt{1 + 4\beta^4}}{2\beta^3},$$

which is related to the homoclinic bifurcation of the 2-cycle of the map ψ giving rise to the transition from 4-cyclical chaotic intervals to 2-cyclical chaotic intervals, $\mathcal{B} \cap \mathcal{H}_2 = \alpha_2$;

4) the curve denoted as $\mathcal{H}_1$ given by

$$\mathcal{H}_1: \qquad \beta = \frac{-1 + \sqrt{1 + 4\alpha^2}}{2\alpha},$$

which is related to the homoclinic bifurcation of the fixed point y^* of the map ψ, giving rise to the transition from 2-cyclical chaotic intervals to one chaotic interval; $\mathcal{B} \cap \mathcal{H}_1 = \alpha_1$.

Other bifurcation curves are also shown in Fig.77, not intersected by $\mathcal{B}$. For example the curve $\mathcal{H}_4$ corresponding to the transition from 4-cyclical chaotic intervals to 8-cyclical chaotic intervals for the map ψ. Indeed, as proved in [75], the point $(\alpha, \beta) = (1, -1)$ is an accumulation point for the curves related to the transition from 2^{i-1}-cyclical chaotic intervals to 2^i-cyclical chaotic intervals, $i = 2, ...$ The bifurcation curves related to the existence and stability of a cycle of period 3 can also be seen, and it is not intersected by the curve $\mathcal{B}$ (which is of interest to us). The "end point" for the curve $\mathcal{B}$ for our map is $(\alpha, \beta) = (1, 1-e)$ corresponding to the parameter value $\sigma = \infty$ (or $\theta = e$).

It is clear that the curve $\mathcal{B}$ corresponds to the vertical line at $G = 1$ in the bifurcation diagram in the (G, σ)-parameter plane shown in Fig.70, and the intersection points there evidenced: The point P corresponds to $\sigma = 2$ and the point α_i corresponds to σ_i, for $i = 4, 2, 1$.

To end our considerations we only have to get the approximate values of the coordinates of the intersection points α_i, $i = 4, 2, 1$ by using the analytical expressions of the bifurcation curves and, via (60), to get the corresponding values of the parameter σ. We obtain that $\sigma_4 \simeq 3.825$, $\sigma_2 \simeq 6.1226$ and $\sigma_1 \simeq 21.231$.

We have thus proved that the, as G increases through 1, the border-collision bifurcation of the fixed point $x^* = 1$ can directly lead to a chaotic interval (for $\sigma > \sigma_1$), as in the example shown in Fig.76b, or to 2-cyclical chaotic intervals (for $\sigma_2 < \sigma < \sigma_1$), as in the example shown in Fig.76a, or to 4-cyclical chaotic intervals (for $\sigma_4 < \sigma < \sigma_2$), as in the example shown in Fig.75b, or to a stable 2-cycle (for $2 < \sigma < \sigma_4$), as in the example shown in Fig.75a.

10.2 2D Business Cycle map.

As a relevant application in the economic context let us recall here the classical works on the business cycle. As well known (we refer to [97] for details), Hicks (1950 [58]) modified the Samuelson (1939 [102]) linear multiplier-accelerator model through introducing two constraints. The linear multiplier-accelerator model itself only has two options: Exponentially explosive or damped motion. According to Hicks, only the explosive case is interesting, as only this produces persistent motion endogenously, but it had to be limited through two (linear) constraints for which Hicks gave factual explanations.

When the cycle is in its depression phase it may happen that income decreases so fast that more capital can be dispensed with than what disappears through depreciation, i.e., natural wear and aging. As a result, the linear accelerator would predict not only negative investments (disinvestments), but to an extent that implies active destruction of capital. To avoid this, Hicks introduced his floor to disinvestment at the natural depreciation level.

When the cycle is in its prosperity phase, then it may happen that income would grow at a pace which does not fit available resources. Hicks has a discussion about what then happens, in terms of inflation, but he contended himself with stating that (real) income could not grow faster than available resources which put a ceiling on the income variable.

Hicks never formulated his final model with floor and ceiling mathematically, it seems that this was eventually done by Rau (1974 [100]), where the accelerator-generated investments were limited downwards through the natural depreciation floor, and where the income is limited upwards through the ceiling, determined by available resources. Formally:

$$I_t = \max(a(Y_{t-1} - Y_{t-2}), -I^f);$$
$$C_t = cY_{t-1};$$
$$Y_t = \min(C_t + I_t, Y^c).$$

Eliminating C_t and I_t, one has the single recurrence equation:

$$Y_t = \min(cY_{t-1} + \max(a(Y_{t-1} - Y_{t-2}), -I^f), Y^c). \tag{62}$$

It remains to say that Hicks's original discussion included an exponential growth in autonomous expenditures, combined with the bounds I^f and Y^c growing at the same pace, but taking the bounds as constant and deleting the autonomous expenditures, gives a more clear-cut version. It was this that was originally analyzed in detail by Hommes (1991 [59]). However, the full understanding of the bifurcation mechanisms occurring in that two-dimensional piecewise linear model is a recent result (see [37], [97], [109]), and mainly due to a particular degeneracy existing in that model. In fact, for the BCB occurring in the generic 2D continuous piecewise linear map, as we shall recall below, only recent studies have been published up to now, and the study is very far from being completed. And such studies are basic tools for the more general case of piecewise smooth continuous maps: some examples may be found in [112], [111], [98], [99], [113]

Description of the Business Cycle map

Let $x_t := Y_t$, $y_t := Y_{t-1}$, $d := I^f$ and $r := Y^c$. Then the model given in (62) can be rewritten as a two-dimensional piecewise linear continuous map $F : \mathbb{R}^2 \to \mathbb{R}^2$:

$$F : \begin{pmatrix} x \\ y \end{pmatrix} \mapsto \begin{pmatrix} \min(cx + \max(a(x-y), -d), r) \\ x \end{pmatrix}, \tag{63}$$

which depends on four real parameters: $a > 0$, $0 < c < 1$, $d > 0$, $r > 0$.

The map F is given by three linear maps F_i, $i = 1, 2, 3$, defined, respectively, in three regions R_i of the phase plane:

$$F_1 : \begin{pmatrix} x \\ y \end{pmatrix} \mapsto \begin{pmatrix} (c+a)x - ay \\ x \end{pmatrix}; \tag{64}$$
$$R_1 = \{(x, y) : (1 + c/a)x - r/a \le y \le x + d/a\};$$

$$F_2 : \begin{pmatrix} x \\ y \end{pmatrix} \mapsto \begin{pmatrix} cx - d \\ x \end{pmatrix}; \tag{65}$$
$$R_2 = \{(x, y) : y > x + d/a, x \leq (d + r)/c\};$$

$$F_3 : \begin{pmatrix} x \\ y \end{pmatrix} \mapsto \begin{pmatrix} r \\ x \end{pmatrix}; \tag{66}$$
$$R_3 = \mathbb{R}^2 / R_1 / R_2.$$

Three half lines denoted LC_{-1}, LC'_{-1} and LC''_{-1} are boundaries of the regions R_i:

$$\begin{aligned} &LC_{-1} : y = x + d/a, \ x \leq (r + d)/c, \\ &LC'_{-1} : y = (1 + c/a)x - r/a, \ x < (r + d)/c, \\ &LC''_{-1} : x = (r + d)/c, \ y > (r + d)/c + d/a. \end{aligned}$$

Their images by F are called critical lines:

$$\begin{aligned} &LC_0 : y = (x + d)/c, \ x \leq r, \\ &LC'_0 : x = r, \ y < (r + d)/c. \end{aligned}$$

The image of LC''_{-1} by F is a point $(r, (r + d)/c)$. A qualitative view of the phase plane of the map F for $a > 1$, $d < r$ and $a > c^2/(1 - c)$ is shown in Fig.78 (the last inequality indicates that the intersection point of LC'_{-1} and LC_0 is in the negative quadrant).

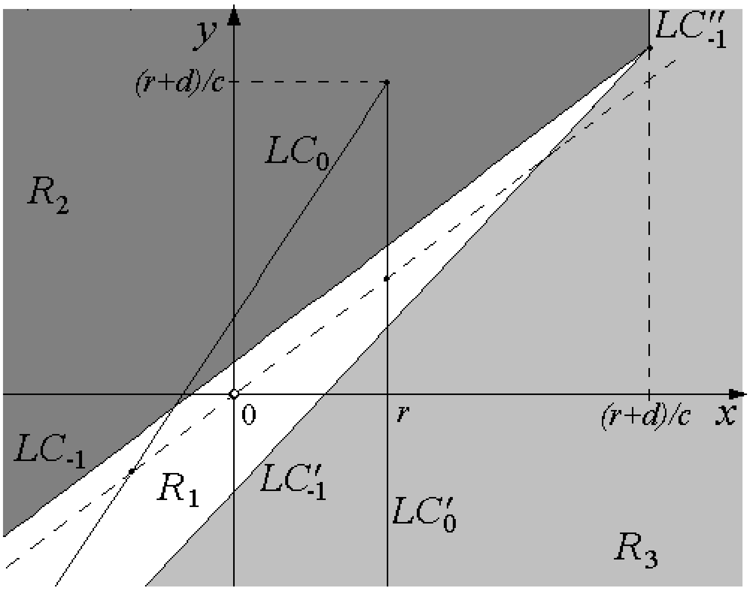

Fig.78 Critical lines of the map F for $a > 1$, $d < r$, $a > c^2/(1 - c)$.

As mentioned above, an analogous model has been studied by Hommes in [59], and the main conclusions there given hold also for the map F, namely, for $a > 1$ the map F has an attracting set $\mathcal{C}$ homeomorphic to a circle and all the trajectories of F (except for the fixed point) are attracted to this set. It was also proved that the dynamics of the map F on $\mathcal{C}$ are either periodic or quasiperiodic. We show how the set $\mathcal{C}$ appears related to the center bifurcation of the fixed point, showing the structure of the two-dimensional bifurcation diagram in the (a, c)-parameter plane.

First note that the maps F_2 and F_3 have simple dynamics: The eigenvalues of F_2 are $\mu_1 = c$, $0 < c < 1$, $\mu_2 = 0$, so that any initial point $(x_0, y_0) \in R_2$ is mapped into a point of LC_0, while the map F_3 has two zero eigenvalues, and any $(x_0, y_0) \in R_3$ is mapped into a point of the straight line $x = r$. In such a way the whole phase plane is mapped in one step to the straight line $x = r$ and a cone $D = \{(x, y) : y \leq (x + d)/c,\ x \leq r\}$ (see Fig.78). Thus, the map F is a noninvertible map of so-called $(Z_\infty - Z_1 - Z_0)$ type: Any point belonging to the critical lines or to the half line $x = r$, $y > (r + d)/c$, has infinitely many preimages, any inner point of D has one preimage and any other point of the plane has no preimages.

The map F has a unique fixed point $(x^*, y^*) = (0, 0)$ which is the fixed point of the map F_1 (while the fixed points of the maps F_2 and F_3 belong to R_1, thus, they are not fixed points for the map F). The eigenvalues of the Jacobian matrix of F_1 are

$$\lambda_{1,2} = (a + c \pm \sqrt{(a + c)^2 - 4a})/2, \tag{67}$$

so that for the parameter range considered the fixed point (x^*, y^*) is a node if $(c + a)^2 > 4a$, and a focus if $(c + a)^2 < 4a$, being attracting for $a < 1$ and repelling for $a > 1$. Thus, for $a < 1$ the fixed point (x^*, y^*) is the unique global attractor of the map F (given that F_2 and F_3 are contractions).

Center bifurcation $(a = 1)$

At $a = 1$ the fixed point (x^*, y^*) loses stability with a pair of complex-conjugate eigenvalues crossing the unit circle, that is the center bifurcation occurs. First we describe the phase portrait of the map F exactly at the bifurcation value $a = 1$. Analogous description is presented in Section 2.2 of Chapter 2 for a two-dimensional piecewise linear map defined by two linear maps, which for the particular parameter value $b = 0$ are the maps F_1 and F_2 given in (64) and (65). It is proved that for the parameter values corresponding to the center bifurcation there exists an invariant region in the phase plane, which either is a polygon bounded by a finite number of images of a proper segment of the critical line, or the invariant region is bounded by an ellipse and all the images of the critical line are tangent to this ellipse (see Propositions 1 and 2 of Chapter 2). In the following we use these results for the considered map F specifying which critical lines are involved in the construction of the invariant region.

The map F_1 at $a = 1$ is defined by a rotation matrix. Moreover, if

$$c = c_{m/n} \overset{def}{=} 2\cos(2\pi m/n) - 1, \tag{68}$$

then the fixed point (x^*, y^*) is locally a center with rotation number m/n, so that any point in some neighborhood of (x^*, y^*) is periodic with rotation number m/n, and all points of the same periodic orbit are located on an invariant ellipse of the map F_1. Note that from $c > 0$ it follows that $m/n < 1/6$. Denote

$$c = c^* \overset{def}{=} 1 - (d/r)^2. \tag{69}$$

Proposition. *Let $a = 1$, $c = c_{m/n}$, then in the phase space of the map F there exists an invariant polygon P such that*

- *if $c_{m/n} < c^*$ then P has n edges which are the generating segment $S_1 \subset LC_{-1}$ and its $n-1$ images $S_{i+1} = F_1(S_i) \subset LC_{i-1}$, $i = 1, ..., n-1$;*
- *if $c_{m/n} > c^*$ then P has n edges which are the generating segment $S'_1 \subset LC'_{-1}$ and its $n-1$ images $S'_{i+1} = F_1(S'_i) \subset LC'_{i-1}$;*
- *if $c_{m/n} = c^*$ then P has $2n$ edges which are the segments S_i and S'_i, $i = 1, ..., n$.*

Any initial point $(x_0, y_0) \in P$ is periodic with rotation number m/n, while any $(x_0, y_0) \notin P$ is mapped in a finite number of steps into the boundary of P.

The value c^* is obtained from the condition of an invariant ellipse of F_1 to be tangent to both critical lines LC_{-1} and LC'_{-1}. It can be shown that for $c_{m/n} < c^*$ only the upper boundary LC_{-1} is involved in the construction of the invariant region, while if $c_{m/n} > c^*$ we have to iterate the generating segment of the lower boundary LC'_{-1} to get the boundary of the invariant region.

An example of the invariant polygon P in the case $c_{m/n} = c^*$ is presented in Fig.79, where $a = 1$, $d = 10$, $r = 10/\sqrt{2-\sqrt{2}}$, $c = c_{1/8} = c^* = \sqrt{2} - 1$. For such parameter values the polygon P has 16 edges, which are the segments $S_i \subset LC_{i-2}$ and $S'_i \subset LC'_{i-2}$, $i = 1, ..., 8$. Any point of P is periodic with rotation number $1/8$ (in Fig.79 the points of two such cycles belonging to the boundary of P are shown by black and gray circles), while any point $(x_0, y_0) \notin P$ is mapped to the boundary of P.

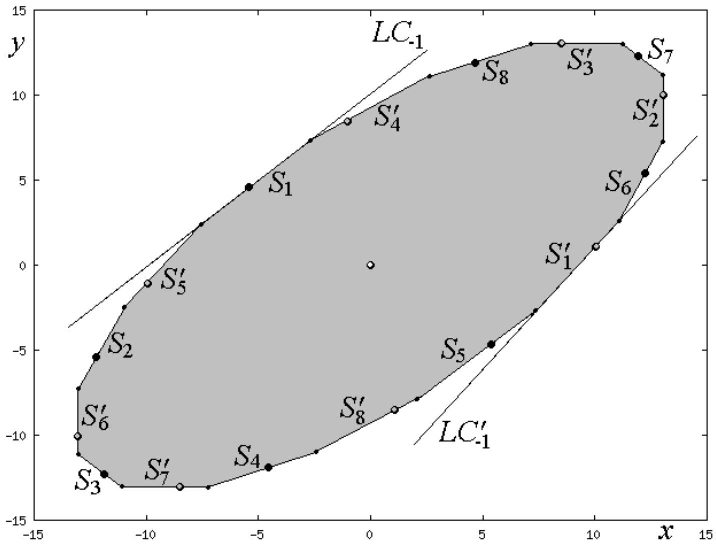

Fig.79 The invariant polygon P with 16 edges at $a = 1$,
$c = c_{1/8} = \sqrt{2} - 1 = c^*$, $d = 10$, $r = 10/\sqrt{2 - \sqrt{2}}$.

Consider now the case in which the map F_1 is defined by the rotation matrix with an irrational rotation number ρ, which holds if

$$c = c_\rho \overset{def}{=} 2\cos(2\pi\rho) - 1, \tag{70}$$

where $\rho < 1/6$. Then any point in some neighborhood of the fixed point (x^*, y^*) is quasiperiodic, and all points of the same quasiperiodic orbit are dense on the corresponding invariant ellipse of the map F_1. Using the values c^* given in (69) we can state the following

Proposition. *Let $a = 1$, $c = c_\rho$. Then in the phase space of the map F there exists an invariant region Q, bounded by an invariant ellipse $\mathcal{E}$ of the map F_1 which is tangent to LC_{-1} (and to all its images) if $c < c^*$, to LC'_{-1} if $c > c^*$, and to both critical lines LC_{-1} and LC'_{-1} if $c = c^*$. Any initial point $(x_0, y_0) \in Q$ belongs to a quasiperiodic orbit dense in the corresponding invariant ellipse of F_1, while any initial point $(x_0, y_0) \notin Q$ is mapped to $\mathcal{E}$.*

Note that from (69) it follows that if $d > r$ then the inequality $c^* < 0$ holds, thus, given $c > 0$, for $d > r$ only the lower boundary LC'_{-1} is involved in the construction of the invariant region of the map F at $a = 1$.

Bifurcation structure of the (a, c)-parameter plane

We describe now the dynamics of the map F after the center bifurcation, that is for $a > 1$. In short, an initial point (x_0, y_0) from some neighborhood of the unstable fixed point (x^*, y^*) moves away from it under the map F_1 and in a finite number k of iterations it necessarily enters either the region R_2, or R_3 (in the case in which (x^*, y^*) is a focus the statement is obvious, while if (x^*, y^*) is a repelling node this can be easy verified using the eigenvalues $\lambda_{1,2}$ given in (67) and the corresponding eigenvectors). If $(x_k, y_k) \in R_2$, then the map F_2 is applied: $F_2(x_k, y_k) = (x_{k+1}, y_{k+1}) \in LC_0$. All consequent iterations by F_2 give points on LC_0 approaching the attracting fixed point of F_2 (which belongs to R_1), until the trajectory enters R_1 where the map F_1 is applied again. If $(x_k, y_k) \in R_3$, then the map F_3 is applied: $F_3(x_k, y_k) = (x_{k+1}, y_{k+1}) \in LC_0'$. We have that either $(x_{k+1}, y_{k+1}) \in R_1$, or $(x_{k+1}, y_{k+1}) \in R_3$ and one more application of F_3 gives its fixed point $(r, r) \in R_1$, so, the map F_1 is applied to this point. In such a way the dynamics appear to be bounded.

Indeed, it was proved in Hommes [59], that for $a > 1$ any trajectory of F rotates with the same rotation number around the unstable fixed point, and it is attracted to a closed invariant curve $\mathcal{C}$ homeomorphic to a circle. It was also proved that the dynamics of F on $\mathcal{C}$, depending on the parameters, are either periodic or quasiperiodic. We can state that such a curve $\mathcal{C}$ is born due to the center bifurcation of the fixed point, described in the previous section: Namely, the bounded region P (or Q), which is invariant for $a = 1$, exists also for $a > 1$, but only its boundary remains invariant, and this boundary is the curve $\mathcal{C}$.

In the subsection below we shown that also in a more generic case of a two-dimensional piecewise linear map, defined by two linear maps, the center bifurcation can give rise to the appearance of a closed invariant attracting curve $\mathcal{C}$, on which the map is reduced to a rotation with rational or irrational rotation number. Recall that in the case of a rational rotation number m/n the map has an attracting and a saddle m/n-cycle on $\mathcal{C}$, so that the curve $\mathcal{C}$ is formed by the unstable set of the saddle cycle, approaching the points of the attracting cycle. While in the case of an irrational rotation number the map has quasiperiodic orbits on $\mathcal{C}$. In Section 2.3 of Chapter 2 the curve $\mathcal{C}$ is described in detail for the map defined by the linear maps F_1 and F_2 given in (64) and (65). So, we can use these results for the considered map F if the curve $\mathcal{C}$ belongs to the regions R_1, R_2 and has no intersection with the region R_3, thus, only the maps F_1 and F_2 are involved in the asymptotic dynamics. Obviously, we have a qualitatively similar case if the curve $\mathcal{C}$ has no intersection with the region R_2 and, thus, only the maps F_1 and F_3 are applied to the points on $\mathcal{C}$. One more possibility is the case in which the curve

$\mathcal{C}$ belongs to all the three regions R_i, $i = 1, 2, 3$. We can state that in the first and second cases the curve $\mathcal{C}$ can be obtained by iterating the generating segment of LC_{-1} and LC'_{-1}, respectively, while in the third case both generating segments can be used to get the curve $\mathcal{C}$.

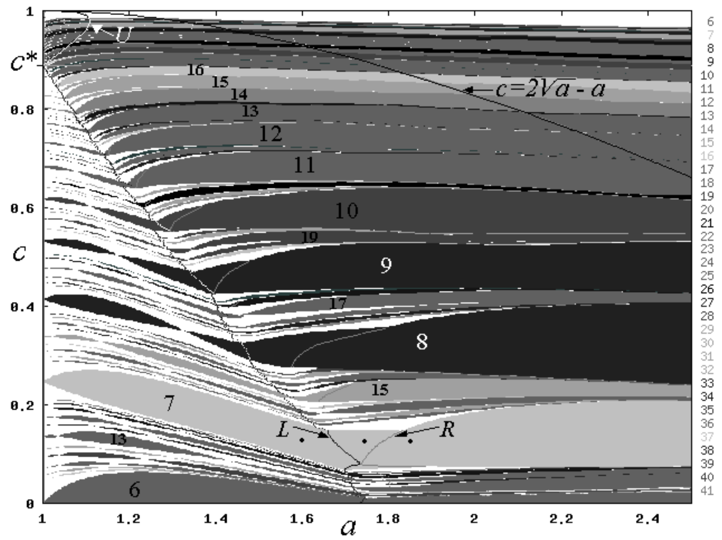

Fig.80 Two-dimensional bifurcation diagram of the map F in the (a, c)-parameter plane at $d = 10$, $r = 30$. Regions corresponding to attracting cycles of different periods $n \leq 41$ are shown by various gray tonalities.

To see which parameter values correspond to the cases described above we present in Fig.80 a two-dimensional bifurcation diagram in the (a, c)-parameter plane for fixed values $d = 10$, $r = 30$. Different gray tonalities indicate regions corresponding to attracting cycles of different periods $n \leq 41$ (note that regions related to the attracting cycles of the same period n, but with different rotation numbers are shown by the same gray tonality). The white region in Fig.80 is related either to periodic orbits of period $n > 41$, or to quasiperiodic orbits. Let us first comment on some particular parameter values of the bifurcation line $a = 1$. As described in the previous section, at $a = 1$, $c = c_{m/n}$ given in (68), in the phase plane of F there exists an invariant polygon P such that any point of P is periodic with the rotation number m/n. So, the points $a = 1$, $c = c_{m/n}$, for different $m/n < 1/6$, are starting points for the corresponding periodicity tongues. For example, $a = 1$, $c = c_{1/8} = \sqrt{2} - 1$ is the point from which the 8-periodicity tongue starts, corresponding to the attracting cycle with the rotation number $1/8$. Recall that according to the summation rule (see Hao and Zheng, 1998 [55]), between any two rotation numbers m_1/n_1 and m_2/n_2 there is also the rotation number $m'/n' = (m_1 + m_2)/(n_1 + n_2)$, so that $a = 1$, $c = c_{m'/n'}$ is the starting point for the corresponding periodicity region. If the (a, c)-parameter point is taken inside the periodicity region, then the map F has the attracting and saddle cycles with corresponding rotation number, and the unstable set of the saddle cycle form the closed invariant attracting curve $\mathcal{C}$. Note, that in the case in which both constrains are involved in the asymptotic dynamics, the map F may have two attracting cycles and two saddles of the same period coexisting on the invariant curve (as it occurs, for example, inside the 7-periodicity tongue at $a = 2.9$, $c = 0.136$, $d = 10$, $r = 30$). While if the (a, c)-parameter point belongs to the boundary of the periodicity region, then the border-collision bifurcation occurs (see [95]) for the attracting and saddle cycles, giving rise to their merging and disappearance.

The parameter points $a = 1$, $c = c_\rho$ given in (70), for different irrational numbers $\rho < 1/6$ correspond to the case in which any point of the invariant region Q is quasiperiodic. Such parameter points are starting points for the curves related to quasiperiodic orbits of the map F.

At $a = 1$, $c = c^* = 8/9$, (which is the value c^* given in (69) at $d = 10$ and $r = 30$) there exists an invariant ellipse of F_1 tangent to both critical lines LC_{-1} and LC'_{-1}, so that for $c < c^*$ the boundary of the invariant region can be obtained by iterating the generating segment of LC_{-1}, while for $c > c^*$ we can iterate the segment of LC'_{-1}. Thus, after the center bifurcation for $c < c^*$ at first only LC_{-1} is involved in the asymptotic dynamics, and then increasing a there is a contact of the curve $\mathcal{C}$ with the lower boundary LC'_{-1}. And vice versa for $c > c^*$. For example, the curve denoted by L inside the 7-periodicity region in Fig.80 indicates a collision of the curve $\mathcal{C}$ with the lower boundary LC'_{-1}. The curves related to similar collision are shown also inside some other periodicity regions. Before this collision the dynamics of F on $\mathcal{C}$ is as described in the above proposition, while after both boundaries LC_{-1} and LC'_{-1} are involved in the asymptotic dynamics. One more curve shown inside the periodicity regions (for example, the one denoted by R inside the 7-periodicity region) indicates that the point $(x, y) = (r, r)$ becomes a point of the corresponding attracting cycle.

To clarify, let us present examples of the phase portrait of the map F corresponding to three different parameter points inside the 7-periodicity region, indicated in Fig.80. Fig.81a shows the closed invariant attracting curve $\mathcal{C}$ at $a = 1.6$, $c = 0.125$, when $\mathcal{C}$ has no intersection with the region R_3, being made up by 7 segments of the images of the generating segment of LC_{-1}.

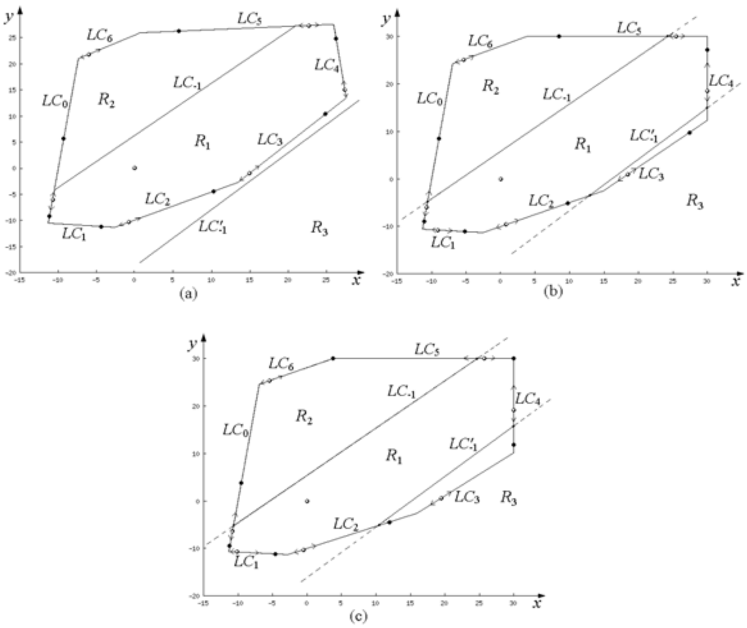

Fig.81 The attracting closed invariant curve C with the attracting and saddle cycles of period 7 at $c = 0.125$, $d = 10$, $r = 30$, and $a = 1.6$ in (a); $a = 1.75$ in (b); and $a = 1.85$ in (c).

The closed invariant curve $\mathcal{C}$ corresponding to the parameter values $a = 1.75$, $c = 0.125$, is shown in Fig.81b. In such a case both boundaries LC_{-1} and LC'_{-1} are involved in the dynamics. It can be easily seen that images of the generating segments of LC_{-1} and LC'_{-1} form the same set, so it does not matter which segment is iterating to get the curve $\mathcal{C}$.

Fig.81c presents an example of $\mathcal{C}$ at $a = 1.85$, $c = 0.125$, when two consequent points of the attracting cycle belong to the region R_3, so that $(x, y) = (r, r)$ is a point of the attracting cycle.

10.3 2D canonical form.

In the recent years more and more works on the BCB concerned the stuy of the one- and two-dimensional canonical forms, proposed in Nusse and Yorke [94], which are piecewise linear maps defined by two linear functions, being this analysis at the basis also of the BCB occurring in piecewise smooth systems. The two-dimensional canonical form has been mainly considered in *dissipative* cases associated with *real* eigenvalues of the point which undergoes the BCB. Among the effects studied up to now are uncertainty about the occurrence after the BCB (see e.g. [64], [34]), multistability and unpredictability of the number of coexisting attractors (see e.g. in [119]), as well as the so-called dangerous BCB ([56], [38]), related to the case in which a fixed point is attracting before and after the BCB, while at the bifurcation value the dynamics are divergent. However, in the last years the problem of BCB associated with points having *complex* eigenvalues, was raised in several applied models, see e.g. a sigma-delta modulation model in Feely et al. [35], several physical and engineering models in [118], a dc-dc converter in [120], business cycles models in economics as previously recolled ([37], [112], [108], [41], [42]). The so-called *center bifurcation*, first described in [112], associated with the transition of a fixed point to an unstable focus and the appearance of an attracting closed invariant curve, in piecewise linear maps is completely new with respect to the theory existing for smooth maps, the Neimark-Sacker (NS) bifurcation, although, as we shall see, there is a certain analogy: For example, the closed invariant curve made up by the saddle-node connections of a pair of cycles (a saddle and a node) is clearly similar to those occurring in smooth maps, however such a curve is not smooth but made up of finitely or infinitely many (depending on the type of noninvertibility of the map) segments and corner points. While similarly to the Arnold tongues in the smooth case, the periodicity regions in the piecewise linear case may be classified with respect to the rotation numbers, the boundaries of these periodicity regions, issuing from the center bifurcation line at points associated with rational rotation numbers, are BCB curves, instead of saddle-node bifurcation curves issuing from the NS bifurcation curve. Moreover, while the emanating point from the NS curve of an Arnold tongue is a cusp point (except for the strong resonance cases $1 : n$, $n = 1, 2, 3, 4$), in the piecewise linear case the periodicity regions are issuing with a nonzero opening angle.

So let us consider here the two-dimensional piecewise linear map which is a normal form to study BCB in piecewise smooth two-dimensional maps, describing the case in which one of the fixed points considered is a focus which undergoes a center bifurcation, and some BCB associated with it. The normal form for the border-collision bifurcation in a 2D phase space, a real plane, is represented by a family of two-dimensional piecewise linear maps $F : \mathbb{R}^2 \to \mathbb{R}^2$ given by two linear maps F_1 and F_2 which are defined in two half planes L and R:

$$F : (x, y) \mapsto \begin{cases} F_1(x, y), \ (x, y) \in L; \\ F_2(x, y), \ (x, y) \in R; \end{cases} \tag{71}$$

where

$$F_1 : \begin{pmatrix} x \\ y \end{pmatrix} \mapsto \begin{pmatrix} \tau_L x + y + \mu \\ -\delta_L x \end{pmatrix}, \ L = \{(x, y) : x \leq 0\}; \tag{72}$$

$$F_2 : \begin{pmatrix} x \\ y \end{pmatrix} \mapsto \begin{pmatrix} \tau_R x + y + \mu \\ -\delta_R x \end{pmatrix}, \ R = \{(x, y) : x > 0\}. \tag{73}$$

Here τ_L, τ_R are traces and δ_L, δ_R are determinants of the Jacobian matrix of the map F in the left and right halfplanes, i.e., in L and R, respectively, $\mathbb{R}^2 = L \cup R$.

The straight line $x = 0$ separating the regions L and R, and its images (backward by F^{-1} and forward by F) are called *critical lines* of the corresponding rank, that is, $LC_{-1} = \{(x, y) : x = 0\}$ is called basic critical line separating the definition regions of the two maps; $LC = F(LC_{-1}) = \{(x, y) : y = 0\}$ is the critical line (of rank 1) and $LC_i = F^i(LC)$ is the critical line of rank i. For convenience of notation we shall identify LC_i, $i = 0$, with LC. Note that due to continuity of the map F the first image of the straight line $x = 0$ by either F_1 or F_2 is the same straight line $y = 0$, i.e., $F_1(LC_{-1}) = F_2(LC_{-1}) = LC_0$, while LC_i, $i > 0$, is in general a broken line.

Property. The map F is invertible for $\delta_L\delta_R > 0$, noninvertible of $(Z_0 - Z_2)$-type for $\delta_L\delta_R < 0$, noninvertible of $(Z_0 - Z_\infty - Z_1)$-type for $\delta_L = 0$, $\delta_R \neq 0$ or $\delta_R = 0$, $\delta_L \neq 0$ and noninvertible of $(Z_0 - Z_\infty - Z_0)$-type for $\delta_L = 0$, $\delta_R = 0$.

To check this property it is enough to consider images of the regions L and R, i.e., $F_1(L)$ and $F_2(R)$. Let $\delta_R \neq 0$, $\delta_L \neq 0$. Then the map F is invertible if $F_1(L) \cap F_2(R) = LC$, i.e., L and R are mapped into two different halfplanes, that is true for $\delta_L\delta_R > 0$. The map F is noninvertible if $F_1(L) = F_2(R)$, i.e., if L and R are mapped into the same halfplane, so that the image of the plane is folded into a halfplane, in each part of which F has two distinct preimages. The map F is noninvertible of $(Z_0 - Z_2)$-type. It is easily to check that this is true for $\delta_L\delta_R < 0$.

If one of the two determinants is 0 then the related halfplane is mapped into the straight line LC, that is any point of LC has an infinity of preimages (a whole halfline), one of the two halfplanes separated by LC has no preimages, and another has one preimage, so that we have $(Z_0 - Z_\infty - Z_1)$-noninvertibility. In such a case the asymptotic dynamics of F are often reduced to a one-dimensional subspace of the phase space, as we have seen in the subsection above. In the case in which both the determinants are 0 we have two halfplanes mapped into LC. The map F on LC is reduced to the border-collision normal form for one-dimensional piecewise smooth continuous maps that we have already seen in the first subsection.

Following Banerjee and Grebogi [14] we denote by L^* and R^* the fixed points of F_1 and F_2 determined, respectively, by

$$\left(\frac{\mu}{1 - \tau_i + \delta_i}, \frac{-\delta_i\mu}{1 - \tau_i + \delta_i}\right), \; i = L, R.$$

Obviously, L^* and R^* become fixed points of the map F if they belong to the related regions L and R. Namely, L^* is the fixed point of the map F if $\mu/(1-\tau_L+\delta_L) \leq 0$, otherwise it is a so-called virtual fixed point which we denote by $\overline{L}^*$. Similarly, R^* is the fixed point of F if $\mu/(1-\tau_R+\delta_R) \geq 0$, otherwise it is a virtual fixed point denoted by $\overline{R}^*$. Clearly, if the parameter μ varies through 0, the fixed points (actual or/and virtual) cross the border LC_{-1}, so that the collision with it occurs at $\mu=0$, value at which L^* and R^* merge with the origin $(0,0)$.

Let μ vary from a negative to a positive value. As it was noted in [14], if some bifurcation occurs for μ increasing through 0, then the same bifurcation occurs also for μ decreasing through 0 if we interchange the parameters of the maps F_1 and F_2, i.e., there is a symmetry of the bifurcation structure with respect to $\tau_R=\tau_L$, $\delta_R=\delta_L$ in the $(\tau_R,\tau_L,\delta_R,\delta_L)$-parameter space. Thus, it is enough to consider μ varying from negative to positive.

We consider the parameter values such that the fixed point of the map F is attracting for $\mu<0$, i.e., before the border-collision. For $\mu<0$, and $1-\tau_L+\delta_L>0$, the point L^* is a fixed point of F. Its stability is defined by the eigenvalues $\lambda_{1,2(L)}$ of the Jacobian matrix of the map F_1, which are

$$\lambda_{1,2(L)} = \left(\tau_L \pm \sqrt{\tau_L^2 - 4\delta_L}\right)/2. \tag{74}$$

The triangle of stability of L^*, say S_L, is defined as follows:

$$S_L = \left\{(\tau_L,\delta_L) : 1+\tau_L+\delta_L>0, 1-\tau_L+\delta_L>0, 1-\delta_L>0\right\}. \tag{75}$$

Thus, let $(\tau_L,\delta_L)\in S_L$.

At $\mu=0$ we have $L^*=R^*=(0,0)$, i.e., the fixed points collide with the border line LC_{-1}. For $\mu>0$ (i.e., after the border-collision) and for $1-\tau_R+\delta_R>0$ the point R^* is the fixed point of F. The eigenvalues $\lambda_{1,2(R)}$ of the Jacobian matrix of the map F_2, and the triangle of stability S_R of R^* are defined as in (74) and (75), respectively, putting the index R instead of L.

Our main purpose is to describe the bifurcation structures of the (δ_R,τ_R) - parameter plane depending on the parameters $(\tau_L,\delta_L)\in S_L$ at some fixed $\mu>0$. Such a bifurcation diagram reflects the possible results of the border-collision bifurcation occurring when the attracting fixed point of F crosses the border $x=0$ while μ passes through 0. A classification of the different types of border-collision bifurcation depending on the parameters of F is presented in [14], [16], but related only to the case in which this map is dissipative on both sides of the border, i.e., for $|\delta_L|<1$, $|\delta_R|<1$.

We consider here a different case, with $|\delta_L| < 1$, $\delta_R > 1$, related, in particular, to a specific type of border-collision bifurcations, giving rise to closed invariant attracting curves. A similar problem is posed in [119] where among other results there is a descriptive analysis of the bifurcation structure of the (τ_L, τ_R)-parameter plane (called there as a chart of dynamical modes) for some fixed $\delta_R > 1$. Our approach to investigate the dynamical modes in the (δ_R, τ_R)-parameter plane gives the advantage of discussing the origin of the periodicity regions, namely to connect this problem to the center bifurcation occurring for $\delta_R = 1$, $-2 < \tau_R < 2$, $\mu > 0$.

10.3.1 Center bifurcation ($\delta_R = 1$)

Without loss of generality we can fix $\mu = 1$ in the following consideration. Indeed, one can easily see that $\mu > 0$ is a scale parameter: Due to linearity of the maps F_1 and F_2 with respect to x, y and μ, any invariant set of F contracts linearly with μ as μ tends to 0, collapsing to the point $(0, 0)$ at $\mu = 0$.

For $(\tau_L, \delta_L) \in S_L$, $(\tau_R, \delta_R) \in S_R$, $\mu = 1$, the map F has the stable fixed point R^* and the virtual fixed point $\overline{L}^*$. For $\tau_R^2 - 4\delta_R < 0$ the fixed point R^* is an attracting focus. If the (τ_R, δ_R)-parameter point leaves the stability triangle S_R crossing the straight line $\delta_R = 1$, then the complex-conjugate eigenvalues $\lambda_{1,2(R)}$ cross the unit circle, i.e., the fixed point R^* becomes a repelling focus.

At $\delta_R = 1$ the fixed point $R^* = (x^*, y^*)$, $x^* = 1/(2 - \tau_R)$, $y^* = -x^*$, is locally a center. What is the phase portrait of the map F in such a case? Note that at $\delta_R = 1$ the map F_2 is defined by a rotation matrix characterized by a rotation number which may be rational, say m/n, or irrational, say ρ. Obviously, there exists some neighborhood of the fixed point in which the behavior of F is defined only by the linear map F_2, i.e., there exists an invariant region included in R filled with invariant ellipses, each point of which is either periodic of period n (in case of a rational rotation number m/n, and we recall that the integer n denotes the period of the periodic orbit while m denotes the number of tours around the fixed point which are necessary to get the whole orbit), or quasiperiodic (in case of an irrational rotation number ρ).

Let F_2 be defined by a rotation matrix with an irrational rotation number ρ, which holds for $\delta_R = 1$, and

$$\tau_R = \tau_{R,\rho} \stackrel{def}{=} 2\cos(2\pi\rho). \tag{76}$$

Then any point from some neighborhood of the fixed point is quasiperiodic, and all the points of the same quasiperiodic orbit are dense on the invariant ellipse to which they belong. In such a case an invariant region

Q exists in the phase space, bounded by an invariant ellipse $\mathcal{E}$ of the map F_2, tangent to LC_{-1}, and, thus, also tangent to LC_i, $i = 0, 1, ...$ The equation of an invariant ellipse of F_2 with the center (x^*, y^*) through (x_0, y_0) is given by:

$$x^2 + y^2 + \tau_{R,\rho} xy - x + y = x_0^2 + y_0^2 + \tau_{R,\rho} x_0 y_0 - x_0 + y_0. \tag{77}$$

In order to obtain an ellipse tangent to LC_{-1}, we first get a tangency point

$$(\overline{x}, \overline{y}) = (0, -1/2), \tag{78}$$

which is *the same for any rotation number*. Then we write the equation of the ellipse (77) through $(\overline{x}, \overline{y})$, that gives us the equation of $\mathcal{E}$:

$$x^2 + y^2 + \tau_{R,\rho} xy - x + y = -1/4. \tag{79}$$

Thus, we can state the following

Proposition. *Let $\delta_R = 1$, $\tau_R = \tau_{R,\rho}$ given in (76). Then in the phase space of the map F there exists an invariant region Q, bounded by the invariant ellipse $\mathcal{E}$ given in (79). Any initial point $(x_0, y_0) \in Q$ belongs to a quasiperiodic orbit dense in the corresponding invariant ellipse (77).*

Let now F_2 be defined by the rotation matrix with a rational rotation number m/n, which holds for $\delta_R = 1$, and

$$\tau_R = \tau_{R,m/n} \overset{def}{=} 2\cos(2\pi m/n). \tag{80}$$

Then any point in some neighborhood of the fixed point R^* is periodic with rotation number m/n, and all the points of the same periodic orbit are located on an invariant ellipse of F_2. As before, the invariant region we are looking for includes obviously the region bounded by an invariant ellipse, say $\mathcal{E}_1$, tangent to LC_{-1}, given by

$$x^2 + y^2 + \tau_{R,m/n} xy - x + y = -1/4. \tag{81}$$

But in the case of a rational rotation number the invariant region is wider: There are other periodic orbits belonging to R. To see this, note that there exists a segment $S_{-1} = [a_0, b_0] \subset LC_{-1}$, which we call *generating segment*, such that its end points a_0 and b_0 belong to the same m/n-cycle located on an invariant ellipse of F_2 which crosses LC_{-1}, denoted $\mathcal{E}_2$ (note that $\mathcal{E}_2$ is not invariant for the map F). Obviously, the generating segment S_{-1} and its images by F_2, that is, the segments $S_i = F_2(S_{i-1})$, $S_i \subset LC_i = F_2(LC_{i-1})$, $i = 0, ..., n-2$, form a boundary of an invariant polygon denoted by P, with n sides, completely included in the region R. The polygon P is inscribed by $\mathcal{E}_1$ and circumscribed by $\mathcal{E}_2$ (see Fig.82 where such a polygon is shown in the case $m/n = 3/11$).

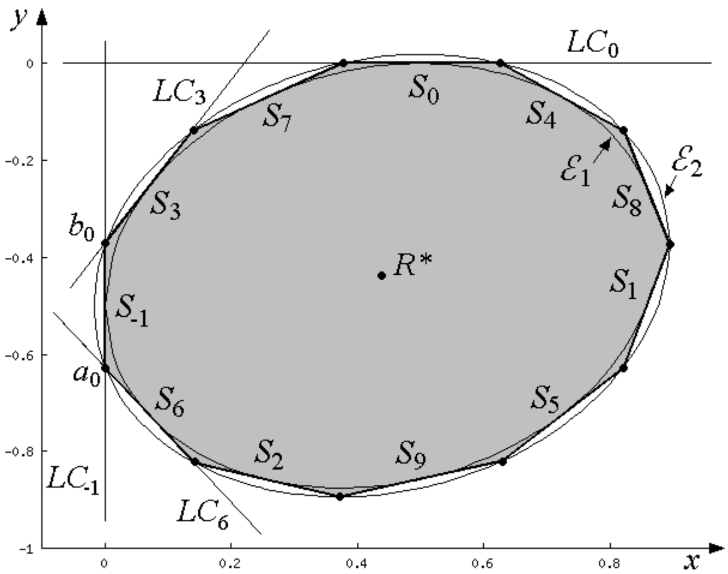

Fig.82 The invariant polygon P of the map F at $\delta_R = 1$, $\tau_R = 2\cos(2\pi m/n)$, $m/n = 3/11$.

The case $m/n = 1/n$ is the simplest one: It can be easily shown that the point $LC_{-1} \cap LC_0 = (0,0)$ and its $n-1$ images form a cycle of period n, all points of which are in R. The ellipse $\mathcal{E}_2$ through $(0,0)$ is given by

$$x^2 + y^2 + \tau_{R,1/n}xy - x + y = 0,$$

and the generating segment S_{-1} for any n has the end points $a_0 = (-1,0)$ and $b_0 = (0,0)$.

The case m/n for $m \neq 1$ is more tricky. To clarify our exposition we use the example of the rotation number $m/n = 3/11$ (see Fig.82). The end points of the generating segment S_{-1} are obtained as intersection points of LC_{-1} with two critical lines of proper ranks. We first obtain an equation for the image of LC_{-1} of any rank i by F_2 (for convenience, in this section we denote these images by LC_i, as in the general case, but recall that in the general case the images by F_1 have to be also considered so that LC_i is indeed a broken line). Let A denote the matrix defining F_2, i.e.,

$$A = \begin{pmatrix} \tau_{R,m/n} & 1 \\ -1 & 0 \end{pmatrix} = \begin{pmatrix} 2\cos(2\pi m/n) & 1 \\ -1 & 0 \end{pmatrix}.$$

For any integer $0 < i < n$ we can write down

$$A^i = \frac{1}{\sin(2\pi m/n)} \begin{pmatrix} \sin(2\pi(i+1)m/n) & \sin(2\pi i m/n) \\ -\sin(2\pi i m/n) & -\sin(2\pi(i-1)m/n) \end{pmatrix}. \qquad (82)$$

(Note that for $i = n$ we get an identity matrix). Making a proper change of coordinates and using (82) we get the following equation for the straight line LC_i for $0 \leq i < n$:

$$LC_i : \qquad y = -\frac{\sin(2\pi im/n)}{\sin(2\pi(i+1)m/n)}x + \frac{\tan(\pi(i+1)m/n)}{2\tan(\pi m/n)} - \frac{1}{2}.$$

The point of intersection of LC_{-1} and LC_i has the following coordinates:

$$\left(0, \frac{\tan(\pi(i+1)m/n)}{2\tan(\pi m/n)} - \frac{1}{2}\right). \tag{83}$$

Now we need to determine the proper rank k_1 such that the side $S_{k_1} \subset LC_{k_1}$ of the polygon P is an upper adjacent segment of the generating segment S_{-1}. The number n which is the period of the m/n-cycle, can be written as $n = rm + l$, where an integer $r = \lfloor n/m \rfloor$ is the number of periodic points visited for one turn around the fixed point, and an integer $l < m$ is the rest. For our example $m/n = 3/11$ we have $r = 3$ and $l = 2$. Following some geometrical reasoning, which we omit here, one can get that if $(m-1)/l$ is an integer, then

$$k_1 = \frac{(m-1)r}{l}, \tag{84}$$

so that the coordinates of the point b_0 are determined through m and n by substituting $i = k_1$ into (83). It can be easily shown that the coordinates of the other end point a_0 of S_{-1} are determined by substituting $i = k_2$ into (83), where

$$k_2 = n - 2 - k_1. \tag{85}$$

For the example shown in Fig.82 we have $k_1 = 3$ and $k_2 = 6$, so that the end points of S_{-1} are $a_0 = LC_{-1} \cap LC_6$ and $b_0 = LC_{-1} \cap LC_3$, whose coordinates are obtained by substituting $m/n = 3/11$ and, respectively, $i = 6$ and $i = 3$ into (83).

If $(m-1)/l$ is not an integer number, then we use a numerical algorithm to determine k_1 as the rank of the critical line whose intersection with LC_{-1} is m/n-periodic point; k_2 is determined by (85) as before.

Obviously, such a polygon P can be constructed for any rotation number m/n. Summarizing we can state the following

Proposition. *Let $\delta_R = 1$, $\tau_R = \tau_{R,m/n}$ given in (80). Then in the phase space of the map F there exists an invariant polygon P with n edges whose boundary is made up by the generating segment $S_{-1} \subset LC_{-1}$ and its $n-1$ images $S_i = F_2(S_{i-1}) \subset LC_i$, $i = 0, ..., n-2$. Any initial point $(x_0, y_0) \in P$ is periodic with rotation number m/n.*

Up to now we have not discussed the behavior of a trajectory with an initial point (x_0, y_0) not belonging to the invariant region (either P or Q), which obviously depends on the parameters δ_L, τ_L of the map F_1. Such a behavior can be quite rich, even in the case we are restricted to, that is for $(\delta_L, \tau_L) \in S_L$ in which the fixed point $\overline{L}^*$ of F_1 is attracting being virtual for F. Without going into a detailed description we give here different examples: A trajectory initiated outside P or Q can be

- attracted to a periodic or quasiperiodic trajectory belonging to the boundary of the invariant region (as, for example, for $\delta_L = 0.3$, $\tau_L = -0.4$, when F is invertible, $\overline{L}^*$ is a focus);

- mapped inside the invariant region (it is possible if F is $(Z_0 - Z_2)$ - noninvertible, like, for example, for $\delta_L = -0.5$, $\tau_L = 0.3$; $\overline{L}^*$ is a flip node);

- mapped to the boundary of the invariant region (it is possible for $(Z_0 - Z_\infty - Z_1)$ - noninvertibility, for example, at $\delta_L = 0$, $\tau_L = -0.3$; $\overline{L}^*$ is a flip node);

- attracted to some other attractor, regular, i.e., periodic or quasi-periodic (e.g., to a periodic attractor for $\tau_R = 0.25$, $\delta_L = 0.9$, $\tau_L = -0.7$) or chaotic (e.g., for $\tau_R = -1.5$, $\delta_L = 0.1$, $\tau_L = 0.63$), coexisting with the invariant region (for both examples $\overline{L}^*$ is a focus);

- divergent (e.g., for $\tau_R = -1.5$, $\delta_L = 0.9$, $\tau_L = -0.7$; $\overline{L}^*$ is a focus).

In the following we investigate the dynamics of the map F 'after' the center bifurcation, that is for $\delta_R > 1$. Among all the infinitely many invariant curves filling the invariant region (P or Q) at $\delta_R = 1$, only the boundary of it survives, being modified, after the bifurcation, that is for $\delta_R = 1 + \varepsilon$ at some sufficiently small $\varepsilon > 0$. Roughly speaking, the boundary of the former invariant region is transformed into an attracting closed invariant curve $\mathcal{C}$ on which the map F is reduced to a rotation. Similar to the NS bifurcation occurring for smooth maps, we can use the notion of rotation numbers: In case of a rational rotation number m/n two cycles of period n with rotation number m/n are born at the center bifurcation, one attracting and one saddle, and the closure of the unstable set of the saddle cycle approaching points of the attracting cycle forms the curve $\mathcal{C}$. In the piecewise linear case such a curve is not smooth, but a piecewise linear set, which in general has infinitely many corner points accumulating at the points of the attracting cycle. Differently from the smooth case such a curve is born not in a neighborhood of the fixed point: Obviously, its position is defined by the distance of the fixed point from the critical line LC. Description of such a curve, born due to the center bifurcation for some piecewise linear maps, as well as proof of its existence in particular cases, can be found in [37], [112], [119], [108], [109]. Our main interest here is related to the bifurcation structure of the (δ_R, τ_R)-parameter plane, namely, to the periodicity regions corresponding to the attracting cycles born due to the center bifurcation.

10.3.2 Bifurcation Diagrams in the (δ_R, τ_R)-parameter plane

Before entering into some general considerations we present examples of the 2D bifurcation diagram in the (δ_R, τ_R)-parameter plane for different values of δ_L and τ_L giving some comments on the bifurcation structure of the parameter plane. Note that each of these examples deserves more detailed investigation being quite rich in a sense of possible bifurcation scenarios. Some properties of similar bifurcation diagrams for piecewise linear and piecewise smooth dynamical systems were described, e. g., in [54], [112], [118], [108]. Referring to these papers, we recall here a few properties using our examples.

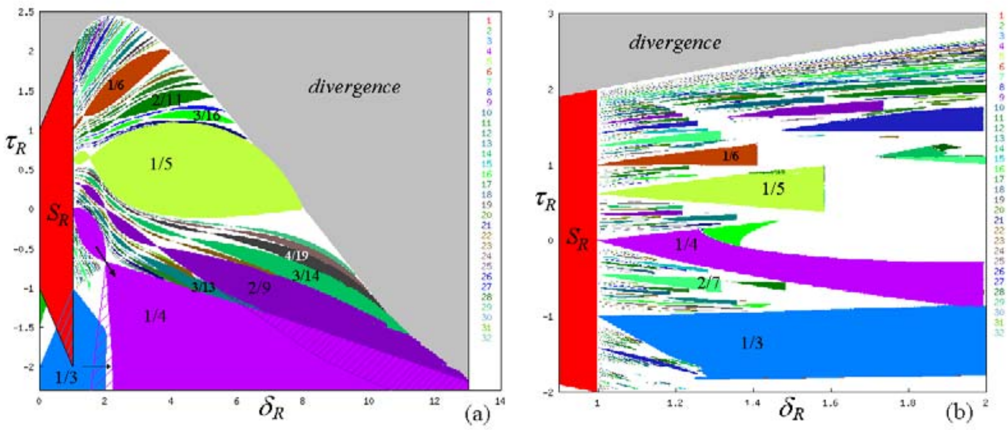

Fig.83 Two-dimensional bifurcation diargams of the map F in the (δ_R, τ_R)-parameter plane. In (a) $\delta_L = 0.25$, $\tau_L = 0.5$. F is invertible and $\overline{L}^*$ is an attracting focus. In (b) $\delta_L = -0.5$, $\tau_L = 0.3$. F is noninvertible, of $(Z_0 - Z_2)$-type, and $\overline{L}^*$ is an attracting flip node.

In the bifurcation diagrams presented in Fig.83a,b the parameter regions corresponding to attracting cycles of different periods n, $n \leq 32$, are shown in different colors (note that the periodicity regions related to attracting cycles with the same period n, but different rotation numbers, say m_1/n and m_2/n, are shown by the same color). If one takes the (δ_R, τ_R)-parameter point belonging to some m/n-periodicity region, denoted by $P_{m/n}$, then the corresponding map F has an attracting cycle of period n, which in general may be not the unique attractor. Some periodicity regions are marked also by the corresponding rotation numbers. White region on these figures is related either to higher periodicities, or to chaotic trajectories. Gray color corresponds to divergent trajectories.

Fig.83a presents the 2D bifurcation diagram for $\delta_L = 0.25$, $\tau_L =$

0.5. In such a case the map F is invertible (given that we consider $\delta_R > 1$, see Property 1); $\overline{L}^*$ is an attracting focus. Fig.83b presents the bifurcation diagram at $\delta_L = -0.5$, $\tau_L = 0.3$: For such parameter values F is noninvertible, of $(Z_0 - Z_2)$-type; $\overline{L}^*$ is an attracting flip node (i.e. one negative eigenvalue exists). Recall that such bifurcation diagrams representing qualitatively different dynamic regimes, reflect also possible results of the border-collision bifurcation of the attracting fixed point of the map F occurring when μ changes from a negative to a positive value. For example, if we fix $\delta_L = 0.25$, $\tau_L = 0.5$, $\delta_R = 4$, $\tau_L = 0.5$ (the parameter point is inside the region $P_{1/5}$ on Fig.83a), then for $\mu < 0$ the map F has the attracting focus L^* which at $\mu = 0$ undergoes the border-collision bifurcation resulting (for $\mu > 0$) in the attracting and saddle cycles of period 5. First of all we recall that an issuing point for the periodicity region $P_{m/n}$ is $(\delta_R, \tau_R) = (1, \tau_{R,m/n})$, where $\tau_{R,m/n}$ is given in (80). In the vicinity of the bifurcation line $\delta_R = 1$ the periodicity regions are ordered in a way similar to that of the Arnold tongues associated with the NS bifurcation occurring for smooth maps. In short, the periodicity regions follow a summation rule, or Farey sequence rule, holding for the related rotation numbers (see, e.g., [87], [76]). In particular, according to this rule if, for example, $r_1 = m_1/n_1$ and $r_2 = m_2/n_2$ are two rotation numbers, associated at $\delta_R = 1$ with $\tau_R = \tau_{R,r_1}$ and $\tau_R = \tau_{R,r_2}$, $\tau_{R,r_1} < \tau_{R,r_2}$, then there exists also a value $\tau_R = \tau_{R,r_3}$, $\tau_{R,r_1} < \tau_{R,r_3} < \tau_{R,r_2}$, related to the rotation number $r_3 = (m_1 + m_2)/(n_1 + n_2)$, so that $(\delta_R, \tau_R) = (1, \tau_{R,r_3})$ is an emanating point for the region P_{r_3}. To illustrate the summation rule some periodicity regions are marked in Fig.83 by the rotation numbers of the related cycles.

The kind of bifurcations associated with the boundaries of the periodicity regions differs from the smooth case: It is known that the boundaries of the Arnold tongues issuing from the Neimark-Sacker bifurcation curve are related to saddle-node bifurcations, and the other boundaries correspond to stability loss of the related cycle. While for piecewise linear maps the boundaries of the periodicity regions issuing from the center bifurcation line correspond to so-called border-collision pair bifurcations (a piecewise linear analogue of the saddle-node bifurcation), which we shall consider in detail in the next section.

Note also that differently from the smooth case the periodicity regions can have a 'sausage' structure (see Fig.83) with several subregions, first described in [54], which is typical for piecewise smooth and piecewise linear systems (see also [118], [112]). In fact, different subregions of the same periodicity region for the considered map F are related to different compositions of the maps F_1 and F_2 applied to get the corresponding cycle (attracting or saddle). It can be shown that the first (leftmost) subregion of the m/n-periodicity region, denoted by $P^1_{m/n}$, is related to an attracting m/n-cycle with two periodic points located in L and $n-2$ points in R, that is, the related composition can be written as $F^n = F_1^2 \circ F_2^{n-2}$ for $m = 1$, and $F^n = F_1 \circ F_2^i \circ F_1 \circ F_2^{n-2-i}$, for $m \neq 1$, where $i > 1$ depends on m and n. The corresponding saddle m/n-cycle for any m for parameters from $P^1_{m/n}$ has one periodic point in L and $n-1$ points in R, that is, for such a cycle $F^n = F_1 \circ F_2^{n-1}$.

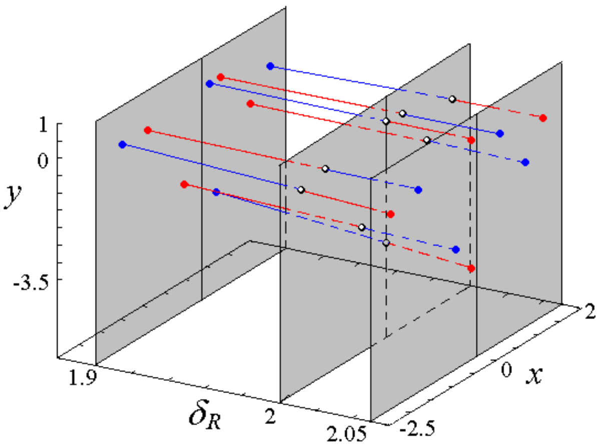

Fig.84 Bifurcation diagram for $\delta_R \in [1.9, 2.05]$, $\delta_L = 0.5$, $\tau_L = 0.25$, related to the parameter path shown in Fig.83a by the thick straight line with an arrow. The points of the attracting and saddle cycles are shown in red and blue, respectively.

The 'waist' points separating subregions are related to a particular border-collision bifurcation at which points of the attracting and saddle cycles exchange their stability colliding with the border: Namely, after the collision the former attracting cycle becomes a saddle one while the saddle cycle becomes attracting (for details see [31], [112]). To illustrate such a border-collision bifurcation we have chosen the waist point $(\delta_R, \tau_R) \approx (2, -0.6666)$ of the region $P_{1/4}$ at $\delta_L = 0.5$, $\tau_L = 0.25$ (see Fig.83a). Fig.84 presents a bifurcation diagram for $\delta_R \in [1.9, 2.05]$, $\tau_R = -1.6665\delta_R + 2.66635$, so that the parameter point moves from the first subregion $P^1_{1/4}$, to the second one, denoted $P^2_{1/4}$ (the related parameter path is shown by the thick straight line with an arrow in Fig.83a). On this diagram the points of the attracting and saddle cycles are shown in red and blue, respectively. Three (x, y)-planes shown in gray represent a part of the phase portrait of the system: Before the bifurcation, i.e., for $(\delta_R, \tau_R) \in P^1_{1/4}$; at the moment of the border-collision related to the waist point $(\delta_R, \tau_R) \approx (2, -0.6666)$; and after the bifurcation, i.e., for $(\delta_R, \tau_R) \in P^2_{1/4}$. Comparing the phase portrait related to the subregion

$P^2_{1/4}$ with the one related to $P^1_{1/4}$, one can see that the number of periodic points in L is increased: Now three points of the attracting cycle are in L and one in R, and for the saddle cycle we have two points in L and two in R.

Let us comment also the overlapping of periodicity regions, which corresponds to multistability (as an example, see Fig.83a on which several multistability regions are dashed, related with the periodicity regions $P_{1/3}$ and $P_{1/4}$. Some other overlapping zones can be seen in the same figure, as well as in Fig.83b). Recall that considering the initial problem of the BCB of the fixed point of F, we have that in the case of multistability, varying μ through 0, the fixed point bifurcates into several attractors. As it was already mentioned, any invariant set of F contracts linearly with μ as μ tends to 0 collapsing to the origin at $\mu = 0$. Among such invariant sets we have the basins of attraction of coexisting attractors which shrink to 0 as well. Thus, one cannot answer a priori to which attractor the initial point will be attracted after the bifurcation. This gives a source of unpredictability of the results of the BCB. This problem was posed first in [64], see also [34]. To give an example, we fix $\delta_L = 0.25$, $\tau_L = 0.5$, $\tau_R = -2$ and will increase the value of δ_R starting from $\delta_R = 1.5$, when the map F has attracting and saddle cycles of period 3 (see the arrow in Fig.83a). At $\delta_R \approx 1.64$ a border-collision pair bifurcation occurs giving birth to attracting and saddle cycles of period 4, i.e., the parameter point enters the bistability region. Fig.85a presents a part of the phase portrait of the system at $\delta_R = 1.65$ when there are coexisting attracting cycles of period 3 and 4 whose basins of attraction, separated by the stable set of the period 4 saddle, are shown in yellow and green, respectively. The unstable set (shown in blue) of the saddle 3-cycle, approaching points of the attracting 3-cycle, forms a saddle-node connection which is wrinkled due to two negative eigenvalues of the attracting 3 cycle. With further increasing δ_R the stable set of the period 3 saddle (shown in red) tends to get a tangency with its unstable set. Indeed, at $\delta_R \approx 1.68$ a homoclinic bifurcation occurs after which the saddle-node connection is destroyed. Another qualitative change of the phase space occurs when the attracting 3-cycle undergoes a 'flip' bifurcation (an eigenvalue passing through -1) resulting in a cyclic chaotic attractor of period 6. After pairwise merging of the pieces of the attractor it becomes a 3-piece cyclic chaotic attractor shown in Fig.85b (for further details related to the 'flip' bifurcation in a piecewise linear map see [78]). Note that the boundary separating the basins of attraction is no longer regular as in Fig.85a but fractal. Such a basin transformation is a result of the homoclinic bifurcation of the saddle 4-cycle.

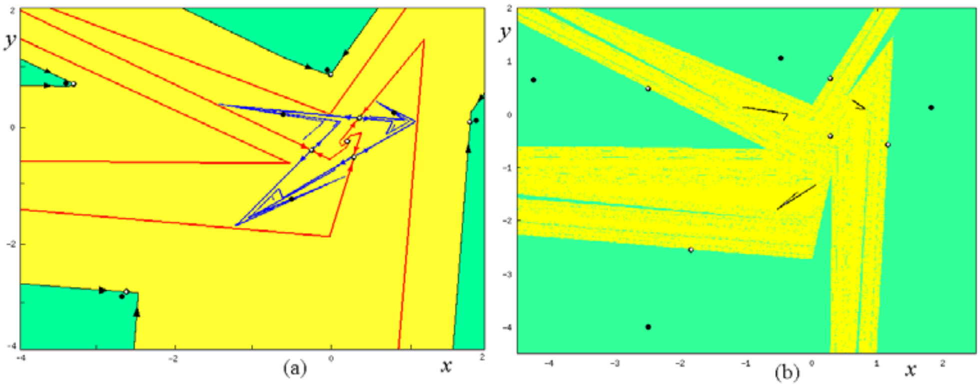

Fig.85 In (a) $\delta_L = 0.25$, $\tau_L = 0.5$, $\delta_R = 1.65$, $\tau_R = -2$. Attracting cycles of periods 3 and 4 with their basins of attraction (shown in yellow and green, respectively) separated by the stable set of the 4-saddle; The unstable set (in blue) of the 3-saddle forms a saddle-node connection which is near to be destroyed by homoclinic tangency with the stable set (in red). In (b) $\delta_R = 2.2$. Basins of attraction of the 3-piece cyclic chaotic attractor and 4-cycle are shown in yellow and green, respectively.

A contact with the fractal basin boundary leads to the disappearance of the chaotic attractor at $\delta_R \approx 2.25$. Thus, in the considered sequence of bifurcations, the attracting 4-cycle coexists first with the attracting 3-cycle, then with the 6-piece chaotic attractor and finally with the 3-piece chaotic attractor. To illustrate the border-collision bifurcation of the fixed point of F in a case of multistability we present in Fig.86 a bifurcation diagram for $\mu \in [-0.2 : 1]$, related to Fig.85b. The problem of multiple attractors and the role of homoclinic bifurcation is discussed in [119], [108].

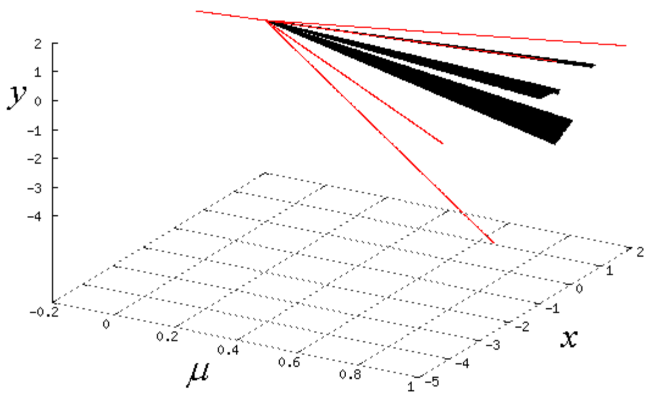

Fig.86 Phase space (x, y) as μ changes in the interval $\mu \in [-0.2 : 1]$ at $\delta_L = 0.25$, $\tau_L = 0.5$, $\delta_R = 2.2$, $\tau_R = -2$. After the BCB at $\mu = 0$ the attractor in red is the attracting 4-cycle, while the attractor in black is the 3-piece chaotic attractor.

10.3.3 $1/n$ periodicity regions and their BCB boundaries

Let us consider now the first subregion, denoted by $P^1_{1/n}$, of the main periodicity region $P_{1/n}$. For such regions in the parameter space we can get the analytic representations for their boundaries related to the BCB, that is, the two boundaries of the regions issuing from the center bifurcation line, which we shall call BC boundaries for short. Note that in general any periodicity region has two BC boundaries and may have also other boundaries which are related to the stability loss of the corresponding attracting cycle. Note that (similarly to the smooth case) inside a periodicity region it is not guaranteed the existence of a closed invariant curve, which can be destroyed in several ways (for a list of mechanisms of destruction of a closed invariant attracting curve in the piecewise linear case see [108]).

So let us consider a periodicity region $P_{1/n}$ and let $(\delta_R, \tau_R) \in P^1_{1/n}$. Denote the related attracting and saddle cycles by $p = \{p_0, ..., p_{n-1}\}$ and $p' = \{p'_0, ..., p'_{n-1}\}$, respectively. Let $p_0, p_{n-1} \in L$ and $p_1, ..., p_{n-2} \in R$. As for the saddle cycle, let $p'_0 \in L$ and $p'_1, ..., p'_{n-1} \in R$. We shall see what happens with these cycles if the (δ_R, τ_R)-parameter point crosses the two BC boundaries of $P^1_{1/n}$. To illustrate our consideration we use an example shown in Fig.87a for $\delta_L = 0.25$, $\tau_L = 0.5$, i.e., $(\delta_R, \tau_R) \in P^1_{1/5}$ (see Fig.83a).

We consider a fixed value $\delta_R = \delta^*_R$ inside the periodicity tongue, such that the qualitative position of the periodic points in the (x, y) phase plane is presented in Fig.87a. Now let us increase the value of τ_R, then the point p_{n-1} of the cycle moves towards the critical line LC_{-1}, so that at some $\tau_R = \tau^*_R$ we have $p_{n-1} \in LC_{-1}$ (and, as a consequence, $p_0 \in LC_0$) which indicates a BCB. It occurs not only for the attracting cycle: Indeed, also the saddle cycle undergoes the BCB, namely, at $\tau_R = \tau^*_R$ we have $p'_{n-1} \in LC_{-1}$, moreover, $p'_{n-1} = p_{n-1}$, as well as all the other points of the cycles p and p' are pairwise merging on the critical lines of the proper ranks (see Fig.87c). In such a way the 'saddle-node' BCB occurs (not related to an eigenvalue equal to 1). The value $\tau_R = \tau^*_R$ corresponds to the (δ_R, τ_R)-parameter point crossing the upper boundary of $P^1_{1/n}$, which we denote by $BC_{1/n(1)}$. While if at the fixed $\delta_R = \delta^*_R$ the value τ_R is decreased, then p_0 and p'_1 move towards the critical line LC_{-1}, so that at some $\tau_R = \tau^{**}_R$ we have $p_0 = p'_1 \in LC_{-1}$, thus one more 'saddle-node' BCB occurs (see Fig.87b), related to the (δ_R, τ_R)-parameter point crossing the lower boundary of $P^1_{1/n}$, denoted by $BC_{1/n(2)}$.

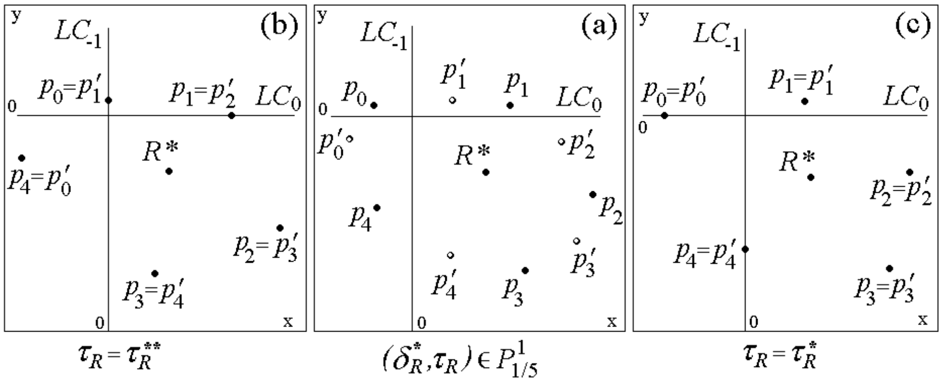

Fig.87 Examples of the 'saddle-node' BCB for (δ_R,τ_R)-parameter points crossing the boundaries of $P^1_{1/5}$ at $\delta_L=0.25$, $\tau_L=0.5$: (a) $(\delta^*_R,\tau_R)=(1.25,0.65)\in P^1_{1/5}$; (b) $(\delta^*_R,\tau^{**}_R)\in BC_{1/5(2)}$ where $\tau^{**}_R\approx 0.575$; (c) $(\delta^*_R,\tau^*_R)\in BC_{1/5(1)}$ where $\tau^*_R\approx 0.726$.

Independently on the way the parameters τ_R and δ_R are varying, the two conditions for the BCB of the cycle p (at this moment we say nothing about its stability before the bifurcation), are $p_0\in LC_{-1}$ and $p_0\in LC_0$, or, more precisely,

$$BC_{1/n(1)} \qquad (x_0,0)=F_2^{n-1}\circ F_1(x_0,0), \tag{86}$$
$$BC_{1/n(2)} \qquad (0,y_0)=F_1\circ F_2^{n-1}(0,y_0), \tag{87}$$

where (x_0,y_0) are coordinates of the point p_0.

Let the matrix defining the map F_2 be denoted by A, that is

$$A=\begin{pmatrix}\tau_R & 1\\ -\delta_R & 0\end{pmatrix}.$$

It is not difficult to note that A^i, $i>1$, can be written as follows:

$$A^i=\begin{pmatrix}a_i & a_{i-1}\\ -\delta_R a_{i-1} & -\delta_R a_{i-2}\end{pmatrix}, \tag{88}$$

where a_i is a solution of the second order difference equation

$$a_i-\tau_R a_{i-1}+\delta_R a_{i-2}=0 \tag{89}$$

with the initial conditions

$$a_0=1,\ a_1=\tau_R. \tag{90}$$

We know that the eigenvalues of the corresponding characteristic equation of (89) are complex-conjugate: $\lambda_{1,2(R)}=\left(\tau_R\pm\sqrt{\tau_R^2-4\delta_R}\right)/2$, where $\tau_R^2 < 4\delta_R$, so the general solution of (89) with the initial conditions (90) can be written as

$$a_i = \left(\sqrt{\delta_R}\right)^i \left(\cos(2\pi i/n) + \frac{\tau_R}{\sqrt{4\delta_R - \tau_R^2}} \sin(2\pi i/n)\right).$$

For example, $a_2 = \tau_R^2 - \delta_R$, $a_3 = \tau_R^3 - 2\tau_R\delta_R$, and so on.

Now, to get the condition in (86) in terms of the parameters of the system, we first shift the coordinate system so that the origin becomes the fixed point of F_2, that is we make a change of variables: $x' = x - x^*$, $y' = y - y^*$. Note that $y^* = -\delta_R x^*$. Then, in the new variables the maps F_1 and F_2, say $\widetilde{F}_1$ and $\widetilde{F}_2$, become

$$\widetilde{F}_1 : \begin{pmatrix} x' \\ y' \end{pmatrix} \mapsto \begin{pmatrix} \tau_L(x' + x^*) + y' + y^* + 1 - x^* \\ -\delta_L(x' + x^*) - y^* \end{pmatrix}, \quad x' \leq -x^*;$$
$$\widetilde{F}_2 : \begin{pmatrix} x' \\ y' \end{pmatrix} \mapsto \begin{pmatrix} \tau_R x' + y' \\ -\delta_R x' \end{pmatrix}, \quad x' \geq -x^*.$$

The equality (86) in the new variables is

$$(x'_0 - x^*, \delta_R x^*) = \widetilde{F}_2^{n-1} \circ \widetilde{F}_1(x'_0 - x^*, \delta_R x^*). \tag{91}$$

Note that $\widetilde{F}_2^i$ can be written as

$$\widetilde{F}_2^i : \begin{pmatrix} x' \\ y' \end{pmatrix} \mapsto A^i \begin{pmatrix} x' \\ y' \end{pmatrix},$$

where A^i is given in (88). So, substituting (88) with $i = n - 1$ into (91) and equating the two expressions for x'_0, we get the equality

$$\frac{\delta_R a_{n-1} - a_n + 1}{\delta_L a_{n-2} - \tau_L a_{n-1} + 1} = \frac{\delta_R a_{n-2} - a_{n-1} + 1}{\delta_L a_{n-3} - \tau_L a_{n-2}}$$

which can be also written as

$$BC_{1/n(1)}: \qquad \frac{a_{n-1} + a_{n-2} + ... + a_1 + 1}{\delta_L a_{n-2} - \tau_L a_{n-1} + 1} = \frac{a_{n-2} + a_{n-3} + ... + a_1 + 1}{\delta_L a_{n-3} - \tau_L a_{n-2}}. \tag{92}$$

Similarly, the equality in (87) in the new variables (x', y') is written as

$$(-x^*, y'_0 + \delta_R x^*) = \widetilde{F}_1 \circ \widetilde{F}_2^{n-1}(-x^*, y'_0 + \delta_R x^*),$$

from which we get the equality

$$BC_{1/n(2)}: \quad \frac{\delta_L(a_{n-1} - 1) + \delta_R}{\delta_L a_{n-2} + 1} = \frac{\tau_L(a_{n-1} - 1) - \delta_R a_{n-2} + \tau_R - 1}{\tau_L a_{n-2} - \delta_R a_{n-3}}. \tag{93}$$

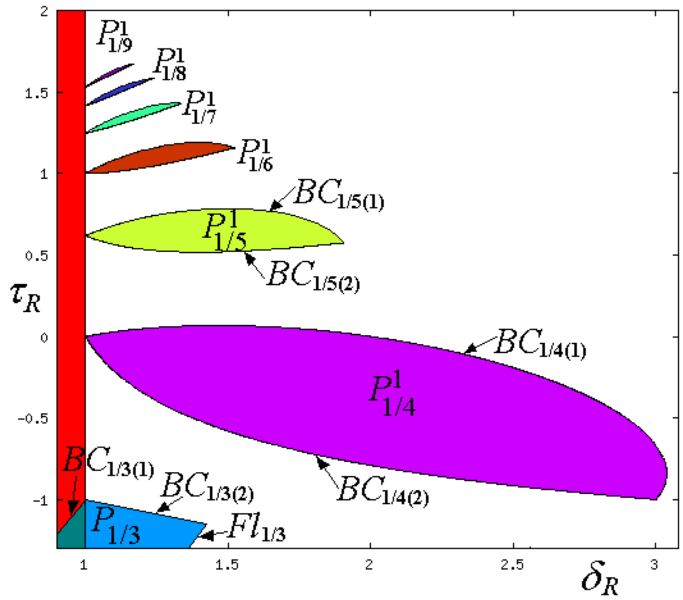

Fig.88 The border-collision bifurcation curves $BC_{1/n(1)}$ and $BC_{1/n(2)}$, $n = 3, ..., 9$; $\delta_L = 0$, $\tau_L = 0.5$.

For fixed values of the parameters δ_L and τ_L, the equalities (92) and (93) represent, in an implicit form, two curves in the (δ_R, τ_R)-parameter plane. As an example, in Fig.88 the curves $BC_{1/n(1)}$ and $BC_{1/n(2)}$ are plotted for $n = 3, ..., 9$, where $\delta_L = 0$, $\tau_L = 0.5$. Obviously, only particular arcs of the curves given in (92) and (93) are related to the BCB of the attracting cycle. The end points of such arcs are the waist points issuing from the NS curve, being two intersection points of (92) and (93), and one of them belongs, obviously, to the center bifurcation line, i.e., $\delta_R = 1$, $\tau_R = \tau_{R,1/n} = 2\cos(2\pi/n)$ (see (80)).

For example, let us consider in more details the region $P^1_{1/4}$ at $\delta_L = 0$, $\tau_L = 0.5$ (see Fig.88). The BC boundaries of $P^1_{1/4}$ are given by

$$BC_{1/4(1)}: \quad \tau_R - \delta_R - \tau_L\delta_R + \tau_L\tau_R\delta_R + \tau_R^2 + \tau_L\tau_R^2 + \tau_L\delta_R^2 + 1 = 0, \quad (94)$$

$$BC_{1/4(2)}: \quad -\tau_L\tau_R - \tau_L + \delta_R - 1 - \tau_L\tau_R^2 + \tau_L\delta_R + \delta_R\tau_R = 0. \quad (95)$$

For $\tau_L = 0.5$ we can easily obtain the waist points, which are $(\delta_R, \tau_R) = (1, 0)$ and $(\delta_R, \tau_R) = (3, -1)$. We can also check that for the curve $BC_{1/4(1)}$ the derivative of τ_R with respect to δ_R, evaluated at $(\delta_R, \tau_R) = (1, 0)$ is

$$\tau'_R|^{(1)}_{(\delta_R,\tau_R)=(1,0)} = \frac{1-\tau_L}{1+\tau_L},$$

while for the curve $BC_{1/4(2)}$ we have

$$\tau'_R\big|^{(2)}_{(\delta_R,\tau_R)=(1,0)} = \frac{\tau_L+1}{\tau_L-1} = \frac{1}{\tau'_R\big|^{(1)}_{(\delta_R,\tau_R)=(1,0)}}$$

These two derivatives are not equal (in effect they are reciprocal), thus the point $(\delta_R, \tau_R) = (1, 0)$, which is an issuing point for the region $P^1_{1/4}$, is not a cusp point.

1/3 periodicity region

Let us consider in more details the region $P_{1/3}$ in the (δ_R, τ_R)-parameter plane for $(\delta_L, \tau_L) \in S_L$. Let $p = \{p_0, p_1, p_2\}$ be a cycle of period 3 of the map F such that $p_0, p_1 \in L$ and $p_2 \in R$. Substituting $n = 3$ to (92) and (93) we get the equations for the BC boundaries of $P_{1/3}$, which are the straight lines in the (δ_R, τ_R)-parameter plane:

$$BC_{1/3(1)}: \quad \begin{cases} \tau_R = (\delta_R - \delta_R\delta_L - 1 - \tau_L)/(\delta_L + \tau_L), & \text{for } \delta_L \neq -\tau_L; \\ \delta_R = 1, & \text{for } \delta_L = -\tau_L; \end{cases} \tag{96}$$

$$BC_{1/3(2)}: \quad \begin{cases} \tau_R = (-\delta_R\delta_L - \delta_R\tau_L + \delta_L - 1)/(1 + \tau_L), & \text{for } \tau_L \neq -1; \\ \delta_R = 1, & \text{for } \tau_L = -1. \end{cases} \tag{97}$$

We can also obtain the equations defining the boundaries of the triangle of stability of the cycle p. Indeed, the map F^3 corresponding to the considered cycle is $F^3 = F_2 \circ F_1^2$, for which the related eigenvalues $\eta_{1,2}$ are less then 1 in modulus for

$$\left\{ \begin{array}{l} \left\{ \begin{array}{l} \tau_R > (\delta_R(\tau_L - \delta_L^2) - 1 + \delta_L\tau_L)/(\tau_L^2 - \delta_L), \\ \tau_R > (\delta_R(\tau_L + \delta_L^2) + 1 + \delta_L\tau_L)/(\tau_L^2 - \delta_L), \end{array} \right. \quad \text{for } \tau_L^2 > \delta_L; \\ \left\{ \begin{array}{l} \tau_R < (\delta_R(\tau_L - \delta_L^2) - 1 + \delta_L\tau_L)/(\tau_L^2 - \delta_L), \\ \tau_R < (\delta_R(\tau_L + \delta_L^2) + 1 + \delta_L\tau_L)/(\tau_L^2 - \delta_L), \end{array} \right. \quad \text{for } \tau_L^2 < \delta_L; \\ \qquad\qquad \delta_R < \frac{1}{\delta_L^2}, \end{array} \right. \tag{98}$$

so that the 'flip' bifurcation line denoted by $Fl_{1/3}$ and related to $\eta_2 = -1$, is given by

$$Fl_{1/3}: \quad \begin{cases} \tau_R = (\delta_R(\tau_L - \delta_L^2) - 1 + \delta_L\tau_L)/(\tau_L^2 - \delta_L), & \text{for } \tau_L^2 \neq \delta_L; \\ \delta_R = (\delta_L\tau_L - 1)/(\delta_L^2 - \tau_L), & \text{for } \tau_L^2 = \delta_L; \end{cases} \tag{99}$$

the bifurcation line related to $\eta_1 = 1$, denoted by $T_{1/3}$ (a particular "transcritical" bifurcation in our examples, as we shall see), is given by

$$T_{1/3}: \quad \begin{cases} \tau_R = (\delta_R(\tau_L + \delta_L^2) + 1 + \delta_L\tau_L)/(\tau_L^2 - \delta_L), & \text{for } \tau_L^2 \neq \delta_L; \\ \delta_R = -(\delta_L\tau_L + 1)/(\delta_L^2 + \tau_L), & \text{for } \tau_L^2 = \delta_L; \end{cases} \tag{100}$$

and by $C_{1/3}$ we denote the center bifurcation line (related to $\left|\eta_{1,2}\right| = 1$ for the complex-conjugate $\eta_{1,2}$), which is given by

$$C_{1/3}: \quad \delta_R = \frac{1}{\delta_L^2}, \ \delta_L \neq 0. \tag{101}$$

Thus, in the (δ_R, τ_R)-parameter plane we have 5 straight lines such that two of them, namely, $BC_{1/3(1)}$, $BC_{1/3(2)}$ are necessarily the boundaries of $P_{1/3}$, while three others depend on δ_L and τ_L : All the three lines may be involved as boundaries of $P_{1/3}$, or only two of them, or only one. Note that it may also happen that $P_{1/3} = \varnothing$, as well as $P_{1/3}$ may be an unbounded set (as, for example, in the case shown in Fig.88, in which the straight line $BC_{1/3(1)}$ is parallel to the straight line $Fl_{1/3}$). All the above cases can be classified depending on the values of δ_L and τ_L.

Coming back to the initial problem of the BCB of the attracting fixed point of F occurring for μ varying through 0 at some fixed values of the other parameters of the normal form (71), one can check analytically, using (96)-(101), whether an attracting cycle of period 3 is born due to the bifurcation.

11 Appendix on the Myrber's map.

In this Appendix we summarize some of the properties of the maps which are topologically conjugated to the logistic map or Myrberg's map T : $x' = x^2 - b$, say $T : X \to X$, $X = [q_1^{-1}, q_1]$ where q_1 is the fixed point always repelling for $b \in [-1/4, 2]$. The critical point is denoted as x_c, and the absorbing interval is $I = [T(x_c), T^2(x_c)]$.

On the x-axis, the repelling cycles and their preimages and limit points have a fractal organization when $b \geq b_{1s}$ where b_{1s} denotes the Feigenbaum point, i.e. the limit point of the first flip bifurcation sequence of the $2-$cycle of T. For each value of the parameter b, $b \geq b_{1s}$, the fractal structure of the map singularities is completely identified from the *box-within-a-box* bifurcation structure described in the years 1975 by Mira (see [87] and references therein). Consider b ($b \geq b_{1s}$) such that the map has an attracting $k-$cycle $\mathcal{C}$, then for the map T^k this cycle gives k attracting fixed points P_i, $i = 1, ..., k$, each of them with an immediate basin $d_0(P_i)$, and a total non connected basin $d(P_i) = \cup_{n>0} T^{-kn} d_0(P_i)$. The total basins $d(P_i)$ have a fractal structure, and a strange repeller Λ_i belongs to the boundary of $\cup_{n=1}^{k} d(P_i)$. For the map T this is reflected in a cyclical property, so that the basin $d(\mathcal{C})$ is the union of the k basins and its fronties is a strange repeller Λ, i.e. an invariant set, $T(\Lambda) = \Lambda$, such that the restriction $T : \Lambda \to \Lambda$ is chaotic (in the sense of Devaney, i.e. topological chaos with positive topological entropy). This frontier (on which the map is chaotic) if a set of zero measure in the interval X.

For any value of b almost all the points x of the interval $]q_1^{-1}, q_1[$ (i.e. apart from at most a set of points of zero Lebesgue measure) have the same asymptotic behavior, which sometimes is called metric attractor A_λ, due to this property, and independently on its nature. This metric attractor A_λ can only be one of the following three typologies ([24], [104]):

(1) a $k-$cycle (of any period $k \geq 1$, either stable ($|S| < 1$), or neutral ($|S| = 1$);

(2) a critical attractor (A_{cr}) with Cantor like structure, of zero Lebesgue measure;

(3) $k-$cyclic chaotic intervals, $k \geq 1$.

In the case (1) the generic omega limit set $\omega(x)$ is equal to the omega limit set of the critical point x_c, and the trajectory of x_c tends to the $k-$cycle, stable or neutral A_λ, $\omega(x_c) = A_\lambda$. In the case in which $|S| = 1$ the cycle belongs to the frontier of its basin (or better, stable set). In the case in which $|S| < 1$ *the cycle is an attractor of* T. For $b > b_{1s}$ the frontier of the basin of attraction is a strange repeller Λ, i.e. an invariant set, $T(\Lambda) = \Lambda$ such that the restriction $T : \Lambda \to \Lambda$ is chaotic (in the sense of Devaney). This frontier (on which the map is chaotic) if a set of zero measure in the interval X, and it is a topological repellor, i.e. a repelling set in the definition given above.

In the case (2) the generic omega limit set $\omega(x)$ is equal to $\omega(x_c) = A_{cr}$ and $x_c \in A_{cr}$. In this case $T : A_{cr} \to A_{cr}$ is chaotic, however A_{cr} is not a topological attractor, that is, an "attractor of T" in the usual definition, but an "attractor in Milnor' sense" and its stable set is the whole interval, so that we can say that it is globally attracting in the interval.

We recall that an invariant set is an "attractor in Milnor' sense" when its stable set has positive Lebesgue measure in the space of the map.

In the case (3) the critical point x_c is either periodic or preperiodic, merging into a repelling cycle ($|S| > 1$), which is called a critical periodic orbit, and at this parameter value a homoclinic bifurcation of this cycle occurs. The critical periodic orbit belongs to the chaotic intervals A_λ. In this case $T : A_\lambda \to A_\lambda$ is chaotic, and A_λ may be a topological attractor or an "attractor in Milnor' sense" depending on the parameter value (for example, at the closure of a box of second kind it is a topological attractor, while at the closure of a box of first kind it is an attractor in Milnor's sense, globally attracting in the whole interval).

In all the cases (1), (2) and (3), *the chaotic set is the closure of all the repelling points in I.*

Noticing that in (2) and (3) above the chaotic sets attracts all the points of the interval, we may generically speak of "chaotic attractors", but the chaotic set is of *full measure* only in the case (3).

Let us define as b_p the set of parameter values in the interval $[-1/4, 2]$ at which the typology (1) occurs, b_{cr} and b_{ch} respectively the set of parameter values in the same interval $[-1/4, 2]$ at which the typology (2) and (3) respectively occurs. Then it is important to notice that the set b_p consists of infinitely many nontrivial intervals having a fractal structure in the interval $[-1/4, 2]$ and dense in it (i.e. $\overline{b_p} = [-1/4, 2]$). The set b_{cr} is a completely disconnected set of zero Lebesgue measure while the set b_{ch} is a completely disconnected set of positive Lebesgue measure (for the proofs we refer to Thunberg [2001] and references therein).

Thus the set of points in the parameter space $[-1/4, 2]$ in which we have chaotic attracting sets of full measure in X is a set of positive Lebesgue measure.

When the parameter b varies in the interval $-1/4 \leq b \leq 2$ sequences of "boxes" occur, with the related bifurcations. Each box of the first kind is opened by a fold bifurcation giving rise to a pair of cycles, such a box of first kind closes when the cycle with $S > 1$ becomes critical for the first time (i.e. the first time that a critical point merges in it, at its first homoclinic bifurcation). Inside each box of first kind the cycle with $S < 1$ starts an infinite sequence of flip bifurcations, each of which opens a box of second class which closes when it becomes critical for the first time (i.e. at its first homoclinic bifurcation). Such sequences of boxes have a fractal structure due to the self similar property. All the boundaries of boxes of first or second class are bifurcation values. At all the opening values the map is of typology (1), while all the closure values are global (homoclinic) bifurcations (belonging to the set b_{ch}), and the map is of typology (3). Inside each box of first kind there exists a limit value of boxes of second kind at which the the map is of typology (2) (the so called Feigenbaum point). Particular bifurcation values of b are those which are limit points of other bifurcation values (for example boundaries of boxes of first class), such bifurcation values belong to the set b_{ch} and the map is of typology (3). In particular, when the critical point x_c is periodic or preperiodic the map is of typology (3).

12 References

References

[1] Abraham R., L. Gardini, C. Mira "Chaos in Discrete Dynamical Systems (A visual introduction in 2 dimensions)", TELOS, Springer-Verlag, N-Y 1997.

[2] A. Agliari, G.I. Bischi and L. Gardini, Some methods for thr Global Analysis of Dynamic Games represented by Noninvertible Maps, Chapter 3 in *Oligopoly and Complex Dynamics: Tools & Models*, T. Puu and I. Sushko (eds.), Springer Verlag (in press).

[3] A. Agliari, Gardini, Puu (2005), Some global bifurcations related to the appearance of closed invariant curves, *Computers and Mathematics in Simulation* 68, pp.201-219

[4] A. Agliari, Gardini, Puu (2006),Global bifurcation in duopoly when the fixed point is destabilized via a subcritical Neimark bifurcation, *International Game Theory Review* 8, pp. 1-20

[5] Agliari A. (2006), Homoclinic connections and subcritical Neimark bifurcations in a duopoly model with adaptively adjusted productions, *Chaos Solitons & Fractals* 29, pp. 739-755

[6] A. Agliari, G. I. Bischi, R. Dieci, L. Gardini (2005) "Global bifurcations of closed invariant curves in two-dimensional maps: A computer assisted study" International Journal of Bifurcations and Chaos, vol. 15 (4), pp. 1285-1328

[7] A. Agliari, G.I. Bischi, R. Dieci, L. Gardini (2006) "Homoclinic tangles associated with closed invariant curves in families of 2D maps" Grazer Math. Ber. N. 350, pp. 1-14

[8] Agliari, Dieci (2006), Coexistence of attractors and homoclinic loops in a Kaldor-like business cycle model, In: T. Puu and I Sushko (eds.): *Business cycle dynamics: Models and tools.* Springer-Verlag, pp.223-254.

[9] Agliari A. (2007), On the bifurcation mechanisms causing the appearance of invariant closed curves, *Grazer Math. Ber.*, N.351, pp. 1-20

[10] Agliari, Dieci, Gardini (2007), Homoclinic tangle in Kaldor's like business cycle models, *Journal of Economic Behavior and Organization* 62, pp. 324-347

[11] A. Agliari, C. Chiarella, L. Gardini (2006) "A Re-evaluation of the Adaptive Expectations in Light of Global Nonlinear Dynamic Analysis " *Journal of Economic Behavior and Organization*, Vol 60/4, pp 526-552.

[12] V. Avrutin, M. Schanz. On fully developed bandcount adding sce-

nario. Nonlinearity 21 (2008), 1077-1103.

[13] Azariadis, C. and Guesnerie, R., 1986, "Sunspots and cycles". *Review of Economic Studies* 53, 725-736.

[14] Banerjee, S. and C. Grebogi [1999] "Border-collision bifurcations in two-dimensional piecewise smooth maps", *Physical Review E*, 59, No. 4, 4052-4061.

[15] S. Banerjee, M.S. Karthik, G. Yuan and J.A. Yorke, *Bifurcations in One-Dimensional Piecewise Smooth Maps - Theory and Applications in Switching Circuits,* IEEE Trans. Circuits Syst.-I: Fund. Theory Appl. 47 No. 3 (2000), 389-394.

[16] Banerjee, S., Ranjan, P., and Grebogi, C., *Bifurcations in 2D Piecewise Smooth Maps - Theory and Applications in Switching Circuits,* IEEE Trans. Circuits Syst.-I: Fund. Theory Appl. 47 No. 5 (2000), 633-64.

[17] Barnsley M.F. and S. Demko (1985): Iterated function systems and the global construction of fractals. The Proceedings of the Royal Society of London A399, 243-275.

[18] Barnsley M.F. "Fractals everywhere", Academic Press, CA, (1988).

[19] Bignami F., Agliari A. (2008) "Synchronization and on-off intermittency phenomena in a market model with complementary goods and adaptive expectations" *Working paper n.51 del Dipartimento di Scienze Economiche e Sociali*, Serie verde "Metodi quantitativi ed informatica" Università Cattolica, sede di Piacenza.

[20] Bischi, G.I., Mammana, C., Gardini, L., Multistability and cyclic attractors in duopoly games, *Chaos Solitons & Fractals* 11 (2000), 543-564.

[21] G.I. Bischi, L. Gardini and M. Kopel, Analysis of Global Bifurcations in a Market Share Attraction Model, *Journal of Economic Dynamics and Control*, 24, pp. 855-879, (2000).

[22] G.I. Bischi and M. Kopel, Equilibrium Selection in a Nonlinear Duopoly Game with Adaptive Expectations, *Journal of Economic Behavior and Organization*, vol. 46/1, pp. 73-100, (2001).

[23] Bischi, G.I., Dieci, R., Rodano, G., and Saltari, E., 2001, "Multiple attractors and global bifurcations in a Kaldor-type business cycle model", *Journal of Evolutionary Economics* 11, pp.527-554.

[24] Blockh A.M. & M. Yu. Lyubich [1991] "Measurable dynamics of S-unimodal maps of the interval", *Ann. Scuola Norm. Sup.* Pisa Cl. Sci.4, 24, pp. 545-573.

[25] Cass, D. and Shell, C., 1983, " Do sunspots matter?" *Journal of Political Economy* 91. 193-227.

[26] Cournot, A.,.*Researches into the principles of the theory of wealth.*

Engl. transl., Chapter VII, 1963, Irwin Paperback Classics in Economics, (1838).

[27] R. Day, *Irregular growth cycles*, The American Economic Review 72(3) (1982), 406-414.

[28] R. Day, “Complex Economic Dynamics”, MIT Press, Cambridge, 1994.

[29] W. De Melo and S. van Strien, “One-Dimensional Dynamics”, Springer, New York , 1993.

[30] Devaney R., An Introduction to Chaotic Dynamical Systems, The Benjamin/Cummings Publishing Co., Menlo Park, California, 1986.

[31] M. Di Bernardo, M.I. Feigen, S.J. Hogan and M.E. Homer, Local analysis of C-bifurcations in n-dimensional piecewise smooth dynamical systems, Chaos, Solitons & Fractals 10(11) (1999), 1881-1908.

[32] M. di Bernardo C.J. Budd A.R. Champneys P. Kowalczyk, Piecewise-smooth Dynamical Systems Theory and Applications, Springer-Verlag London, 2008.

[33] Dohtani, A., Misawa, T., Inaba, T., Yokoo, M., and Owase, T., 1996, "Chaos, complex transients and noise: Illustration with a Kaldor model", *Chaos Solitons & Fractals* 7, pp.2157-2174.

[34] Dutta, M., Nusse, H. E., Ott, E., Yorke, J. A., and Yuan, G. H. [1999] "Multiple attractor bifurcations: A source of unpredictability in piecewise smooth systems", *Phys. Rev. Lett.* 83, 4281–4284.

[35] Feely, O., D. Fournier-Prunaret, I. Taralova-Roux, and D. Fitzgerald [2000], "Nonlinear dynamics of bandpass sigma-delta modulation. An investigation by means of the critical lines tool", *International Journal of Bifurcation and Chaos*, 10(2), 303-327.

[36] Foroni I., Agliari A. (2008), Complex price dynamics in a financial market with imitation, *Computational Economics* 32, pp. 21-36

[37] Gallegati, M., Gardini, L., Puu, T., and Sushko, I., 2003, "Hicks's trade cycle revisited: cycles and bifurcations", *Mathematics and Computers in Simulations,* 63:505-527

[38] Ganguli, A. and S. Banerjee [2005] "Dangerous bifurcation at border collision: when does it occur? ", *Phys. Rev.E* 71 057202 (1-4)

[39] Laura Gardini, Iryna Sushko and Ahmad Naimzada. Growing Through Chaotic Intervals. *Journal of Economic Theory 143* (2008), 541-557.

[40] Gardini L., "Homoclinic bifurcations in n-dimensional endomorphisms, due to expanding periodic points”, Nonlinear Analysis, Theory, Methods & Applications, 23(8), pp. 1039-1089. 1994.

[41] Gardini, L., Puu, T. and Sushko, I.[2006], "The Hicksian Model

with Investment Floor and Income Ceiling". In: *Business Cycles Dynamics. Models and Tools* (T. Puu and I. Sushko Ed.s), Springer.Verlag, N.Y.

[42] Gardini, L., Puu, T., Sushko, I. [2006] "A Goodwin-type Model with a Piecewise Linear Investment Function". In: *Business Cycles Dynamics. Models and Tools* (T. Puu and I. Sushko Ed.s), Springer Verlag, N.Y.

[43] Gardini L., Cars Hommes, Fabio Tramontana, Robin de Vilder, 2008, "Forward and Backward Dnamics in implicitly defined Overlapping Generations Models" Journal of Economic Behavior and Organization (to appear).

[44] Gaunersdorfer A., Hommes C.H., Wagener F.O.O. (2008), Bifurcation routes to volatility clustering under evolutionary learning, *Journal of Economic Behavior & Organization* 67, pp. 27-47 JEBO forthcoming

[45] Grandmont, J.M., 1985, "On endogenous competitive business cycles". *Econometrica* 53, 995-1045.

[46] Grandmont, J.M. and Laroque, G., 1986, Stability of cycles and expectations. *Journal of Economic Theory* 40, 138-151.

[47] Grandmont, J.M., 1993, "Expectations driven nonlinear business cycles". In: RheinischwestfÄalische akademie der wissenschaften, vortrÄage N 397. Westdeutcher Verlag.

[48] Grasman, J., and Wentzel, J.J., 1994, "Coexistence of a limit cycle and an equilibrium in a Kaldor's business cycle model and its consequences", *Journal of Economic Behavior and Organization* 24, pp.369-377.

[49] Guckenheimer, J., On the bifurcaiton of maps on the interval, Invent. Math., 39 (1977), 165-178.

[50] Guckenheimer, J., Holmes, P., Nonlinear Oscillations, Dynamical Systems, and Bifurcations of Vector Fields, Springer-Verlag New-York 1983.

[51] Gumowski I. & Mira C. 1980 *Dynamique chaotique. Transformations ponctuelles. Transition ordre désordre,* Cépadues Editions, Toulouse.

[52] Gumowski I. and Mira C., 1980, "Recurrences and discrete dynamic systems", Lecture notes in Mathematics, Springer.

[53] C. Halse, M. Homer and M. di Bernardo, *C-bifurcations and period-adding in one-dimensional piecewise-smooth maps*, Chaos, Solitons & Fractals 18 (2003), 953-976.

[54] B.L. Hao, "Elementary Symbolic Dynamics and Chaos in Dissipative Systems", World Scientific, Singapore, 1989.

[55] Hao, B.-L., Zheng, W.-M., 1998, *Applied Symbolic Dynamics and*

Chaos, World Scientific

[56] Hassouned, M.A., E.H. Abed and H.E. Nusse [2004] "Robust dangerous Border-Collision Bifurcations in piecewise smooth systems", *Phys. Rev. Letters*, 92(7) 070201 (1-4).

[57] Herrmann, R., 1985, "Stability and chaos in a Kaldor-type model", DP22, Department of Economics, University of Gottingen.

[58] Hicks, J.R., 1950, *A Contribution to the Theory of the Trade Cycle*, Clarendon Press, Oxford

[59] C.H. Hommes, H. Nusse, Period three to period two bifurcations for piecewise linear models, Journal of Economics 54(2) (1991) 157-169.

[60] Ingram, W.T. 2002, "Invariant sets and inverse limits", *Topology and its Applications* 126, pp. 393-408.

[61] Ingram, W.T. and W.S. Mahavier, 2004, "Interesting dynamics and inverse limits in a family of one dimensional maps", *American Mathematical Monthly*, 111(3), pp. 198-215.

[62] Iooss, G., 1979, *Bifurcation of Maps and Applications*, North-Holland Publishing Company, Amsterdam.

[63] Iooss, G., and Joseph, D.D., 1980, *Elementary Stability and Bifurcation Theory*, Springer-Verlag (New York).

[64] Kapitaniak, T. and Maistrenko, Yu. L. [1998] "Multiple choice bifurcations as a source of unpredictability in dynamical systems" *Phys. Rev. E 5*8(4), 5161–5163.

[65] Kennedy, J.,A., Stockman, D.R. and Yorke J.A. 2007. Inverse limits and an implicitly defined difference equation from economics. *Topology and its Applications* 154, pp. 2533-2552

[66] Kennedy, J.,A. and Stockman, D.R., 2008. "Chaotic equilibria in models with backward dynamics". *Journal of Economic Dynamics and Control* 32, 939-955.

[67] Kind, C., 1999, "Remarks on the economic interpretation of Hopf bifurcations", *Economic Letters* 62, pp.147-154.

[68] Kocic, V. L., Ladas, G., *Global Behavior of Nonlinear Difference Equations of Higher Order with Applications*, Kluwer Academic Publishers 1993

[69] Kopel, M., Simple and complex adjustment dynamics in Cournot Duopoly Models, Chaos, Solitons, and Fractals, 7, 2031-2048, (1996).

[70] Kuznetsov, Y. A. Elements of applied bifurcation theory, Springer-Verlag New-York 1998.

[71] Li T. and Yorke J.A. "Period Three Implies Caos", American Mathematical Monthly, 82, 985-992, (1975).

[72] Lines M., Westerhoff F. (2006), Expectations and the Multiplier-

Accelerator Model, In: T. Puu and I Sushko (eds.): *Business cycle dynamics: Models and tools*. Springer-Verlag, pp.255-276

[73] Lines M. (2005), Bifurcation scenarios in a heterogeneous agent, multiplier-accelerator model, *PUMA* 16, pp.429-442

[74] Lorenz, H.W., 1992, "Multiple attractors, Complex Basin Boundaries, and Transient Motion in Deterministic Economic Systems", in *Dynamic Economic Models and Optimal Control*, G. Feichtinger (Ed.), North-Holland, Amsterdam, pp.411-430

[75] Yu.L. Maistrenko, V.L. Maistrenko and L.O. Chua, *Cycles of chaotic intervals in a time-delayed Chua's circuit*, International Journal of Bifurcation and Chaos 3(6) (1993), 1557-1572.

[76] Maistrenko Y.L., V.L. Maistrenko, S.I. Vikul and L. Chua [1995] "Bifurcations of attracting cycles from time-delayed Chua's circuit", *International Journal of Bifurcation and Chaos* 5(3), 653-671.

[77] Y.L. Maistrenko, V.L. Maistrenko and S.I. Vikul, On period-adding sequences of attracting cycles in piecewise linear maps, Chaos, Solitons & Fractals 9(1) (1998) 67-75.

[78] Maistrenko, Y., Sushko, I., and Gardini, L. [1998] "About two mechanisms of reunion of chaotic attractors", *Chaos, Solitons & Fractals*, 9(8), 1373-1390.

[79] Marotto F. R. (1978): "Snap-Back Repellers Imply Chaos in R^n " Journal of Mathematical Analysis and Applications, 63(1), 199-223.

[80] Marotto, F. R. (2005): "On Redefining a Snap-Back Repeller," Chaos, Solitons & Fractals, 25, 25-28.

[81] K. Matsuyama, Growing through cycles, Econometrica 67(2) (1999), 335-347.

[82] R.M. May "Simple mathematical models with very complicated dynamics" Nature, vol. 261, June 10 1976.

[83] Medio, A. and Raines, B., 2007, "Backward dynamics in economics. The inverse limit approach", *Journal of Economic Dynamics and Control* 31, 1633-1671.

[84] Michener, R. and Ravikumar, B., 1998. Chaotic dynamics in a cash-in-advance economy. *Journal of Economic Dynamics and Control* 22, 1117–1137.

[85] Mira C. [1975] "Accumulations de bifurcations et structures boîtes-emboîtées dans les récurrences et transformations ponctuelles." *Proceedings of the 7th International Conference On Nonlinear Oscillations*. Berlin sept. 1975. Akademic Verlag, Berlin 1977, Band I 2, 81-93.

[86] Mira C. [1976] "Sur la double interprétation , déterministe et sta-

tistique, de certaines bifurcations complexes". *Comptes Rendus Acad. Sc. Paris,*. Série A, 283, 911-914.

[87] C. Mira, "Chaotic Dynamics", World Scientific, Singapore, 1987.

[88] Mira, C., Fournier-Prunaret, D., Gardini, L., Kawakami, H. and Cathala, J.C.,.Basin bifurcations of two-dimensional noninvertible maps: fractalization of basins, *International Journal of Bifurcations and Chaos*, 4, 343-381, (1994).

[89] Mira C., L. Gardini, A. Barugola, J.C. Cathala "Chaotic Dynamics in Two-Dimensional NonivertibIe Maps", World-Scientific Publ. Co., "Nonlinear Sciences, Series A", Singapore 1996.

[90] T. Mitra, A sufficient condition for topological chaos with an application to a model of endogenous growth, J. of Economic Theory, 96, (2001), 133-152.

[91] A. Mukherji, Robust cyclical growth, International J. of Economic Theory, 1 (2005), 233-246.

[92] Myrberg P. J. (1963) "Iteration von Quadratwurzeloperationen. III". *Ann. Acad. Sci.. Fenn.*, ser. A, 336, 1-10.

[93] A. Norin and T. Puu, Cournot duopoly when the competitors operate under capacity constraints, *Chaos, Solitons and Fractals* 18 (2003) 577-592

[94] H.E. Nusse and J.A. Yorke, *Border-collision bifurcations including period two to period three for piecewise smooth systems*, Physica D 57 (1992), 39-57.

[95] H.E. Nusse and J.A. Yorke, *Border-collision bifurcations for piecewise smooth one-dimensional maps*, International Journal of Bifurcation and Chaos 5(1) (1995), 189-207.

[96] T. Puu and I. Sushko Ed.s, "Oligopoly and Complex Dynamics: Models and Tools", Springer, New York, 2002.

[97] T. Puu and I. Sushko Ed.s, "Business Cycles Dynamics: Models and Tools", Springer, New York, 2006.

[98] Puu, T., Gardini, L., Sushko, I., 2005. A Hicksian multiplier-accelerator model with floor determined by capital stock. Journal of Economic Behavior and Organization 56, 331-348.

[99] Puu, T., 2007. The Hicksian trade cycle with floor and ceiling dependent on capital stock, Journal of Economic Dynamics & Control 31:575-592.

[100] Rau, N., 1974, *Trade Cycle: Theory and Evidence*, Macmillan, London

[101] Reichlin, P., 1986, "Equilibrium cycles in an overlapping generations economy with production", *Journal of Economic Theory* 40, 89-102.

[102] Samuelson, P.A., 1939, "Interactions between the multiplier analy-

sis and the principle of acceleration", *Review of Economics and Statistics 21: 75-78*
[103] A.N. Sharkovsky (1964) "Coexistence of cycles of a continuous map of a line into itself" Ukr. Math. Z. 16, pp.61-71.
[104] A.N. Sharkovsky, S.F. Kolyada, A.G. Sivak and V.V. Fedorenko, “Dynamics of One-dimensional Maps”, Kluwer Academic Publ., Boston, 1997.
[105] Simpson, D. J. W., and Meiss, J. D., *Neimark–Sacker Bifurcations in Planar, Piecewise-Smooth, Continuous Maps*, SIAM J. Applied Dynamical Systems, Vol. 7 (2008), No. 3, 795–824.
[106] I. Sushko, A. Agliari and L. Gardini, Bistability and border-collision bifurcations for a family of unimodal piecewise smooth maps, Discrete and Continuous Dynamical Systems, Serie B, 5(3) (2005), 881-897.
[107] I. Sushko, A. Agliari and L. Gardini, Bifurcation Structure of Parameter Plane for a Family of Unimodal Piecewise Smooth Maps: Border-Collision Bifurcation Curves, Chaos, Solitons & Fractals, 29(3), (2006), 756-770.
[108] Sushko, I., and Gardini, L. [2006] "Center Bifurcation for a 2D Piecewise Linear Map". In: *Business Cycles Dynamics. Models and Tools* (T. Puu and I. Sushko Ed.s), Springer Verlag, N.Y.
[109] Sushko, I., and Gardini, L. *Center Bifurcation for Two-Dimensional Border-Collision Normal Form*, Int. J. Bifurcation and Chaos, Vol. 18, Issue 4 (2008), 1029-1050.
[110] Sushko, I., Gardini, L., *Center Bifurcation of a point on the Poincaré Equator*, Submitted to Grazer Mathematische Berichte (2009).
[111] Sushko, I., Gardini, L., and Puu, T., *Tongues of Periodicity in a Family of Two-dimensional Discontinuous Maps of Real Möbius Type*, Chaos, Solitons & Fractals 21 (2004), 403-412.
[112] I. Sushko, T. Puu and L. Gardini, *The Hicksian floor-roof model for two regions linked by interregional trade*, Chaos Solitons & Fractals *18 (2003), 593-612.*
[113] Iryna Sushko, Laura Gardini and Tönu Puu: "Regular and Chaotic Grouwth Cyckles in a Hicksian Floor/Roof Model ", Journal of Economic Behavior and Organization. 2009 (to appear).
[114] F. Tramontana, L. Gardini and T. Puu “Duopoly games with alternative technologies”, JEDC, 33, pp. 250-265, 2008.
[115] F. Tramontana, L. Gardini “Use of homoclinic orbits and Iterated Function Systems in backward models.” Grazer Mathematische Berichte, 2009 (to appear).
[116] Wiggins, S., 1988, *Global Bifurcations and Chaos, Analytical Meth-*

ods, Springer Verlag, New York.

[117] Woodford, M., 1986, "Stationary sunspot equilibria in a finance constrained economy", *Journal of Economic Theory* 40, 128–137.

[118] Z.T. Zhusubaliyev and E. Mosekilde, “Bifurcations and Chaos in Piecewise - Smooth Dynamical Systems”, World Scientific, Singapore, 2003.

[119] Zhusubaliyev, Z. T., Mosekilde, E., Maity, S., Mohanan, S., and Banerjee, S., *Border collision route to quasiperiodicity: Numerical investigation and experimental confirmation*, Chaos 16, 023122 (2006), 1-11.

[120] Zhusubaliyev, Z.T., E. Soukhoterin and E. Mosekilde [2007] "Quasiperiodicity and torus breakdown in a power electronic dc/dc converter" Mathematics and Computers in Simulation 73, 364-377.